

**Using Forced Degradation to Aid the Development of Biopharmaceutical Products**

by

Alexander Benet

A dissertation submitted in partial fulfillment  
of the requirements for the degree of  
Doctor of Philosophy  
(Pharmaceutical Sciences)  
in the University of Michigan  
2021

Doctoral Committee:

Professor Anna Schwendeman, Chair  
Professor Brandon Ruotolo  
Professor Steven Schendeman  
Professor Peter Tessier

Alexander Benet

[abenet@umich.edu](mailto:abenet@umich.edu)

ORCID iD: [0000-0003-4178-1985](https://orcid.org/0000-0003-4178-1985)

© Alexander Benet 2021

## **Dedication**

This thesis is first dedicated to my family. Firstly, my parents Reed and Jacqueline, for all their love and support, providing a loving and nurturing environment each and every day. Also, my grandparents, Ninette, Leslie and Carol, who continue to dole out unconditional love and support at all turns, who I can turn to for advice and amazing life lessons. Lastly, my brother and sister, two people who continue to grow in unique ways.

This thesis is also dedicated to God, “the knowledge, the knower and the known” -Maimonides. The world of science and the complexity of the human body continue to serve as a proof that everything has a purpose in this world. As humans, we must interact and elevate the world, from the inanimate to vegetation, from animals to humans, revealing sparks of Godliness like diamonds covered beneath layers of dirt.

Lastly, I want to dedicate this thesis in the honor of the Lubavitcher Rebbe, whose teachings continue to inspire me. It is through self-nullification and lack of haughtiness that we continue to grow. Chabad on Campus and the Goldstein and Zwiebel families, as my spiritual accountants, have continued to inspire me to grow. There is only so much that is within our environment that we can control and we must take full advantage of these opportunities. We must realize that factors outside of our control are direct challenges to our true essence and serve as distractions that pull us away from such growth.

## **Acknowledgements**

I would first like to thank my advisor, Dr. Anna Schwendeman, who I've gotten to know since we met 7 years ago. It's been quite the ride and we've managed to make it through without tearing each other's heads off. I had chosen to work in this lab because of your sense of humor and contagious personality. It has been interesting watching you grow in your professorship and your path towards a recent advancement to tenure. Continue to keep a positive attitude and your self-awareness will let you go far. I would next like to thank Dr. Ara Paul who was my mentor since the first two years of grad school, continuously supporting me and providing me with advice, all while giving me a needed kick in the butt to persevere throughout grad school. I would also like to thank my dissertation committee for their support and guidance; Prof. Brandon Ruotolo, Prof. Steve Schwendeman and Prof. Pete Tessier, thank you for helping me develop my ability to think about science. Thank you to the College of Pharmacy, other professors, mentors and administrative staff for your help.

I have been extremely lucky to have been surrounded by good and supportive friends in the Schwendeman labs. Those who struggle together, strive together. First and foremost I am obligated to thank Jukyung (Jay) Kang (주나) who has been my best friend in grad school. Without your help, mentorship, guidance and support I don't know if I could have made it through the program. Next, I'd like to acknowledge another best friend and cubicle mate Jenna Walker, who was always there to listen to my silly ideas,

investigate the world of coffee and espresso and participation in the Kroger Crew, which also included Jay, Emily Morin, Maria Fawaz and Minzhi Yu. I'd also like to thank our dear leader (and my lab father) Karthik Pisupati who continues to give me advice to this day. I'd like to also thank the future of the team Karthik family, Jill Coghlan and Troy Halseth. Thank you to our lab managers Rose Ackermann and Karl Olsen, without you I don't know what would happen to our lab.

Shout out to the legendary suite 3030 (Mac, Vyas, Dom, Efe, Adrian, Aaron, Jean, Joel, Brian) and the many friends I have made over the course of grad school. Shout out to the Munger crew (Hayden, Dwarf etc...) as the shenanigans never end when the filter comes off.

Shout out to the Chabad crew (Isaac, Avi, Alan, Ethan, Scott, Max, Aviv etc...) and my friends who I met in undergrad here at U of M (Tony, David and Jordan).

Thank you to everyone not mentioned in this list, it is not that I have forgotten but this section would go on for a while if I included everyone.

## Table of Contents

<b>Dedication</b> .....	<b>ii</b>
<b>Acknowledgements</b> .....	<b>iii</b>
<b>List of Figures</b> .....	<b>vii</b>
<b>List of Tables</b> .....	<b>xiv</b>
<b>Abstract</b> .....	<b>xv</b>
<b>Chapter 1: Introduction</b> .....	<b>1</b>
1.1 Background and Significance of the Analytical Characterization of Biologics .....	1
1.2 Forced Degradation Studies as a Tool to Characterize Biopharmaceuticals .....	6
1.3 Chemical and Physical Stability of mAb Therapeutics .....	8
1.4 Chemical and Physical Stability of Peptide Therapeutics.....	25
1.5 Background: GLP-1 Receptor Agonists .....	30
1.6 Exenatide: An Approved GLP-1 Receptor Agonist.....	34
1.7 Infliximab: An Anti-TNF- $\alpha$ mAb.....	39
1.8 Aspects of Peptide/mAb Formulations and Delivery Devices.....	47
<b>Chapter 2: The Effects of pH and Excipients on the Stability of Exenatide</b> .....	<b>1</b>
2.1 Abstract.....	57
2.2 Introduction .....	58
2.3 Materials and Methods.....	60
2.4 Results .....	64
2.5 Discussion.....	78

<b>Chapter 3: Biosimilarity Under Stress: A Forced Degradation Study .....</b>	<b>81</b>
3.1 Abstract.....	81
3.2 Introduction .....	82
3.3 Materials and Methods.....	85
3.4 Results .....	95
3.5 Discussion.....	111
<b>Chapter 4: Disulfide Shuffling Comparability Studies .....</b>	<b>117</b>
4.1 Abstract.....	117
4.2 Introduction .....	118
4.3 Methods .....	122
4.4 Results .....	127
4.5 Discussion.....	149
<b>Chapter 5: Conclusions and Future Directions .....</b>	<b>154</b>
<b>Bibliography .....</b>	<b>161</b>

## List of Figures

Figure 1-1. Molecular weight and complexity differences between small molecules, small biologics and biologics, which are respectively represented as bicycles, cars and airplanes.	2
Figure 1-2. Differences in the drug development processes for biologics/small molecules.	3
Figure 1-3. Methionine oxidation pathway that leads to the formation of methionine sulfoxide (MetO), a single oxygen addition, and methionine sulfone, a double oxygen addition.	10
Figure 1-4. Typical Asn deamidation pathway, proceeding through a succinimide intermediate, which undergoes isomerization, resulting in the formation of aspartic acid (Asp) and isoaspartic acid (isoAsp).	11
Figure 1-5. Typical PyroQ formation pathways that occurs at glutamine and glutamic acid residues.	11
Figure 1-6. Intra- and inter-molecular disulfide shuffling that occurs (A) between a free thiol and an existing disulfide bond within a molecule or (B) between two molecules. Here, free thiols are shown as thiolate anions, which commonly occur at elevated pH. Figure adapted with permission from [113].	13
Figure 1-7. (A) Correlation of % potency (TNF- $\alpha$ neutralization) with % incorrect disulfide bonding at C78-C88 for etanercept. (B) Etanercept structures with correct/incorrect disulfide bonding. <sup>137</sup>	14
Figure 1-8. Atomic Force Microscopy (AFM) images of IgG when subject to freeze-thaw, pH, heat, shake and oxidation stress, resulting in various aggregate types. Figure adapted with permission from [160].	16
Figure 1-9. Size-dependent analysis methods of various aggregates and particle sizes from monomer to visible aggregates. <sup>10</sup>	17
Figure 1-10. Far-UV CD spectra for GLP-1 subject to freeze-thaw, pH, heat, shake and oxidation stress. Figure adapted with permission from [160].	20
Figure 1-11. Methods that compare higher order structure of innovator/biosimilar infliximab. (A) far-UV CD. MRE: Molar Residue Ellipticity; RMP: Reference Medicinal Product. <sup>136</sup> (B) DSC thermal overlay plot. <sup>136</sup> (D) HDX-MS butterfly plots. <sup>202</sup> (E) deuterium uptake difference plots. <sup>202</sup> (F) IM-MS collision induced unfolding (CIU) fingerprints, showing averages (left) and Standard Deviations (right) of innovator (top) and biosimilar (bottom). <sup>211</sup> Figures adapted with permission.	22



Figure 1-12. Types of ADAs from “binding” to neutralizing to cross-reactive neutralizing, where frequency is inversely related to clinical impact. Figure adapted with permission from [215]. .....	22
Figure 1-13. In vitro interactions of protein aggregates with antigen presenting cells (APCs) that can potentially trigger an immune response through different kinds of receptors - FcγRs, TLRs and/or CRs. In addition, following receptor-mediated phagocytosis of aggregates, lysosome digested peptides are presented on the cell surface, resulting in naïve T-cell stimulation. Figure adapted with permission from [170].	23
Figure 1-14. Cytokine response profiles for IgG1 subjected to thermal, pH, stir and syringe stress. Figure adapted with permission from [221].	24
Figure 1-15 Molecular weight and complexity differences between small molecules, peptides, small biologics and biologics, respectively represented as bicycles, mopeds, cars and airplanes.	25
Figure 1-16. Peptide sequences and molecular structures of FDA approved GLP-1RA, including GLP-1, exenatide, liraglutide, lixisenatide, semaglutide, dulaglutide and albiglutide. Yellow: key amino acids related to potency; Red: substituted amino acids; Blue: spacers; Green: IgG. Figure adapted with permission from [263].	31
Figure 1-17 Chemical impurity formation of exenatide released from hydrogels over 56 days of incubation at 37°C. Black: 0 days; Red: 8 days; Blue: 28 days; Green: 56 days. Figure adapted with permission from [284].	35
Figure 1-18. Far-UV CD spectra of exenatide concentrations from 2 to 600 μM. Green: 2 μM; Purple: 40 μM; Red: 240 μM; Yellow: 600 μM. Figure adapted with permission from [285].	37
Figure 1-19. Potential conformational isomers and oligomeric species that could contribute to the solvent-dependent equilibrium in exenatide at different concentrations as a function of Trp-cage unfolding. Figure adapted with permission from [285].	38
Figure 1-20 Sources of mAb manufacturing, including mouse derived, chimeric, humanized and human. Shown in the order of highest to lowest potential to elicit immunogenic response. Figure adapted with permission from [294].	40
Figure 1-21. Range of rates (%) of ADAbs formation to biologics in patients with IDBs. Only studies reporting rates of ADAbs were included, immunogenicity analyses are product- and assay-specific, infliximab excluded one study that had a small sample size (n = 28) and high rate of immunogenicity (79%). -: no publications available; ADAbs: anti-drug antibodies; CD: Crohn’s Disease; UC: Ulcerative Colitis. Figure adapted with permission from [160].	41
Figure 1-22. Results and Statistical Analysis of Binding of soluble TNF-α. Dark Blue: CT-P13; Light Blue: ALAG CT-P13; Grey: EU Remicade; Yellow: US Remicade; ALAG: artificially elevated afucosylated glycans.	43
Figure 1-23. Results and Statistical Analysis of ELISA Binding of Transmembrane-Bound TNF-α. Dark Blue: CT-P13; Light Blue: ALAG CT-P13; Grey: EU Remicade; Yellow: US Remicade; ALAG: artificially elevated afucosylated glycans.	43

Figure 1-24. Quality Range Analysis of FcγRIIIa F variant binding by SPR. Dark Blue: CT-P13; Light Blue: ALAG CT-P13; Grey: EU Remicade; Yellow: US Remicade; ALAG: artificially elevated afucosylated glycans; Red: QR limits of variability. ....	44
Figure 1-25. Quality Range Analysis of FcγRIIIa V variant binding by SPR. Dark Blue: CT-P13; Light Blue: ALAG CT-P13; Grey: EU Remicade; Yellow: US Remicade; ALAG: artificially elevated afucosylated glycans; Red: QR limits of variability. ....	44
Figure 1-26. Scatter Plots Showing Relationship of % Afucosylated Glycan Species (G0 + Man 5) with FcγR3a Binding Affinity and ADCC Activity. Dark Blue: CT-P13; Grey: EU Remicade; Yellow: US Remicade. ....	44
Figure 1-27. Quantification by LC-MS/MS. (A) N-glycans. (B) Total mannose-terminated forms. (C) Total afucosylated forms. (D) Average $K_D$ values for binding to FcγR3a as measured by BLI. (n = 4 lots, mean ± SEM; *: p < 0.05). Figure adapted with permission from [211]. ....	45
Figure 1-28. Forest plot of risk difference according to disease. Figure shows data for the per-protocol set. Risk difference adjusted for treatment duration of infliximab originator at baseline. Figure adapted with permission from [312]. ....	46
Figure 1-29. Conformation states of insulin, including the monomer, dimer, tetramer and stable hexamer and factors affecting conformational equilibrium. Decreased pH favors the monomer while Zn and insulin concentration favor the hexamer. Figure adapted with permission from [319]. ....	48
Figure 1-30. Examples of excipients and their main function in peptide and protein formulations and their common, expected effects. Figure adapted with permission from [318]. ....	49
Figure 1-31. Three proposed theories how sugars may protect proteins from degradation. Vitrification: increase of viscosity; Water Replacement: preferential sugar binding with protein; Preferential Exclusion: preferential sugar binding with water. Figure adapted with permission from [320]. ....	50
Figure 1-32. Major landmark events in the evolution of insulin and insulin delivery devices. Figure adapted with permission from [338]. ....	52
Figure 1-33. Components of a closed-loop insulin delivery system. Sensor: measures interstitial glucose levels; Controller modifies the pump control algorithm in response to the sensor; Pump: infuses insulin through the catheter. All communication is wireless. Figure adapted with permission from [344]. ....	53
Figure 1-34. Optical appearance and properties of pen injection devices for approved GLP-1 receptor agonists (as mono substances or fixed-dose combinations with basal insulin). ....	55
Figure 2-1. Identification (w/ deconvoluted masses) of exenatide's chemical impurities by RPLC-MS QToF following incubation of peptide solution (pH 8.5) at 60°C for 24 hours. RP-HPLC C4 UV absorbance (A) total ion chromatograms (TIC) and (B-E, G-J) exenatide chemical impurities and their reported respective mass shifts, which include a combination of oxidation, deamidation and PyroQ formation, from (F) native exenatide's MW of 4186 Da. 65	

Figure 2-2. Kinetics of chemical degradation determined by RP-LC separating (A) parent peak from (B) oxidation and (C) deamidation chemical impurities during incubation of exenatide solutions pH 4.5 – pH 8.5 at 37°C for 4 weeks. (n = 3, mean ± SEM). ..... 66

Figure 2-3. A) RP-LC chromatograms after 4 weeks of incubation and B) AUCs (relative to day 0) and C) SEC-LC chromatograms after 4 weeks of incubation and D) AUCs (relative to day 0) for exenatide samples reconstituted at pH 4.5 – 8.5 over the course of incubation at 37°C for 4 weeks. .... 67

Figure 2-4. Kinetics of physical degradation determined by SEC-LC, separating (A) monomer from (B) aggregate and (C) fragment physical impurities of exenatide reconstituted at pH 4.5 – pH 8.5 after incubation at 37°C for 4 weeks. (n = 3, mean ± SEM).and Orange = 8.5. .... 68

Figure 2-5. Structural and conformational changes characterized and measured by (A-C) intrinsic fluorescence and (D-F) circular dichroism, with secondary structures (G-I) quantified by CDPro analysis (n = 3, mean ± SEM) for exenatide that was reconstituted at pH 4. .... 71

Figure 2-6. Kinetics of degradation determined by RP-LC and SEC-LC, with RP-LC separating (A) parent peak from (B) oxidation and (C) deamidation chemical impurities and SEC-LC separating (D) monomer from (E) aggregate and (F) fragment physical impurities of exenatide reconstituted at pH 4.5 w/ mannitol and pH 7.5 with specified excipients after incubation at 37°C for 4 weeks. (n = 3, mean ± SEM, \* p < 0.05 \*\* p < 0.01 \*\*\* p < 0.001). 74

Figure 2-7. RP-LC chromatograms after 4 weeks of incubation and B) AUCs (relative to day 0) and C) SEC-LC chromatograms after 4 weeks of incubation and D) AUCs (relative to day 0) for exenatide samples reconstituted at pH 4.5 w/ mannitol vs pH 7.5 w/ specified excipients over the course of incubation at 37°C for 4 weeks. .... 75

Figure 2-8. Particle size distribution determined by DLS (by volume) and separated into 0.3 – 10, 10 – 100, 100 – 500, 500 – 1000 and 1000+ µm size ranges for exenatide that was reconstituted at pH 4.5 w/ mannitol and pH 7.5 w/ specified excipients when incubated at 37C after weeks; (n = 3, mean). ..... **Error! Bookmark not defined.**

Figure 2-9. Structural and conformational changes characterized and measured by intrinsic fluorescence (A,D) and circular dichroism (B,E), with secondary structure quantified by CDPro analysis (C,F) for exenatide that was reconstituted at pH 4.5 w/mannitol and pH 7.5 w/ specified excipients after incubation at 37°C for 4 weeks. (n = 3, mean ± SEM). ..... **Error! Bookmark not defined.**

Figure 3-1. Schematic of stress study design. Humidity/thermal stress of infliximab samples were performed by incubating the drug powders at 40°C at different %RH for 0–4 weeks, followed by reconstitution (in WFI) and analysis. .... 95

Figure 3-2. (A) SEC-LC infliximab chromatograms over incubation at 97% RH/40°C and (B) Kinetics of monomer loss. (n = 4, n ± SEM) Characterization by (C) SDS PAGE and (D) Reducing SDS PAGE of RC/RS after 4 weeks of incubation at various humidities/40°C. .... 97

Figure 3-3. (A) Nanoparticle tracking analysis and (B) DSC thermal melts of unstressed (light) and stressed (dark) RC and RS that was incubated at 97% RH/40°C for 4 weeks. .... 98

Figure 3-4. Characterization of RC (blue) and RS (orange) incubated at 60°C. (A) Kinetics of monomer (SEC-LC) and (B) ThT fluorescence. (C) NTA analysis after 2 hrs of incubation. LC-MS/MS analysis of (D) deamidation, (E) oxidation and (F) dioxidation after 1 hr of incubation.....	100
Figure 3-5 . IM-MS spectra and corresponding mass to charge spectrograms of unstressed (A) RC and (B) RS before incubation and (C) RC and (D) RS after 4 weeks incubation at 97% RH/ 40°C. Fragment, monomer, dimer and trimer species are annotated in the ion mobility spectra. ....	102
Figure 3-6. Biophysical characterization of humidity stressed samples of RC (solid) and RS (dashed). (A,B) IF (C,D) near-UV CD and (E,F) far-UV CD. Blue: 0 weeks; Red: 2 weeks; Green: 4 weeks. ....	104
Figure 3-7. LC-MS/MS analysis of chemical modifications over the course of incubation at 97% RH/40°C for RC (blues) and RS (oranges). (A) Deamidation. (B) Oxidation. (C) N-glycosylation. (n = 2, average ± SEM). ....	106
Figure 3-8 (A) TNF-α binding (measured by ELISA) (B) FcγRIIIa binding (measured by BLITZ) (n = 2, mean ± SEM; P < 0.05) for RC and RS over the course of incubation 97% RH/40°C. ....	109
Figure 4-1. Comparison of infliximab originator/biosimilar by (A) relative expected contributions and (b) normalized contributions; Relative = divided by XIC AUC Totals of expected disulfide, shuffled disulfide and trisulfide bonds; Normalized = divided by specified XIC AUC total. ....	127
Figure 4-2. Comparison of shuffled disulfide bonds when trypsin digested at pH 5 for originator/biosimilar infliximab by (A) relative shuffled contributions and (B) normalized shuffled contributions for the top 10 shuffled bond locations. ....	128
Figure 4-3. Comparison of trisulfide bonds for originator/biosimilar infliximab (A) relative trisulfide contributions and (B) prevalent normalized contribution locations. ....	129
Figure 4-4. Comparison of originator/biosimilar rituximab by (A) relative expected contributions and (b) normalized contributions.....	130
Figure 4-5. Comparison of originator/biosimilar rituximab by (A) relative shuffled contributions and (b) normalized contributions.....	130
Figure 4-6. Comparison of originator/biosimilar bevacizumab by (A) relative expected contributions and (b) normalized contributions. ....	131
Figure 4-7. Comparison of originator/biosimilar bevacizumab by (A) relative shuffled contributions and (b) normalized contributions. ....	132
Figure 4-8. Comparison of trisulfide bonds for originator/biosimilar bevacizumab (A) relative trisulfide contributions and (B) prevalent normalized contribution locations. ....	133
Figure 4-9. SEC-LC chromatogram overlays of originator/biosimilar (A) infliximab, (B) rituximab and (C) bevacizumab when labeled overnight with bodipy maleimide.....	134

Figure 4-10. Quantified AUCs for SEC-LC chromatogram of originator/biosimilar infliximab, rituximab and bevacizumab when labeled overnight with bodipy maleimide. ....	134
Figure 4-11. SDS PAGE gels for bevacizumab and rituximab originator and biosimilar mAb pairs at (A) 0.25 and (B) 0.4 mg/mL comparing HiMark Prestained Protein Ladder against mAb pairs after 0, 2 and 4 weeks of incubation at 37°C; n = 1.....	136
Figure 4-12. SDS-PAGE relative contributions for rituximab originator/biosimilar (A) aggregates, (B) monomer and (C) fragments and relative contributions for bevacizumab originator/biosimilar (D) aggregates, (E) monomer and (F) fragments over the course of 4 weeks of incubation at 37°C; n = 1.....	137
Figure 4-13. SEC-LC chromatograms of rituximab originator at (A) 0 and (B) 4 and biosimilar at (C) 0 and (D) 4 weeks of incubation at 37°C. Bevacizumab originator at (E) 0 and (F) 4 and biosimilar at (G) 0 and (H) 4 weeks of incubation at 37°C. ....	138
Figure 4-14. SEC relative contributions for rituximab originator/biosimilar (A) aggregates, (B) monomer and (C) fragments and relative contributions for bevacizumab originator/biosimilar (D) aggregates, (E) monomer and (F) fragments over the course of 4 weeks of incubation at 37°C. (n = 1).....	138
Figure 4-15. Labeled cysteines and expected disulfide bond locations for (A) rituximab and (B) bevacizumab.....	140
Figure 4-16. Relative contributions of expected disulfide bonds, shuffled disulfide bonds and trisulfide bonds for (A) rituximab originator/biosimilar and (B) bevacizumab originator/biosimilar over the course of 4 weeks of incubation at 37°C. n = 3, mean ± SEM. ....	141
Figure 4-17. Normalized contributions of shuffled bonds comparing originator/biosimilar rituximab at (A) 0, (B) 2 and (C) 4 weeks and bevacizumab at (D) 0, (E) 2 and (F) 4 weeks of incubation at 37°C; n = 3, mean ± SEM.....	143
Figure 4-18. Normalized trisulfide contributions for bevacizumab at (A) 0, (B) 2 and (C) 4 weeks of incubation at 37°C; n = 3, mean ± SEM.....	145
Figure 4-19. Fluorescence SEC-LC chromatograms overlays of OR/BS at 0,2 and 4 weeks of incubation for rituximab (A) OR and (B) BS and bevacizumab (C) OR and (D) BS incubated with bodipy maleimide.....	146
Figure 4-20. Free thiol total fluorescence AUCs for rituximab and bevacizumab OR/BS at 0, 2 and 4 weeks of incubation at 37°C; n = 1. ....	147
Figure 5-1. Currently marketed GLP-1 receptor agonist/long-acting insulin analog co-formulations.....	159
Figure 5-2 Hypothesis of TD mechanism of ADA formation by aggregates. (1) Early stage: activated APCs stimulate naïve T-cells through interactions of MHC-II and costimulatory molecules (presented on the surface of activated APCs) with TCRs and CD28 (presented on T-cells), respectively, turning them into activated T-cells. (2) Late-stage: activated T cells differentiate into cytokine secreting T helper cells type 2 (Th2). Both antigen binding to	

BCRs (IgM or IgD) and costimulation of B-cells with antigen-specific Th2 cells are required to activate naïve B-cells in the T-cell-rich zones of the secondary lymphoid tissues into B2-cells. Mature B2-cells develop oligoclonal monoreactive GCs in the B-cell follicles, in which B-cells undergo site-directed hypermutation in the Ig variable domain and clonal expansion. Finally, B-cells proliferate and differentiate into memory and antibody-secreting plasma cells. The response also involves antibody isotype class switching, in which the Ig class is switched (i.e., from IgM or IgD to IgG, IgE, or IgA) by alternatively splicing the Ig heavy chain in the constant region. Green rectangles denote stages at which studies have evaluated the potential immunogenicity of protein aggregates. BCR = B-cell receptors; GC = germinal centers; TCR = T-cell receptor; TD = thymus dependent. Adapted with permission..... 160

## List of Tables

Table 1-1. Top 10 selling mAb/mAb-related products, brands, indications and 2020 sales .....	3
Table 1-2. Examples of analytical biosimilarity assessment of infliximab CQAs, criticality and impacts. **Relatively assigned by each developer based on literature and experiments. <sup>10,32,33</sup> .....	4
Table 1-3. The 3-tiered approach for biosimilar statistical quality attribute evaluation. EM: equivalence margin; QR: quality range; SD: standard deviation. <sup>10,32-34</sup> .....	5
Table 1-4. Analytical methods to assess different types of degradation products. <sup>10</sup> .....	6
Table 1-5. Top-10 marketed peptide products (2019) by brand, manufacturer, sales revenue, molecule class, synthetic/biologic nature, presence of a generic/biosimilar, estimated patent expiration date and indication. ....	26
Table 1-6. GLP-1RAs, modification types, half-lives and dosing regimens. ....	32
Table 1-7. GLP-1RA products, manufacturers, revenues (2019*), Y/Y % change, synthetic/biologic nature and estimated patent expiration date. *: 2018 revenue. ....	33
Table 1-8. mAb products, US/EU biosimilar presence, manufacturer and mAb type. ....	39
Table 2-1. Particle size distribution determined by DLS (by volume) and separated into 0.3 – 10, 10 – 100, 100 – 500, 500 – 1000 and 1000+ $\mu\text{m}$ size ranges for exenatide that was reconstituted at pH 4.5 – 8.5 after incubation at 37°C for 4 weeks; (n = 3, mean). ....	70
Table 2-2 Particle size distribution determined by DLS (by volume) and separated into 0.3 – 10, 10 – 100, 100 – 500, 500 – 1000 and 1000+ $\mu\text{m}$ size ranges for exenatide that was reconstituted at pH 4.5 w/ mannitol and pH 7.5 w/ specified excipients when incubated at 37C after weeks; (n = 3, mean).....	76
Table 3-1. Lot numbers and expiration dates of studied Remicade/Remsima products.....	86
Table 3-2. Rates of monomer loss for RC/RS after incubation at various humidities/40°C. ....	98
Table 3-3 Impurity profiles of RC and RS before and after 4 weeks of incubation at 97% RH/40°C (n = 2, mean $\pm$ SD) NA: not applicable; NS: not significant. ....	101

## **Abstract**

Biotherapeutic products are lifesaving medicines for cancer, autoimmune and infectious diseases. In the last few years, the pharmaceutical industry has seen a massive spike in the development of biologics – over 2,700 biologics in development reported in 2018 alone. This trend fuels an ever-growing need for the development of new analytical methodologies to characterize the structure and function of biopharmaceutical products. The application of such new methodologies advances the understanding of their degradation mechanisms and provides useful knowledge in designing and meeting regulatory criteria.

An overview of biopharmaceutical peptides, mAbs and biosimilars available on the market, along with their currently published analytical characterizations and typical instability mechanisms, are summarized in the first chapter. In the second chapter, we investigated the long-term stability of exenatide, a 39 amino acid GLP-1 receptor agonist peptide used to treat type 2 diabetes, under different experimental conditions. When exenatide was incubated at an elevated pH, rapid chemical and physical degradation occurred. Chemical degradation was characterized by a pH-dependent increase of deamidation impurities while physical degradation was mainly attributed to dimerization, aggregation and loss of  $\alpha$ -helicity. The addition of excipients such as sucrose, mannitol and sorbitol showed a slight reduction of monomer loss at pH 7.5.

In the third chapter, a comparability study between originator and biosimilar infliximab (Remicade® and Remsima™) was performed. Forced degradation was



implemented to understand whether initial minor analytical differences could be amplified over the course of incubation. Some minor differences were found over incubation, including differences of heat capacity, intrinsic fluorescence, subvisible particulates, deamidation tendencies and fragmentation levels. Differences were not determined to be statistically significant and degradation mechanisms and kinetics were found to be highly similar.

In the fourth chapter, a tandem mass-spectrometry method was employed to detect, identify and quantify disulfide bonds and related impurities (shuffled disulfide and trisulfide bonds) in originator and biosimilar pairs of infliximab, rituximab and bevacizumab. Infliximab and bevacizumab biosimilars had higher levels of shuffled and trisulfide bonds relative to the originators, while rituximab biosimilar and originator had the similar levels of impurities. The bevacizumab and rituximab pairs were then incubated for 4 weeks at 37°C to examine the kinetics of physical degradation by size exclusion chromatography and electrophoresis gels and disulfide shuffling by tandem mass-spectrometry. The two mAb pairs responded differently to forced degradation. The rituximab biosimilar had a slightly higher initial level of aggregation over incubation, relative to the originator, though degradation products were low and not exacerbated over the 4-week incubation. In contrast, the bevacizumab biosimilar had higher initial levels of protein aggregates and shuffled disulfide bonds, relative to the originator product, but also had exacerbated extent of aggregation and disulfide shuffling over the incubation than rituximab. This study indicates that originator and biosimilar pairs respond differently to forced degradation and that tandem mass-spectrometry is a useful tool to track the formation of covalent aggregates.

Taken altogether, the thesis highlights the importance of the combination of classical analytical methodologies with new mass-spectrometry techniques to characterize instability mechanisms for peptide and mAb products subjected to forced-degradation conditions. The application of these techniques allows researchers, manufacturers and regulators to explore differences and similarities between reference biopharmaceutical products and their biosimilar (or generic) versions.

## Chapter 1: Introduction

### 1.1 Background and Significance of the Analytical Characterization of Biologics

Biologic product development has been a growing field with a breadth of therapeutic applications including, but not limited to autoimmune, cancer, hematologic, and infectious diseases.<sup>1-4</sup> The massive spike in the development of biologics (over 2700 reported in 2018) has been fueled by improvements in the understanding and emphasis of biologic drug efficacy and safety. These improvements have been made possible by recent advancements in protein analytics technologies as well as by the development of regulatory pathways.<sup>5-8</sup> Biologic products are large, complex molecules derived from living cells that include (but are not limited to) therapeutic recombinant proteins, vaccines and blood components.<sup>9</sup> As shown in Fig. 1-1, small molecules like acetaminophen (151.2 Da) can be thought of as bicycles relative to small biologics (e.g. erythropoietin, 30kDa) and large biologics (e.g. IgG, 150 kDa), respectively thought of as cars and airplanes.<sup>10</sup> Biologics are not only more complex in structure but are also more complex in their manufacturing processes. Biologic manufacturing relies on dynamic and environmentally sensitive living cell systems, which can pose problems such as high molecular heterogeneity within batches; and high potential for elicitation of immunogenic response in patients.<sup>11-13</sup> For these reasons, development of methods for the extensive analytical characterization of biologics has been deemed necessary. This is especially the case with respect to the development and regulatory approval of

biosimilars, generic biologics that have no clinically meaningful differences from a previously approved biologic.<sup>14</sup> Extensive analytical characterization is required to ensure similarity of characteristics that could potentially lead to alteration of a biologic's safety, purity and potency.<sup>15</sup>

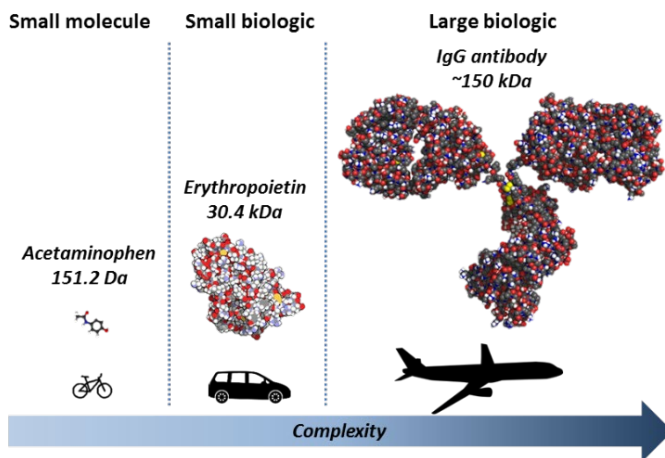


Figure 1-1. Molecular weight and complexity differences between small molecules, small biologics and biologics, which are respectively represented as bicycles, cars and airplanes.

The phenomenon of developing extensive analytical characterization techniques has grown significantly since the approval and entry of the first biosimilar into the European market by the European Medical Association's (EMA) in 2016.<sup>16</sup> The EMA and U.S. Food and Drug Administration (FDA) have since together approved over 75 biosimilars.<sup>17,18</sup> Many companies continue to design and submit new biosimilars for approval in hopes that a successful drug will gain entry into a market space worth over \$80 billion in revenue as of 2020 for the top 10 mAb and mAb-like products alone (Table 1-1). In order to reach regulatory approval, extensive characterization of biologics and biosimilars must first be conducted to ensure safety, efficacy and overall "similarity".

Molecule Name	Brand Name	Indication Area	Revenue (\$Bn)
Adalimumab	Humira	Immunology	19.8
Pembrolizumab	Keytruda	Oncology	14.4
Nivolumab	Opdivo	Oncology	7.9
Aflibercept	Eylea	AMD	7.9
Ustekinumab	Stelara	Immunology	7.2
Bevacizumab	Avastin	Oncology	5.0
Etanercept	Enbrel	Immunology	5.0
Rituximab	Rituxan	Oncology	4.2
Trastuzumab	Herceptin	Oncology	3.7
Infliximab	Remicade	Immunology	3.7

Table 1-1. Top 10 selling mAb/mAb-related products, brands, indications and 2020 sales

Fig. 1-2 visually represents the differences in development processes between innovator biologics, biosimilars and generic small molecules. Small molecule generics are passed through the abbreviated new drug application (ANDA) process, where approval only requires proof of matching bioequivalence and bioavailability data in healthy subjects.<sup>10,19,20</sup> On the other hand, biosimilar development focuses on extensive analytical characterization to ensure no differences in terms of clinical efficacy or safety when compared with its innovator counterpart.<sup>21-27</sup> Not only does this increase the time to market but also the number of steps and money required to develop biosimilars.

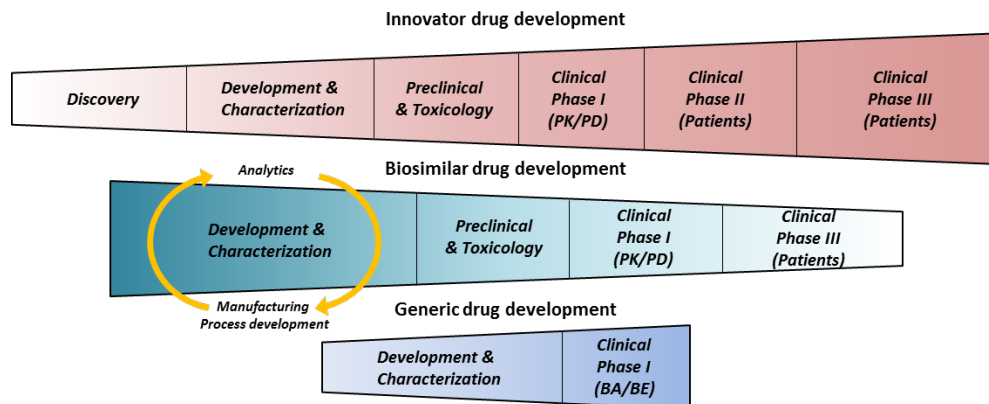


Figure 1-2. Differences in the drug development processes for biologics/small molecules.

## Analytical Characterization of Critical Quality Attributes

Critical quality attributes (CQAs) are defined as the physical, chemical, biological, or microbiological properties that must be studied to ensure a desired product quality.<sup>28</sup> Certain CQAs must be characterized in order to claim biosimilarity. Analysis of CQAs for biosimilar products starts by selecting individual attributes, including molecular structure, mechanism of action, safety and efficacy and then defining appropriate analytical characterization methods for their analysis.<sup>29,30</sup> Through various models, utilizing both quantitative and/or qualitative methods, each CQA is assessed for its relative criticality and the potential risk of impact on clinical outcomes (PK, PD, etc.).<sup>31</sup>

Examples of CQAs based on their criticality that are used for analytical biosimilarity assessment of an infliximab molecule are shown in Table 1-2 from high to low criticality.<sup>32,33</sup>

CQAs	Criticality**	Impacts
Primary structure	High	Efficacy, safety, immunogenicity
Protein content	High	Efficacy
FcRn binding	High	PK
Target binding to TNF- $\alpha$	High	Efficacy
Purity/impurity	High	Efficacy, Immunogenicity
Size variants/aggregation	High-moderate	Efficacy, immunogenicity
Excipient	Moderate	Efficacy, safety, immunogenicity
Charge variants	Moderate-low	Efficacy
Glycosylation	Moderate-low	Immunogenicity
Target binding to <u>tm</u> TNF- $\alpha$	Moderate-low	Efficacy
C1q binding & CDC activity	Low	Immune system mediator
Fc binding	Low	Immune system mediator

Table 1-2. Examples of analytical biosimilarity assessment of infliximab CQAs, criticality and impacts.  
 \*\*Relatively assigned by each developer based on literature and experiments.<sup>10,32,33</sup>

CQAs are categorized into three tiers (Table 1-3).<sup>32-34</sup> Tier 1 (high criticality) is assumed to impact biological activity, PK/PD, immunogenicity, and safety. Tier 2 (moderate criticality) can potentially impact biological activity, PK/PD, immunogenicity, and safety, requiring a “quality range approach”, where values must fall within a specified number of standard deviations from a mean (depending on the assessment). Tier 3 (low criticality) is assumed to have little to no impact on biological activity, PK/PD, immunogenicity and safety and are typically assigned and assessed both comparatively and qualitatively.<sup>30,35</sup> The FDA has not officially determined a preferred approach for analysis of CQAs or the determination of criticality. Their previously draft guidance document on “statistical approaches to evaluate analytical similarity” was withdrawn due to unforeseen complexities.<sup>31,36-38</sup> In contrast, the EMA does not require tier assignment for analytical assessments nor a specific subsequent statistical analysis method but is currently, in conjunction with the FDA, discussing ways to improve and define the analytical assessment of biosimilarity definitions.<sup>32</sup> Examples of CQAs of analytical relevance that require characterization include amino acid sequences, disulfide bonds, carbohydrate attachments, molecular weights, extinction coefficients, and electrophoretic, liquid chromatographic, and spectroscopic patterns.<sup>33,39</sup>

Tier	Tier assignment condition	Example 1: Infliximab	Recommended assessment method	EM/QR limit
1	Critical quality attributes most relevant to clinical outcomes	Target binding (e.g., TNF- $\alpha$ binding), protein concentration	Equivalency test with null hypothesis	1.5 <u>sd</u>
2	Less critical quality attributes moderately relevant to clinical outcomes	Peptide mapping, Glycosylation	Quality range approach: mean $\pm$ <u><math>x\bar{\sigma}</math></u>	3 <u>sd</u>
3	Least critical quality attributes least relevant to clinical outcomes	High-order structure	Raw data and graphical comparison	-

Table 1-3. The 3-tiered approach for biosimilar statistical quality attribute evaluation. EM: equivalence margin; QR: quality range; SD: standard deviation.<sup>10,32-34</sup>

## 1.2 Forced Degradation Studies as a Tool to Characterize Biopharmaceuticals

Forced degradation studies have been used to support the drug development process and to evaluate manufacturability through the application of various stress conditions that include (but are not limited to) thermal (elevated temperature, freeze/thaw thermocycling), light (UV, daylight), chemical (low/high pH, metal-catalyzed oxidation) and physical (agitation) stresses.<sup>40,41</sup> The objectives of these studies are to: (1) determine degradation pathways, (2) develop formulations, (3) develop analytical methods, (4) determine shelf-life, (5) mimic shipping and storage conditions (6) evaluate manufacturability, (7) assess CQAs and (8) determine intrinsic stability.<sup>42</sup> Forced degradation through the use of stress conditions has recently been implemented during biosimilar comparability studies. Examples of such can be found in the literature and in Biologic License Application submissions, where analytical methods are used to assess degradation and the formation of impurities, such as those shown in Table 1-4.<sup>10,43-47</sup>

Types of Degradation	Selected Analytical Methods
Soluble aggregates/fragments	SEC-HPLC, AF4, AUC, SDS-PAGE, Capillary electrophoresis
Subvisible aggregates (nm)	DLS, NTA, AF4, MALLS, Turbidity, Static light scattering
Subvisible aggregates ( $\mu\text{m}$ )	Light obscuration
Visible particles	Visual inspection
Secondary structure	Far-UV CD, IR, Raman spectroscopy
Tertiary structure	Near-UV CD, Intrinsic fluorescence, NMR, Second derivative UV spectrometry
Hydrophobicity	RP-LC, extrinsic fluorescent dyes, Hydrophobic chromatography
Chemical (e.g., oxidation)	LC-MS, Peptide mapping, RP-LC, IEX-LC, IEF

Table 1-4. Analytical methods to assess different types of degradation products.<sup>10</sup>



## Significance of Forced Degradation Conditions

The most common method of forced degradation is through the application of a thermal stress that exceeds typical and recommended storage conditions. These typically include storage at room temperature, 25°C, and temperatures above 35°C, and are commonly referred to as accelerated stability studies as specified in ICH guidelines.<sup>48</sup> MAb products stressed at elevated temperatures for a shortened period of time above the typical storage temperature (2-8°C) can facilitate the formation of degradant impurities. High humidity may also be introduced in addition to thermal stress for drug substances stored in a solid form, including lyophilized mAbs.<sup>49,50</sup> Freeze-thaw is another form of thermal stress often utilized for forced degradation studies for drug substances that may be exposed to multiple temperature transitions. An example biologic is insulin analog delivery devices that contain up to a month's supply of injections that are potentially exposed to multiple transition temperatures as products are stored in the refrigerator but may be brought to room temperature multiple times during consumer handling. Freeze thaw studies also come in handy to determine the appropriate use of protective and stabilizing excipients in lyophilized drug products.<sup>51</sup> The major degradation pathway for freeze-thaw is aggregation, though precipitation and particle formation have been observed. To prevent this degradation, certain excipients can be added into the final product.<sup>52,53</sup>

Biopharmaceuticals can also encounter physical (mechanical) stresses such as agitation, stirring or shaking during manufacturing, shipping and patient handling. Stirring, shaking, vortexing and sonication are all mechanical stresses commonly used to confirm a drug's robustness and stability against agitation.<sup>51,54-58</sup> Often, mechanical

stress can be found applied in combination with thermal stress, both sharing a major degradation pathway of aggregation. It should be noted that the underlying mechanisms of impurity formation may not only differ between one stress condition and the next, but also between two different molecules.<sup>59</sup>

Another stress condition category called chemical stresses may occur when drug substances such as mAbs are exposed to low or high pH conditions during purification. Low pH can lead to aggregation and fragmentation that can be further exacerbated by the high concentration typical of mAb products, resulting in precipitation.<sup>60</sup> High pH is known to drive asparagine deamidation and disulfide bond shuffling, also resulting in aggregation and fragmentation.<sup>61</sup> Another chemical stress that can occur during the manufacturing of biologics is oxidation caused by dissolved oxygen and/or metal and surfactant impurity-derived free radicals.<sup>59</sup> Hydrogen peroxide and tert-butyl hydrogen peroxide, in combination with or without zinc and copper metal ions, are the most widely used forced degradation reagents to test for oxidation.<sup>62</sup> Peracetic acid (PAA) has been studied as an alternative oxidizing agent that specifically oxidizes methionine but not tryptophan<sup>63</sup>. Probing oxidation susceptible residues by forced oxidation is important since oxidation of site-specific residues (mainly methionine) can result in decreased drug potency when located at the site of antigen binding, or oxidation-induced conformational changes in the Fc domain that can lead to aggregation.<sup>60</sup>

### **1.3 Chemical and Physical Stability of mAb Therapeutics**

#### **Chemical Stability**

Over the course of their lifetime, mAb biologics are subject to both enzymatic and non-enzymatic modifications that contribute to the alteration of their chemical and

physical stability and the formation of related impurities. These modifications are further separated into two categories. The first category is that of product variants, modifications that occur during the cell culture, extraction, and purification of the manufacturing process while the second category is that of product-related impurities, modifications that occur from storage onwards.<sup>64,65</sup> Both categories of modifications can affect the final products' stability, safety, and immunogenicity, and thus necessitate investigation. By applying the previously mentioned extensive analytical characterization techniques, abundant modifications including (but not limited to) amino acid modifications, charge variants and glycosylations can be identified and correlated with their potential to impede the approval of a final product.<sup>66-69</sup>

The most commonly seen chemical impurities are those that form as a result of the modification of amino acids, including oxidation, deamidation and disulfide shuffling. Many of these impurities can also be classified as charge variants as modification of amino acids lead to changes of a molecules' surface properties such as charge and hydrophobicity.<sup>70,71</sup> Oxidation is a major chemical impurity induced by a reactive oxygen species (ROS) where an oxygen is inserted at an amino acid residue site. This mainly occurs at methionine residues though it has been observed at other amino acid residues including tryptophan, cysteine, histidine and lysine.<sup>72-77</sup> When oxidation occurs at methionine, it results in the formation of methionine sulfoxide (MetO) and, to a significantly lesser extent, the formation of an irreversible double oxidation impurity methionine sulfone (MetOO)(Fig. 1-3).<sup>78</sup> Oxidation results in the disruption of the hydrophobic bond found in the aromatic side chains of some of the listed amino acid residues. Disruption of this bond is likely to alter the molecule's 3-D structure, exposing

typically buried residues and increasing the number and type of surface exposed hydrophobic amino acid residues.<sup>79-82</sup>

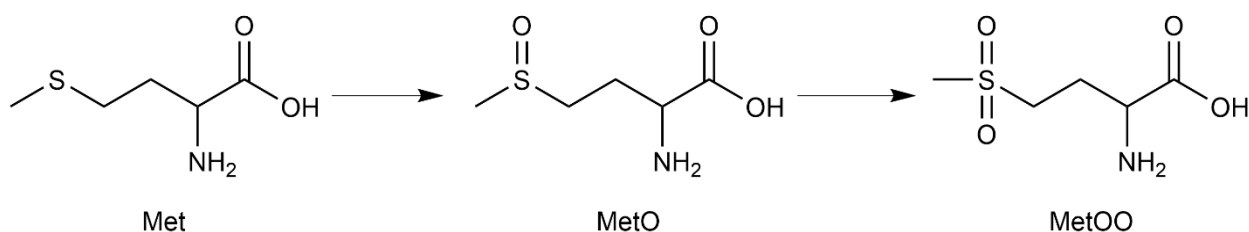


Figure 1-3. Methionine oxidation pathway that leads to the formation of methionine sulfoxide (MetO), a single oxygen addition, and methionine sulfone, a double oxygen addition.

Deamidation is another major process leading to chemical impurity, described as the loss of an amide group that occurs mainly at asparagine (Asn) amino acid residues (as shown in Fig. 1-4) and at glutamine (Gln) amino acid residues. Asn deamidation in peptides and proteins has been shown to be highly pH and buffer dependent. In general, Asn deamidation is base-catalyzed, occurring between pH 5 and pH 8. Some common buffers including phosphate, tris and carbonate buffers, exhibit increased deamidation propensity at pH greater than 7.<sup>83,84</sup> Asn deamidation is known to form 3 major impurities. The first is a succinimide intermediate that forms as a result of the loss of the amide group. The succinimide intermediate, which then racemizes into aspartic acid (Asp) and isoaspartic acid (Iso-Asp) impurities that are present in either the D or L conformation of Iso-Asp.<sup>85</sup> Even at pH < 5, Asn deamidation can still occur through via a slightly different acid-driven mechanism. This phenomenon, where the succinimide and Asp impurities form at lower pH values and occur increasingly when followed by Serine (Ser) and Histidine (His) residues.<sup>83-92</sup>

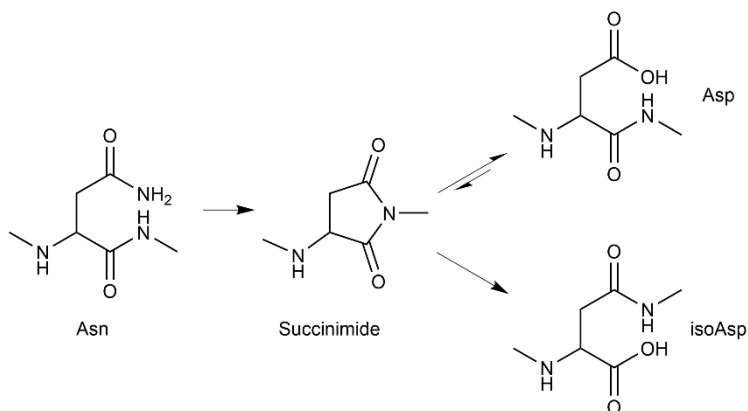


Figure 1-4. Typical Asn deamidation pathway, proceeding through a succinimide intermediate, which undergoes isomerization, resulting in the formation of aspartic acid (Asp) and isoaspartic acid (isoAsp).

Gln deamidation has been shown to be barely detectable in biological products as a result of its approximately 100-fold slower rate of occurrence; nevertheless, it can still occur.<sup>86,87,93–97</sup> N-terminal terminal pyroglutamic acid (PyroQ) formation (Fig. 1-5), also titled pyroE, pGlu and pyrELA, is a common chemical impurity that occurs as a result of removal of an amide group at N-terminal glutamine and glutamic acid amino acid residues. PyroQ formation has been observed in a variety of proteins, including mAbs and peptides both in solution and in the dry state.<sup>98–101</sup> PyroQ formation generates acidic variants also through the loss of the positively charged primary amine.<sup>102,103</sup> Although we have mainly touched on pH dependence, deamidation relies on many other factors, including the primary structure of nearby amino acid residues, tertiary molecular structure, storage temperature, and formulation components (i.e. buffer strength and ionic strength).<sup>85,104,105</sup>

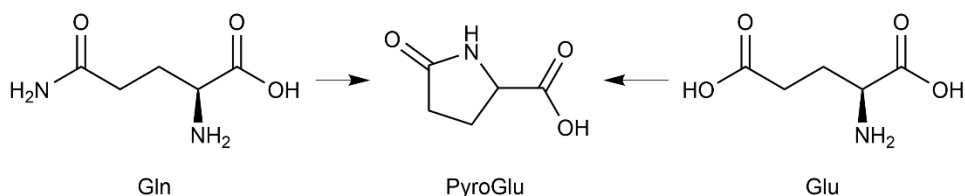


Figure 1-5. Typical PyroQ formation pathways that occurs at glutamine and glutamic acid residues.

Disulfide bond related impurities also fall into the chemical impurity category since they yield an amino acid modification. Disulfide bonding plays a critical role in the structure and function of proteins as its presence is necessary for the correct folding of proteins during translation and is responsible for stabilization.<sup>106,107</sup> In IgGs, at least 12 disulfide bonds are conserved. Disulfide bonds linking the light chain with heavy chains, called “inter-chain” disulfide bonds, are necessary to conserve quaternary structure, while bonds found within each sub-domain component, called “intra-chain” disulfide bonds, are necessary for stability.<sup>108</sup> The heterogeneity of recombinant mAb disulfide bonding has been previously reported.<sup>102,109,110</sup> Disulfide bond related impurities, including incorrect disulfide bonding, also known as disulfide shuffling, occurs when biologics are exposed to environmental stresses during downstream processing steps.<sup>111,112</sup> Disulfide bonding is the exchange of a covalent bond location between the sulfur group of two cysteines and commonly occurs when the sulfur group of a free thiol attacks an existing disulfide bond, hence shuffling its location. Disulfide shuffling can occur either intra-molecularly, within a molecule, or inter-molecularly, between two molecules (Fig. 1-6). Free thiols and/or high pH conditions are implicated to be the main culprits of disulfide shuffling induction.<sup>113–116</sup> Trisulfide bonding, whereby a third sulfur is inserted into an existing disulfide bond, is another chemical impurity that arises from the use of H<sub>2</sub>S during cell culture.<sup>117</sup> It is a rare modification that is not currently implicated to alter mAb function but may be of use as an indicator of variations of manufacturing process controls.<sup>118,119</sup>

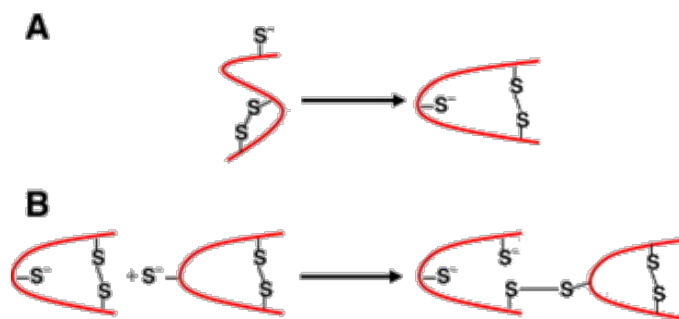


Figure 1-6. Intra- and inter-molecular disulfide shuffling that occurs (A) between a free thiol and an existing disulfide bond within a molecule or (B) between two molecules. Here, free thiols are shown as thiolate anions, which commonly occur at elevated pH. Figure adapted with permission from [113].

In summary, oxidation has been shown to induce the formation of aggregate impurities and the loss of function of various proteins.<sup>59,120–125</sup> For IgG1 and IgG2, several studies have reported that methionine (Met) oxidation in the Fc domain is related to weakened neonatal Fc receptor (FcRn) binding, which is a function related to IgG recycling and transcytosis.<sup>126</sup> Due to the proximity of Met residues to the FcRn binding interface, oxidation can disrupt antibody conformation and the oligomerization of IgG, leading to decreased C1q binding and CDC activity.<sup>127–130</sup> Deamidation is a main cause of chemical degradation and may introduce a local charge-related structure distortion.<sup>94,131</sup> It has been reported that deamidation at the Asn30 location in the light chains of Herceptin® (the trastuzumab originator) showed a reduction of potency by 70%, while deamidation at the Asn55 residue showed a 14-fold decrease in antigen binding affinity.<sup>94,97</sup> Furthermore, Iso-Asp is a non-natural amino acid residue and deamidation induced impurity which means it is potentially immunogenic.<sup>132</sup> It has been shown that the formation of pGlu impurities do not have significant clinical impact, but need to be monitored and identified as indicators of the introduction of heterogeneous species that may reflect a lack of manufacturing process control.<sup>133–136</sup> One example of how modifications of disulfide bonds and the formation of related impurities impact

molecular function has been evaluated in originator and biosimilar etanercept, an IgG-like TNF- $\alpha$  inhibitor. Etanercept has a complex disulfide bonding pattern containing 29 disulfide bridges throughout its structure. Various shuffled disulfide bond variants were investigated, whereby an increase of the percentage of samples with incorrect disulfide bonding at the 78-88 location were shown to be correlated with a potency loss (Fig. 1-7).<sup>137-139</sup>

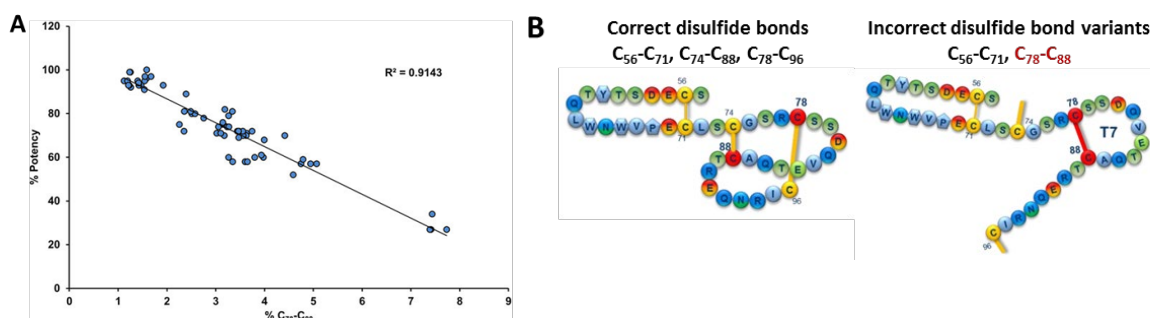


Figure 1-7. (A) Correlation of % potency (TNF- $\alpha$  neutralization) with % incorrect disulfide bonding at C78-C88 for etanercept. (B) Etanercept structures with correct/incorrect disulfide bonding.<sup>137</sup>

Analytical characterization methods of chemical impurities are commonly liquid chromatography (LC) based and vary based on the desired impurities of interest. The most widely used analytical method for characterization of large proteins is digestion and analysis by LC-MS or MS/MS.<sup>94,140-143</sup> These techniques have been implemented in comparability studies between innovator and biosimilar mAb pairs. Many additional methods have been used orthogonally as method-to-method variability has been observed for different techniques.<sup>144,145</sup>

Other desired attributes of interest that result from chemical impurity formation include the formation of charge variants. These are commonly characterized by ion exchange chromatography (IEX), which separates proteins according to their overall net surface charge and can even differentiate isoforms that have single charge differences.<sup>43,44,46,47,146-149</sup> To further identify the nature of each peak separated by IEX,



subsequent orthogonal MS analysis is necessary. Proteins with high isoelectric points (pI), such as mAbs, are generally separated by cation exchange chromatography (CEX).<sup>147,150–152</sup> Further details on mAb impurities differentiated by IEX can be found in the literature. CE-based methods in combination with MS can provide more rapid analyses leading to the use of small amounts of samples and reagents.<sup>153</sup>

To characterize disulfide bonding for mAbs, analysis by RP-LC-MS/MS is currently regarded as the standard method. In this set of techniques, peptide fragments are generated using enzymatic digestion (such as trypsin) then separated by RP-LC and analyzed by MS/MS.<sup>154–156</sup> This technique requires very low sample volume and outputs very large amounts of data, which requires the use of an analysis software that allows for the identification of disulfide bonds and their related impurities. As free thiols are implicated as the main factor for disulfide shuffling, the levels of surface exposed free thiols can be measured using Ellman's reagent, assuming large amounts of free thiols present.<sup>44,157</sup> Other techniques to analyze free thiols include the use of maleimide, which conjugates to free thiols and allows for analysis by RP-LC, as conjugated maleimide will form a more hydrophilic mAb species. Studies have been performed to optimize the combination of column conditions and maleimide reagents in order to improve species peak resolutions.<sup>158</sup>

## Physical Stability

The physical stability of mAbs, and therefore prevalent physical degradation pathways, are highly related to the formation of chemical impurities. As previously mentioned, chemical modifications can result in altered surface properties, including changes of charge and hydrophobicity. It is well understood that changes in surface properties are related to the formation of physical impurities, which include structural modifications and the formation of aggregate and fragment impurities. MAb aggregates fall under the category called higher order structures (HOS), which covers impurities ranging from dimers to high molecular weight species.<sup>159</sup> These differences in types of fragment and aggregate impurities can reflect the use of various forced degradation stress conditions as one condition may induce physical impurities differently than the next.<sup>59</sup> Fig. 1-8 shows microscopy images of IgGs that were subjected to various stress conditions, where different types of aggregation were shown to occur under various stress conditions.<sup>160</sup> These differences can also potentially reflect underlying changes of secondary, tertiary and quaternary structures that can be analytically characterized through the application of orthogonal methods.<sup>161</sup>

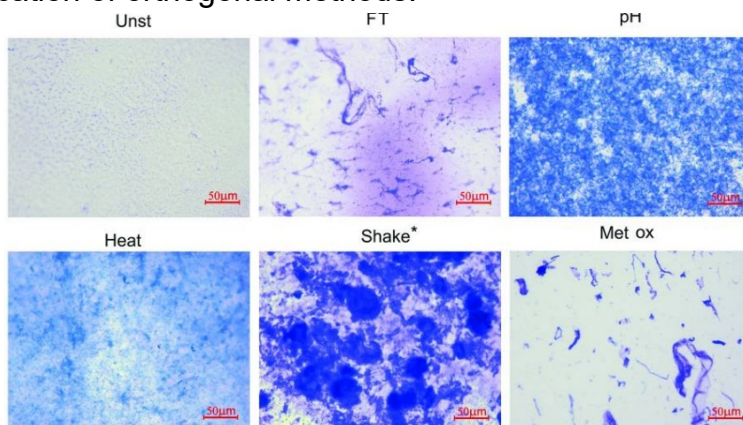


Figure 1-8. Atomic Force Microscopy (AFM) images of IgG when subject to freeze-thaw, pH, heat, shake and oxidation stress, resulting in various aggregate types. Figure adapted with permission from [160].

Another major challenge in producing biologics is their natural propensity to form complex aggregates.<sup>162</sup> These aggregates vary in size (nm- $\mu$ m), structure (native/non-native), morphology (spherical/strand-like) aggregate type (fibrillar/amorphous) and reversibility.<sup>163</sup> Not only does the presence of protein aggregates compromise therapeutic efficacy and bioavailability, it may also elicit immune responses to the protein drug that are measured by the formation of anti-drug antibodies (ADAs).<sup>164–168</sup> The elicited immune response can result from any combination of changes in solubility, viscosity and exposure of neo-epitopes that cause a protein to be recognized as foreign by the immune system.<sup>165,169,170</sup> In the case of the infliximab biosimilar, there have been reports that aggregates might affect TNF- $\alpha$  binding, which is a critical mechanism of action. Aggregates have also been linked to infliximab immunogenicity.<sup>43</sup> However, there is no single method that can assess a wide size range of aggregates. Therefore, biosimilar developers should analyze aggregates by employing several orthogonal methods (Fig. 1-9) for cross-validation to ensure the presence of comparable or lower levels of aggregates with the reference throughout the product's life cycle.

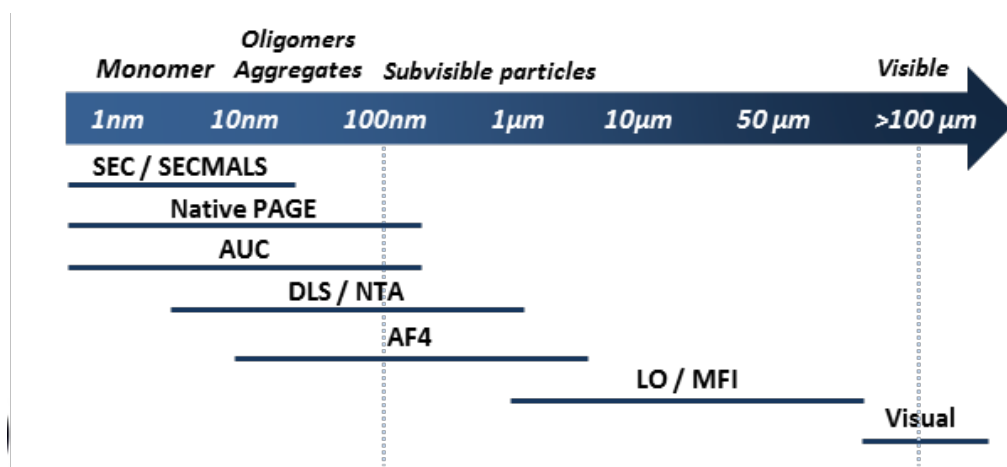


Figure 1-9. Size-dependent analysis methods of various aggregates and particle sizes from monomer to visible aggregates.<sup>10</sup>

Among the diverse methods of aggregate determination, size exclusion chromatography (SEC) is most commonly used for aggregate quantification and size estimation. SEC is based on the interaction of molecules with a column's bead pores, which separates molecules from large to small depending on their size in solution.<sup>163</sup> In addition, SEC can be combined with UV, fluorescence, multi-angle laser light scattering (MALS) and other detectors, though SEC-MALS is highly valuable, providing increased accuracy by acquiring absolute molar mass for each eluted fraction.<sup>171</sup> However, it has been reported that SEC can incorrectly detect aggregates due to either unwanted secondary interactions with the stationary phase (adsorption), removal of large insoluble aggregates during sample preparation, or dissociation of reversible aggregates as a result of dilution.<sup>172-174</sup> Further details of SEC and mAb aggregates can be found in the literature. Another alternative technique is asymmetric flow field-flow fraction (AF4), which determines particle size as a function of diffusion coefficient through the use of laminar and a perpendicular cross-flows across two different plates.<sup>175</sup> AF4 can be combined with various detection methods such as UV, MALS and refractive-index.<sup>176</sup> However, method validation has been shown to be difficult.<sup>173</sup> Analytical ultracentrifugation (AUC) is another commonly used method for size detection and can be utilized by sedimentation velocity (SV), a hydrodynamic approach, and sedimentation equilibrium (SE), a thermodynamic approach. In general, AUC separates particles of various shapes and sizes by centrifugal force and by detection with attached optical systems (absorbance/interference/fluorescence). The biggest advantage of AUC is the ability to directly measure aggregates in various native solutions over a wide

range of sample concentrations.<sup>177</sup> While useful for absolute size measurements, AUC is low-throughput requiring high quality instrumentation and complicated analysis.<sup>163,178</sup>

In terms of particle analysis, dynamic light scattering (DLS) and nanoparticle tracking analysis (NTA) are often used. Both techniques generate data as a function of particle diffusion coefficients based on Brownian motion and light scattering. DLS is a useful tool for quickly assessing size, providing a wider range of particle size and sample concentrations than NTA. DLS requires low sample volume ( $\mu\text{L}$ ) where samples can be recollected for further analyses. DLS's major limitation is that the reported intensity distribution of particle sizes is sensitive to the presence of large particle contaminants, which may dominate scattering signals and result in misrepresented particle size distributions.<sup>163,179,180</sup> NTA tracks and visualizes movement of particles using a microscope coupled to a camera system and provides size distribution as a function of number distribution. Compared to DLS, NTA generates information on particle concentration in solution with a better resolution on samples with polydisperse size distribution. However, the reproducibility of NTA is low, often requires sample dilution for analysis, and is not useful for molecules that are too small, which constitutes several limiting factors when compared to DLS.<sup>179,181,182</sup>

For the determination of secondary structure, Fourier transform infrared spectroscopy (FTIR), far-UV circular dichroism (CD), x-ray crystallography and nuclear magnetic resonance (NMR) are typically used, with FTIR and CD being most commonly employed.<sup>136,183–189</sup> FTIR spectroscopy can be used regardless of the physical sample state with no limitation on protein size. It requires a relatively small amount of sample (10-100  $\mu\text{g}$ ) and provides a high signal to noise ratio, allowing for rapid data collection

(10 ms).<sup>190,191</sup> CD provides data in a relatively short time period with small amounts of sample (<20 µg), but requires aqueous samples. UV CD spectra are derived from the peptide bond region (<240 nm), therefore allowing conformational information to be obtained while secondary structure is estimated using various algorithms.<sup>73,74</sup> These techniques are prevalent in literature for proteins that undergo changes of secondary structure such as the detection of β-fibrillation, a common physical impurity also formed in insulin and insulin analogs. Fig. 1-10 shows an example CD spectra for IgGs that were subjected to various stress conditions.<sup>160</sup> NMR can be used to generate useful protein secondary structural data but requires high sample concentration and is time consuming. 1-D NMR is typically used more for smaller biopharmaceuticals and can be used as a fingerprint comparison to show the structural similarity between innovator and biosimilar products.<sup>139,193,194</sup>

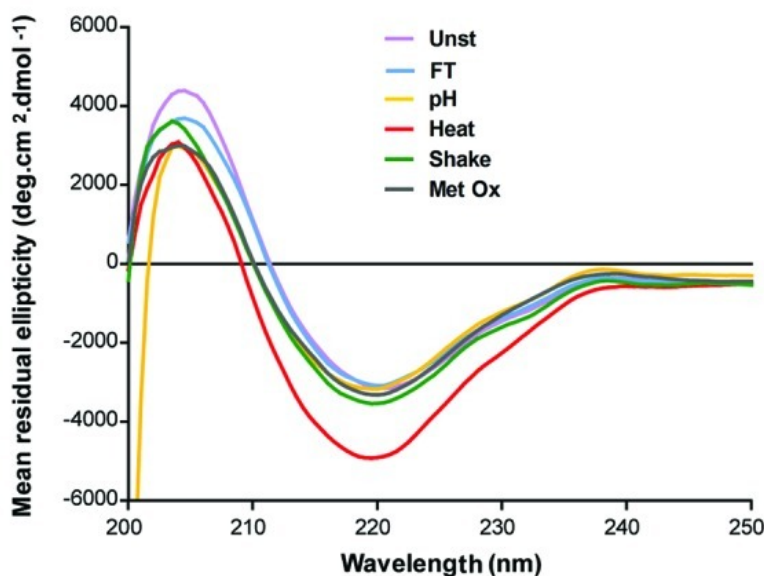


Figure 1-10. Far-UV CD spectra for GLP-1 subject to freeze-thaw, pH, heat, shake and oxidation stress. Figure adapted with permission from [160].

Applications of the following analytical techniques are shown in Fig. 1-11. Tertiary structure can be determined through near-UV CD, differential scanning calorimetry (DSC), 2D-NMR and mass spectrometry techniques such as hydrogen deuterium exchange (HDX-MS) and ion mobility (IM-MS). Near-UV CD (250-320 nm) can detect differences in the tertiary structural environment of disulfide bonds and highly environmentally sensitive aromatic residues.<sup>195-197</sup> DSC is widely used to evaluate thermal and conformational stability during processing and manufacturing.<sup>198-200</sup> Highly similar thermograms and  $T_m$ s denote the similarity of tertiary structures as a result of thermal stability. Recently, 2D NMR has been utilized to provide sensitive, robust and precise structural assessment of biologics, but requires highly concentrated samples and long acquisition times.<sup>201</sup> HDX-MS can monitor conformational protein dynamics, relying on the deuteration of labile hydrogen in amide bonds along the polypeptide backbone. These subtle HOS differences are detected by LC-MS analysis and quantified based on degrees and rates of deuterium exchange.<sup>54,55,64,97</sup> The advantages of HDX-MS are its analytical capacities to measure exchange in complex buffer systems and large proteins, as well as its minimal sample requirement (5-100 pmol).<sup>203</sup> IM-MS is a rapid (msec) and sensitive (nmol) emerging technique for generating HOS biologic fingerprints.<sup>204-207</sup> In addition to IM-MS, collision induced unfolding (CIU) has been applied for structural analysis, yielding distinct protein unfolding patterns as a function of collisional heat, while resolving small variations in protein structures.<sup>204,208-210</sup> Recently, CIUs were applied in an infliximab comparability study that showed comparable quantitative unfolding patterns.<sup>136,202,211,212</sup>

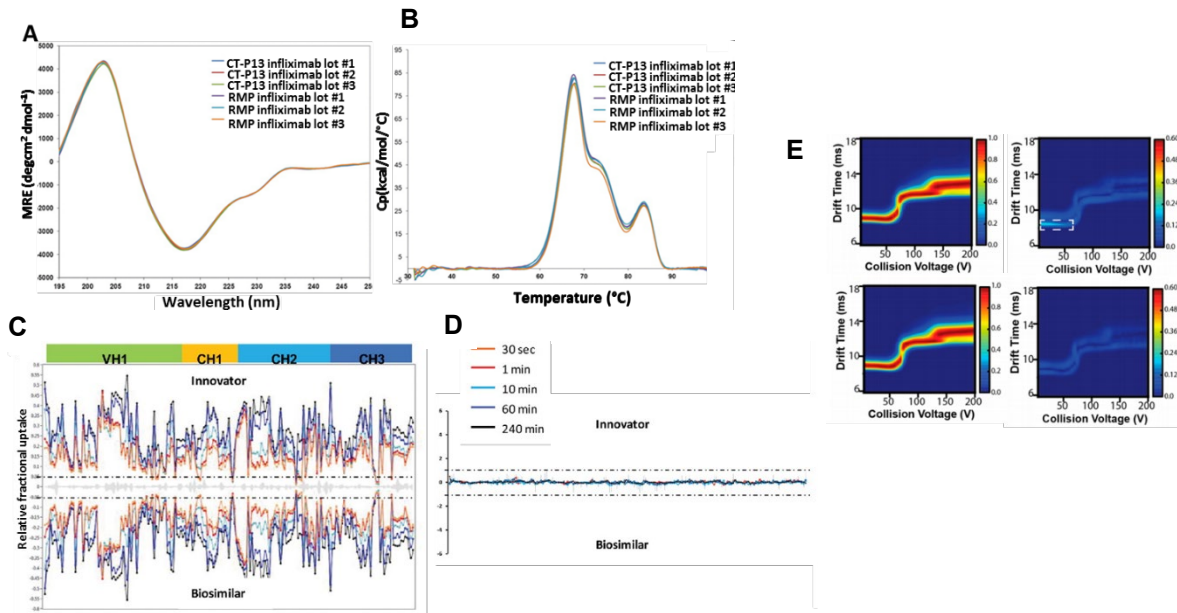


Figure 1-11. Methods that compare higher order structure of innovator/biosimilar infliximab. (A) far-UV CD. MRE: Molar Residue Ellipticity; RMP: Reference Medicinal Product.<sup>136</sup> (B) DSC thermal overlay plot.<sup>136</sup> (D) HDX-MS butterfly plots.<sup>202</sup> (E) deuterium uptake difference plots.<sup>202</sup> (F) IM-MS collision induced unfolding (CIU) fingerprints, showing averages (left) and Standard Deviations (right) of innovator (top) and biosimilar (bottom).<sup>211</sup> Figures adapted with permission.

## Impurities and Immunogenicity

Immunogenicity is the elicitation of an immune response by a patient to a therapeutic protein product. Immunogenic responses can range from no apparent clinical manifestations to life-threatening ones.<sup>213</sup> Immunogenic response to the biologic erythropoietin is an example of a life-threatening immunogenic response whereby neutralizing anti-erythropoietin antibodies induce pure red-cell aplasia, resulting in fatal anemia.<sup>214</sup> Currently, immunogenic responses are characterized by the formation of binding to neutralizing anti-drug antibodies (ADAs). (Fig. 1-12).<sup>213,215</sup>

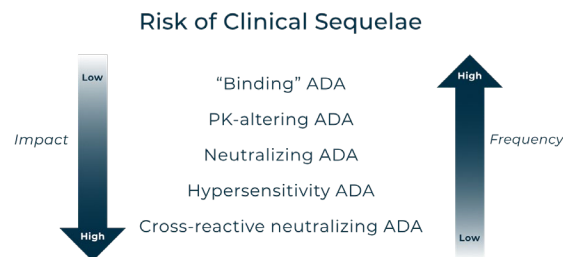


Figure 1-12. Types of ADAs from “binding” to neutralizing to cross-reactive neutralizing, where frequency is inversely related to clinical impact. Figure adapted with permission from [215].



While long-term, adaptive immune response is the current focus for determining immunogenicity, the innate immune response has recently generated interest as well. People are studying the innate immune response to determine initial immune response mechanisms that may then lead to downstream elicitation of an adaptive immune response.<sup>170</sup> Fig. 1-13 shows the exposure of protein aggregates to an antigen presenting cell (APC), which can trigger immune responses through various kinds of pathways, including interactions with Fc $\gamma$ , Toll-like and T-cell receptors. Following this interaction, the protein can then undergo receptor mediated phagocytosis, lysosomal digestion and presenting cell maturation.<sup>170,216</sup>

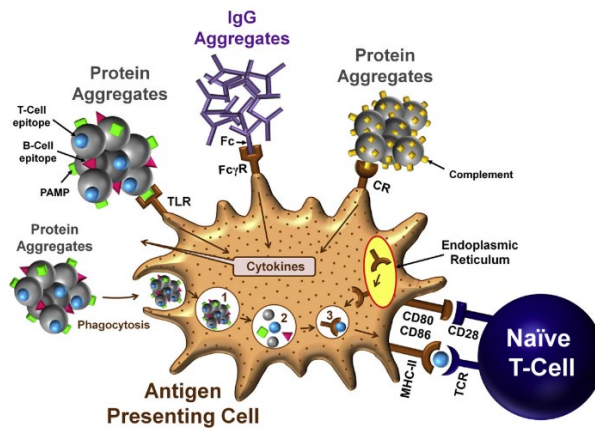


Figure 1-13. In vitro interactions of protein aggregates with antigen presenting cells (APCs) that can potentially trigger an immune response through different kinds of receptors - Fc $\gamma$ R, TLRs and/or CRs. In addition, following receptor-mediated phagocytosis of aggregates, lysosome digested peptides are presented on the cell surface, resulting in naïve T-cell stimulation. Figure adapted with permission from [170].

APCs being studied for maturation in the literature mainly include dendritic cells and monocytes, though THP-1 is being used as a robust *in vitro* alternative that does not require derivatization from a human source.<sup>217</sup> Following APC maturation, antigen peptide sequences can be investigated by the MHC associated peptide proteomics (MAPPs) assay, which allows for further elucidation of underlying immune response elicitation.<sup>218</sup> Another common technique used to investigate immunogenicity is through

a whole blood assay, whereby a multiplex cytokine assay is used to determine cytokine responses in whole blood that has been taken from human patients.<sup>219</sup>

As previously mentioned, various impurities have been suggested to be related to the elicitation of immunogenic response; though correlation between individual components and responses are highly complex and molecule dependent.<sup>220</sup> Several papers have been published investigating this relationship using forced degradation and the application of various stress conditions. It has been shown that different stress conditions applied to an IgG1 resulted in different cytokine responses, though it should be noted that these trends may not translate from one mAb to the next (Fig. 1-14).<sup>221</sup>

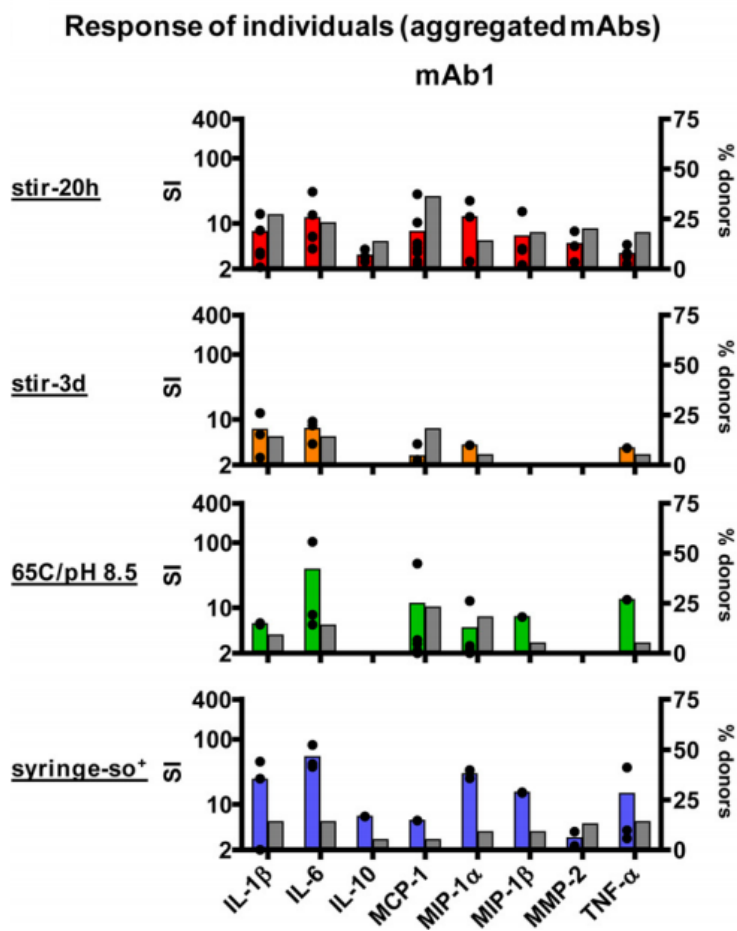


Figure 1-14. Cytokine response profiles for IgG1 subjected to thermal, pH, stir and syringe stress. Figure adapted with permission from [221].

## 1.4 Chemical and Physical Stability of Peptide Therapeutics

Peptides are located in a unique space between small molecules and small biologics and can be thought of as mopeds relative to small molecules and large biologics (Fig. 1-15). Peptides can be manufactured synthetically, produced by recombinant technology, or purified from a biological source.<sup>222</sup> Peptides generally serve as replacement therapies in cases of the dysregulation of the production or secretion of endogenous peptides and hormones. They have access to unique targets inaccessible by mAbs and small molecule products.<sup>223</sup> The top 10 non-insulin peptide drug products are shown in Table 1-5. As peptides are composed of an underlying amino acid sequence, characterization of their chemical and physical stability is highly translatable from mAb characterization.

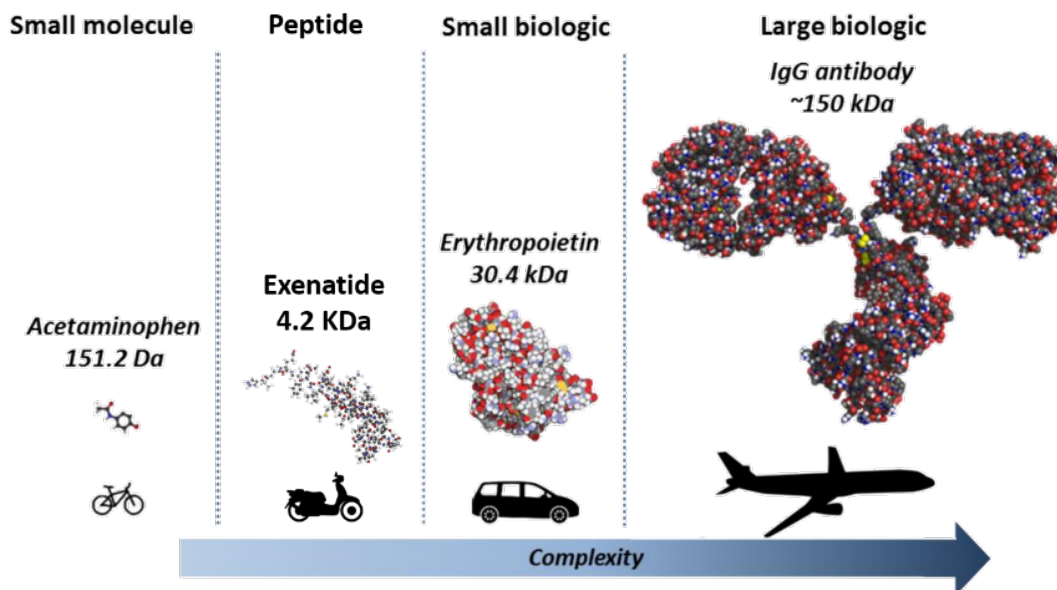


Figure 1-15 Molecular weight and complexity differences between small molecules, peptides, small biologics and biologics, respectively represented as bicycles, mopeds, cars and airplanes.

Molecule	Brand	Manufacturer	Global Revenue (\$Mn)	Class	Synthetic/Biologic	Generic/Biosimilar? (US/EU)	Patent Expiration (US/EU)	Indication
Liraglutide	Victoza	Novo Nordisk	3,319	GLP-1 Analog	Biologic	No	2022	Diabetes
Dulaglutide	Trulicity	Lilly	4,128	GLP-1 Analog	Biologic	No	2024 (2026)	Diabetes
Octreotide	<a href="#">Sandostatin</a>	Novartis	1,585	Somatostatin Analog	Synthetic	Yes	N/A	Growth hormone producing tumors
Teriparatide	<a href="#">Forteo</a>	Lilly	1,405	<a href="#">rPTH</a>	Biologic	No/Yes	2019/ N/A	Osteoporosis
Glatiramer	Copaxone	Teva	1,017	Myelin basic protein random polymer	Synthetic	Yes	N/A	MS
Carfilzomib	<a href="#">Kyprolis</a>	Amgen	1,044	Epoxomicin Analog	Synthetic	No	2025	20S Proteasome inhibitor
Linaclotide	<a href="#">Linzess</a>	Allergan	827	<a href="#">Guanylin/uroguanylin</a> mimetic	Synthetic	No	2024 (2031)	IBS
<a href="#">Goserelin</a>	<a href="#">Zoladex</a>	AstraZeneca/ <a href="#">TerSera</a>	813	GnRH Agonist	Synthetic	No/Yes	2022/ N/A	Hormone sensitive breast/prostate cancer
<a href="#">Lanreotide</a>	<a href="#">Somatuline</a>	Ipsen	322	Somatostatin Analog	Synthetic	No	2024	Acromegaly, neuroendocrine tumors
Leuprolide	Lupron	AbbVie	219	Multiple	Synthetic	No	2022 (2031)	Prostate cancer, endometriosis, puberty blocker
<a href="#">Corticotropin</a>	<a href="#">Acthrel</a>	Ferring		ACTH	Synthetic			Cushing's

Table 1-5. Top-10 marketed peptide products (2019) by brand, manufacturer, sales revenue, molecule class, synthetic/biologic nature, presence of a generic/biosimilar, estimated patent expiration date and indication.

Like mAb products, oxidation and deamidation are also the most prevalent peptide chemical impurities.<sup>224,225</sup> While the impact that chemical impurities have on mAb function depends on the location of the modification, the shortened sequence of peptides would imply that any chemical modification could significantly impact its function. In addition to the globular structure of proteins like IgG limits solvent accessibility because of imparted structural rigidity. Peptides, on the other hand, commonly lack quaternary structure and therefore steric hindrances, typically allowing for greater molecular flexibility. This flexibility makes them more susceptible to instability, as is the case for deamidation and oxidation chemical impurity formation in peptides.<sup>92,113,226–229</sup> While this molecular flexibility can contribute to the presence of certain chemical degradation hotspots (i.e. NG amino acid combinations), such flexibility is also a consideration that must be accounted for when it comes to the conservation of receptor binding.<sup>222</sup> As such, it is necessary to investigate a peptide's chemical stability, including the formation of chemical impurities such as deamidation and oxidation, and its relationship with a peptide's physical stability and function. Peptides, in comparison to large proteins that have highly defined quaternary structures, are generally understood to be more complex in nature and are known to have a distribution of conformational native states, sometimes in equilibrium between monomer, dimer and hexamer as is the case for native insulin.<sup>230</sup> These native states are typically influenced by the secondary structure of each peptide that arises from the primary amino acid sequences. Shifts in secondary structure can arise from either one or a combination of  $\alpha$ -helical,  $\beta$ -sheet and unordered secondary structural portions. Chemical impurities can then propagate the shifting of secondary structures through the formation of

complex physical impurities, including amorphous aggregation and  $\beta$ -sheet fibrillation.<sup>231,232</sup>  $\beta$ -sheet fibrillation has been well studied in insulin and insulin analogs and is a well-known physical impurity formed in peptides.<sup>233</sup>

Deamidation has been determined as critical for insulin and insulin analogs.<sup>234</sup> Deamidation in peptides occurs as a result of many factors including pH, temperature, buffer species, ionic strength, structure and neighboring amino acid residues.<sup>87,235,236</sup> Asn followed by a glycine is a well-known deamidation hotspot in peptides and has been determined to undergo the most rapid rate of deamidation when compared to other peptide sequences.<sup>237</sup> Deamidation of insulin has been shown to affect the tertiary structure via exposure of its hydrophobic core.<sup>238</sup> Deamidation has also been shown to induce aggregation in the peptides such as amylin and  $\beta$ -B<sub>1</sub>-crystallin and has been established to correlate with bovine growth hormone aggregation.<sup>239-241</sup> Oxidation in peptides has been shown to have mixed effects on aggregation, especially in terms of the type of aggregation that occurs (fibrillar or amorphous).<sup>242-244</sup> PyroQ formation has been shown to occur at N-terminal glutamine and glutamic acid amino acid residues in peptides in both solution and solid states though its impact is complex and molecule-dependent.<sup>99-101</sup> Several peptides that are prone to PyroQ formation have been designed and modified to initially have pyroGlu substituted at these N-terminal locations. This design method is meant to prevent degradation and the potential loss of binding activity and efficacy.<sup>101</sup> The complex nature of peptide aggregation has been shown for GLP-1, exhibiting the ability to form amorphous aggregates and  $\beta$ -sheet fibrils. These different aggregation types were formed as a result of many factors including pH, buffer, buffer strength and peptide concentration.<sup>245</sup>

While there are many analytical techniques that overlap between proteins and peptides for the determination of chemical and physical stability, the small nature of peptides does allow for the use of certain techniques that are not specified for larger proteins. Whereas large proteins like mAbs require digestion into small pieces for the analysis of chemical impurities, small peptides subject to analysis can be analyzed through direct application onto MS. LC interfaced with a time of flight (ToF) mass spectrometer allows for the identification of small mass changes that can be translated into amino acid modifications. Another commonly used technique for the detection and identification of physical impurities-aggregation or fragmentation is SEC. Aggregates can be further visualized with the use of microscopy techniques like TEM and by turbidity studies.<sup>233</sup> In terms of the formation of physical impurities, secondary structure shifting is analyzed by CD. Since peptides are well known for their tertiary structures, the use of peptide absorbance techniques and tagging with fluorescent dyes have been implemented to detect various changes of structure. These techniques commonly include intrinsic fluorescence, whereby tertiary structure is detected through the solvent exposure of a tryptophan amino acid and thioflavin T (ThT), which binds to  $\beta$ -sheets and fluoresces to indicate  $\beta$ -fibrillation. Meanwhile, extrinsic fluorescent are of importance, such as anilino-naphthalene-8-sulfonic acid (ANS) that can bind to hydrophobic pockets that are commonly exposed with the breakdown of tertiary structure.<sup>233,246-248</sup> Another technique often used for analysis of amyloid fibrillation for insulin and insulin analogs is Fourier transform IR spectroscopy.<sup>249</sup> Other techniques such as HDX-MS have been used to investigate the amino acids responsible for the formation and interaction of  $\beta$ -sheet fibrils in glucagon.<sup>250</sup>

## 1.5 Background: GLP-1 Receptor Agonists

Glucagon like peptide-1 receptor agonists (GLP-1 RAs) are a class of peptide drug products that are used to treat type II diabetes mellitus patients that have developed an insulin resistance. These agonists were developed as safer, and more effective, glucose-dependent alternatives to previously used diabetes therapies, including metformin, insulins, sulfonylureas and thiazolidinediones, that have previously been associated with poor glucose homeostasis, weight gain and hypoglycemic events.<sup>251–253</sup>

GLP-1 RAs are also known as mimetics of incretin, an endogenous hormone produced by intestinal enteroendocrine L-cells following nutrient ingestion, at high glucose levels.<sup>254</sup> This class of therapies interacts with GLP-1 receptors (GLP-1Rs) that are located in various organs, including the pancreas, gastrointestinal tract, brain, heart and kidneys. Upon receptor binding, a multi-faceted physiological response is elicited that goes beyond the simple secretion of insulin.<sup>255,256</sup> Physiological responses include activating the nervous system, decreasing body weight through the enhancement of satiety and energy uptake, slowing gastric emptying, regulating glucagon secretion, and inducing  $\beta$ -cell proliferation and enhancing their resistance to apoptosis. The induction of apoptosis resistant  $\beta$ -cells is especially important as it has been hypothesized to prevent further loss of endocrine pancreatic function.<sup>254,257–259</sup> Additionally, recent literature has delved into the neuroprotective application of GLP-1 RAs in brain diseases like Parkinson's.<sup>260–262</sup>



GLP-1 is impractical for therapeutic use itself as it rapidly degraded by the peptidase NEP 24.11 and by DPP4 at the Alanine 8 amino acid residue. This degradation means that *in vivo* GLP-1 only has a half-life of approximately 2.4 minutes.<sup>263</sup> As part of the effort to design and develop therapies with improved longer half-lives, Alanine 8 is typically substituted in GLP-1 RAs.<sup>263</sup> Not only does improving half-life allow for greater glucose control, but it also eases the use and improves the compliance for the administration of these therapies. The different GLP-1 RAs are shown in Fig. 1-16 with the details of modification types and half-lives shown in Table 1-6.<sup>263</sup> GLP-1 RAs include synthetically manufactured molecules exenatide and lixisenatide and molecules derived from a biologic source, including dulaglutide, liraglutide, albiglutide and semaglutide.

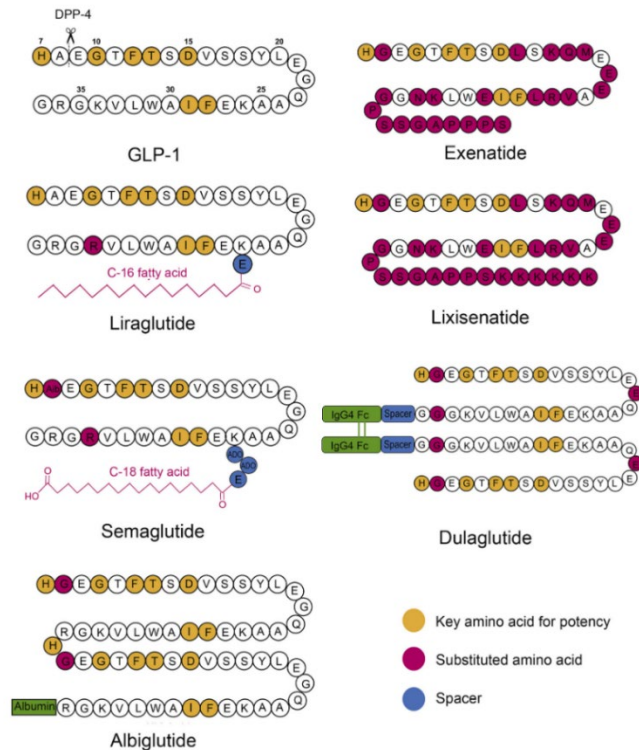


Figure 1-16. Peptide sequences and molecular structures of FDA approved GLP-1RA, including GLP-1, exenatide, liraglutide, lixisenatide, semaglutide, dulaglutide and albiglutide. Yellow: key amino acids related to potency; Red: substituted amino acids; Blue: spacers; Green: IgG. Figure adapted with permission from [263].

Molecule	Modification Type	Half-Life	Q
GLP-1	None	2.4 Min	N/A
Exenatide	Substitutions + Additions	2.4 <u>Hrs</u>	Daily (weekly)
<u>Lixisenitide</u>	Substitutions + Additions	3 <u>Hrs</u>	Daily
Liraglutide	Substitution + Conjugation	13 <u>Hrs</u>	Daily
<u>Semaglutide</u>	Substitutions + Conjugation	7 Days	Weekly
Dulaglutide	Substitutions + Fusion	5 Days	Weekly
Albiglutide	Substitutions + Fusion	5 Days	Weekly

Table 1-6. GLP-1RAs, modification types, half-lives and dosing regimens.

GLP-1Rs are part of the G-protein coupled receptor (GPCR) super ‘family B’, ‘secretin receptor-like family’ that includes receptors composed of an N-terminal domain of 100-150 residues connected to an integral membrane core domain that is typically GPCR-associated.<sup>264</sup> GLP-1Rs, first cloned from rat pancreatic islets and then humans, show similarities to secretin, parathyroid hormone and calcitonin receptors.<sup>265–267</sup> Ligand-receptor binding has been proposed to occur through what is called the ‘two-domain model’, where a ligand’s C-terminal helical region enables N-terminal interaction with the receptor’s core domain.<sup>264,268</sup> Various GLP-1 like molecules, including several GLP-1 truncations, were studied in view of this “two-domain model”. These studies showed that the N-terminal residue was required to be a histidine in order to enable such interaction with the core domain. GLP-1 C-terminal variants that were truncated at the 6<sup>th</sup>/8<sup>th</sup> amino acid showed reduction of activity by approximately 300 fold, whereas cleavage of the single C-terminal residue only reduced activity up to 10 fold.<sup>269–271</sup> Micelle-forming lipids sodium dodecyl sulfate (SDS) and dodecyl phosphocholine (DPC)

are commonly used to mimic membrane- or receptor-bound states, as most membrane binding peptides are unstructured in the monomeric solution state.<sup>272–275</sup> Use of these micelle-forming lipids allows for GLP-1 variants to exist in a preferred, analysis friendly, conformational state.<sup>272–275</sup> Altogether, these results show that modifications and conjugations must be designed with receptor binding in mind. Currently marketed GLP-1 products are listed below in table 1-7 and includes several products that are co-administered with insulin analogs.

Molecule	Brand	Manufacturer	Global Revenue (\$Mn)	Y/Y (%)	Synthetic/Biologic	Patent Expiration (US/EU)
Dulaglutide	Trulicity	Lilly	4,128	+29%	Biologic	2027 (2029)
Liraglutide	Victoza	Novo Nordisk	3,319	-	Biologic	2023
Exenatide	Byetta	AZ	110	-13%	Synthetic	2020 (2021)
Exenatide	Bydureon	AZ	549	-6%	Synthetic	2028
Lixisenatide/Insulin Glargine	Suliqa/Soliqua	Sanofi-Aventis	122	+60.3%	Synthetic	2035
Semaglutide	Rybelsus (oral)	Novo Nordisk	50	N/A	Biologic	2031
Lixisenatide	Adlyxin/Lyxumia	Sanofi-Aventis	26*	-21%	Synthetic	2035
Semaglutide	Ozempic	Novo Nordisk	11	+525%	Biologic	2031
Liraglutide/Insulin Degludec	Xultophy	Novo Nordisk	2.2	+37%	Biologic	2029 (2028)
Albiglutide	Tanzeum/Eperzan	GSK	Discontinued	N/A	Biologic	2025

Table 1-7. GLP-1RA products, manufacturers, revenues (2019\*), Y/Y % change, synthetic/biologic nature and estimated patent expiration date. \*: 2018 revenue.

## 1.6 Exenatide: An Approved GLP-1 Receptor Agonist

Exenatide is a synthetic GLP-1 agonist that was initially derived from the venom of the Gila Monster (*Heloderma Suspectum*), a lizard that is native to the southwestern United States. Exenatide, also referred to as exendin-4 (Ex4), differs from exendin-3 (Ex3) at two amino acid residues. Switching Ser2-Asp3 (Ex3) to Gly2-Glu3 (Ex4) results in distinct bioactivities and greatly eliminates the vasodilation side effect exhibited in Ex3.<sup>276</sup> Aside from amino acid switching, truncation of amino acids has also been studied in Ex4 and Ex3. It was found that truncation of the first 8 residues of Ex3 yielded an antagonist, while similar truncation of the first two residues of Ex4 also rendered it an antagonist. Clearly, amino acid modifications of Ex3 and Ex4 are important and are worth further exploration, showing the importance and drastic effects of amino acid modifications.<sup>277-280</sup>

Exenatide is the active pharmaceutical ingredient (API) found in AstraZeneca's marketed product Byetta<sup>®</sup>, a solution formulation for twice-daily injection. Byetta<sup>®</sup> has since been superseded by the more successful Bydureon<sup>®</sup>, which contains exenatide encapsulated in poly(lactide-co-glycolic acid) (PLGA) microspheres for extended release, allowing it to be injected weekly.<sup>281,282</sup> Exenatide's isoelectric point (pI) has been reported to be approximately 4.86 and, therefore, both Byetta<sup>®</sup> and Bydureon<sup>®</sup> are formulated at pH 4.5. Byetta<sup>®</sup> is formulated with mannitol and m-cresol excipients and is administered subcutaneously from a pen that contains a month's worth of injections (60). Bydureon<sup>®</sup> microspheres are encapsulated with sucrose, where each pen contains a single dose containing a lyophilized powder (formulated with sucrose) that is resuspended prior to injection.<sup>283</sup> While many current GLP-1RAs are dosed weekly,

ongoing research has been focusing on potential formulation approaches to develop exenatide into a monthly injection.<sup>263</sup>

The amino acid sequence of exenatide is shown below with the locations of exenatide's most likely chemical degradation sites highlighted in red, Asn28 followed by Gly29, a deamidation hotspot, as well as Met10 and Trp25, oxidation hotspots. Other potential chemical degradation sites include Asp (D) and Ser (S) hydrolysis and Gly (G), which undergoes formation to pyroglutamic acid (PyroQ).



The chemical stability of exenatide and the impact of its chemical impurities on GLP-1R has been previously studied in relation to a novel hydrogel technology, whereby exenatide was covalently attached to hydrogel microspheres.<sup>284</sup> Exenatide was analyzed for the formation of chemical impurities after 8 (red), 28 (blue) and 56 days (green) of incubation at 37°C (Fig. 1-17).

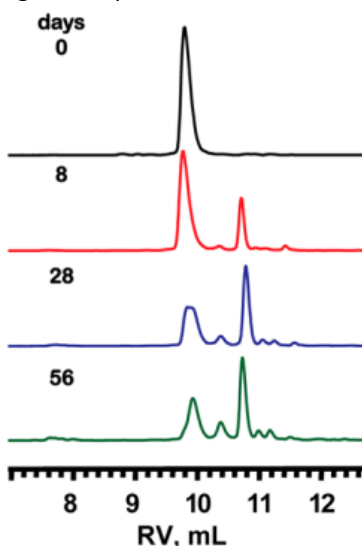


Figure 1-17 Chemical impurity formation of exenatide released from hydrogels over 56 days of incubation at 37°C. Black: 0 days; Red: 8 days; Blue: 28 days; Green: 56 days. Figure adapted with permission from [284].

They found that major impurity for all time points was deamidation at Asn28, which appears at a retention volume of 10.8 mL.<sup>284</sup> They showed that deamidation resulted in the formation of L-Asp, L-isoAsp and D-isoAsp impurities, which all showed decreased GLP-1R binding affinity in terms of increased EC<sub>50</sub> relative to day 0.<sup>284</sup> In attempt to avoid these deamidation impurities, the deamidation prone Asn28 was substituted with Gln28, where they were able to show reduced formation of the deamidation impurity while simultaneously maintaining similar activity and PK profiles to those seen without Asn28 modification.<sup>284</sup> The lack of oxidation observed in this study implies that different formulation strategies can have different chemical instability pathways and tendencies when compared to exenatide alone in aqueous solution, where we observed similar trends for deamidation at pH 6.5 and above, although we observed the formation of oxidation impurities.

Exenatide's secondary structure is composed of the following: 1) an N-terminal strand from amino acids 1 - 8, with amino acids 1-6 being responsible for receptor binding; 2) an  $\alpha$ -helical structure making up the majority of the structure from amino acids 9-27; 3) a C-terminal Trp cage that forms via the interaction between the side chains of Trp25 and the several proline residues (28 - 39).<sup>285</sup> The  $\alpha$ -helix has been suggested to be stabilized through salt bridging of positive and negative side chains and polar H-bonding, which can be disrupted by drastic changes of pH. The C-terminal Trp cage interaction has also been suggested to stabilize tertiary conformations of small proteins, hairpin peptides and peptide protein complexes.<sup>286-289</sup> The physical stability of the Trp-cage miniprotein and other modified Trp-cage miniproteins have been independently investigated and was found to have a melting temperature of

approximately 42°C at pH 7, though in isolation. The cage was not found to interact with exenatide's N-terminus, hence the reason it's stability was investigated in isolation.<sup>290,291</sup>

Concentration-dependent differences in secondary structure between exenatide samples at pH 4.4 were observed at 2°C for 2 (green), 40 (blue), 240 (red) and 600 μM (yellow) concentrations (Fig. 1-18). Similar trends were observed over CD melts at peptide concentrations that were between 2 (~0.0084 mg/mL) and 240 μM (1 mg/mL) when ramping from 10 to 90°C.<sup>285</sup> It was concluded that exenatide is only monomeric with a partially formed Trp cage at concentrations < 10 μM., Samples at higher concentrations participate in aggregation via helix-helix interactions at residues 11-26.<sup>285</sup> The presence of helix-helix interactions and concentration dependence aligns with the general understanding that peptides can exist in multiple conformational states.

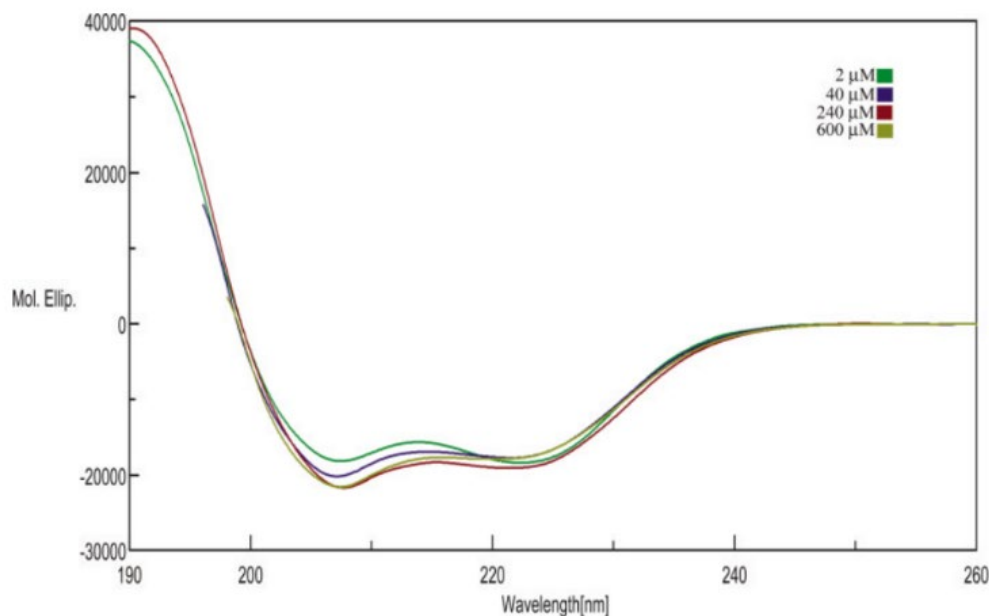


Figure 1-18. Far-UV CD spectra of exenatide concentrations from 2 to 600 μM. Green: 2 μM; Purple: 40 μM; Red: 240 μM; Yellow: 600 μM. Figure adapted with permission from [285].

In the presence of fluoro-alcohols, exenatide has been shown to induce an increasingly helical tertiary structure with fully folded Trp-cage domains.<sup>285,292</sup> This is contrary to the typical behavior of fluoro-alcohols, which entails β-sheet formation of

proteins to enhance stabilization through “solvophobic effects”.<sup>275,285,293</sup> SDS and DPC micelles were used to investigate receptor binding and its effect on tertiary structure for a truncated 26-residue analog. It was observed that DPC micelle binding resulted in a loss of tertiary structure, likely attributed to the favorable interactions between Trp and the PC head groups. The Trp cage also showed SDS micelle binding, a phenomenon that has been previously reported in other Trp-containing peptides.<sup>272–274,287</sup> While this does not elucidate the exact role of the Trp cage, it remains useful information for the design of receptor binding models. Several conformational isomers and their suggested role in aggregation are shown in Fig. 1-19.

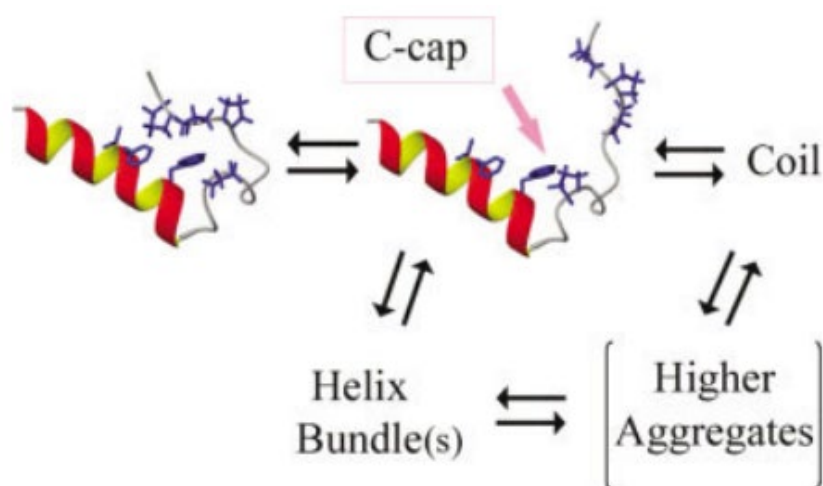


Figure 1-19. Potential conformational isomers and oligomeric species that could contribute to the solvent-dependent equilibrium in exenatide at different concentrations as a function of Trp-cage unfolding. Figure adapted with permission from [285].



## 1.7 Infliximab: An Anti-TNF- $\alpha$ mAb

There are a handful of biological products on the market that target TNF- $\alpha$  (commonly known as TNF- $\alpha$  inhibitors) to treat various autoimmune diseases, including rheumatoid arthritis (RA), psoriasis, ankylosing spondylitis, ulcerative colitis (UC) and Crohn's disease (CD). Table 1-8 shows a list of products in the TNF- $\alpha$  inhibitor class, as well as their molecular name and type and whether a biosimilar version is available. While these molecules share overlapping mechanisms of action, there are a few important differences that must be identified in terms of molecule type, route of administration and potential for immunogenicity.

Brand Name	Molecule Name	Biosimilar?	Company	Molecule Type
Humira <sup>®</sup>	Adalimumab	-	AbbVie	Human
<u>Cyltezo<sup>®</sup></u>	Adalimumab	Y	Boehringer Ingelheim	Human
<u>Hyrimoz</u>	Adalimumab	Y	Sandoz	Human
<u>Amjevita<sup>™</sup></u>	Adalimumab	Y	Amgen	Human
Cimzia <sup>®</sup>	Certolizumab Pegol	-	UCB	Humanized
Avastin <sup>®</sup>	Bevacizumab	-	Genentech	Humanized
<u>Mvasi<sup>™</sup></u>	Bevacizumab	Y	Amgen/Allergan	Humanized
<u>Zirabev<sup>®</sup></u>	Bevacizumab	Y	Pfizer	Humanized
Enbrel <sup>®</sup>	Etanercept	-	Amgen	Human
<u>Erelzi<sup>®</sup></u>	Etanercept	Y	Sandoz	Human
Simponi <sup>®</sup>	Golimumab	-	Janssen	Human
Remicade <sup>®</sup>	Infliximab	-	Janssen	Chimeric
<u>Renflexis<sup>®</sup></u>	Infliximab	Y	Merck	Chimeric
<u>Inflectra<sup>®</sup></u>	Infliximab	Y	Pfizer	Chimeric

Table 1-8. mAb products, US/EU biosimilar presence, manufacturer and mAb type.

Amongst the listed anti TNF- $\alpha$  molecules, etanercept and infliximab stand out as outliers. Enbrel is a mAb-like biologic that is comprised of a TNF- $\alpha$  receptor 2 protein coupled to an IgG1-derived Fc domain. Without the Fab domain, etanercept lacks the ability to be approved for multiple inflammatory indications, such as Crohn's and ulcerative colitis. Another difference between listed products is the route of administration. Infliximab products are administered intravenously by infusion while all other products are administered subcutaneously. This infusion is given over the course of 2 hours, which has been the preferred option for patients that consider fear of needles as the most influential factor of choosing a therapy.

Additionally, molecules vary in their inherent potential for immunogenicity depending on their manufacturing source (cell lines). Chimeric molecules, which have mouse derived variable domains, have a higher immunogenicity potential compared to humanized and fully human molecules (Fig. 1-20).<sup>294</sup> Infliximab is chimeric and certolizumab is humanized (mouse derived CDR) while adalimumab and golimumab are fully human.

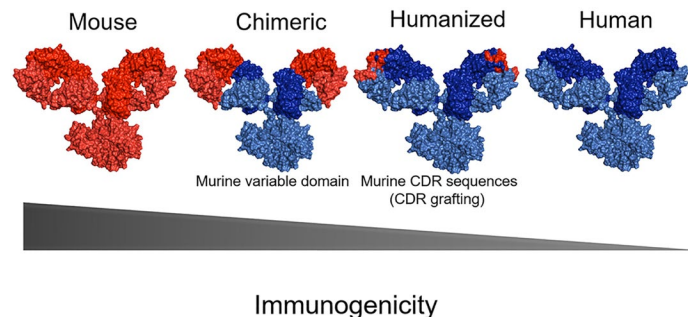


Figure 1-20 Sources of mAb manufacturing, including mouse derived, chimeric, humanized and human. Shown in the order of highest to lowest potential to elicit immunogenic response. Figure adapted with permission from [294].

A review (Fig. 1-21) compared the immunogenic response for several of these molecules in patients with CD and UC.<sup>295</sup> The authors observed that infliximab exhibited the greatest potential for immunogenic response compared to humanized and fully

humanized molecules (though immunogenic responses were highly variable).<sup>295</sup> It is generally understood that these molecules all have the potential to elicit an immunogenic response upon administration, but identification of key modulators resulting in immunogenicity remains complicated and full of confounding factors. Studies have been performed whereby the forced degradation of mAbs has shown that different stress types can lead to variations in immunogenic responses, thus affirming the complicated nature of studying and predicting immunogenicity.<sup>160</sup>

Biologic agent	All studies (n)	CD (n)	UC (n)	CD or UC (n)
Infliximab <sup>c</sup>	0.0–65.3 (73)	2.9–60.8 (22)	6.1–41.0 (8)	0.0–65.3 (43)
Adalimumab	0.3–38.0 (22)	0.3–35.0 (11)	2.9–5.3 (3)	14.0–38.0 (8)
Certolizumab pegol	3.3–25.3 (4)	3.3–25.3 (4)	–	–
Vedolizumab	1.0–4.1 (4)	1.0–4.1 (2)	3.7 (1)	4.0 (1)
Golimumab	0.4–2.9 (2)	–	0.4–2.9 (2)	–
Ustekinumab	0.7 (1)	0.7 (1)	–	–

Figure 1-21. Range of rates (%) of ADABs formation to biologics in patients with IDBs. Only studies reporting rates of ADABs were included, immunogenicity analyses are product- and assay-specific, infliximab excluded one study that had a small sample size (n = 28) and high rate of immunogenicity (79%). -: no publications available; ADABs: anti-drug antibodies; CD: Crohn’s Disease; UC: Ulcerative Colitis. Figure adapted with permission from [160]

Despite the potential for immunogenicity, these TNF- $\alpha$  inhibitors are undeniably successful on the market. Due to their success, many companies have begun to create biosimilar versions of these drug products in hopes of outcompeting the innovator in the market once it has lost exclusivity. Changes in total sales revenues of the innovator and respective biosimilars have reflected this competition.

Between 2016 and 2019 three infliximab biosimilars of Remicade<sup>®</sup> (Johnson & Johnson) were FDA approved, including Inflectra<sup>®</sup>/Remsima<sup>™</sup> (Celltrion), FDA approved in 2016, Fliaxabi<sup>®</sup>/Renflexis<sup>®</sup> (Samsung Bioepis), FDA approved in 2017, and Avsola<sup>™</sup> (Amgen), FDA approved in 2019. The total sales revenues of the innovator Remicade<sup>®</sup> have continued to fall since the approval of the first US approved infliximab biosimilar in 2016, decreasing from \$6.97 Bn in 2016 to \$4.4 Bn in 2019 (-36.9%).<sup>296</sup> US

sales revenues for Inflectra®/Remsima™ (Celltrion) increased from \$259 Mn in 2018 to \$325 Mn in 2019 (+16%), while global sales of Renflexis®/Flixabi® (Samsung Bioepis) increased to \$5.0 Bn in 2019 (+16.7% from 2018), with some contribution from US sales.<sup>297,298,299</sup> 2020 financial reports for some companies were unavailable.

As shown in Fig. 1-2, the major focus for the development of biosimilar mAbs is establishing analytical similarity to an innovator. This information can be found in regulatory filing documents and in published comparability studies. In both, various orthogonal analytical techniques are applied to establish similarity to the innovator product.<sup>43,144,211</sup> Detailed analytical comparisons of the innovator, Remicade®, against biosimilar, Inflectra®/Remsima™, in literature and regulatory documents showed that there were minor differences found for levels of soluble aggregates, levels of basic charge variants and glycan distribution profiles.<sup>136,211,300</sup> However, these differences are small enough that they were not considered to be a clinically relevant concern. When considering whether these minor differences are just that – minor – companies have to determine their potential impact on mAb function. The two main mechanisms of action for mAbs are TNF- $\alpha$  neutralization, via binding to soluble and membrane bound TNF- $\alpha$ , and ADCC, via Fc $\gamma$ R3A binding. Therefore, assays such as TNF- $\alpha$  neutralization and Fc $\gamma$ R binding are also implemented and required for regulatory approval. The FDA's assessment report for Inflectra®/Remsima™ compared TNF- $\alpha$  binding of CT-P13 against US and EU Remicade® by ELISA (Fig. 1-22/23) and Fc $\gamma$ R3A binding to low (F) and high affinity (V) variants (Fig. 1-24/25). While TNF- $\alpha$  binding was similar, we do notice that there is a difference in terms of Fc $\gamma$ R3A binding for both variants (differences in these variants and their importance are highlighted in a paper published by Kang et

a).<sup>301</sup> The difference in binding is further understood by differences of glycan distribution profiles, which are also reported in this document (Fig. 1-26). Pisupati et al. performed a comparability study of these molecules (Fig. 1-27), utilizing LC-MS/MS to quantify glycan distribution and biolayer interferometry (BLI) to measure FcγR3A binding where similar results were reported; Remsima™ (CT-P13) showed fewer afucosylated glycans and a weaker FcγR3A binding affinity when compared with Remicade®.<sup>211</sup> In the end, while minor analytical and functional differences have been found, they are generally assumed as of little importance as long as there are no clinically meaningful differences as defined by the FDA.<sup>14</sup>

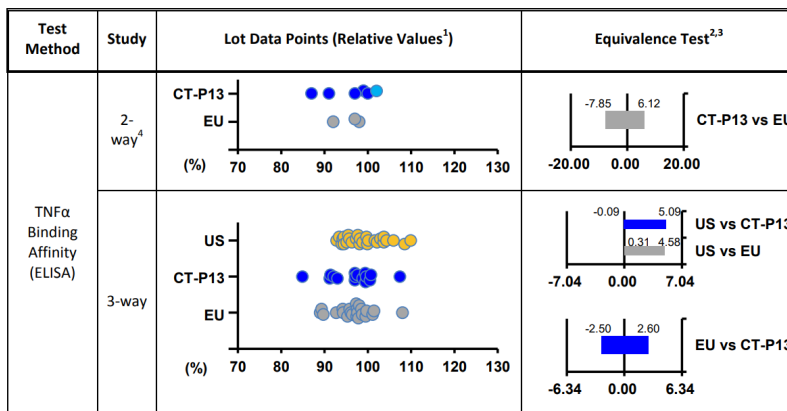


Figure 1-22. Results and Statistical Analysis of Binding of soluble TNF-α. Dark Blue: CT-P13; Light Blue: ALAG CT-P13; Grey: EU Remicade; Yellow: US Remicade; ALAG: artificially elevated afucosylated glycans.

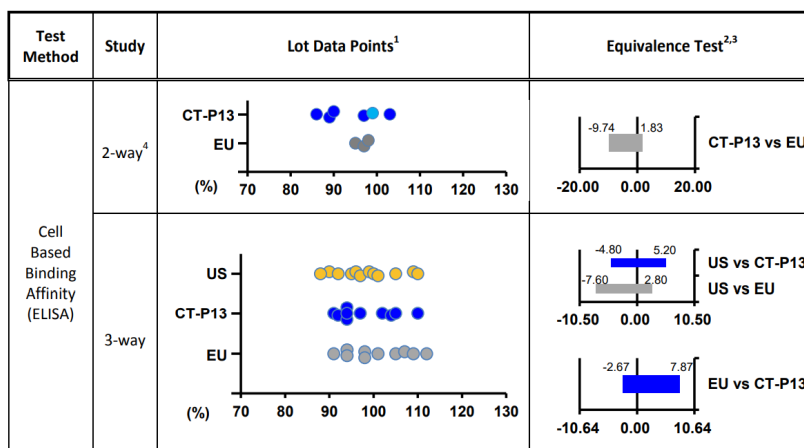


Figure 1-23. Results and Statistical Analysis of ELISA Binding of Transmembrane-Bound TNF-α. Dark Blue: CT-P13; Light Blue: ALAG CT-P13; Grey: EU Remicade; Yellow: US Remicade; ALAG: artificially elevated afucosylated glycans

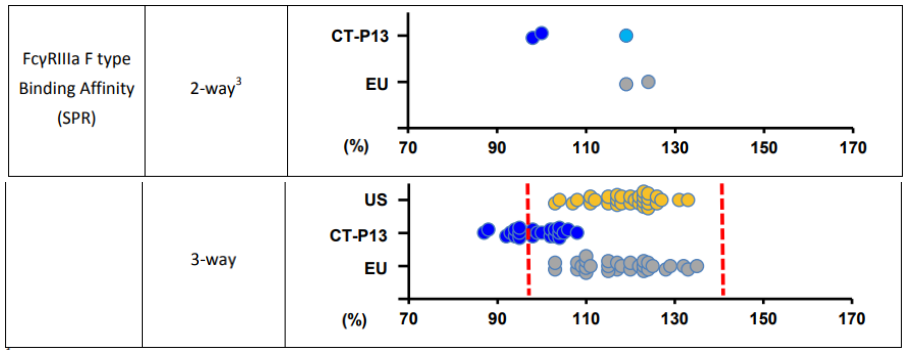


Figure 1-24. Quality Range Analysis of FcγRIIIa F variant binding by SPR. Dark Blue: CT-P13; Light Blue: ALAG CT-P13; Grey: EU Remicade; Yellow: US Remicade; ALAG: artificially elevated afucosylated glycans; Red: QR limits of variability.

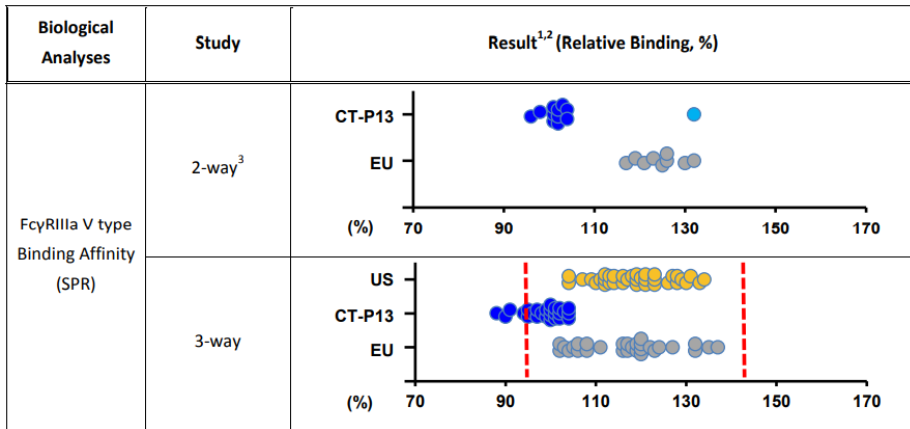
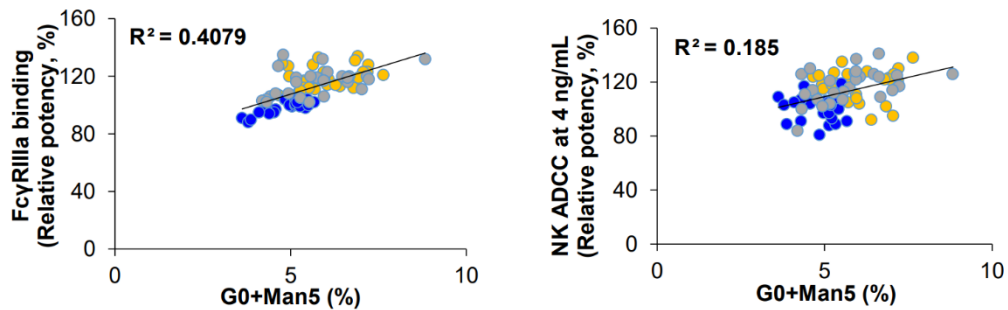


Figure 1-25. Quality Range Analysis of FcγRIIIa V variant binding by SPR. Dark Blue: CT-P13; Light Blue: ALAG CT-P13; Grey: EU Remicade; Yellow: US Remicade; ALAG: artificially elevated afucosylated glycans; Red: QR limits of variability.



CT-P13 lots are shown in blue; US Remicade lots are shown in yellow; EU Remicade lots are shown in grey

Figure 1-26. Scatter Plots Showing Relationship of % Afucosylated Glycan Species (G0 + Man5) with FcγR3a Binding Affinity and ADCC Activity. Dark Blue: CT-P13; Grey: EU Remicade; Yellow: US Remicade.

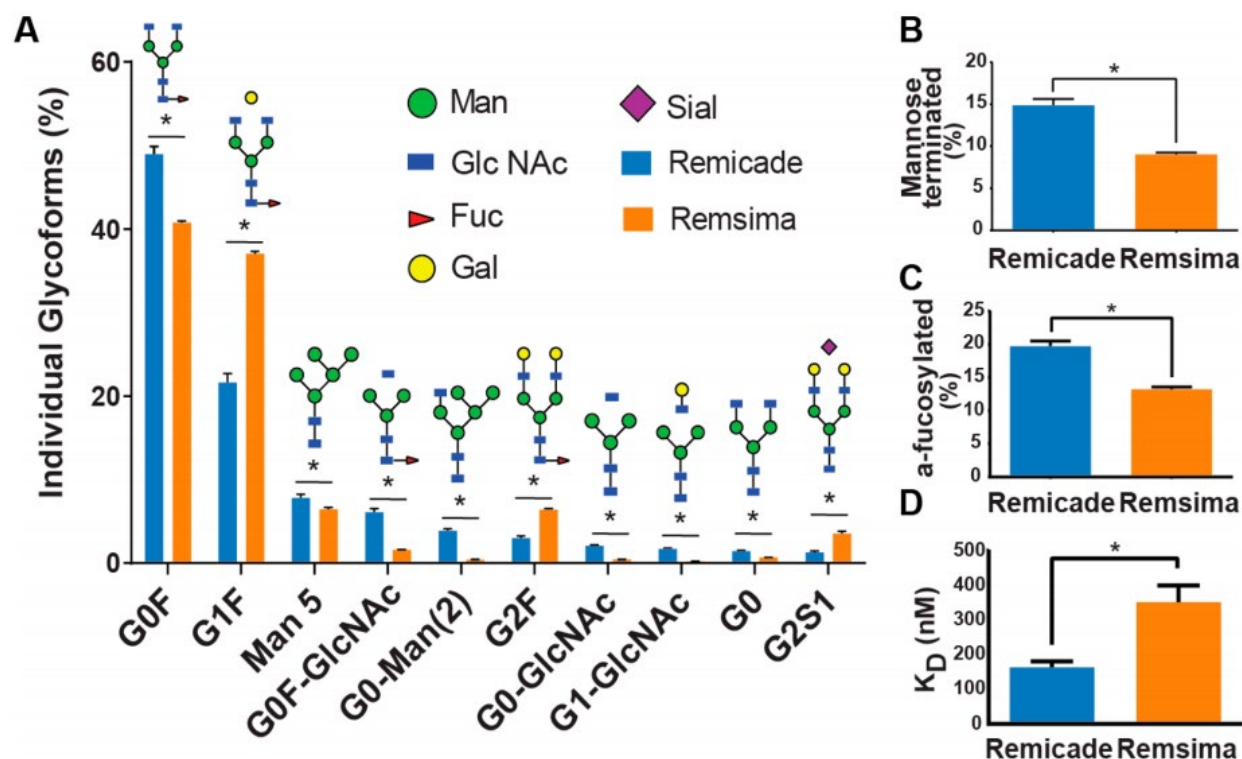


Figure 1-27. Quantification by LC-MS/MS. (A) N-glycans. (B) Total mannose-terminated forms. (C) Total afucosylated forms. (D) Average  $K_D$  values for binding to  $Fc\gamma R3a$  as measured by BLI. (n = 4 lots, mean  $\pm$  SEM; \*: p < 0.05). Figure adapted with permission from [211].

Analytically, biosimilars sufficiently match their innovator. However, there are still concerns surrounding the ability to switch patients, who are stable and doing well on the innovator infliximab, to more cost-effective biosimilars. Concerns have previously been raised regarding efficacy, safety and immunogenicity, resulting in the formation of ADAs once patients have switched to biosimilars.<sup>302,303</sup> Some of these concerns were raised from specific scientific communities (in this case, gastroenterology) that had issues with extrapolations of indications for the biosimilars.<sup>304–306</sup> Some of the early switching studies from infliximab originator to biosimilar included 1) open cohort studies; 2) second year extensions of PLANETAS, a phase 1 study in AS patients, and PLANETRA studies, a phase 3 study in RA patients; 3) NOR-SWITCH study, in which all indications were accounted for.<sup>307–311</sup> The outcome of the PLANETAS and PLANETRA studies

were that switching is safe and does not reduce effectiveness of treatment in terms of serum concentrations of infliximab and ADA occurrence.<sup>307,308,310,311</sup> The NOR-SWITCH study was a randomized, controlled trial conducted in order to assess CT-P13's comparability regarding efficacy, safety and immunogenicity for patients who had been on stable originator for at least 6 months.<sup>309</sup> This study showed that switching to Celltrion's biosimilar (CT-P13) was non-inferior to the originator, meeting acceptability specifications within a margin of 15%.<sup>312</sup> Fig. 1-28 shows the Forest plot of risk difference according to disease, where shifting of results indicate either a favoring of the originator (left shift) or the biosimilar (right shift).<sup>312</sup> A review on switching studies publications in specific disease populations was published in 2018 and as a whole, barring some minor outliers, studies on switching to biosimilar infliximab did not lead to issues of safety, efficacy or immunogenicity.<sup>312</sup>

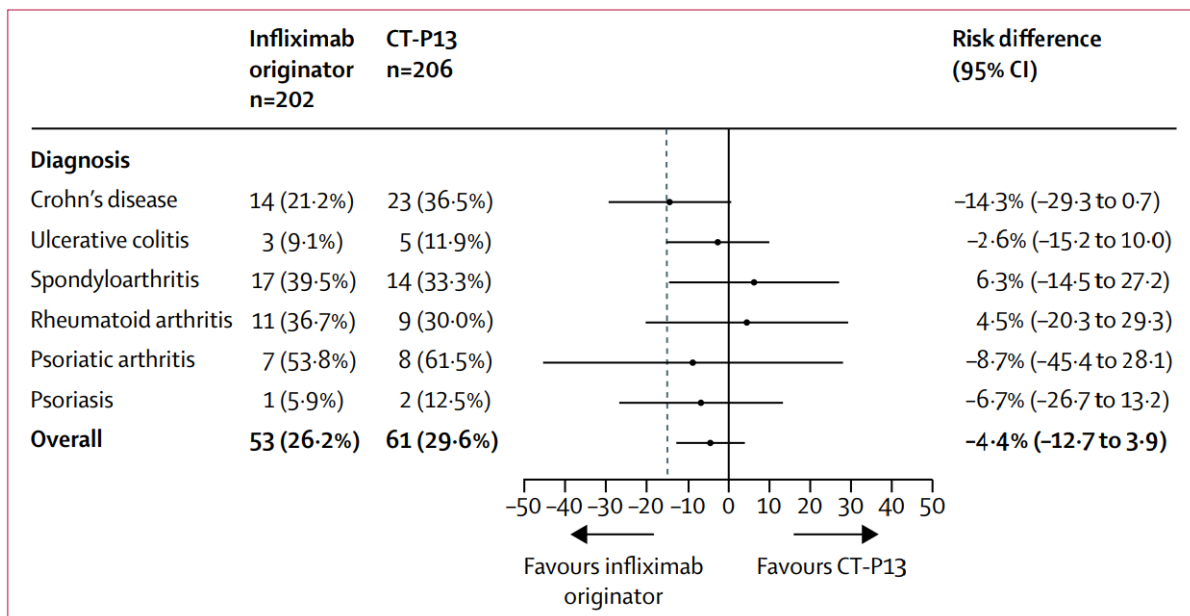


Figure 1-28. Forest plot of risk difference according to disease. Figure shows data for the per-protocol set. Risk difference adjusted for treatment duration of infliximab originator at baseline. Figure adapted with permission from [312]



## 1.8 Aspects of Peptide/mAb Formulations and Delivery Devices

Peptides and proteins are formulated as subcutaneous (SC), intravenous (IV) or intramuscular (IM) parenteral injections as they are not orally bioavailable. There are many aspects that must be simultaneously considered when developing formulations for peptides and proteins including previously mentioned molecular properties, manufacturing conditions, storage conditions, potential impurities, routes of administration, related administration devices and potential responses to physiological conditions.<sup>313</sup>

pH is an example of a parameter that is heavily considered during formulation. Many of the top 10 mAbs are formulated between pH 5.5 and 7.4.<sup>314,315</sup> There is a range because the formulation pH for peptides and proteins has to account for each protein's isoelectric point (pI). If pH is equal to pI (determined by amino acid structure), the molecule has a net neutral charge that can lead to unwanted precipitation. While precipitation is typically considered a potential impurity, there are select cases, such as insulin glargine (Lantus), where isoelectric precipitation is intended upon injection into the physiological environment of the body.<sup>316</sup> In this case, insulin is modified by the attachment of an arginine-arginine tag, increasing the pI from human insulin's typical 5.6 to that of approximately 7.0.<sup>316,317</sup>

Another factor at play in determining the final protein formulation for parenteral solutions is the selection of excipients. Formulation excipients are important given that they can prevent degradation. (Fig. 1-29).<sup>318</sup> When deciding which excipients are best suited for a specific product, manufacturers have to consider the nature of the API. The complexity of peptide and protein products translates to a need for the inclusion of

certain excipients. Insulin and insulin analog products serve as good examples of molecules requiring significant consideration of formulation complexities. Insulin is natively found in equilibrium between the monomer, dimer, tetramer and hexamer conformational states, where the equilibrium can be controlled through concentration, pH and excipients (Fig. 1-30).<sup>319</sup> Insulin analogs have been designed with various modifications to effectively remove the ability of these molecules to form dimers. Likewise, some formulations have added phenolic compounds to drive the insulin into the hexamer conformation.<sup>319</sup>

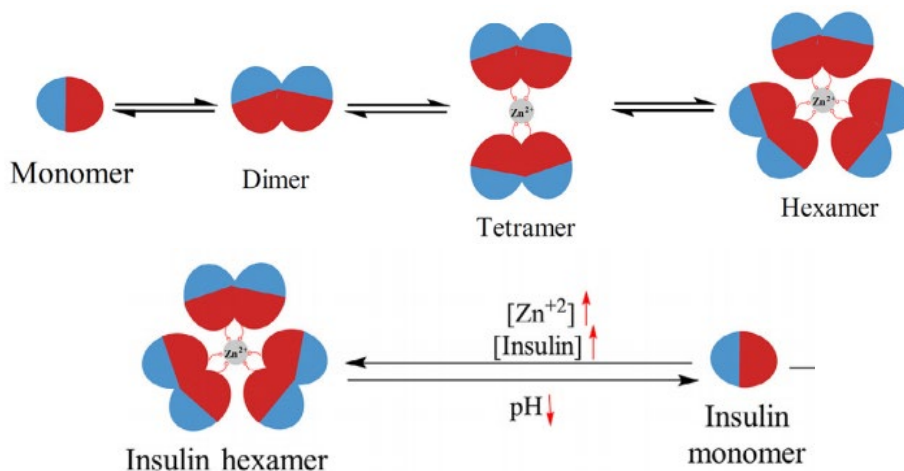


Figure 1-29. Conformation states of insulin, including the monomer, dimer, tetramer and stable hexamer and factors affecting conformational equilibrium. Decreased pH favors the monomer while Zn and insulin concentration favor the hexamer. Figure adapted with permission from [319]

Formulation effect	Excipient type	Example	
Anti-adsorption	Surfactants	Poloxamer [1,57] Polysorbate 20 and 80 [1,34]	
	Polymers	Dextran [11,37] Poly(ethyleneglycol)- <i>b</i> -poly(L-histidine) [59] PEG [1,11,105]	
	Other proteins	BSA and HSA [32]	
Oxidation protection	Antioxidants	Ascorbic acid [1,26-27] Ectoine [24,106] Glutathione [1] Monothioglycerol [25] Morin [107] Poly(ethylenimine) [24] Propyl gallate [2,3] Vitamin E [2,3]	
	Chelating agents	Citric acid [2,3] EDTA [23,27] Hexaphosphate [1] Thioglycolic acid [2,3]	
pH	Buffer salts	Phosphate, bicarbonate, sulphate, nitrate, acetate, chloride, pyruvate [2,29]	
	Antacids	Mg(OH) <sub>2</sub> [31] ZnCO <sub>3</sub> [56]	
Stabilisers	Amino acids	Alanine [1,11] Arginine [1,13,18] Aspartic acid [1] Glycine [1,11] Histidine [108] Lysine [1] Proline [1,11,14]	
	Sugars	Glucose [15] Sucrose [1,11,31,15,45,109,110] Trehalose [1,11,16,45,43]	
	Polyols	Glycerol [1,11,109,75,111] Mannitol [1,11,45] Sorbitol [1,11,24,109,111]	
	Salts	Potassium phosphate [1,11] Sodium sulphate [1,11,82]	
	Chelating agents	EDTA [1,23,27] Hexaphosphate [1]	
	Ligands	Phenol [22] Zinc [21]	
	Polymers	Cyclodextrin [1,19,112,113] Dextran [1,11,114] PEG [1,11,38] PVP [1,11,110]	
	Tonicity	Salts	NaCl and many other salts [80,86]
		Other	Glycerol [75]

BSA: Bovine serum albumin; HSA: Human serum albumin; PEG: Polyethylene glycol; PVP: Poly(vinyl pyrrolidone).

Figure 1-30. Examples of excipients and their main function in peptide and protein formulations and their common, expected effects. Figure adapted with permission from [318].

Sugars have frequently been described as protective excipients against the formation of degradants and impurities in protein/peptide formulations. The mechanism of protection by sugars, depicted in Fig. 1-31, has been largely attributed to preferential exclusion, where the sugar preferentially binds to water in the solution, reducing protein solvation propensity.<sup>320</sup> Other suggested mechanisms of protection by sugars are vitrification, which involves embedding the protein into a glassy matrix to restrict mobility, and water replacement, which occurs when the sugar/protein interaction is greater than the water/protein interaction at hydrophilic residues, thus removing the surrounding water layer.<sup>320</sup> Differences between polyol and sugar excipients are also likely attributed to differences in the number of H-bond donors and H-bond acceptors as well as the variation of hydration volumes occupied by these various excipients.<sup>320</sup>

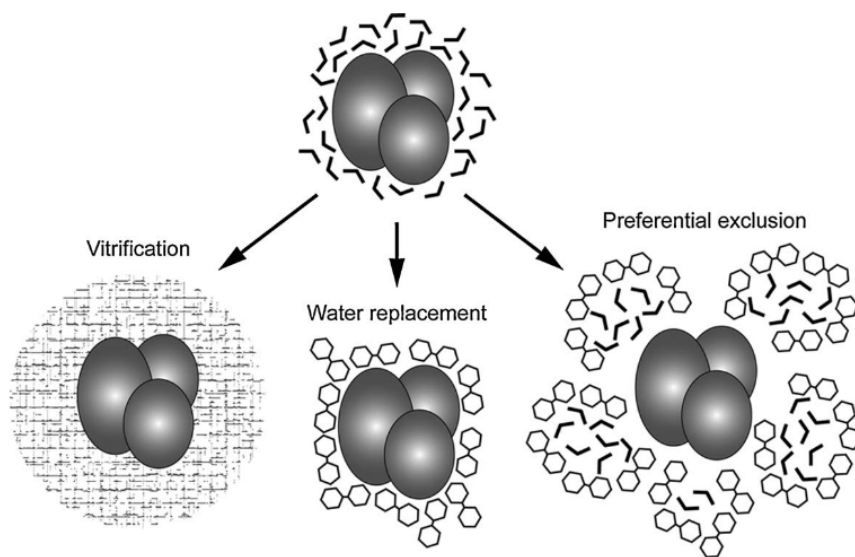


Figure 1-31. Three proposed theories how sugars may protect proteins from degradation. Vitrification: increase of viscosity; Water Replacement: preferential sugar binding with protein; Preferential Exclusion: preferential sugar binding with water. Figure adapted with permission from [320].

While most excipients are known for their protective effects, there have been studies performed where various polyol and sugar excipients have been shown to induce protein destabilization as a factor of the protein itself, concentration, and pH.<sup>313</sup> For example, bromelain in the presence of 1M trehalose was observed to exhibit a 2-state unfolding process. It also exhibited a 3-state unfolding process in the presence of 1M sucrose.<sup>321</sup> The same group then investigated the impact of sucrose and trehalose on intrinsic fluorescence. They observed fluorescence quenching by both sucrose and trehalose, more so by trehalose, indicating these sugars' destabilizing effects on conformation in a manner previously described.<sup>321</sup>

Lyophilization, which entails freeze drying of a solution into a solid state, has been implemented for a number of peptide and protein products to avoid degradations commonly prevalent in the liquid state.<sup>322–324</sup> While lyophilized cakes are well known to achieve adequate shelf-life, the freeze-dry process itself is a source of instability. Sugars and polyols are added to reduce degradation and allow rapid freezing below the glass transition temperature.<sup>325,326</sup> The mechanism of sugar induced stabilization during lyophilization has been suggested to occur by two mechanisms: 1) the “glass dynamics hypothesis”, where formation of a molecularly dispersed matrix limits mobility, solvent induced degradation and bimolecular degradation; and 2) the “water substitute hypothesis”, where site specific hydrogen bonds thermodynamically inhibit protein unfolding.<sup>327–331</sup> Studies comparing the degradation propensity during lyophilization in the presence of sucrose or trehalose have been conducted. From these studies it was found that sucrose was better at preventing degradation.<sup>332</sup> All infliximab products are supplied as lyophilized powders, where others are in solution.

Another major consideration of formulation optimization lies at the interface of delivery devices. Insulin delivery devices serve as a highly useful and comprehensive platform that can be translated to the development of future delivery devices for peptide and protein products and will thus be used here as an example case. Insulin was initially discovered and purified for therapeutic application in 1921 by Banting and Best and has since had a long history marked by many advancements in terms of the development of alternate products and improvements of delivery devices (Fig. 1-32). Now, devices can precisely deliver insulin with minimal invasiveness in a way that improves patient compliance.<sup>333–338</sup>

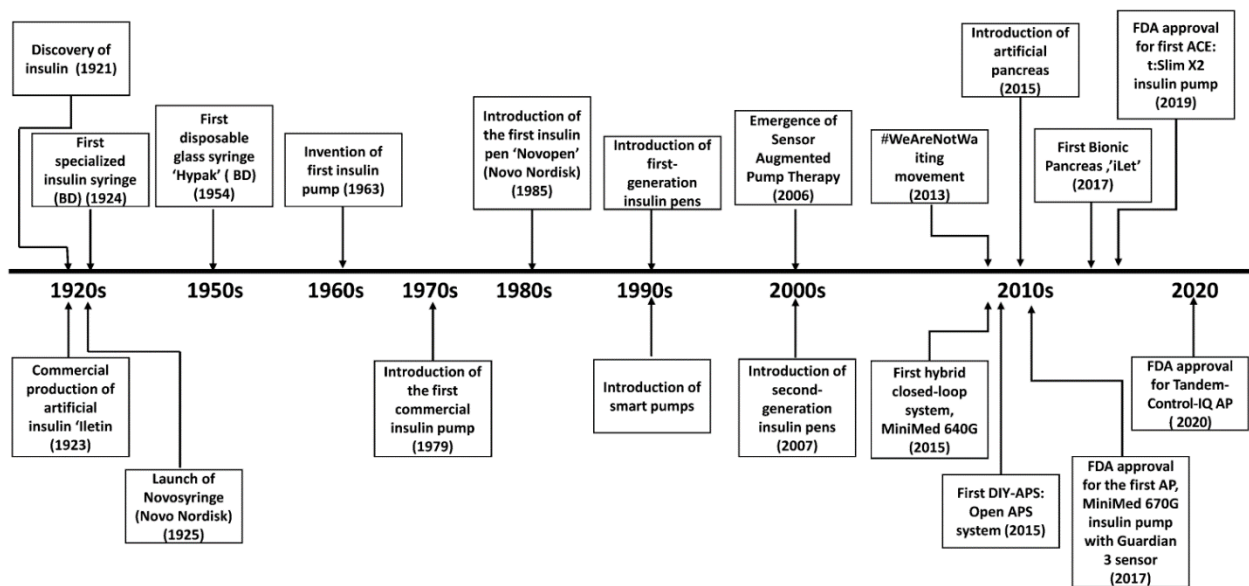


Figure 1-32. Major landmark events in the evolution of insulin and insulin delivery devices. Figure adapted with permission from [338].

Initially, insulin was administered via big, heavy reusable syringes that required sterilization by boiling prior to use. These reusable syringes were then replaced with more specialized needle types, though these were unfavorable due to poor accuracy, requirements for multiple daily injections and patient non-adherence. The first pen was developed by Novo Nordisk in 1985, offering a more simple, accurate and convenient delivery.<sup>339,340</sup> First generation pens were available in the market in the 1990's and have been improved by recent advances in smart technology to track and remember insulin dosing.<sup>341,342</sup> The most recent insulin delivery innovations have been related to continuous subcutaneous insulin infusion (CSII) pumps. These pumps are also called closed-loops systems, where glucose is constantly monitored, and insulin constantly infused. Typical components for these pumps are an insulin reservoir, infusion set and tubing, and a catheter for continuous delivery of insulin. The benefit of this technology is that the user can specify the program to dispense basal rates while fasting and dispense bolus doses prior to meals.<sup>343</sup> The two main insulin pumps currently in use are Medtronic's MiniMed System (represented in Fig. 1-33) and Insulet's Omnipod.<sup>344,345</sup>

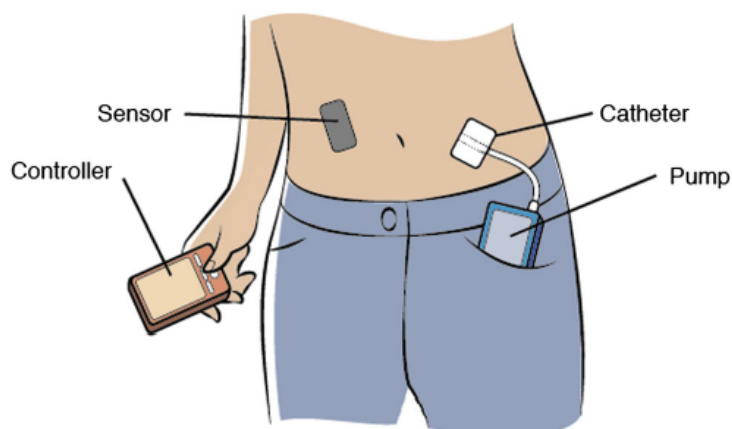


Figure 1-33. Components of a closed-loop insulin delivery system. Sensor: measures interstitial glucose levels; Controller modifies the pump control algorithm in response to the sensor; Pump: infuses insulin through the catheter. All communication is wireless. Figure adapted with permission from [344].

The main concern for insulin pumps is under- or over-delivery of insulin resulting in health consequences, including hyperglycemia and ketoacidosis.<sup>346</sup> Incorrect insulin delivery can occur via occlusion within the pump, infusion set or tubing. Incidence of occlusion has been studied as a function of time and insulin analog used, where occlusions were rare in the first 72 hours of infusion, but substantially increased over time.<sup>347,348</sup> These occlusions have been suggested to be directly related to the physicochemical stability of the molecules and their propensity to form fibrils..<sup>233,349</sup>

While insulin delivery is common now through pens and continuous pumps, delivery of short-term (twice daily) and long-term (weekly) GLP-1 receptor agonists for type 2 diabetes therapy remains common via pre-filled pen devices. These devices are shown below in Fig. 1-34 along with information on use number, dosage type, max dosage strength, whether resuspension is necessary prior to injection and ease of use.<sup>350,351</sup> GLP1RAs and insulin analogs have been compared in early stage diabetes patients in terms of glycemic effectiveness. It was found that there were only minor differences such as GLP1RAs having somewhat greater HbA1C reduction.<sup>352,353</sup> This comparability is important as the current barrier to entry for early stage patients is the initialization of therapeutic treatment. GLP1RAs provide a more simplified route of administration, whereas insulin analogs commonly require significant education on dose titration and administration, making them less user friendly.













	GLP1RAs								GLP1RA/Insulin Co-formulations	
Injection Devices										
Commercial Name(s)	Byetta®	Lyxumia®	Victoza®	Bydureon®	Bydureon BCise®	Dulicity®	Eperzan/Tanzeum®	Ozempic®	Xultophy®	Suliqua/Suliqua®
Generic Name	Exenatide	Lixisenatide	Liraglutide	Exenatide	Exenatide	Dulaglutide	Albiglutide	Semaglutide	Liraglutide/Ins Degludec	Lixisenatide/Ins Glargine
Use:										
Single (s)	m	m	m	s	s	s	s	m	m	m
Multiple (m)										
Dosing:										
Fixed (f)	f	f	v	f	f	f	f	f	v	v
Variable (v)										
Dosage(s)	5/10 µg	10/20 µg	0.6/1.2/1.8 mg	2 mg	2 mg	0.75/1.5 mg	30/50 mg	0.25/0.5/1 mg	1.8 mg/50 IU	20 µg/40 IU 20 µg/60 IU

Figure 1-34. Optical appearance and properties of pen injection devices for approved GLP-1 receptor agonists (as mono substances or fixed-dose combinations with basal insulin).

Additionally, there are 2 successful co-formulated subcutaneous injections of insulin analogs and GLP-1RAs on the market (shown in Table 1-7, Fig. 1-35). Both products, Suliqua (Sanofi) and Xultophy (Novo Nordisk), are intended for use in late-stage type 2 diabetes patients due to the complementary mechanisms of action of the components. While relatively new, the growth rate for sales of Xultophy, which increased 11% (to \$353.6 Mn in 2020), while Suliqua's sales revenues increased 60.3% (to \$146 Mn in 2019 [2020 annual report unavailable]), indicate a high ceiling for the success of these types of products. In a result of being co-formulated, these products lie in a relatively undefined category of biologically derived products in regards to regulatory approval pathways.<sup>354</sup> Suliqua comes in two dosage forms, containing a combination of 300 units of insulin glargine and either 100 or 150 µg of lixisenatide in a 3mL pre-filled pen.<sup>355</sup> Xultophy contains a combination of 300 units of insulin degludec and 10.8 mg of liraglutide in a 3mL pre-filled pen.<sup>356</sup> Both pens allow for adjustment of dosage strength according to desired insulin titration while maintaining the desired

insulin:GLP1RA ratio.<sup>355,356</sup> Clinical data has shown that these combinations have greater efficacy than either product alone while simultaneously mitigating side effects commonly associated with insulin titration.<sup>355–357</sup> Additionally, since basal insulin is limited to fasting plasma glucose, the benefit of co-administration with GLP1RA's mechanism of action (glucose dependent) has been well-documented in terms of its glycemic control.<sup>351,358–364</sup> Even so, there is no literature investigating the stability profiles of these co-formulations, which seems to indicate that this information has remained proprietary. This lack of literature presents an opportunity for further research in the diabetes co-formulation and device spaces.

The following chapters highlight a compilation of analytical techniques that were developed to characterize generic peptide and mAb biopharmaceutical products to address aspects of chemical and physical degradation in relations to their regulatory approval. The scope of these chapters is applicable to mostly all failed, approved and future biopharmaceutical products.

## **Chapter 2: The Effects of pH and Excipients on the Stability of Exenatide**

### **2.1 Abstract**

Exenatide, a glucagon-like peptide-1 receptor agonist, is the active pharmaceutical ingredient in Byetta<sup>®</sup> and Bydureon<sup>®</sup>, two type 2 diabetes drug products that have generics and multiple follow-up formulations currently in development. Even though exenatide is known to be chemically and physically unstable at pH 7.5, there lacks a systematic evaluation of the impact of pH and excipients on the peptide solution stability. In this study we established analytical methods to measure the chemical and physical degradation of the peptide in solution. Exenatide remained relatively stable at pH 4.5 when incubated at 37°C. At pH 5.5-6.5, degradation was driven by oxidation, while driven by deamidation at pH 7.5-8.5. Significant aggregation of exenatide at pH 7.5 and 8.5 was detected by size exclusion chromatography and dynamic light scattering. Each pH value greater than 4.5 exhibited unique profiles corresponding to a loss of  $\alpha$ -helical content and increase of unordered structures. Addition of sugars, including mannitol, sorbitol and sucrose, conferred small protective effects against monomer loss when incubating at pH 7.5 and 37°C, as measured by size-exclusion chromatography and dynamic light scattering. The results of this study will be useful for investigators developing generic exenatide products, peptide analogs and novel exenatide drug delivery systems.

## 2.2 Introduction

Exenatide, also known as exendin-4, is a 39-amino acid glucagon-like peptide-1 (GLP-1) receptor agonist that acts as an incretin mimetic for the treatment of type II diabetes mellitus.<sup>365</sup> Exenatide retains 53% homology with endogenous human GLP-1, while having several amino acid additions and substitutions that give rise to its increased serum half-life and potency.<sup>263,366,367,368</sup> Exenatide has a partially-folded tryptophan (Trp) cage that prevents degradation by NEP 24.11, the main peptidase responsible for GLP-1 breakdown *in vivo*.<sup>2</sup> Exenatide is the active pharmaceutical ingredient (API) found in AstraZeneca's Byetta<sup>®</sup>, a solution formulation for twice-daily injection, and the more successful Bydureon<sup>®</sup>, which consists of exenatide encapsulated in poly(lactide-co-glycolic acid) (PLGA) microspheres for weekly injection.<sup>281,282</sup> In 2019, Byetta<sup>®</sup> and Bydureon<sup>®</sup> sales reached over \$110 and \$549 million, respectively, in a highly competitive GLP-1 product field.<sup>369</sup> There are no FDA approved generic versions of Byetta<sup>®</sup> or Bydureon<sup>®</sup> currently available. Teva Pharmaceuticals reached an agreement with AstraZeneca in 2016, which became effective in October 2017, allowing them to manufacture and commercialize a generic version of Byetta<sup>®</sup>. Teva Pharmaceutical's product has yet to reach the market due to its pending ANDA FDA approval.<sup>370,371,372</sup> Aside from generics, ongoing research is geared towards the development of novel controlled-release formulations of exenatide, such as hydrogels and nanospheres, as alternatives to Bydureon<sup>®</sup>.<sup>263,365,373–375</sup>

A recently published FDA guidance on ANDA submissions for synthetic peptides highlights the importance of characterizing product-related impurities that may affect the safety, immunogenicity and effectiveness of peptide products.<sup>376</sup> Five peptide

products are specifically mentioned, including glucagon, liraglutide, nesiritide, teriparatide and teduglutide. Additionally, the guidance specifically states that analytical characterization data should include elucidation of primary sequence, identification of chemical impurities, as well as characterization of peptide physicochemical properties and oligomer/aggregation states.

Thus, for both the development of potential generic exenatide drug products and novel extended-release formulations, it is critical to understand the chemical and physical stability of exenatide. Identifying the peptide's potential mechanisms of degradation allows for the optimization of formulation and selection of appropriate manufacturing conditions to avoid the formation of product impurities that may impact its safety and efficacy.<sup>377,225</sup> At present, there are no systematic studies available in the literature investigating exenatide's solution stability. Based on exenatide's sequence, several deamidation and oxidation hot spots are evident, as highlighted by the following underlined peptide residues (HGEGT-FTSDL-SKQME-EEAVR-LFIEW-LKNGG-PSSGA-PPPS-NH<sub>2</sub>). Exenatide contains two likely deamidation sites, N28 and Q12, as well as two likely oxidation sites, M14 and W24. Only some of these chemical impurities are identified and noted in the formulation literature.<sup>375,378</sup> Structurally, exenatide contains three major domains, including an N-terminal unordered, hydrophilic strand (residues 1-10), an  $\alpha$ -helical coil (residues 11-28) and a C-terminal hydrophobic, proline rich, partially-folded Trp-cage (residues 29-39).<sup>285</sup> It has been reported that Trp-cage disruption is likely responsible for the physical degradation of exenatide.<sup>285</sup> While a variety of isolated analytical methods for the characterization of exenatide's purity have been mentioned in regulatory and peer-reviewed literature, an analysis of its impurities

and their underlying degradation mechanisms is missing.<sup>285,379</sup> As such, the goals of this study were to identify and characterize exenatide's chemical and physical degradation through the use of accelerated stability testing to elucidate exenatide's potential underlying degradation mechanisms.

In order to do so, we have developed and implemented several orthogonal analytical techniques to investigate the impact of pH and the addition of excipients (NaCl, mannitol, sorbitol, and sucrose) on exenatide solution stability during prolonged incubation at 37°C. During incubation chemical impurities of exenatide were investigated using reverse phase liquid chromatography (RP-LC) and identified by liquid chromatography-mass spectrometry (RP-LC-MS). Exenatide physical impurities were analyzed by size-exclusion chromatography (SEC), with subsequent examination of particle size distributions by dynamic light scattering (DLS). Structural conformation and content were analyzed by intrinsic fluorescence (IF) and circular dichroism (CD). Overall, our study provides a valuable body of information regarding complex exenatide (and peptide) degradation that can be potentially useful for the approval of generic exenatide versions and the development of novel sustained release formulation.

## **2.3 Materials and Methods**

### **Exenatide**

Exenatide powder was generously provided by Amneal® Pharmaceuticals (Ahmedabad, India). All other materials were purchased from commercial suppliers.

### **Exenatide Incubation Conditions**

Exenatide solutions were prepared at a concentration of 0.5 mg/mL in various 30 mM buffer solutions according to their respective buffer capacities, including sodium

acetate [Acetate] (pH 4.5), sodium citrate [Citrate] (pH 5.5), sodium phosphate [Phosphate] (pH 6.5), HEPES (pH 7.5) and HEPBS (pH 8.5). To investigate the impact of excipients, either salt (154 mM NaCl) or sugar (4.3% w/v mannitol, sorbitol, sucrose or trehalose), which were added to exenatide reconstituted at pH 7.5 and compared against exenatide reconstituted at pH 4.5 with 4.3% (w/v) mannitol, the negative control. Reconstituted exenatide samples at various pH and excipient conditions were subjected to 4 weeks of incubation at 37°C. Samples were removed from the incubator at 0-, 1-, 2- and 4-week time points and immediately analyzed. Samples were either left undiluted at 0.5 mg/mL for analysis by dynamic light scattering (DLS) and intrinsic fluorescence (IF) or diluted to 0.125 mg/mL prior to analysis by reverse phase liquid chromatography (RP-LC), RP-LC-mass spectrometry (RPLC-MS), size exclusion chromatography (SEC HPLC), or circular dichroism spectroscopy (CD), as described below.

### **Reverse Phase Liquid Chromatography**

Exenatide and its chemical degradation impurities were separated by hydrophobicity by RP-LC on a C4-Pack column (YMC) with a Waters 2595 Alliance System interfaced to a 2995 Photodiode Array Detector. Samples were filtered and injected at a concentration of 0.125 mg/mL at a volume of 50  $\mu$ L and delivered using a mobile phase of acetonitrile (ACN) (0.1%TFA) / H<sub>2</sub>O (0.1% TFA) at a flow rate of 1 mL/min with a gradient, ramping from 30 to 55% ACN (0.1% TFA) over 25 minutes. The column temperature was held at 40°C. Exenatide samples were detected from UV absorbance chromatograms that were extracted at 280 nm.

## **Impurity Identification by Liquid Chromatography with Mass Spectrometry**

Exenatide chemical degradation impurities were separated by RP-LC on the same C4-Pack column and analyzed by a dual electrospray ionization equipped Agilent 6520 Accurate-Mass Q-ToF (Agilent Technologies, Santa Clara, CA). Samples were filtered and injected at a concentration of 0.125 mg/mL at an injection volume of 20  $\mu$ L and delivered using a mobile phase of ACN (0.05% TFA) / H<sub>2</sub>O (0.05% TFA) at a flow rate of 0.3 mL/min with a gradient, ramping from 30 to 55% ACN (0.05% TFA) over the course of 25 minutes. The column temperature was also held at 40°C. The MS parameters include a capillary voltage between 1.2 and 2.0 kV, a ToF-MS range of 300 – 3200 m/z, a drying-gas temperature of 325 °C, a drying-gas flow rate of 12 L/min, a nebulizer pressure of 45 psi, and a fragmentor voltage of 225 V. Total ion chromatograms (TIC) were detected at 280 nm, with impurity peak mass extractions generated by Qualitative Analysis Mass Hunter Software (Agilent).

## **Size Exclusion Chromatography**

Exenatide and its physical degradation impurities were separated by molecular weight using SEC on a Superdex Increase 75 10/300 GL column (GE Healthcare) with a Waters 2707 autosampler connected to a 1525 binary HPLC pump, interfaced with a 2489 UV/Vis detector. Samples were filtered and injected at a concentration of 0.125 mg/mL at a volume of 50  $\mu$ L and isocratically delivered with a pH 7.4 PBS mobile phase at a flow rate of 1 mL/min over 25 minutes. Molecular weights of exenatide peaks were determined from a standard calibration, generated from the injection of Uracil (MW 114 Da), aprotinin (MW 6.5 kD), Cytochrome C (MW 14.5 kD), Carbonic Anhydrase (MW 19.5 kD) and BSA (MW 65 kD). Maximum peak height retention times for each standard



( $t_{RS}$ ) were correlated with their MWs when imported onto a semi-log plot with the generated equation being used to estimate the MW of exenatide monomer and aggregate peaks (not shown). Exenatide samples were detected from UV absorbance chromatograms that were extracted at 280 nm.

### **Particle Size Distribution by Dynamic Light Scattering**

Size distributions of exenatide solutions were determined by DLS on a Zetasizer ZSP Nano (Malvern, Worcestershire, UK). 100  $\mu$ L aliquots of undiluted exenatide (0.5 mg/mL) were placed into low-volume TruView cuvettes (Biorad, Hercules, CA) at an undiluted concentration of 0.5 mg/mL and analyzed for particle size distribution. Attenuation and accumulation numbers were automatically optimized for each sample by the instrument prior to analysis. Particle size distributions were reported by volume, with distributions being combined into 0.3-10, 10-100, 100-500, 500-1000 and 1000+  $\mu$ m size ranges.

### **Intrinsic Fluorescence**

Intrinsic fluorescence was used to determine the conformational structure of exenatide. Undiluted exenatide samples placed into a QS 1.5 mm quartz cuvette (Hellma, Mullheim, Germany) were analyzed at an undiluted concentration of 0.5 mg/mL on a SpectraMax M3 (Molecular Devices, San Jose, CA) plate/cuvette reader. The fluorescence was measured using a wavelength emission range of 280 – 450 nm and an excitation wavelength of 270 nm while obtaining fluorescence at 6 flashes per read.

### **Far-UV Circular Dichroism**

The secondary structure of exenatide samples were determined on a J-815 (JASCO) that were diluted to a concentration of 0.125 mg/mL. Instrument sample

temperature was held at 37°C using a Peltier attachment. CD spectra were averaged from 5 collected scans over a wavelength range of 245 to 195 nm, with an accumulation rate of 20 nm/min and a data integration time (DIT) of 4 seconds. Percent  $\alpha$ -helix,  $\beta$ -sheet and unordered secondary structures were quantified using a third-party Spectra Manager Suite (JASCO) add-in, CDPPro analysis. In this software, the CONTIN method was chosen, using soluble-membrane protein 56 (SMP 56) as the reference protein for secondary structure analysis.

## 2.4 Results

### Forced Chemical Degradation

#### Identification of Degradation Impurities by LC-MS QToF

LC-MS-QToF was implemented to analyze potential exenatide chemical impurity formation. Short-term accelerated exenatide degradation was induced by reconstituting exenatide at pH 8.5 and incubating at an elevated temperature of 60°C for 24 hours. Exenatide's parent peak was separated from its chemical impurities by reverse phase liquid chromatography (RP-HPLC) on a C4 Pack column. Fig. 2-1A depicts a total ion chromatogram (TIC) with the respective peak identities. A total of 9 different peaks were identified for exenatide (Fig. 2-1B-J) relative to its average mass of 4816 Da, which included the formation of a PyroQ impurity and different combinations of oxidations and deamidations.<sup>380</sup> The peak at a  $m/z$  was an internal standard.

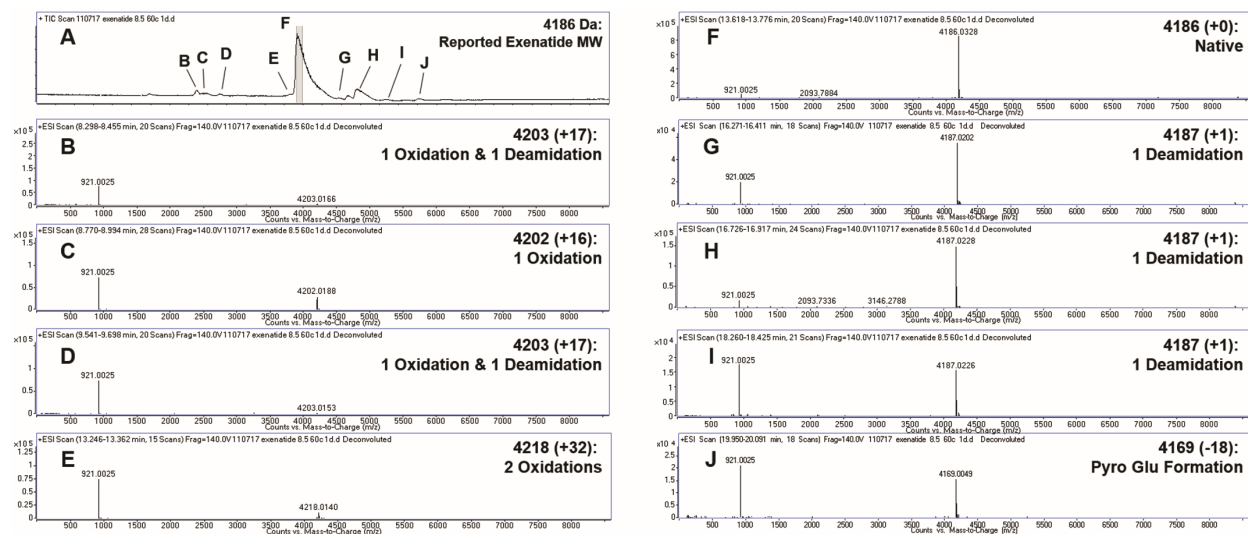


Figure 2-1. Identification (w/ deconvoluted masses) of exenatide's chemical impurities by RPLC-MS QToF following incubation of peptide solution (pH 8.5) at 60°C for 24 hours. RP-HPLC C4 UV absorbance (A) total ion chromatograms (TIC) and (B-E, G-J) exenatide chemical impurities and their reported respective mass shifts, which include a combination of oxidation, deamidation and PyroQ formation, from (F) native exenatide's MW of 4186 Da.

Peak F was identified as exenatide's native state parent peak (+0); peaks C and E, single (+16) and double oxidations (+32), respectively; peaks B and D, a combination of an oxidation and a deamidation (+17); peaks G, H, and I, a single deamidation (+1); and peak J, PyroQ formation from a glutamine (Q12). A previously published study has confirmed that the primary deamidation site for exenatide is N28 when incubated in pH 7.4 phosphate buffer at 37°C for 56 days.<sup>284</sup> As expected, deamidations occurred at the N28 G29 residue combination, a prolific peptide and protein deamidation hotspot.<sup>225,224,381</sup> The major deamidation impurity (Peak H) in both studies had been previously identified as the conversion to L-isoAspartate [L-isoAsp], while the minor impurity (peak G) was identified as the conversion to D-isoAspartate [D-isoAsp]<sup>284</sup>. We would expect that the observed oxidation is occurring at Met14, another primary degradation hotspot that has been implicated to affect peptide and protein stability.<sup>225,224,381,382</sup> Additional LS-MS/MS studies are needed to identify specific oxidation impurities.

## Forced Chemical Degradation at 37°C

Chemical degradation profiles were determined for exenatide solutions that were reconstituted between pH 4.5 - 8.5 and subject to incubation at 37°C for 4 weeks. Exenatide's parent peak was separated from its chemical impurities on an RPLC column. Parent peak (Fig. 2-2A) and oxidation (Fig. 2-2B) and deamidation (Fig. 2-2C) impurities were quantified over the course of incubation.

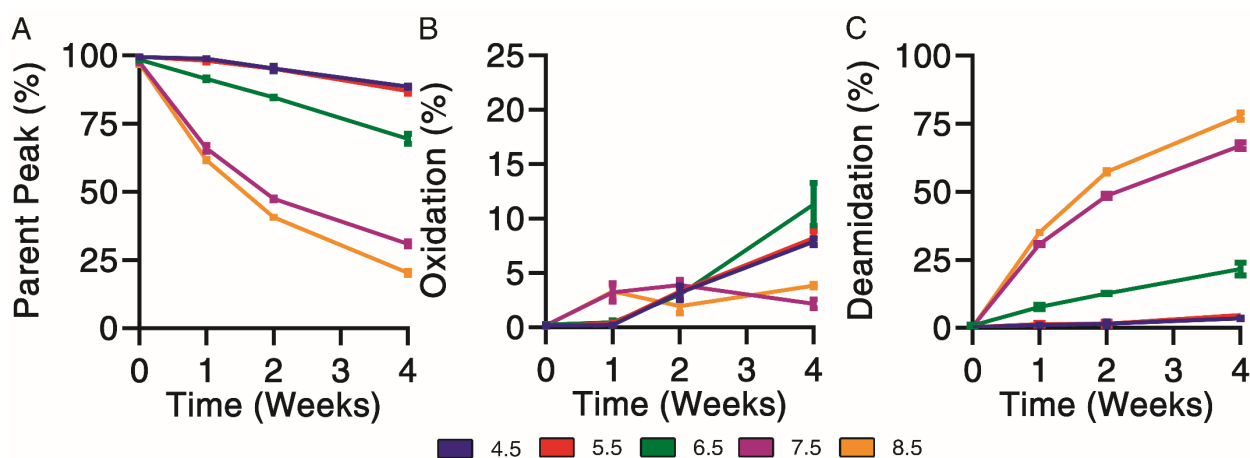


Figure 2-2. Kinetics of chemical degradation determined by RP-LC separating (A) parent peak from (B) oxidation and (C) deamidation chemical impurities during incubation of exenatide solutions pH 4.5 – pH 8.5 at 37°C for 4 weeks. (n = 3, mean ± SEM).

When incubated at pH 4.5 and 5.5, the exenatide parent peak remained relatively stable over the course of incubation, decreasing to  $88.6 \pm 0.7\%$  and  $87.0 \pm 1.4\%$ , after 28 days of incubation, respectively. The relative stability of exenatide at low pH was expected as Byetta® is commercially formulated in an acetate buffer solution of pH 4.5. On the other hand, a rapid, pH-dependent degradation of exenatide was observed when reconstituted at pH 6.5, 7.5 and 8.5. We also observed a loss in total AUC during incubation indicating some precipitation occurring at pH 7.5 and 8.5 over 4 weeks decreasing to an average of  $71.9 \pm 10.1\%$  and  $70.9 \pm 9.8\%$  relative to day 0, respectively (Fig. 2-3B). This precipitation was confirmed by appearance of larger particulates during incubation as measured by DLS.

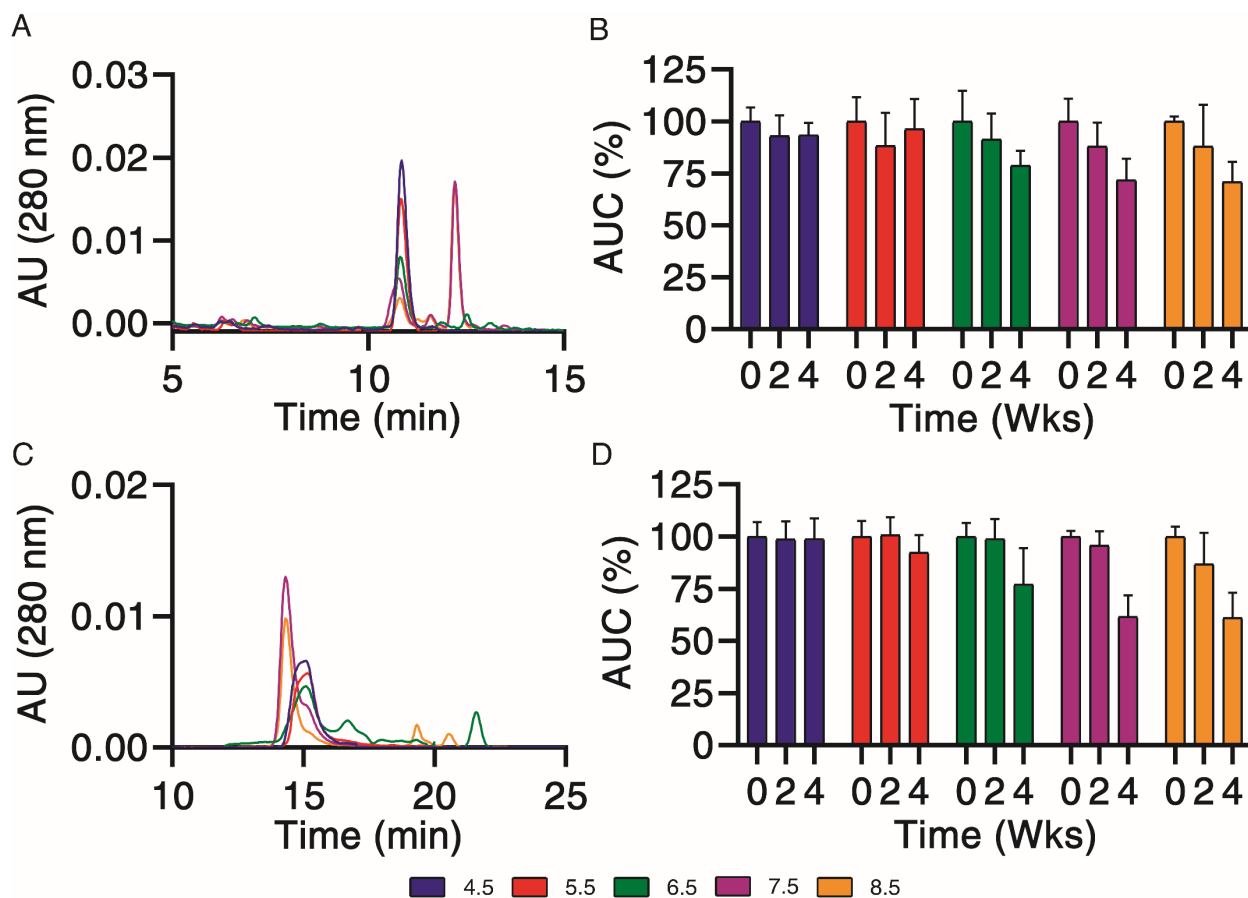


Figure 2-3. A) RP-LC chromatograms after 4 weeks of incubation and B) AUCs (relative to day 0) and C) SEC-LC chromatograms after 4 weeks of incubation and D) AUCs (relative to day 0) for exenatide samples reconstituted at pH 4.5 – 8.5 over the course of incubation at 37°C for 4 weeks.

Chemical degradation appears to be mainly oxidation driven from pH 4.5 to 6.5.

As previously mentioned, we would expect that this would likely occur at the methionine residue. Oxidation was identified by the presence of a split peak around a retention time of 6.5 minutes, with total oxidation being the summation of peaks that elute prior to the parent peak (Supp. Fig. 2-3A). Over the course of long-term incubation, chemical degradation of exenatide at pH 7.5 and 8.5 also appears to be driven mainly by deamidation, with the parent peak decreasing to  $30.9 \pm 1.6\%$  and  $20.3 \pm 1.1\%$  and deamidation impurity peaks increasing to  $67.0 \pm 2.2\%$  and  $77.8 \pm 1.9\%$ . We would expect the formed impurity to occur at the N28 residue, as it is followed by a glycine, a

well-known deamidation hotspot combination.<sup>225,224</sup> A major deamidation impurity, previously identified as the conversion to L-isoAsp, formed at a retention time of 12.4 minutes while a minor deamidation impurity, previously identified as conversion to D-isoAsp, formed at a retention time of 11.8 minutes (D-isoAsp). It has been previously reported that isolated L-isoAsp and isolated D-isoAsp impurities exhibit weaker GLP1 receptor binding.<sup>284</sup>

### Forced Physical Degradation at 37°C

Aggregation has been identified as an important instability mechanism in both peptides and proteins.<sup>225</sup> Specifically, aggregation has been suggested to occur through the disruption of exenatide's partially-folded, protective Trp cage though studies have remained lacking.<sup>285</sup> Physical degradation profiles were also determined for exenatide solutions reconstituted between pH 4.5 - 8.5 that were subject to incubation at 37°C for 4 weeks. An SEC column was used to separate and quantify monomers (Fig. 2-4A), aggregates (Fig. 2-4B) and fragments (Fig. 2-4C) over the course of incubation.

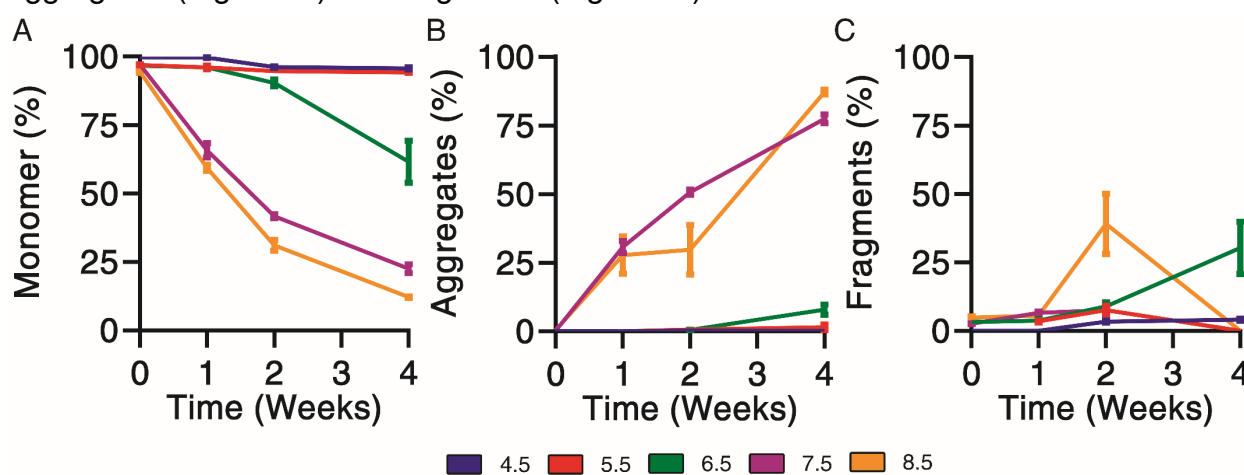


Figure 2-4. Kinetics of physical degradation determined by SEC-LC, separating (A) monomer from (B) aggregate and (C) fragment physical impurities of exenatide reconstituted at pH 4.5 – pH 8.5 after incubation at 37°C for 4 weeks. (n = 3, mean ± SEM).and Orange = 8.5.

Physical degradation, in terms of monomer loss, appears to occur in a pH dependent manner. Exenatide incubated at pH 4.5 and 5.5 remained relatively stable

over the course of incubation, with monomer decreasing to  $95.7 \pm 0.8\%$  and  $94.2 \pm 0.1\%$ , respectively, after 4 weeks of incubation. Again, the relative stability of exenatide at low pH was expected as Byetta® is commercially formulated in acetate buffer (pH 4.5).<sup>383</sup> Physical degradation tendencies vary significantly at pH 6.5 and above in terms of aggregation and fragmentation. Exenatide reconstituted at pH 6.5 tends to form fragments after 2 and 4 weeks of incubation, increasing to  $9.0 \pm 2.5\%$  and  $30.3 \pm 16.4\%$ , rather than aggregates, which increased slightly,  $0.6 \pm 0.2\%$  and  $8.0 \pm 1.9\%$ , respectively. On the other hand, exenatide reconstituted at pH 7.5 forms mainly aggregates, increasing to  $50.6 \pm 1.8\%$  and  $77.4 \pm 2.9\%$  after 2 weeks and 4 weeks of incubation, respectively. The total AUCs for SEC chromatograms decreased over the course of incubation at pH 7.5 and 8.5 reaching  $61.6 \pm 0.3\%$  and  $61.1 \pm 12.1\%$  of the initial values, indicating peptide precipitation.

### **Characterizing Particle Size Distribution by DLS**

To further characterize pH-dependence of aggregation of exenatide during incubation, particle size distributions were determined by DLS. Particles were measured by volume since intensity measurements were skewed by exenatide's non-spherical nature. Particles were combined into 0.3-10, 10-100, 100-500, 500-1000 and 1000+  $\mu\text{m}$  size ranges with distributions shown for an incubation over the course of 4 weeks at 37°C (Table 2-1). While DLS measurement is inherently highly variable, several trends were observed, corroborating the formation of oligomers during incubation at higher pH values as had been observed through the reduction of SEC and C4 AUCs. For pH 4.5 and 5.5, peptide was found to be primarily in the 0.3-10  $\mu\text{m}$  size range throughout incubation, although some formation of oligomers was detected at pH 5.5 following 4

weeks of incubation. At higher pH values (6.5 to 8.5) the reduction of the 0.3-10  $\mu\text{m}$  fraction was observed during incubation, as well as an increase in particulates of 10-1000  $\mu\text{m}$  size range.

<b>DLS (by Volume)</b>		<b>0.3-10 <math>\mu\text{m}</math></b>	<b>10-100 <math>\mu\text{m}</math></b>	<b>100-500 <math>\mu\text{m}</math></b>	<b>500-1000 <math>\mu\text{m}</math></b>	<b>1000+ <math>\mu\text{m}</math></b>
<b>4.5</b>	<b>0 Weeks</b>	77.8	3.5	18.6	0.1	0
	<b>1 Week</b>	100	0	0	0	0
	<b>2 Weeks</b>	100	0	0	0	0
	<b>4 Weeks</b>	100	0	0	0	0
<b>5.5</b>	<b>0 Weeks</b>	100	0	0	0	0
	<b>1 Week</b>	100	0	0	0	0
	<b>2 Weeks</b>	100	0	0	0	0
	<b>4 Weeks</b>	77.8	0	8.8	13.3	0.1
<b>6.5</b>	<b>0 Weeks</b>	100	0	0	0	0
	<b>1 Week</b>	55.6	11.1	28.2	5.1	0
	<b>2 Weeks</b>	88.9	0	1.8	9.3	0
	<b>4 Weeks</b>	33.3	32.5	20.6	13.5	0
<b>7.5</b>	<b>0 Weeks</b>	100	0	0	0	0
	<b>1 Week</b>	88.9	0	9.4	1.8	0
	<b>2 Weeks</b>	100	0	0	0	0
	<b>4 Weeks</b>	33.4	25.2	36.1	5	0.4
<b>8.5</b>	<b>0 Weeks</b>	100	0	0	0	0
	<b>1 Week</b>	44.4	0	54.5	0.9	0.2
	<b>2 Weeks</b>	66.7	29.5	3.8	0	0
	<b>4 Weeks</b>	0	0	27.4	70.1	2.5

Table 2-1. Particle size distribution determined by DLS (by volume) and separated into 0.3 – 10, 10 – 100, 100 – 500, 500 – 1000 and 1000+  $\mu\text{m}$  size ranges for exenatide that was reconstituted at pH 4.5 – 8.5 after incubation at 37°C for 4 weeks; (n = 3, mean).

### Structural Analysis by IF and CD

Understanding the underlying structural changes of peptides is especially important when investigating degradation profiles, as they provide more insight into the impact of chemical and physical degradation profiles on structure. Tertiary and



secondary structures of exenatide samples reconstituted at pH 4.5 - 8.5 were analyzed by IF and CD over 4 weeks of incubation at 37°C (Fig. 2-5).

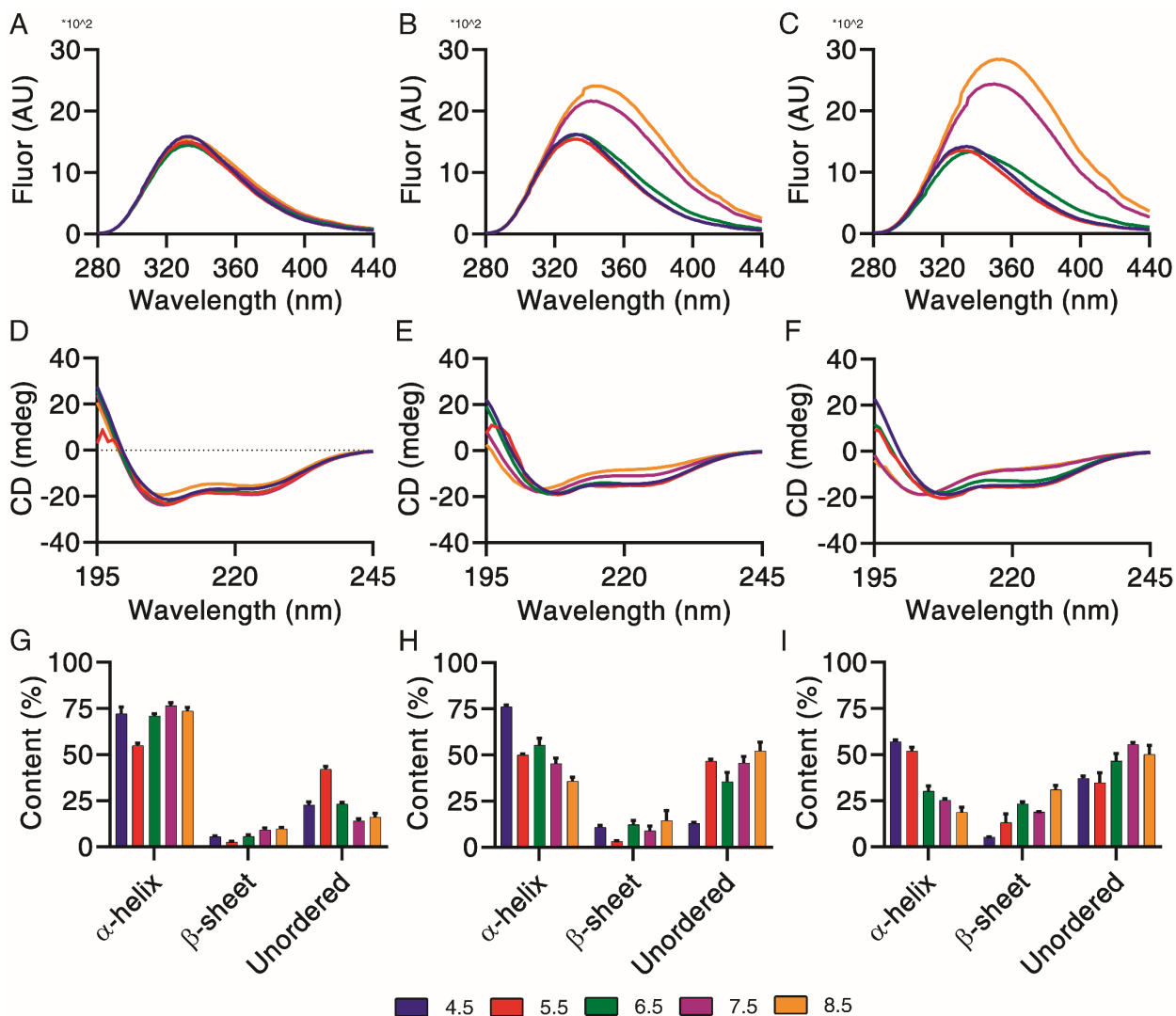


Figure 2-5. Structural and conformational changes characterized and measured by (A-C) intrinsic fluorescence and (D-F) circular dichroism, with secondary structures (G-I) quantified by CDPro analysis ( $n = 3$ , mean  $\pm$  SEM) for exenatide that was reconstituted at pH 4.

IF was used to qualitatively investigate exenatide's conformational structure when subject to incubation, where both increases of intrinsic fluorescence and a right shift of maximum emission wavelengths (red shift) indicated unfolding through increased solvent exposure of Trp (Fig. 2-5A-C). Trp solvent exposure is an important structural indicator in exenatide, as the Trp is typically buried in a proline rich C-terminal cage that stabilizes exenatide<sup>285</sup>. Initially, the intrinsic fluorescence profiles were very

similar for all pH conditions in terms of fluorescence intensity (~1500 units) and maximum emission wavelengths (333 nm). After 2 weeks and 4 weeks of incubation at 37°C, the IF profiles of exenatide reconstituted at pH 4.5 and 5.5 were unchanged, retaining maximum emission wavelengths of 333 nm. After 4 weeks of incubation at pH 6.5, there was an observable right shift of maximum emission wavelength to 341 nm, though with a decrease of fluorescence intensity, which may potentially indicate both Trp cage unfolding and structural rearrangement. Exenatide showed a significant, time-dependent, increase of fluorescence intensity and a right shift of maximum emission wavelength at elevated pHs. Following 2 weeks and 4 weeks of incubation, exenatide reconstituted at pH 7.5 showed an increase of fluorescence intensity to 2150 and 2425 units, respectively, and a right shift of maximum emission wavelengths to 342 and 348 nm, respectively. A similar change was seen for exenatide reconstituted at pH 8.5 where changes were even more drastic than pH 7.5 in terms of fluorescence intensity, increasing to 2390 and 2835 units, respectively, and maximum emission wavelengths, shifting to 344 nm to 354 nm, respectively. Together, they indicate both unfolding and an increase of Trp solvent exposure.

CD is useful in combination with IF, providing further information on underlying secondary structural changes, including shifts of distributions between of  $\alpha$ -helical,  $\beta$ -sheet and unordered content. Exenatide samples were qualitatively measured by CD (Fig. 2-5D-F) and then quantified by CDPro analysis (Fig. 2-5G-I). At week 0, base emission wavelengths were 208 nm for all samples. Quantified secondary structures were similar for all pH conditions, apart from pH 5.5. Over the course of incubation, exenatide incubated at pH 4.5 retained a base emission wavelength of 208 nm, though

quantified secondary structures over the course of incubation showed a loss of  $\alpha$ -helical content ( $72.3 \pm 6.1\%$  at 0 weeks vs  $57.1 \pm 1.6\%$  after 4 weeks) and increase of unordered content ( $22.7 \pm 2.8\%$  at 0 weeks vs  $37.1 \pm 2.1\%$  at 4 weeks). Exenatide reconstituted at pH 5.5 also retained a base emission wavelength of 208nm. While having a lower initial amount of  $\alpha$ -helical content, the distribution of secondary structural content remained unchanged over the course of incubation. The  $\alpha$ -helical content for exenatide reconstituted at pH 6.5, 7.5 and 8.5 decreased in a pH dependent manner from  $70.9 \pm 2.2\%$ ,  $76.6 \pm 2.6\%$  and  $73.7 \pm 3.4\%$  at week 0, respectively, to  $30.1 \pm 5.1\%$ ,  $25.4 \pm 1.3\%$ , and  $18.75 \pm 4.0\%$  after 4 weeks, respectively. Loss of  $\alpha$ -helical content was generally matched by an increase of unordered content for the exenatide samples reconstituted at pH 6.5-8.5.

### **The Impact of Excipients on Degradation at pH 7.5**

It is known that the addition of sugar excipients can generally offer protection from peptide and protein aggregation during freeze/thaw cycles and long-term storage, while other excipients, like salt, may negatively induce aggregation.<sup>225,224</sup> The impact of these types of excipients on chemical and physical degradation profiles was investigated for exenatide reconstituted at pH 7.5 and incubated for 4 weeks at 37°C. Common excipients, including salt (NaCl) and various sugars (mannitol, sorbitol and sucrose) were added at iso-osmolar concentrations (154 mM and 4.3% w/v, respectively), to determine if they would alter degradation profiles. Parent peak (Fig. 2-6A), oxidation (Fig. 2-6B) and deamidation (Fig. 2-6C) profiles for exenatide after 4 weeks of incubation are shown here.

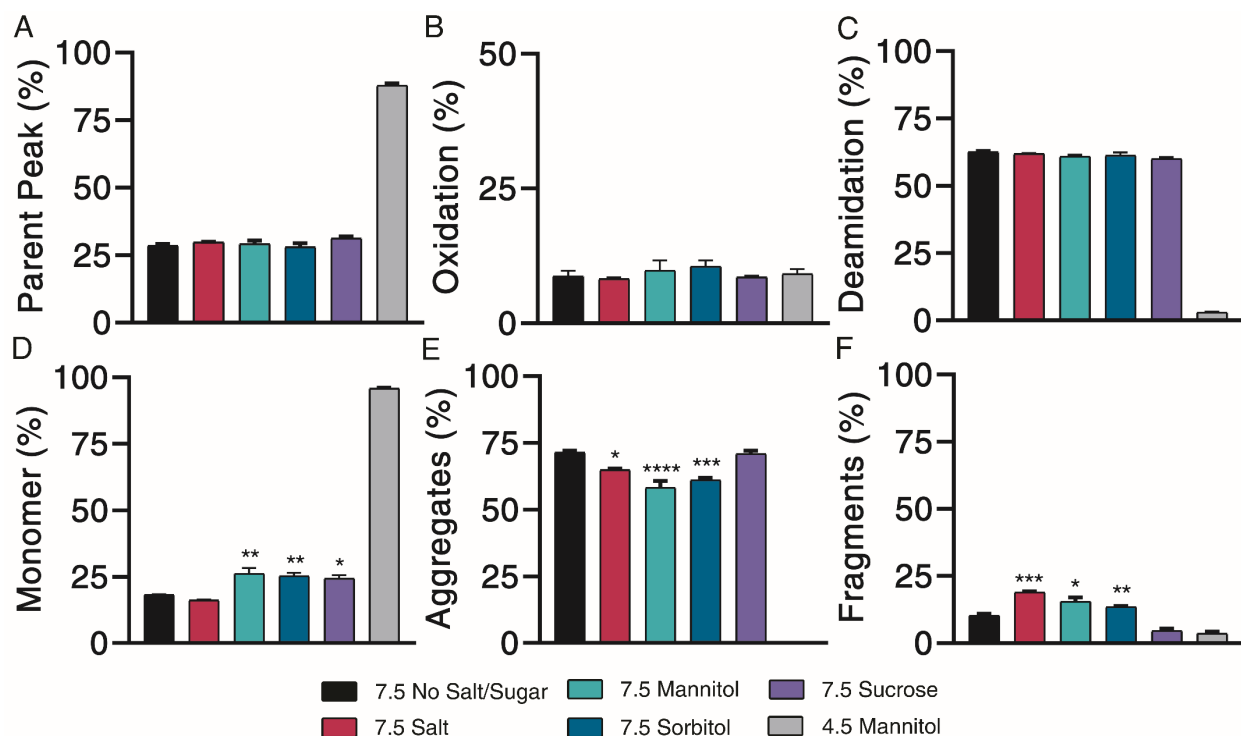


Figure 2-6. Kinetics of degradation determined by RP-LC and SEC-LC, with RP-LC separating (A) parent peak from (B) oxidation and (C) deamidation chemical impurities and SEC-LC separating (D) monomer from (E) aggregate and (F) fragment physical impurities of exenatide reconstituted at pH 4.5 w/ mannitol and pH 7.5 with specified excipients after incubation at 37°C for 4 weeks. (n = 3, mean ± SEM, \* p < 0.05 \*\* p < 0.01 \*\*\* p < 0.001).

Exenatide reconstituted at pH 4.5 with 4.3% mannitol was the negative control (Byetta<sup>®</sup> formulation). Our results indicate that the addition of different excipients had limited effects on chemical exenatide's stability at pH 7.5. Compared to the negative control, where 87.8 ± 0.8% of the parent peak remained intact, pH 7.5 formulations had significant parent peak loss, decreasing to approximately 30% after 4 weeks of incubation. All formulations experienced similar levels of oxidation during the incubation period. The negative control contained significantly less deamidated species compared to pH 7.5 formulations (approximately 3% vs. 60%) after 4 weeks of incubations. We also observed some total AUC loss, decreasing to an average between approximately 60 and 80% at 4 weeks relative to day 0 for all pH 7.5 formulations, indicating some precipitation occurring over the course of incubation (Fig. 2-7B).

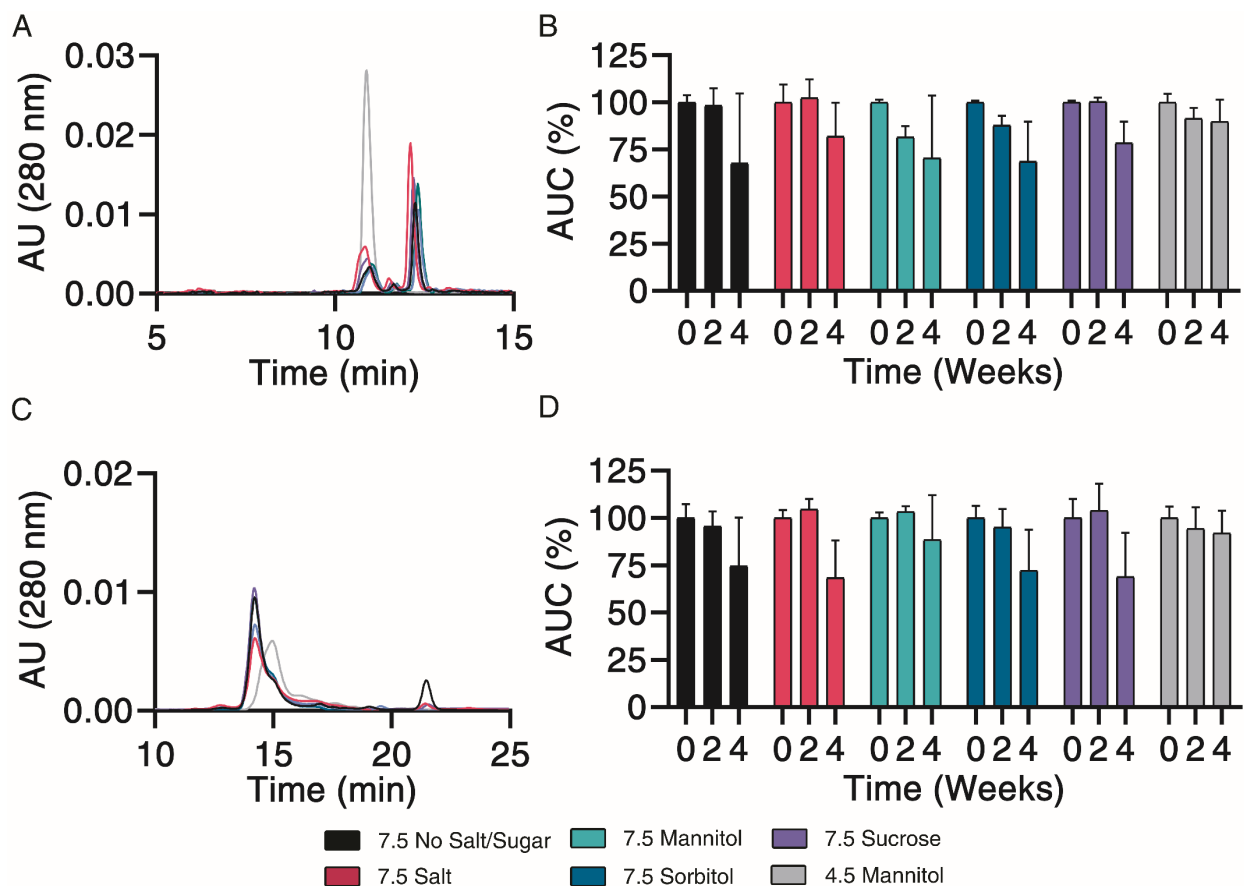


Figure 2-7. RP-LC chromatograms after 4 weeks of incubation and B) AUCs (relative to day 0) and C) SEC-LC chromatograms after 4 weeks of incubation and D) AUCs (relative to day 0) for exenatide samples reconstituted at pH 4.5 w/ mannitol vs pH 7.5 w/ specified excipients over the course of incubation at 37°C for 4 weeks.

An SEC column was used to separate and quantify monomers (Fig. 2-6D), aggregates (Fig. 2-6E) and fragments (Fig. 2-6F) over the course of incubation. SEC analysis after 4 weeks of incubation revealed significant monomer loss for all pH 7.5 formulations compared to the negative control after 4 weeks (approximately 20% vs. 95% remaining). Monomer loss was significantly greater for the pH 7.5 formulation without excipient ( $18.3 \pm 0.1\%$ ) than formulations containing mannitol ( $26.3 \pm 2.0\%$ ), sorbitol ( $25.4 \pm 1.1\%$ ) and sucrose ( $24.4 \pm 1.3\%$ ) ( $p < 0.05$  for all solutions), indicating protective abilities of these excipients against physical instability, though not against

chemical instability. Exenatide physical impurities were present mainly in the form of aggregates at pH 7.5.

Further characterization of peptide aggregates was performed using DLS. Our data showed that exenatide was very stable at pH 4.5, with particles staying in the 0.3-10- $\mu\text{m}$  size range for the entire incubation. At pH 7.5, sucrose, mannitol, and sorbitol exhibited significant stabilizing effects on exenatide against aggregation, as indicated by 100% of particles present in the 0.3-10  $\mu\text{m}$  size range after 4 weeks compared to excipient-free formulation which had 67% in this size range (Table 2-2). The NaCl formulation resulted in significant shifts in particle size distribution, with most particles being in the 10-100  $\mu\text{m}$  range (NaCl) after 4 weeks.

<b>DLS (by Volume)</b>	<b>0.3-10 <math>\mu\text{m}</math></b>	<b>10-100 <math>\mu\text{m}</math></b>	<b>100-500 <math>\mu\text{m}</math></b>	<b>500-1000 <math>\mu\text{m}</math></b>	<b>1000+ <math>\mu\text{m}</math></b>
<b>4.5 Mannitol</b>	100	0	0	0	0
<b>7.5 No Salt/Sugar</b>	66.6	0	19.8	13.6	0
<b>7.5 NaCl</b>	0	41.9	37.5	20.6	0
<b>7.5 Mannitol</b>	100	0	0	0	0
<b>7.5 Sorbitol</b>	100	0	0	0	0
<b>7.5 Sucrose</b>	100	0	0	0	0

Table 2-2 Particle size distribution determined by DLS (by volume) and separated into 0.3 – 10, 10 – 100, 100 – 500, 500 – 1000 and 1000+  $\mu\text{m}$  size ranges for exenatide that was reconstituted at pH 4.5 w/ mannitol and pH 7.5 w/ specified excipients when incubated at 37C after weeks; (n = 3, mean).

Subsequent structural analysis by IF and CD revealed the pH 4.5 mannitol formulation to be the most stable. All pH 7.5 formulations experienced a significant red shift of maximum emission wavelength as well as an increase in maximum fluorescent intensity after 4 weeks, indicative of unfolding and Trp solvent exposure (Fig. 2-8A,D).

CD Pro analysis showed no observable differences between excipient spectra at 0 (Fig. 2-8) and 4 weeks (Fig. 2-8E) of incubation. CD pro analysis prior to incubation showed that all formulations contained similar percentages of  $\alpha$ -helix,  $\beta$ -sheet, and unordered content (Fig. 2-8C). After 4 weeks, the secondary structural content was additionally similar across all formulations, resulting in the formation of unordered content and  $\beta$ -sheet structures. (Fig. 2-8F). Taken together, the addition of sucrose, mannitol, and sorbitol to exenatide formulation at pH 7.5 shown modest stabilization effect against monomer loss, but only by SEC.

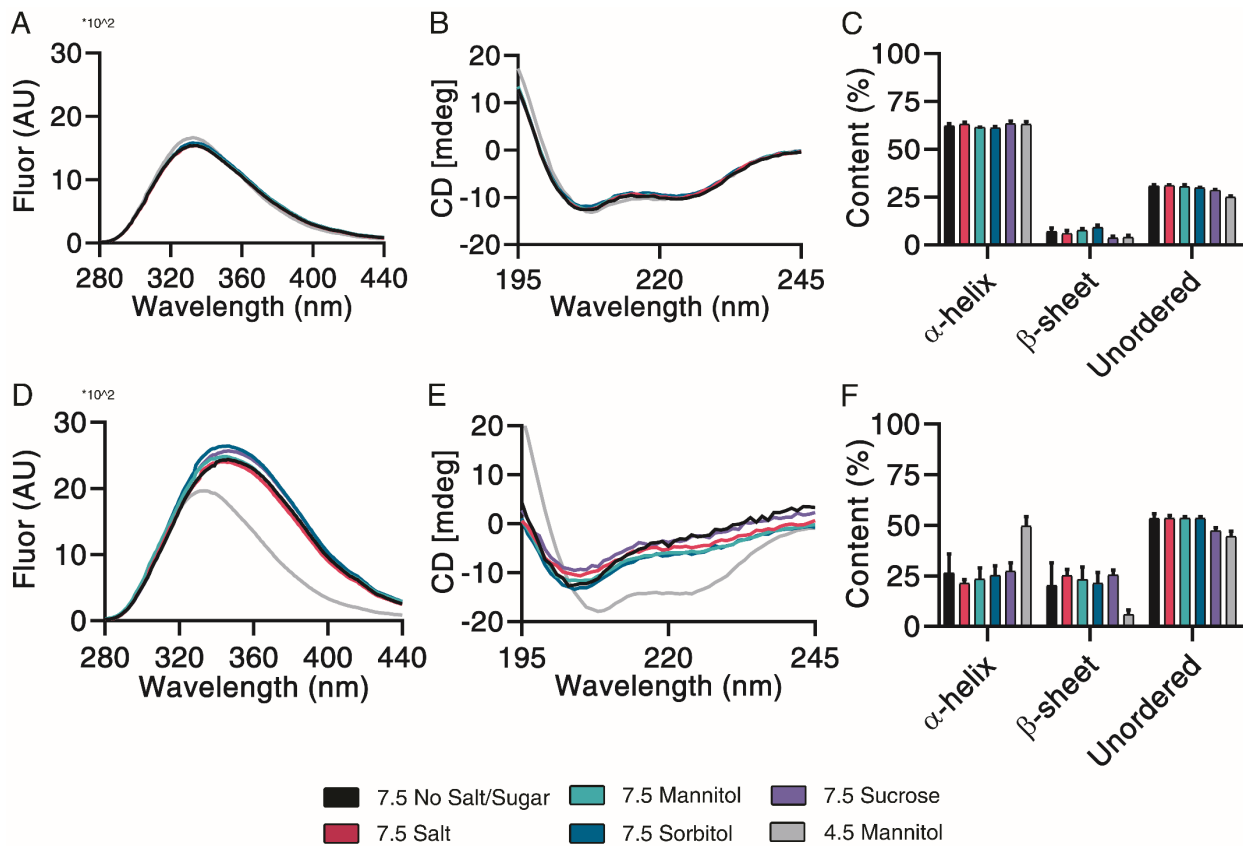


Figure 2-8 Structural and conformational changes characterized and measured by intrinsic fluorescence (A,D) and circular dichroism (B,E), with secondary structure quantified by CDPro analysis (C,F) for exenatide that was reconstituted at pH 4.5 w/mannitol and pH 7.5 w/ specified excipients after incubation at 37°C for 4 weeks. (n = 3, mean  $\pm$  SEM).

## 2.5 Discussion

Exenatide appears to undergo a rapid, pH-dependent degradation at pH 6.5 and above while remaining relatively stable at lower pH over the course of incubation. Analogously, endogenous GLP-1 has also shown degradation when pH was slightly increased, though pH was adjusted on a smaller scale.<sup>384</sup> While loss of exenatide's parent peak and monomer detected by LC is pH-dependent, impurity formation varied, with mainly oxidation and fragmentation occurring at pH 6.5, deamidation and aggregation at pH 7.5 and 8.5. Particle size distributions determined by DLS seemed to further confirm these relationships, indicating size distribution shifts toward the formation of oligomers at higher pH values. Additionally, trends for structural degradation of exenatide reconstituted at an elevated pH seemed to match, where exenatide reconstituted at pH 6.5 and 8.5 had greater amounts of  $\beta$ -sheet formation than exenatide reconstituted at pH 7.5. While deamidation is rapidly occurring at pH 7.5 and above, it remains undetermined whether significant unfolding of structure is related to, or simply simultaneously occurring with, deamidation. Additionally, though not statistically significant, we observed a trend of total AUC loss after 4 weeks of incubation by C4 and SEC for exenatide reconstituted at pH 6.5 – 8.5. This seems to indicate some amount of larger aggregate formation occurring at elevated pH over the course of incubation further confirming DLS findings.

Exenatide chemical impurities were identified by LC-MS QToF, revealing several deamidations (+1 mass shift), oxidations (+16/+32 mass shifts) oxidation/deamidation mixtures (+17 mass shift) and pyro-Q impurity formations. However, we have limited knowledge of the actual amino acid residue location of these modifications, as



exenatide contains two potential deamidation and two potential oxidation sites. We identified three deamidation peaks based on LC-MS QTOF (mass shift +1), with one major peak that rapidly increases at high pH in a solution incubated at an elevated temperature. We speculate that the major deamidation occurred on asparagine (N28) as this amino acid is followed by glycine (G29), the most prominent deamidation hot spot.<sup>237,84</sup> Another deamidation is potentially occurring on the glutamine residue (Q13). In addition, different C4 deamidation peaks with a mass shift of +1 could be attributed to conformational peptide changes resulting from the formation of two different asparagine deamidation products (aspartic or iso-aspartic acid).<sup>225</sup> In terms of oxidation, an impurity that has not been previously studied, we have identified a +32 mass shift that could be attributed to single oxidation of two residues or a double oxidation of one residue. It appears that this oxidation is likely forming at the M14 residue, as the Trp-cage protects the Trp at low pH. Additional analysis of isolated impurity peaks is needed to confirm exenatide degradation product identities.

Our experiments investigating the impact of different excipients on exenatide's stability at pH 7.5 revealed the limited ability of excipients to stabilize exenatide as well as their varied effects on exenatide's degradation profile. We did observe minor stabilizing effects protecting against the loss of monomer by mannitol, sorbitol and sucrose, though they were unable to prevent chemical degradation. The main impurities observed were aggregation and deamidation for all formulations after 4 weeks of incubation. Fragmentation was significantly reduced in the formulation containing sucrose.

While we have determined a pH-dependence in exenatide's degradation kinetics, we have not fully defined the mechanism of peptide aggregation. Currently, we propose that degradation occurs through two different mechanisms. At low pH, M14 would seem to undergo oxidation as the Trp is protected by the Trp cage. M14 oxidation in exenatide's helical region could lead to alpha helix disruption and potential degradation and fragmentation, which was observed at pH 6.5. At high pH, N28 appears deamidated, as shown by RPLC, and unfolded at the Trp-cag, resulting in an increase of unordered structures by CD, which then can lead to further degradation including dimerization, formation of larger aggregates and precipitation, as seen by loss of AUC. Considering the recently published FDA guidance for synthetic peptides, and previously published literature about exenatide's ability to elicit immunogenic responses, further investigation of the impact of formed exenatide impurities on immunogenicity may be warranted.<sup>263,376,385</sup>

## Chapter 3: Biosimilarity Under Stress: A Forced Degradation Study

### 3.1 Abstract

Remsima™, marketed as Inflectra™ in the US, (infliximab) is the first biosimilar monoclonal antibody (mAb) approved by the European Medical Agency and the Food and Drug Administration. Remsima™ is highly similar to its reference product, Remicade®, with identical formulation components. The 2 products, however, are not identical; Remsima™ has higher levels of soluble aggregates, C-terminal lysine truncation, and fucosylated glycans. To understand if these attribute differences could be amplified during forced degradation, solutions and lyophilized powders of the 2 products were subjected to stress at elevated temperature (40–60°C) and humidity (dry-97% relative humidity). Stress-induced aggregation and degradation profiles were similar for the 2 products and resulted in loss of infliximab binding to tumor necrosis factor and FcγRIIIa. Appearances of protein aggregates and hydrolysis products were time- and humidity-dependent, with similar degradation rates observed for the reference and biosimilar products. Protein powder incubations at 40°C/97% relative humidity resulted in partial mAb unfolding and increased asparagine deamidation. Minor differences in heat capacity, fluorescence, levels of subvisible particulates, deamidation and protein fragments were observed in the 2 stressed products, but these differences were not statistically significant. The protein solution instability at 60°C, although quite significant, was also similar for both products. Despite the small initial analytical differences, Remicade® and Remsima™ displayed similar degradation mechanisms and

kinetics. Thus, our results show that the 2 products are highly similar and infliximab's primary sequence largely defines their protein instabilities compared with the limited influence of small initial purity and glycosylation differences in the 2 products.

### 3.2 Introduction

Looming patent expirations for lucrative protein drugs have led to a surge in development, regulatory filings, and approvals for biosimilar products.<sup>386</sup> Infliximab was the first biosimilar monoclonal antibody (mAb) to receive approval by the European Medical Agency and, recently, by the US Food and Drug Administration.<sup>300,3</sup> The approved biosimilar Remsima™, Inflectra™ in the US, is manufactured by Celltrion (Incheon, South Korea) and is a copy of Remicade®, manufactured by Janssen. Infliximab is approved for various indications, including rheumatoid arthritis, ankylosing spondylitis, and inflammatory bowel diseases such as ulcerative colitis and Crohn's disease.<sup>387</sup> Detailed analytical comparison of Remicade® and Remsima™ shows significant product similarity, apart from differences in glycan composition, as well as minor differences in levels of soluble aggregates and basic charged variants.<sup>41,135,300,348</sup> These product variances are not surprising since the biosimilar protein is produced using a different clone of Sp2/0 murine hybridoma cell line, a different manufacturing processes, and in different facilities.<sup>43,300,8</sup> Additionally, while the formulations of the 2 products are identical, the final lyophilization process as well as the sources for formulation excipients are likely different. These process and excipient differences could result in various levels of reactive species, such as reduced sugars and peroxide impurities of polysorbates, capable of protein modification during product

storage. These factors may all contribute to product quality, safety and efficacy, and ultimately make demonstrating biosimilarity challenging.

One strategy to evaluate biosimilarity is to compare biosimilar and reference products in forced degradation studies using thermal, mechanical, or chemical stressors.<sup>389-391</sup> Forced degradation studies are usually performed in the development cycle of biotherapeutics to select formulation excipients, develop dosage forms, and determine product shelf life.<sup>389,391</sup> These studies are also used during manufacturing process validation to define hold times, for process intermediates, and in analytical method development to define resolving abilities of various assays. The stress testing conditions used for these analyses are far more extreme than the actual physical and thermal stresses that the product vials are exposed to during manufacturing, transport, storage, and handling by physicians or patients. The results from stress testing likely over-exaggerates the extent of product difference and should, thus, be interpreted with caution. However, stress conditions accelerate protein degradation, enrich impurity levels, and thereby improve analytical resolution to aid with analytical development. Ultimately, examination of protein products under stressed conditions give insights into the mechanisms of how these proteins may unfold, lose efficacy, aggregate, and become immunogenic. Forced degradation studies generate valuable analytical data, in relatively short periods of time, to compare biosimilar and reference products and to help link protein structural information with product quality, safety and efficacy.<sup>389,391</sup>

In this study, we use Remicade<sup>®</sup> and Remsima<sup>™</sup> as a model reference and biosimilar product pair to investigate whether small variances in initial product purity and

manufacturing process between the 2 products could influence protein instability upon stress degradation. Comparisons between batch release data of biosimilar and reference product provide the most important information for assessment of product safety, efficacy and biosimilarity. However, minor structural differences between products may be amplified upon stressing, and such stress testing could provide additional information for biosimilarity evaluation. When protein products are stressed, their degradation pathways and the extent of modifications are determined by multiple factors, including protein sequence, physical state, formulation, excipients, and the levels of initial impurities. When formulations of innovator and biosimilar products are different, forced degradation studies could be particularly important in determining biosimilarity. While the primary sequence, physical state and formulations are identical for Remsima™ and Remicade®, the levels of various impurities such as soluble aggregates, charged isoforms, misassembled light chain-heavy chain impurities and glycation levels are different.<sup>136,300</sup> These initial impurities could serve as initiators to facilitate further protein unfolding and degradation upon stress. Hence, it could be reasonably expected that a stress-testing based strategy that compares reference and biosimilar products could help to both accentuate product differences and delineate between protein degradative pathways that are defined by protein structure versus product impurities. Consequently, we expect the stress degradation studies to provide further insight into similarity and differences between the 2 products.

To test our concept, we used elevated humidity and temperature incubation to assess how multiple lots of Remsima™ and Remicade® compared. Rigorous analytical characterization was performed to monitor structural (aggregation, hydrolysis, unfolding)

and chemical (oxidation, deamidation) changes brought on due to stressing, to understand infliximab's degradation pathways, and identify modification “hot spots” in the sequence. Lastly, the effect of these modifications on biologic activity was quantified using tumor necrosis factor (TNF) binding ELISA and FcγRIIIa binding assays. Collectively, our results provide both a biosimilarity comparison and information about degradation mechanisms for infliximab in the lyophilized powder form.

### **3.3 Materials and Methods**

#### **Infliximab Products**

Remicade<sup>®</sup> was purchased from the University of Michigan Hospital Pharmacy (Ann Arbor, MI) and Remsima<sup>™</sup> was acquired from Celltrion (Incheon, South Korea). Both Remsima<sup>™</sup> and Remicade<sup>®</sup> are supplied as lyophilized powders in vials containing 100 mg of infliximab, 500 mg of sucrose, 0.5 mg Tween 80, and 8 mg phosphate buffer salts.<sup>387,392</sup> The lot numbers and expiry dates of the products used in this study are listed in Table 3-1. All forced degradation studies were conducted within the expiry dates of the samples. Samples were reconstituted using pure WFI (Thermo-HyClone) to a concentration of 1 mg/mL unless specified otherwise. All chemical reagents were of analytical grade or purer and were purchased from either Fisher or Sigma Aldrich.

Sample	Lot #	Exp Date
Remicade 1	14AO52P1	2017.01
Remicade 2	14GO43P1	2017.09
Remicade 3	EIM74016P1	2017.08
Remicade 4	EKL97011P1	2017.10
<u>Remsima</u> 1	12B1C006BA1	2014.12.19
<u>Remsima</u> 2	12B1C014BA1	2015.05.04
<u>Remsima</u> 3	12B1C015BA6	2015.12.03
<u>Remsima</u> 4	12B1C021BA1	2017.05.08

Table 3-1. Lot numbers and expiration dates of studied Remicade/Remsima products

### **Protein Stress Study Set-up**

Powders of Remicade<sup>®</sup> and Remsima<sup>™</sup> contain ~16% of protein by weight. Vials of both products were opened and aliquoted in 1.5 mL Eppendorf tubes (~6.25 mg of powder or 1 mg of infliximab in each tube). Saturated solutions of NaBr and K<sub>2</sub>SO<sub>4</sub> in distilled water were prepared to simulate 53% and 97% RH, respectively.<sup>393</sup> Desiccant was used to simulate dry conditions. The infliximab powders in open tubes were placed in desiccators at a specific RH and incubated at 40°C for 1, 2, or 4 weeks. Samples were removed from the desiccators and reconstituted with WFI to 1 mg/mL. Reconstituted samples were further aliquoted for the various analytical assays and stored at either 4°C or -80°C until analysis. Reconstituted proteins were also subject to thermal stress and are detailed in the supplemental information.

### **Size Exclusion Chromatography**

SEC was performed using a Waters Binary HPLC pump 1525 equipped with Waters auto-sampler 2707 and UV/visible detector 2489. TSK Gel 3000 SW<sub>xl</sub> column (Tosoh 7.8 mm × 30 cm, 5 μm). The mobile phase, phosphate-buffered saline (PBS; pH 7.4), was delivered at 1 mL/min. Protein samples were filtered through 0.45 μm filter



(Millipore) before injection. A 25  $\mu$ L injection volume was used and the UV signal was monitored at 210 and 280 nm. The area under the curve was used to calculate the percentage of monomer, aggregates and fragments. The monomer content for unstressed samples served as the 100% reference and the loss of monomer content at each stressed time point was calculated by decrease of monomer peak area.

### **Circular Dichroism**

CD was performed using a Jasco J-815 CD spectrometer equipped with temperature controller (CDF-426S/15) and Peltier cell at 25°C. The samples were diluted to 0.1 mg/mL for near UV and to 0.5 mg/mL for far UV measurements. The samples were measured in quartz cuvettes (Hellma) with a path length of 1 mm for far UV and 1 cm for near UV. The spectra were collected in continuous mode at a speed of 50 nm/min, bandwidth of 1 nm and a DIT of 1 s. The average of 10 scans were reported. Blank buffer without the antibody was subtracted from each spectrum using the Jasco spectra manager software (Version 2.1). The raw data were converted to mean residual ellipticity (MRE) using the following equation:

$$[\theta]_{mrw,\lambda} = MRW \times \frac{\theta_{\lambda}}{10 \times d \times c}$$

where  $\theta_{\lambda}$  is the observed ellipticity in degrees at wavelength  $\lambda$ ,  $d$  is the path length in cm,  $c$  is the concentration in g/mL, and mean residual weight (MRW) is 110 for infliximab. Data smoothing was performed using GraphPad Prism Software (Version 6.07) using a 0<sup>th</sup> order polynomial with 4 neighbors at each point.

### **Intrinsic Fluorescence**

Intrinsic fluorescence was performed with a Jasco J-815 spectrometer equipped FMO-427S/15 detector and Peltier controller set at 25°C. The samples were diluted to

0.1 mg/mL and were measured in black window quartz cuvettes (Hellma) with a path length of 1 mm. The spectra were collected in continuous mode with a data pitch of 5 nm, scan speed of 50 nm/min and a DIT of 1sec; data were averages of 5 scans. The excitation wavelength was 280 nm and emission spectra were collected from 300 to 400 nm, with a gain voltage of 850 V. Data smoothing was performed using GraphPad Prism Software (Version 6.07) using a 2<sup>nd</sup> order polynomial with 4 neighbors at each point.

### **Gel Electrophoresis**

Selected samples were analyzed by non-reducing and reducing SDS-PAGE to examine for presence of mAb aggregates and fragments. Samples (~10 µg) were mixed with NuPAGE LDS sample buffer, at 3:7 sample: loading buffer ratio and denatured at 90°C for 3 minutes before gel loading. For reduced samples, 5% v/v β-mercaptoethanol was added before heat denaturation. Samples were run on Invitrogen PowerEase 500 with NuPAGE 4–12% BisTris gel. BioRad Precision Plus Protein™ All Blue Standards were used for molecular weight controls. Gels were stained using Thermo Pierce Silver Stain Kit and accompanying protocol and analyzed using Fluorchem M (ProteinSimple).

### **Nanoparticle Tracking Analysis**

NTA (Nanosight NS300, Malvern) was used to quantify subvisible particulates in protein samples. The NS3000 was fitted with a sCMOS camera, a 405 nm blue laser and the sample chamber. The samples were diluted 10-fold before analysis and transferred to sterile syringes (BD) before injection into the sample chamber. The sample chamber was flushed with antibody buffer and then with sterile water in between

sample analysis. The sample results were averages of three 60s runs measured at 0.1 mL/min flow rate and were analyzed using the NTA 3.0 software.

### **Modulated Differential Scanning Calorimetry**

Modulated DSC (Discovery, TA Instruments, New Castle, DE) was used to determine the T<sub>g</sub> and heat of enthalpy of the lyophilized powders. Sample powders (~10 mg) were sealed in hermetic aluminum pans. The measurements were performed at a heating rate of 2 °C per min from 0 to 180 °C under a nitrogen gas flow of 25 mL/min. The modulation amplitude was 0.5 °C and the period was 40 s. The T<sub>g</sub> and enthalpy were obtained by fitting data with TA Trios software (v4.1.1).

### **Nano-differential Scanning Calorimetry**

The thermal melt profiles for stressed and unstressed samples of Remicade<sup>®</sup> and Remsima<sup>™</sup> were measured using TA Instruments nDSC equipped with an autosampler. The thermograms were obtained using a scan rate of 1°C/min from 10°C to 100°C. The thermograms were analyzed using TA NanoAnalyze software (v2.4.1) after blank buffer subtraction using multiple scaled 2 state models to determine the 3 transition melt temperatures.

### **Thermal Degradation**

Remicade and Remsima powders were reconstituted in water for injection (WFI) to a concentration of 1 mg/ml. Samples were incubated at various temperatures 4°C, 25°C, 40°C and 60°C (n=4 per) for up to 1 week. Periodically, formation of soluble aggregates and partial unfolding were monitored by SEC and Thioflavin-T (ThT) fluorescence assay, respectively. Follow on studies were performed at 60°C, the most stressful temperature, for multiple lots of Remicade and Remsima to assess lot to lot

variability as well as the differences between the two products. Samples were incubated for 3 h and protein aggregation was examined by SEC and ThT fluorescence analyses periodically. Following 2 h incubation, subvisible particulates were analyzed by Nanoparticle Tracking Analysis (NTA). Samples incubated for 1 h were digested and analyzed by LC-MS/MS to assess individual amino acid deamidation, oxidation and dioxidation levels.

### **Thioflavin-T Fluorescence Assay**

Thioflavin-T (ThT) is a fluorescent dye known to bind to beta sheet/hydrophobic rich regions of proteins and increase the fluorescence intensity<sup>1</sup>. ThT assay was performed to assess the exposure of hydrophobic regions and protein unfolding and aggregation as follows: 50 x Stock ThT (Sigma) solutions were prepared by dissolving 8 mg of ThT in 10 mL of 10 mM phosphate/150 mM NaCl and stored away from light. 1x ThT working solutions were prepared by dilution into 10mM phosphate/150 mM NaCl buffer and filtered through 0.45 µm membrane filters prior to use. Samples were plated in triplicate in black walled 96-well plates at 30 µL/well to which 100 µL of 1x ThT working solution was added and allowed to react for 5 min at room temperature. The fluorescence intensity was measured using BioTek Nova plate reader with excitation at 440 nm and emission at 482 nm.

### **Liquid Chromatography-Mass Spectrometry**

Antibody tryptic digests were prepared per manufacturer procedure from the low pH protein digestion kit (Promega, CAS # CS1895A01), designed to prevent non-enzymatic protein modifications during digest. Antibody samples were denatured in 8 M urea, reduced, and alkylated with iodoacetamide. The reactions were diluted 7-fold and

incubated with Trypsin Gold and Lys-C (Promega) at 20:1:1 (w/w/w) ratio overnight at 37°C. After digestion was complete, the reactions were acidified with trifluoroacetic acid.

500 ng of each digested sample was analyzed by nano UPLC-MS/MS with a Proxeon EASY-nLC 1000 HPLC system interfaced to a ThermoFisher Q Exactive HF mass spectrometer. Peptides were loaded on a trapping column and eluted over a 75  $\mu\text{m}$   $\times$  50 cm analytical column (Thermo Fisher P/N ES-803) at 300 nL/min by using a 2-hour reverse phase gradient; both columns were packed with PepMap RSLC C18, 2  $\mu\text{m}$  resin (Thermo Scientific). The mass spectrometer was operated in data-dependent mode, with MS and MS/MS performed in the Orbitrap at 70,000 and 17,500 FWHM resolution, respectively. The 15 most abundant ions were selected for MS/MS.

Data analysis for LC-MS/MS analysis of digested specimens was performed with Byonic search software (Protein Metrics Inc., San Carlos, CA, USA).<sup>394,395</sup> In this instance, the search used the infliximab sequence. Identifications for peptide ions were made by matching the precursor (MS1) mass and expected fragment ion masses (MS2) to infliximab peptides. The search included variable modifications such as mono- and di-oxidation on methionine and tryptophan, deamidation and ammonia loss from asparagine, and a wide range of N-linked glycans.

Quantification of modifications relative to unmodified and other modified peptides was accomplished using the Byologic software (Protein Metrics), which uses a label-free quantification approach with extracted ion chromatogram areas (XIC areas). This software automated the XIC extraction and data organization automatically from the Byonic results or *in silico* generated lists of potentially observed molecular ions.

## **Ion Mobility Mass Spectrometry**

Reconstituted antibody samples for native MS experiments were buffer exchanged into 100 mM ammonium acetate buffer using Micro Bio-Spin 30 columns (Bio-Rad, Hercules, CA) without further purification. Sample aliquots (~7  $\mu$ L) were analyzed by IM-MS on a quadrupole-ion mobility-time-of-flight mass spectrometer (Q-IM-ToF MS) instrument (Synapt G2 HDMS, Waters, Milford, MA).<sup>396,397</sup> Antibody ions were generated using a nESI source in the positive mode. Capillary voltages of 1.4 kV-1.6 kV were applied, and the sampling cone was operated at 60 V. The trap traveling-wave ion guide was pressurized to  $3.4 \times 10^{-2}$  mbar of argon gas. The traveling-wave ion mobility separator was operated at a pressure of ~3.5 mbar and used a series of DC voltage waves (40 V wave height traveling at 600 m/s) to generate ion mobility separation. The ToF-MS was operated over the  $m/z$  range of 1000–10000 at a pressure of  $1.7 \times 10^{-6}$  mbar.

Mass spectra were calibrated externally using a solution of cesium iodide (100 mg/mL) and processed with Masslynx V4.1 software (Waters, Milford, MA). Exact molecular masses of intact mAb samples were calculated by assigning the charge states based on the set that gives lowest standard deviation for a given average mass assignment.<sup>398,399</sup> Relative dimer ratios were calculated from total ion counts of major charge states ( $30^+$  to  $36^+$ ) compared with that of major monomer charge states ( $20^+$  to  $26^+$ ). Peaks were fitted to Gaussian models and integrated using OriginPro 9 software.

## **FcγRIIIa Binding**

The binding of infliximab to FcγRIIIa was tested with biolayer interferometry using a BLITZ instrument (Fortebio, Menlo Park, CA). The procedure used here was adopted from the method reported previously.<sup>400,401</sup> Protein G biosensor tips were used and the binding measurement was performed at 25°C. Infliximab samples at 4.6 μM (1 mg/mL) initial concentration in formulation buffer were diluted to 0.8 μM with PBS containing 1 mg/mL casein as a blocking agent (kinetic buffer). Binding studies were performed as follows: First, the protein G biosensor tip was hydrated in PBS for 10 min and then incubated for 30 min in kinetic buffer. Next, an initial baseline (30 s) was established in the kinetics buffer and then the protein G biosensor tips were loaded (120 s) with infliximab samples at a concentration of 0.8 μM to a response level of ~4 nm. A new baseline (240 s) was then established followed by the association (180 s) and dissociation (360 s) of FcγRIIIa measured by dipping the biosensor into solutions of FcγRIIIa and PBS kinetic buffer, respectively. The biosensor tips were regenerated as described previously<sup>400</sup> after each assay cycle. To determine the dissociation constant ( $K_D$ ), a range of FcγRIIIa concentrations from 0.4 μM-3.2 μM was evaluated. Data generated from the binding of the receptor to infliximab were collected in triplicate for each incubation time point and product, lot and globally fitted to a 1:1 binding model using BLITZ Pro software.

## **ELISA for TNF Binding**

96-well ELISA plates (Nunc Maxisorp) were coated with 1 μg/mL TNF (R&D systems) in PBS (pH 7.4) overnight. The plates were washed for 4 cycles with PBS (pH 7.4) using plate washer (Thermo Wellwash 4 MK-2) and subsequently blocked for 2 h at

room temperature with 1% bovine serum albumin (BSA) in PBS (pH 7.4) solution. The plates were washed again and incubated for 1 h at room temperature with infliximab standards (1 ng/mL to 100,000 ng/mL) and diluted samples of equal concentrations. All standard and sample dilutions were prepared in PBST-BSA (PBS (pH 7.4) containing 0.02% Tween 80 and 1% BSA). The plates were once again washed and then incubated with 1000-fold dilution of AP-conjugated anti-human Fc IgG (Sigma-SKU: A9544) in PBST-BSA for 1 h at room temperature. The plate was then washed again to remove residual secondary antibody and incubated with p-nitrophenyl phosphate (pNPP) (Sigma) for 30 min at room temperature for color development. Absorbance at 405 nm was then read using plate reader (Spectra Max M3, Molecular Devices). A standard curve was built using a sigmoidal fit and concentrations of diluted samples were calculated. The sample concentrations were divided by the initial unstressed Remicade® concentration to determine the relative TNF binding activity.

### **Statistical Analysis**

Statistical analysis was performed using Prism 6 (Graphpad) suite. 2-way ANOVA hypothesis testing was performed using multiple comparisons relative to initial samples of Remicade® or Remsima™. Corrections for multiple comparisons were performed using Dunnett's method and significance levels were set at 0.05 (95% confidence interval).



### 3.4 Results

#### Protein Stress: Monomeric Changes and Particulate Formation

For forced degradation studies, the powders of the 2 products were subjected to incubation at 40°C, at various humidity levels (dry to 97% relative humidity (RH)). A schematic of the study design is depicted in Fig. 3-1. Both Remsima™ (RC) and Remicade® (RS) were supplied as lyophilized powders in vials containing 100 mg of infliximab, 500 mg of sucrose, 0.5 mg Tween 80, and 8 mg phosphate buffer salts.<sup>387,392</sup> Overall, the protein content of the powder cake was ~16% (w/w). The powder melt temperatures, determined by modulated-differential scanning calorimetry (mDSC), were similar, with values of 135.8°C for Remicade® and 138.1°C for Remsima™. Product vials were opened, and powders were aliquoted into Eppendorf tubes and the open tubes were incubated for 0, 1, 2 or 4 weeks at 40°C and elevated humidity. At all incubation conditions, powders visually appeared moist, and those incubated at 97% RH deliquesced.



Figure 3-1. Schematic of stress study design. Humidity/thermal stress of infliximab samples were performed by incubating the drug powders at 40°C at different %RH for 0–4 weeks, followed by reconstitution (in WFI) and analysis.

After incubation, water for injection (WFI) was added to the samples and levels of protein aggregation were examined by size-exclusion chromatography (SEC). Analysis revealed a time- and humidity-dependent loss of native monomer and formation of soluble aggregate. The kinetics of monomer loss were similar for the 2 products (Fig. 3-2A,C). The rates of monomer loss were calculated using linear regression and are summarized in Table 1. The fastest rate of protein aggregation was observed at 97% RH with 0.42% monomer loss per day for Remicade<sup>®</sup> and 0.44% per day for Remsima<sup>™</sup>, and virtually no monomer loss was observed for the dry samples. Samples incubated for 4 weeks were further characterized by non-reducing SDS-PAGE (Fig. 3-2B). The gel showed increased levels of aggregates with increasing relative humidity, but also the presence of mAb fragments not previously detected by SEC. Further characterization was performed using reducing SDS-PAGE (Fig. 3-2D). The absence of some aggregate bands after reduction suggests the aggregate formation was partially mediated by disulfide bonds. Jung et al. reported ~0.12 free –SH mol/mol IgG for infliximab, which may play a role in disulfide bond shuffling.<sup>136</sup>

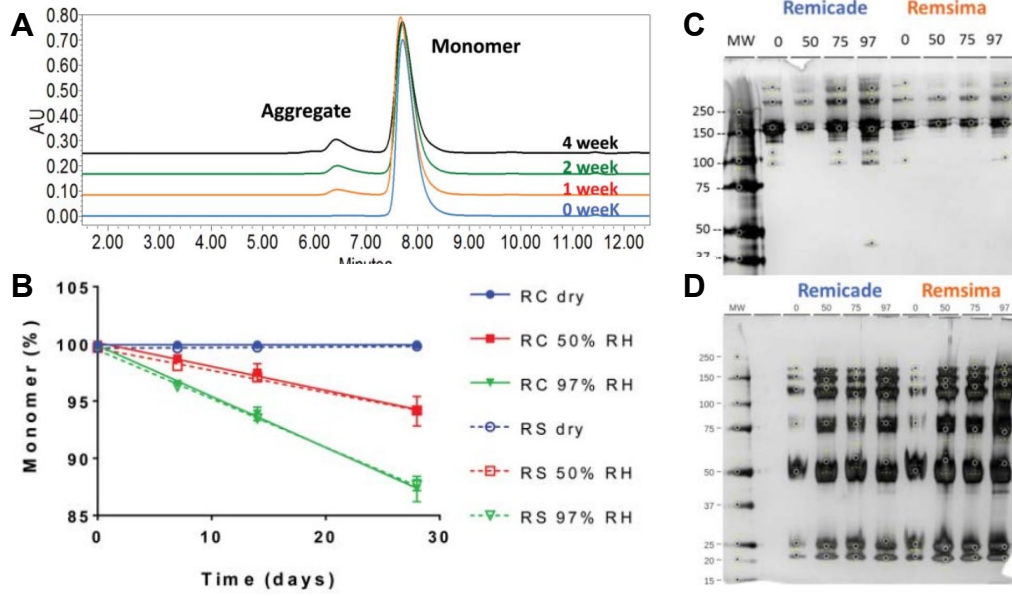


Figure 3-2. (A) SEC-LC infliximab chromatograms over incubation at 97% RH/40°C and (B) Kinetics of monomer loss. ( $n = 4$ ,  $n \pm$  SEM) Characterization by (C) SDS PAGE and (D) Reducing SDS PAGE of RC/RS after 4 weeks of incubation at various humidities/40°C.

Particulate size for the reconstituted samples was measured using nanoparticle tracking analysis (NTA). Particulates from 50–350 nm were observed for both products, as shown in Fig. 3-3A,B. Remicade<sup>®</sup> had fewer observed particulates than Remsima<sup>™</sup>, both initially and after humidity stressing. Although the counts exceed several millions, the particle sizes measured were quite small, and, overall, the particulate counts showed large variability (Table 3-2). Further characterization of these samples was performed using nano-differential scanning calorimetry (nDSC)(Fig. 3-3C,D). The 3 characteristic melt temperatures were determined ( $T_{m1}$ : 67°C,  $T_{m2}$ : 72°C, and  $T_{m3}$ : 86°C) and were similar for the 2 products, in agreement with previously published values.<sup>136</sup> No thermal shifts in the melt temperatures were observed for either product following stress; however, a decrease in overall heat capacity was noticed for the stressed samples. Since the amount of material was held constant, this suggests less energy is required for unfolding after stressing.

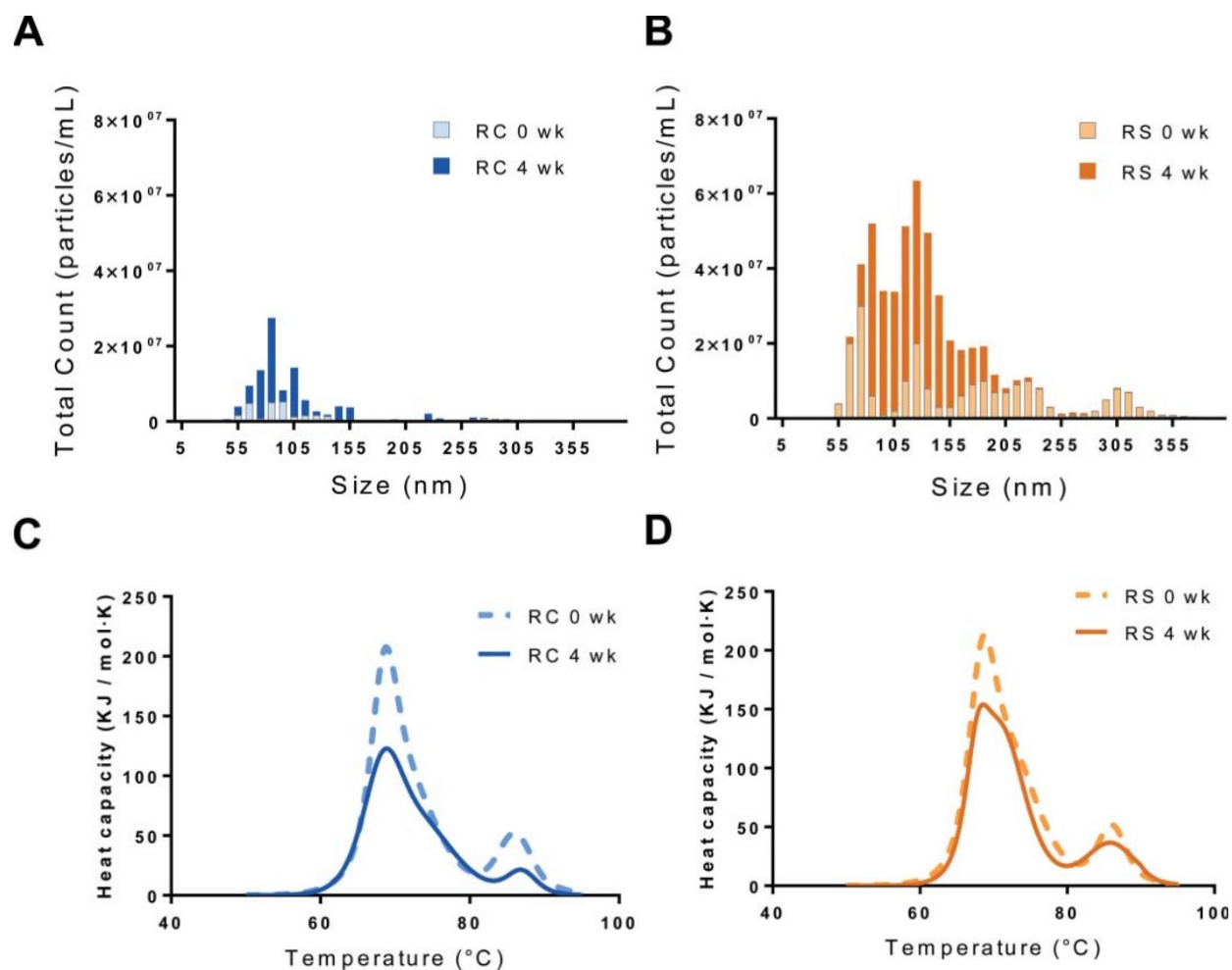


Figure 3-3. (A) Nanoparticle tracking analysis and (B) DSC thermal melts of unstressed (light) and stressed (dark) RC and RS that was incubated at 97% RH/40°C for 4 weeks.

	Monomer Loss Rate ( $\text{day}^{-1}$ ) $\pm$ SD ( $R^2$ )		
	50% RH	75% RH	97% RH
Remsima	$-0.19 \pm 0.01$ (0.99)	$-0.23 \pm 0.06$ (0.86)	$-0.42 \pm 0.01$ (0.99)
Remicade	$-0.20 \pm 0.01$ (0.99)	$-0.18 \pm 0.03$ (0.92)	$-0.44 \pm 0.01$ (0.99)

Table 3-2. Rates of monomer loss for RC/RS after incubation at various humidities/40°C.

Additional forced degradation studies were performed to evaluate antibody stability in solution. Little to no change, as measured by SEC and ThT, was seen for protein samples incubated at 4-40°C over the course of 1 week. However, samples incubated at 60°C showed rapid aggregation and precipitation. Follow on studies were performed at 60°C with multiple lots of Remicade and Remsima incubated for up to 3 hours to establish lot-to-lot variability after thermal stressing for each product as well as to explore differences between two products. All samples were analyzed by SEC, ThT, and selected samples were analyzed by Nanosight (NTA) and LC-MS/MS after trypsin digest. Results from the different assays are summarized in Fig. 3-4. Nearly all the protein appeared to be aggregated after 1hr at 60°C as indicated by Fig. 3-4A,B. Following thermal stress, aggregate particle sizes were measured by DLS which yielded similar particles sizes for both products, but with wide size distributions. NTA was subsequently used to resolve smaller particle sizes (Fig. 3-4C). Several million particles less than 600 nm in size were observed for both products with Remicade having a broader particle size distribution than Remsima. LC-MS characterization (Fig. 3-4D-F) shows the propensity of a few sites for chemical modifications (deamidation at N392, N424 as well as increase in dioxidation at various W sites). Thermal stress at the high temperature of 60°C (near the protein melt temperatures as determined by nDSC) seems to induce protein unfolding that leads to rapid aggregation. In some instances we also observed simultaneous changes in chemical purity. Overall, due to the strong parallel between SEC and ThT results, thermal stress likely induces protein aggregation due rapid unfolding and increased hydrophobic

exposure rather than by chemically mediated process. Overall, the response of both products to thermal stress is similar, again reinforcing the biosimilarity of the products.

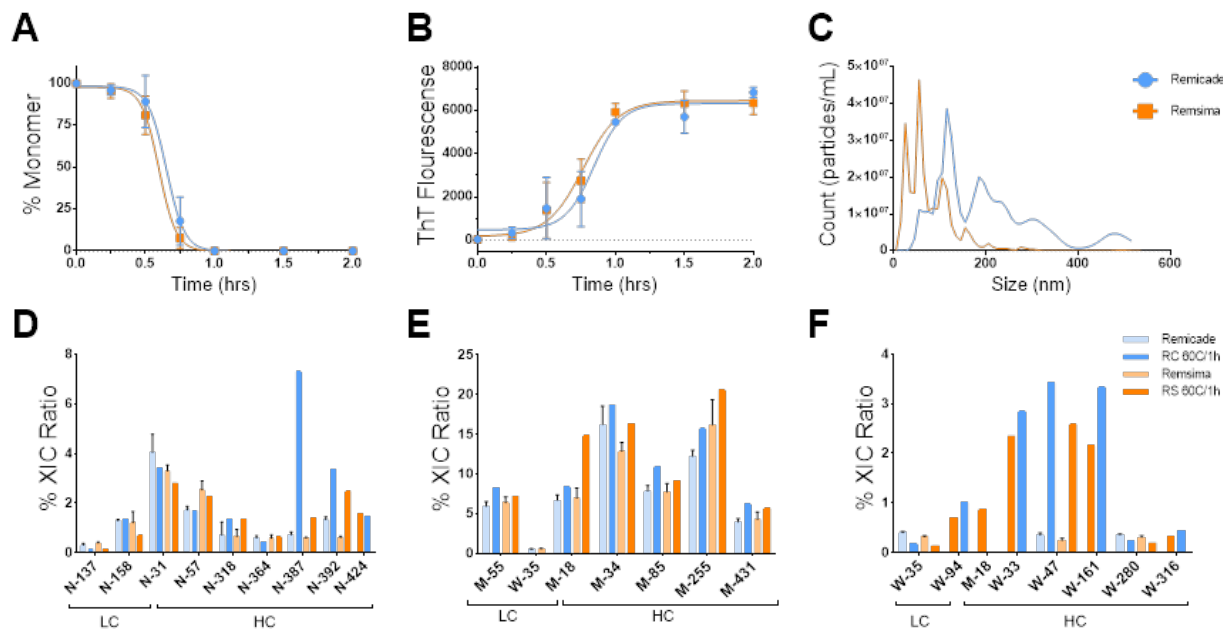


Figure 3-4. Characterization of RC (blue) and RS (orange) incubated at 60°C. (A) Kinetics of monomer (SEC-LC) and (B) ThT fluorescence. (C) NTA analysis after 2 hrs of incubation. LC-MS/MS analysis of (D) deamidation, (E) oxidation and (F) dioxidation after 1 hr of incubation.

### Characterization of Protein Aggregates and Hydrolysis Products

To augment SEC and SDS-PAGE analyses, unstressed and 97% RH/4-week incubated samples for both products were further characterized by ion mobility mass spectrometry (IM-MS). The IM-MS analysis is capable of examining antibodies under native conditions with minimal handling of samples compared with other MS-based methods. Relatively weak electric fields are used to separate gas-phase protein ions accordingly to their orientationally averaged collision cross sections (CCSs) and charge. IM-MS spectra displayed similar IM drift times for Remicade<sup>®</sup> and Remsima<sup>™</sup> with discrete positions in drift time vs.  $m/z$  space for antibody fragments, monomers, dimers, and trimers (Fig. 3-5). The IM-MS results suggested that small initial levels of antibody impurities increase significantly after humidity and temperature stressing (Table 3-3).

For example, the presence of dimer and trimer protein aggregates, as well as 50 and 100 kDa antibody fragments, were observed in stressed samples. Appearance of these species was evident from the different drift times relative to protein monomer drift time, as observed in IM-MS spectra (Fig. 3-5). While the initial levels of aggregates were slightly higher for Remsima™ (0.35% by SEC, 2.0% by IM-MS) than for Remicade® (0.08% by SEC, 0.8% by IM-MS), these differences did not result in faster aggregation upon stress for Remsima™. The large initial dimer differences between the 2 products as measured by IM-MS may be attributed to method variability and should be interpreted with caution, as only 2 batches of each product were analyzed. The levels of dimer were similar in stressed samples for Remsima™ (12.4% by SEC and 3.5% by IM-MS) and Remicade® (12.7% by SEC and 3.0% by IM-MS), and the presence of trimers was detected at 0.1% in both products by IM-MS.

Method	Attribute	Remicade®			Remsima™		
		0 days	4 weeks	Statistics	0 days	4 weeks	Statistics
SEC	Dimer, %	0.1 ± 0.0	12.7 ± 1.1	P < 0.005	0.4 ± 0.0	12.4 ± 0.5	P < 0.005
NTA	Number of subvisible particulates 50–350 nm, 10 <sup>*7</sup>	2.99 ± 0.49	7.43 ± 1.96	NS	21.1 ± 1.60	33.9 ± 3.59	P < 0.005
IM MS	Fragment 50 kDa, %	—	19.7 ± 2.7	N/A	—	26.5 ± 14.2	N/A
	Fragment 100 kDa, %	—	6.0 ± 1.1	N/A	—	9.1 ± 3.4	N/A
	Dimer, %	0.8 ± 0.2	3.3 ± 0.6	P < 0.1	2.0 ± 2.5	2.9 ± 1.2	NS
	Trimer, %	—	0.2 ± 0.1	N/A	—	0.2 ± 0.1	N/A
SDS	Aggregate, %	24.1	37.5	N/A	23.8	40.8	N/A
	Fragment, %	7.0	14.1	N/A	0.0	0.4	N/A
LC-MS	Deamidation LC-N <sub>158</sub> , %	0.6 ± 0.1	7.5 ± 0.7	P < 0.05	0.5 ± 0.4	7.5 ± 0.5	P < 0.05
	Deamidation HC-N <sub>57</sub> , %	1.7 ± 0.2	17.6 ± 1.9	P < 0.05	2.2 ± 0.1	18.9 ± 0.8	P < 0.05
	Deamidation HC-N <sub>392</sub> , %	1.3 ± 0.1	10.3 ± 1.8	NS	0.5 ± 0.1	11.2 ± 1.5	P < 0.05
Activity	TNF binding, %	100.0 ± 3.0	81.8 ± 4.4	NS	111.7 ± 3.1	77.2 ± 5.9	P < 0.01
	FcγRIIIa binding, K <sub>D</sub> (nM)	173 ± 56	545 ± 117	P < 0.1	368 ± 160	680 ± 22	NS

Data shown are percentages (n = 2 lots ± SD), N/A – not applicable, NS – not significant.

Table 3-3 Impurity profiles of RC and RS before and after 4 weeks of incubation at 97% RH/40°C (n = 2, mean ± SD) NA: not applicable; NS: not significant.

The levels of dimers in stressed samples measured by IM-MS appear to be lower than the levels measured by SEC, indicating that possibly some of the newly formed dimers dissociate during mass spectrometry analysis or during sample preparation, e.g., buffer exchange before mass analysis. Prominent fragment sizes of 50 and 100 kDa were observed by IM-MS and may be antibody fragments corresponding to 1 heavy

chain or 2 linked heavy chains, respectively, whereas fragments of 125 kDa by SDS PAGE suggest the loss of one light chain from the mAb. These modifications confirm the susceptibility of infliximab to undergo inter-chain disulfide rearrangements upon humidity stressing. While the levels of protein fragments appear to be higher for Remsima™ than for Remicade® following forced degradation, there is high variability in the measurements and a limited number of samples were available for analysis. Overall, while a significant degree of infliximab aggregation and hydrolysis was observed after the 4-week stress, there were no statistically significant differences in the levels of impurities between the 2 stressed products.

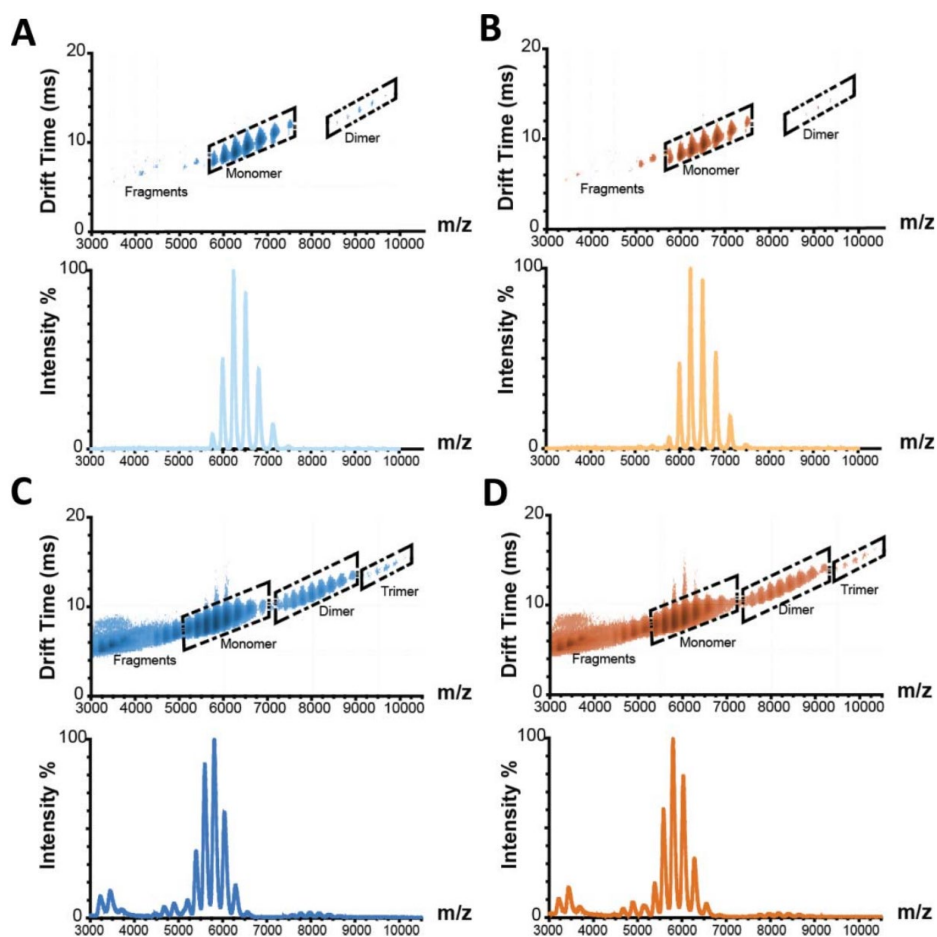


Figure 3-5 . IM-MS spectra and corresponding mass to charge spectrograms of unstressed (A) RC and (B) RS before incubation and (C) RC and (D) RS after 4 weeks incubation at 97% RH/ 40°C. Fragment, monomer, dimer and trimer species are annotated in the ion mobility spectra.



## Structural Characterization

To better understand the structural changes induced by humidity stressing, selected samples were probed using bulk-averaging spectroscopic techniques. Intrinsic fluorescence and near UV circular dichroism (CD; 250–320 nm) were used to gather information about the tertiary structure, while far UV CD (190–250 nm) measurements were used to probe the secondary structure. Intrinsic fluorescence examines changes in the local environment surrounding aromatic amino acids and it assesses how this local hydrophobicity alters the emission profile upon protein stress.<sup>402</sup> The intrinsic fluorescence curves for Remicade<sup>®</sup> and Remsima<sup>™</sup> samples incubated for 0, 2 and 4 weeks at 97% RH are shown in Fig. 3-6A,B. Both products had a maximum intensity at 335 nm and they showed no substantial differences upon humidity stressing, apart from a slight decrease in maximum relative fluorescence intensity. Linear drop-offs in the maximum intensity ( $\lambda_{335}$ ) are observed with increasing incubation times, suggestive of partial unfolding, aggregation, or monomer loss. Our results, which show high homology between the 2 products, also demonstrate comparable intrinsic fluorescence profiles to published results for other IgG1s.<sup>160,403,404</sup>

Near UV and Far UV CD spectra were collected to confirm the intrinsic fluorescence findings, as shown in Fig. 3-6C,D. The Remicade<sup>®</sup> spectra did not change substantially with the increased duration of protein incubation. The Remsima<sup>™</sup> samples showed little change over 2 weeks but showed a large deviation for the 4-week sample at 250–280 nm not observed for Remicade<sup>®</sup>. The initial near UV spectrums look similar to published results for infliximab.<sup>136</sup> A small shift in absorbance was observed at the near UV region between 280 nm and 300 nm corresponding to the aromatic residues,

similar to the earlier drops in the intrinsic fluorescent spectra. Regarding the deviation in the near UV spectrum between 250 nm and 280 nm in the 4-week Remsima™ sample, the spectral pattern suggests a change in the sulfide linkage profile for this sample, in agreement with the earlier findings from IM-MS and SDS-PAGE. It is unclear, however, why similar shifts were not observed for other samples, which should have also undergone similar disulfide rearrangements as suggested by previous data.

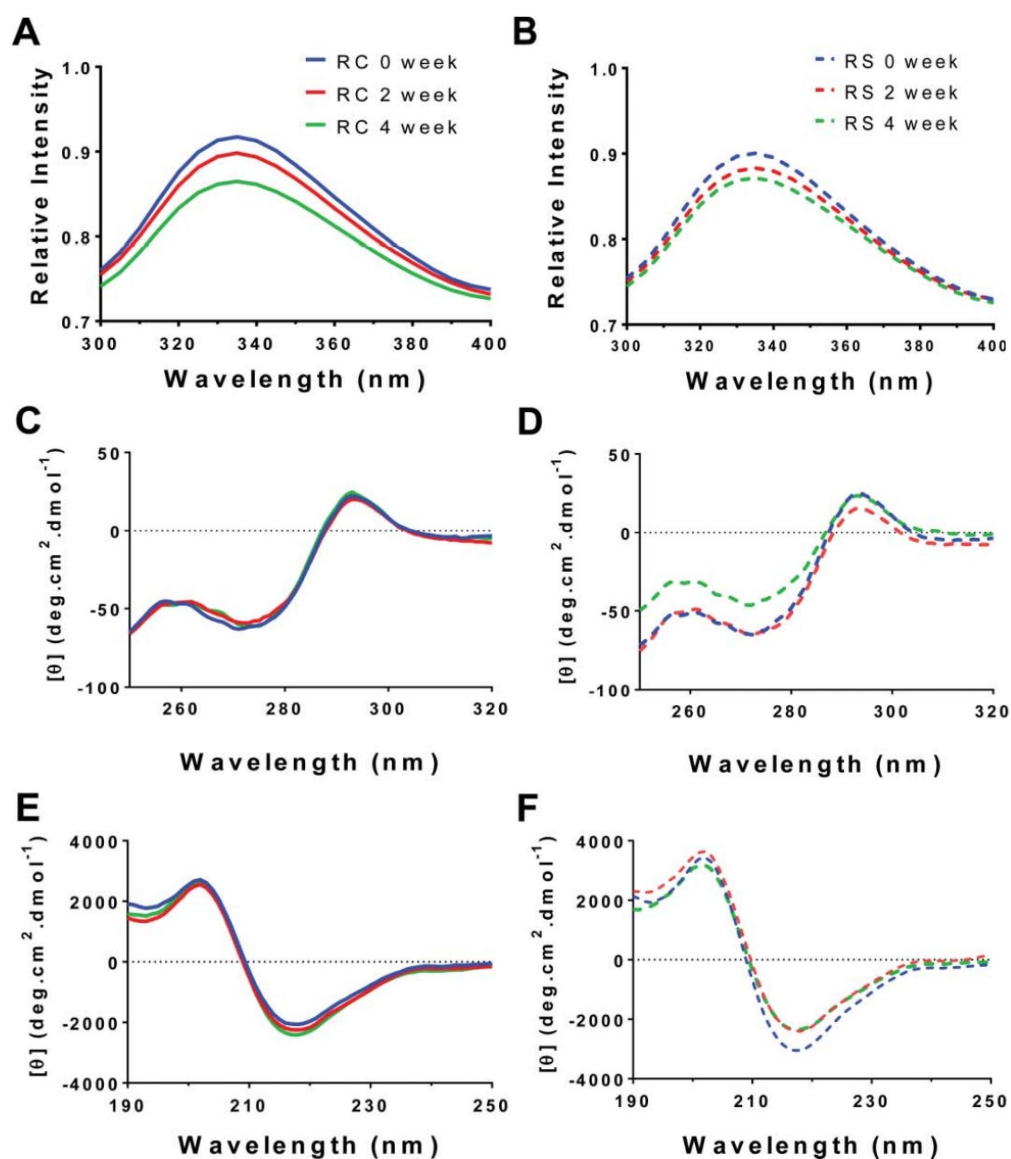


Figure 3-6. Biophysical characterization of humidity stressed samples of RC (solid) and RS (dashed). (A,B) IF (C,D) near-UV CD and (E,F) far-UV CD. Blue: 0 weeks; Red: 2 weeks; Green: 4 weeks.

We next assessed the far UV CD to capture any secondary structural changes that might have occurred due to humidity stressing. Far UV CD from 190 nm to 250 nm has been used extensively to study secondary structure of proteins and antibodies.<sup>405–407</sup> As shown in Fig. 3-6E,F, the far UV CD spectra showed considerable similarity between the 2 products. In addition, Remicade<sup>®</sup> samples displayed small time-dependent deviations in their secondary structure. By contrast, Remsima<sup>™</sup> samples showed a slight increase in positive signal at 218 nm, suggesting a greater anti-parallel  $\beta$  structure. Yet, the overall shapes of spectra were similar for the 2 products, indicating that secondary structural differences between Remicade<sup>®</sup> and Remsima<sup>™</sup> following a 4-week incubation were negligible. The variability of native protein concentration in stressed samples somewhat limits the utility of these intrinsically low resolution spectroscopic methods for biosimilarity characterization.

### **Individual Amino Acid Modifications**

To further characterize how humidity stress leads to chemical modifications of the individual amino acids, the proteins were enzymatically digested and analyzed by LC-MS. As shown earlier by LC-MS, both products exhibit similar but significant degrees of oxidation and deamidation, as well as rather different distributions of N-linked glycans.<sup>7</sup> Here we applied LC-MS methodology to examine whether initial small differences in chemical modifications can be amplified upon stress, as well as to identify infliximab's “hot spots,” i.e., the amino acid residues easily susceptible to modifications upon elevated humidity and temperature stress.

Chemical modifications of the stressed samples were analyzed by LC-MS and depicted in Fig. 3-7. The asparagine deamidation levels were initially similar for Remsima™ and Remicade® at light chain residues N-137 and N-158, and at heavy chain residues N-31, N-57, N-318, N-364, N-387, N-392, and N-424. After humidity stress, deamidation levels for both Remsima™ and Remicade® increased at all measured residues (Fig. 3-7A). The highest levels of deamidation after 4-week incubations were observed for LC N-158 (7.5%), HC N-57 (18–19%) and HC-N-392 (10–11%). The deamidation of conserved Asn 384 (N-387, 384+3 due to different numbering schemes) and 389 (N-392), located in the Fc region, that is responsible for antibody binding to Fcγ and neonatal Fc (FcRn) receptors, might be expected to be significant. While we observed significant increases in deamidation of N-387 and N-392 residues, the extent of deamidation was similar between Remicade® and Remsima™. It also has been shown for other antibodies that deamidation of Fc region residues did not significantly alter Fc receptor binding.<sup>128,129,390,408</sup> The Fc receptor binding is primarily dictated by glycosylation of mAb, specifically the levels of afucosylated species.

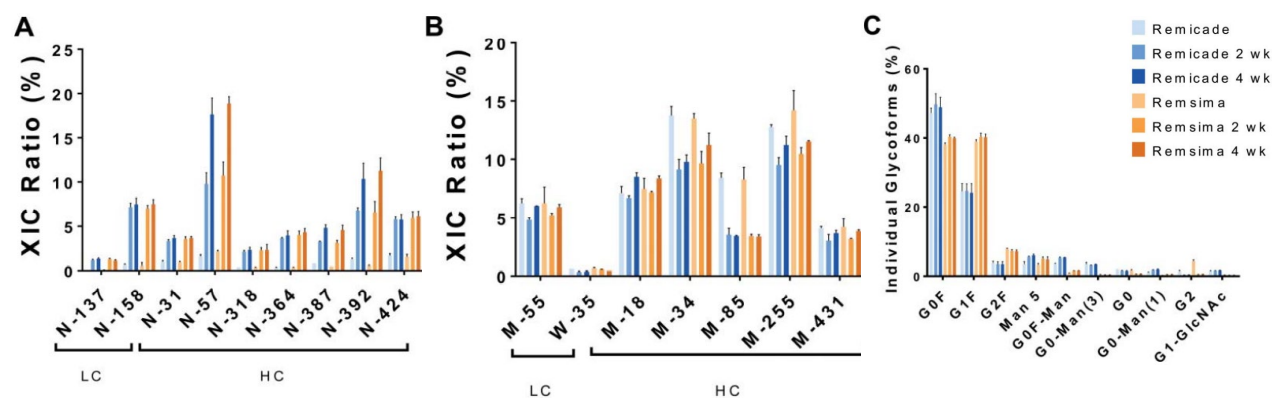


Figure 3-7. LC-MS/MS analysis of chemical modifications over the course of incubation at 97% RH/40°C for RC (blues) and RS (oranges). (A) Deamidation. (B) Oxidation. (C) N-glycosylation. (n = 2, average ± SEM).

In contrast, deamidation of HC N-57 could be significant due to the residue's location in the complementarity-determining region (CDR); thus, deamidation of HC-N-57 could potentially reduce infliximab's binding to TNF. Other antibodies have been shown to exhibit reduced binding abilities to their respective antigens upon chemical modifications of amino acids in the CDR.<sup>103,390,408</sup> Interestingly, while deamidation appears to increase with the duration of incubation for some asparagine residues (N57, N318, and N392), others exhibit the same deamidation levels after 2 and 4 weeks. This provides information regarding the conformational flexibility of the mAbs and the propensity and accessibility of select residues to deamidation. Overall, levels of deamidation appear to be very similar between Remicade® and Remsima™ products both initially and following stressed degradation.

The levels of initial and stress-induced methionine oxidation were analyzed as well (Fig. 6B). Our results indicate significant initial oxidation levels for M-55 at 6.3% (LC) and M-18 (~7%), M-34 (~13%), M-85 (8.2%), M-255 (~12%) and M-431 (~4%) on the heavy chain. However, oxidation levels appeared to be unchanged following forced degradation. Overall, the levels of oxidation are very similar for the 2 products. The oxidation of methionine residues in the Fc region of IgG1 (M-252 and M-431) is known to reduce binding to FcRn and decrease circulation *in vivo*.<sup>409</sup> In addition, oxidation of these methionine residues leads to reduced IgG1 binding to Protein-A column during purification.<sup>128,129,390,408</sup> While we also observe oxidation of the critical methionine residues HC M-255 (252+3) and HC M-431 (428+3), the levels are similar in the 2 products and do not appear to increase during powder temperature/humidity stressing.

The results of our exploratory infliximab solution thermal stability study indicated significantly increased HC M-255 oxidation levels after incubation at 60°C (Fig. S1D-E), highlighting the importance of this residue as a “hot-spot” for infliximab degradation pathways. In addition, increases in tryptophan di-oxidation were observed in heat-stressed protein solutions, specifically the di-oxidation of HC W-33, W-47 and W-161, which increased from <0.5% to ~2–4%. We also observed an increase in deamidation, especially for HC N-387, N-392 and N-424.

In addition to oxidation and deamidation, we examined conserved N-glycosylation of the Fc domain by LC-MS. Glycosylation occurs during recombinant production of infliximab and is defined to a large degree by the specific cell line clone as well as cell culture conditions.<sup>410</sup> Both products were produced using murine hybridoma cell line Sp2/0, but using different infliximab expressing clones generated by the innovator and biosimilar companies.<sup>300,8</sup> Thus, it is not surprising that a biosimilar product like Remsima™ exhibits different distributions of glycans relative to the reference product Remicade®.<sup>43,300,388</sup> We also confirmed initial differences in glycan distribution, with G0F, G0F-Man, G0F-Man(3) and G0F-Man(1) being more abundant in Remicade® while G1F, G2F and G2 more prevalent in Remsima™ (Fig. 6C). These initial differences are important, as it appears that overall levels of mannose and afucosylated glycans are higher in Remicade® than in Remsima™, and this is known to affect Fc receptor binding, antibody dependent cell-mediated cytotoxicity (ADCC), circulation time and immunogenicity.<sup>411</sup> We also observed that glycan distribution remained virtually unchanged for both Remicade® and Remsima™, as expected. Proteins are glycosylated enzymatically during production by the host cell; thus, it is

unlikely that glycosylation could be altered during stressed stability studies apart from possible selective aggregation/degradation of a specific glycan type.

### ***In Vitro* Efficacy**

In addition to the analytical characterization of the humidity stressed samples, we also performed *in vitro* bioactivity assays to gauge how stressing affects infliximab's abilities to bind TNF and FcγRIIIa (Fig. 3-8). We expected that stressed-induced individual amino acid modification in the CDR could reduce infliximab's binding to TNF, while modification of the Fc domain could alter FcγRIIIa interactions. In addition, the reduction of intact infliximab monomer content over the duration of the forced degradation study could lead to further reduction in antigen and receptor binding.

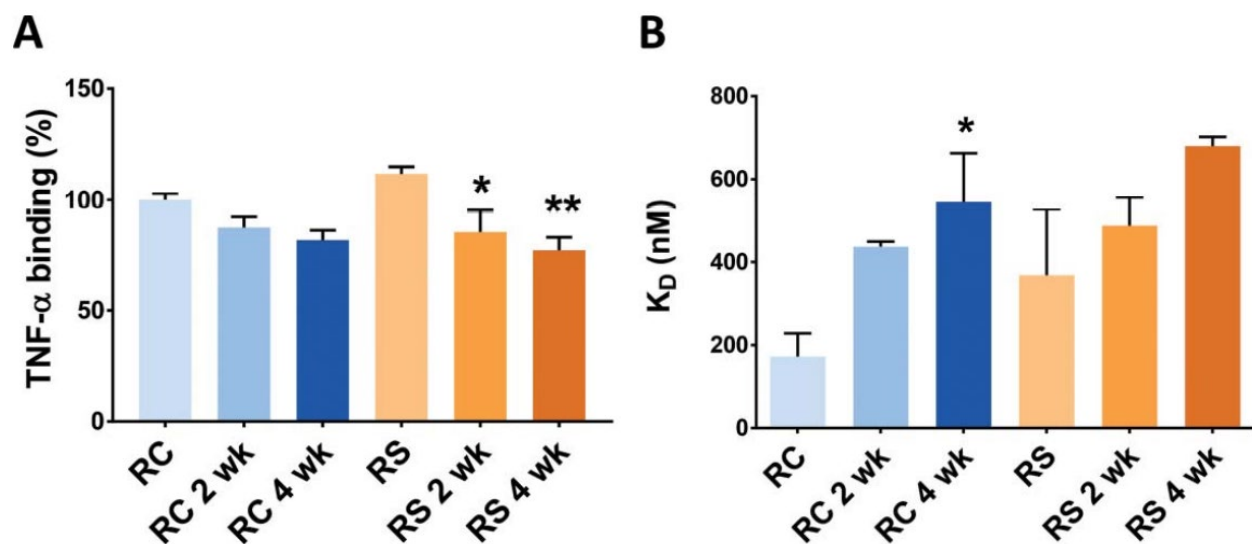


Figure 3-8 (A) TNF-α binding (measured by ELISA) (B) FcγRIIIa binding (measured by BLITZ) (n = 2, mean ± SEM; P < 0.05) for RC and RS over the course of incubation 97% RH/40°C.

According to regulatory filings, Remicade® and Remsima™ exhibit similar initial ability to bind and neutralize TNF.<sup>43,300</sup> The 90% confidence interval for the mean difference between Remicade® and Remsima™ TNF binding affinity measured by ELISA falls entirely within the equivalence margin.<sup>346</sup> Our measurements, derived from only 2 lots for each product, indicated that the TNF binding affinity was slightly higher for

Remsima™, at 111.7% of the initial Remicade® value, but this result was not statistically significant (Fig. 3-9A). Following 4 weeks of forced degradation, TNF neutralization decreased to 81.8% (Remicade®) and 77.2% (Remsima™) of the initial value for unstressed Remicade® standard. This decrease could be attributed to increased deamidation levels of HC-N-57 or reduced infliximab monomer content or both. However, there was no statistically significant difference in TNF binding affinity between 2 stressed products at the corresponding time points.

The differences in FcγRIIIa binding corresponding to the lower levels of afucosylation for Remsima™ relative to Remicade® were reported previously.<sup>388</sup> In the regulatory filing, decreased afucosylation was reported, and corresponded to a 20% lower binding efficiency to FcγRIIIa and 20% lowered ADCC for Remsima™ relative to Remicade®.<sup>346</sup> The initial unstressed samples of Remicade® showed tighter binding to FcγRIIIa relative to Remsima™ with the respective  $K_D$  of  $173 \pm 56$  nM and  $368 \pm 160$  nM, as measured by biolayer interferometry (Fig. 3-9B). The receptor binding progressively weakened following stress degradation of the 2 products, and the  $K_D$  increased to  $545 \pm 117$  nM for Remicade® and  $680 \pm 22$  nM for Remsima™ after 4 weeks at elevated humidity and temperature. Since no significant changes in glycosylation between the 2 products were detected upon incubation, the reduction in Fc receptor binding is likely attributed to the progressive increase in aggregation and fragmentation of the 2 antibodies, in conjunction with the chemical modifications, thus reducing the total amount of bioactive monomer available to bind receptors. Additionally, the initial differences in Fc binding between the 2 products appear to largely diminish upon stressing, highlighting the importance of structural integrity over



glycosylation patterns for bioactivity. Overall, no statistically significant differences in FcγRIIIa binding were observed throughout the entire study, which was possibly due to the small number of lots tested (n = 2).

### 3.5 Discussion

In this study, humidity- and temperature-induced forced degradation was used to analytically compare a biosimilar mAb, Remsima™, with its reference product, Remicade®. Despite the minor differences in initial product profiles (glycosylation pattern, levels of dimer and basic variants), as well as differences in the manufacturing processes of 2 mAbs, the 2 products behaved remarkably similarly in the forced degradation studies.<sup>43,136,300</sup> Very similar rates of degradation, along with similar types and levels of impurities were detected in the 2 stressed products. Hence, for products with high analytical similarity and identical formulations, such as Remsima™ and Remicade®, the degradation mechanisms appear to be defined primarily by protein sequence and structure rather than by minor initial product differences. However, other biosimilar products may be formulated differently or produced in different expression systems compared with their reference products, both potentially leading to greater product differences and varying mechanisms of protein instability in forced degradation studies.<sup>139,29</sup>

Our results revealed the main infliximab degradation products to be protein aggregates and antibody fragments of 50 and 100 kDa. The rate of monomer loss was nearly identical for the 2 products under the various humidities tested, and higher initial levels of dimers in Remsima™ did not result in faster protein aggregation. The actual

levels of formed aggregates and antibody fragments varied slightly when measured by SDS-PAGE, IM-MS and SEC. An increase in the level of subvisible particulates was observed for both products by NTA after stressing. Each analytical method has inherent limitations due to variations in the sample handling, e.g., concentration/dilution, buffer exchange, mixing with gel loading buffer and binding to column matrix, which is known to affect aggregate before the detection.<sup>412</sup> Hence, use of orthogonal methods allows for a more complete picture of protein aggregation and hydrolysis.

Structural changes in the 2 products were compared spectroscopically. The near- and far-UV spectral results for the initial samples are in agreement with the published results for the native protein and small changes in spectra were observed in stressed samples.<sup>136</sup> No thermal shifts were observed in stressed samples by nDSC, but lower enthalpy indicated minimal structural changes. Further analysis suggests these products slightly unfold, but undergo significant deamidation at specific “hot spots” upon stressing, as measured by LC-MS. Overall, structural and chemical modifications were comparable between the products. The TNF neutralizing ability of both antibodies was reduced significantly upon stress, by ~20–30% relative to the unstressed protein levels. This reduction could be attributed to individual amino acids modifications in the CDR domain (LC-M-55, HC-M-34, HC-N-31 and HC-N-57), as well as to the decrease in functional protein monomer content. Nonetheless, regardless of mechanism, the 2 products exhibited a similar magnitude of reduction in TNF binding. Additionally, post-stress FcγRIIIa binding was reduced significantly for both products, by 2–3-fold, with slightly larger mean decreases for Remsima™ binding at each time point. However, there were no statistically significant differences between the reference and biosimilar

products. Interestingly, using a larger number of lots for Remicade<sup>®</sup> and Remsima<sup>™</sup>, we showed that the level of afucosylation was significantly higher in unstressed Remicade, which corresponded to stronger FcγRIIIa binding relative to Remsima<sup>™</sup>. Such differences in glycosylation, along with the reduction in FcγRIIIa binding and ADCC were reported in the regulatory filings for Remsima<sup>™</sup>, resulting in the deferral of biosimilar approval for inflammatory bowel disease indications by Health Canada.<sup>43,300,413,414</sup> While glycosylation differences between products did not change following forced degradation, the FcγRIIIa binding decreased similarly for the 2 products. A several fold reduction in the FcγRIIIa binding after forced degradation could be attributed to individual amino acid modifications in the Fc domain, as well as to extensive aggregation and hydrolysis of the 2 mAbs. However, this finding shows that forced degradation could mute rather than amplify initial differences between biosimilar and reference product, which was surprising and contradictory to the initial expectations for this study.

Stress testing is often used to identify instabilities in proteins, select optimal formulations to reduce protein degradation during stability testing, and to define shelf-life and storage conditions. Antibodies, particularly IgG1s, have been stressed in a variety of ways, including thermally, physically (e.g., stirring, shaking), and chemically (e.g., oxidation, pH).<sup>160,415</sup> Overall, different mechanisms of stressing have yielded different by-products; however, in general, IgG1s are prone to aggregation and chemical modification of several conserved residues identified as “hot-spots.”<sup>390</sup> Most stress conditions lead to aggregate formation, either insoluble, soluble, or both.<sup>389,391</sup> Additionally, structural studies have characterized changes in secondary and

tertiary features of mAbs that may initiate aggregation.<sup>403,406</sup> Chemical stressing has also identified several oxidation hot-spots on mAbs and accessibility of various residues.<sup>160,390,416</sup> Aggregates formed via different stressors are heterogeneous and express differing immunogenic patterns test in various immunogenicity models.<sup>160,417,418</sup> In general, physical stressing (thermal, agitation) leads to greater particulate formation and yields a stronger immune response than chemically stressed samples.<sup>377,378</sup> Stress-induced particulate formation highlights a need for characterizing how process parameters, excipients and formulation differences in biosimilars affect protein aggregation, as they may ultimately affect product immunogenicity and safety.

To demonstrate biosimilarity, the 2 products should have no “clinically meaningful” differences. Thus, comparison of lot release data for biosimilar and reference products are the most critical for determining biosimilarity. However, the rates and mechanisms of degradation of reference and biosimilar products can also be compared during forced degradation studies. These comparisons are particularly useful if the biosimilar is formulated differently compared with the reference product, as it could result in new types of degradation products observed in the biosimilar that are not present in the reference product. The presence of new types of degradation products raises additional questions if these degradants could potentially affect product efficacy and safety.

While forced degradation studies allow rapid generation of a large volume of analytical comparability data, the mechanism of protein instability and type of degradation products formed are largely determined by the stress conditions. Often the

conditions of forced degradation studies are more extreme than the actual stresses that product vials are exposed to during transport, storage, and clinical administration. In this study, to accelerate protein degradation, the vials were opened, and products were exposed to much higher temperatures and humidity than the environment inside sealed and refrigerated vials. For traditional biosimilarity comparisons the analyses are performed using several lots of each product. In our constrained study, only 2 lots of each product were subjected to the forced degradation, which limits our ability to perform rigorous statistical analysis. We observed large deviations in product modifications in the stressed samples, which, in addition to limited sample size, may also arise from the heterogeneous nature of degradant formation, especially at the primary chemical levels. Due to the limited amount of protein, we did not examine the effects of oxidative, mechanical, and chemical stress on reconstituted infliximab solutions for every time point. Furthermore, we have not characterized the type, shapes, and sizes of formed protein aggregates and have not examined the levels of protein glycation in this study, which may be of interest for immunogenicity characterizations.

The immunogenic propensity of biologics is a key safety parameter identified by regulatory agencies. To date, several studies have used a variety of stresses to form immunogenic products, and characterized their immunogenicity in various *in vitro* and *in vivo* models.<sup>160,417,418</sup> General correlations between characteristics of stressed protein (type, shape and size of protein aggregates) and the immunogenicity of these degradation products were developed.<sup>390,415–418</sup> Thus, forced degradation could provide valuable predictive data regarding the immunogenic propensity of the biosimilar product, and this data could ultimately be used in product regulatory licensing applications. The

challenge in applying this stress testing strategy is the lack of universal conditions/guidelines to perform the studies, which leads to different setup conditions and, thus, difficulty in extrapolating results. Ideally, the solution would be to adopt guidelines to perform these tests, but this is confounded by the diverse nature of biotherapeutics, each of which may display different behaviors. Given these concerns, it is recommended that stress studies be designed with specific ends in mind, and that several orthogonal robust analytical techniques be used to ensure confidence in the final outcomes.

Biosimilar approvals are poised to bring substantial positive change to healthcare yet establishing biosimilarity is challenging. Forced degradation studies provide a unique approach to examine the appearance of any minor differences that may have clinical safety, immunogenicity, and efficacy implications. In this study, we used thermal and humidity stress testing on both reference, Remicade®, and biosimilar, Remsima™, infliximab products. Our results show similar levels of aggregate formation, structural variation, and chemical modifications to support the notion that the products are biosimilar. We anticipate stress testing will be used widely for biosimilar assessment as patents for more biologic products expire and new biosimilar products permeate the markets, and this work will help guide future studies.

## **Chapter 4: Disulfide Shuffling Comparability of Originator/Biosimilar mAb Pairs**

### **4.1 Abstract**

Disulfide bonds play a critical role in maintaining the structure, stability, and function of monoclonal antibodies (mAbs). The modification of disulfide bonds can result in altered safety, efficacy and immunogenicity. Since the regulatory approval of a biosimilar mAb requires extensive characterization, it is important to understand the sights of potential disulfide shuffling and the formation of potentially immunogenic impurities.

In the first part of this project, tandem mass spectrometry (LC-MS/MS) was used to compare disulfide bonding for an originator/biosimilar infliximab, rituximab and bevacizumab pairs, where LC-MS/MS outputs were analyzed using a Protein Metrics' Byonic™ and Byologic® workflow, which allows for the detection, identification, quantification and comparison of expected disulfide bonds and related impurities (shuffled disulfide and trisulfide bonds). The relative contribution of shuffled and trisulfide bonds were found to be higher for biosimilar infliximab and biosimilar bevacizumab than their respective originators. On the other hand, for rituximab, the relative contribution of shuffling for the biosimilar was identical to that seen for originator and no trisulfides were detected. These differences of disulfide shuffling would seem to indicate underlying differences between originator and biosimilar infliximab and bevacizumab.

In the second part of this project, originator and biosimilar rituximab and bevacizumab were subject to forced degradation, where these pairs were incubated at 37°C for 4 weeks. LC-MS/MS was used to compare changes of shuffled disulfide and trisulfide bonds over the course of incubation. The relative contribution of shuffled disulfide bonds for originator/biosimilar rituximab were similar over the course of incubation. The relative contribution of disulfide shuffling for originator and biosimilar bevacizumab not only started with higher initial levels of disulfide shuffling and trisulfide bonding but also had greater extents of shuffling over incubation. In addition, the relative contribution of disulfide shuffling for biosimilar bevacizumab was greater than the originator. Physical degradant characterization (SDS PAGE and SEC) was then used to assess and confirm the relationship of protein degradation to disulfide shuffling. It was observed that bevacizumab was more prone to both physical degradation and disulfide shuffling than rituximab, where again the biosimilar bevacizumab had more initial degradation than the originator. Lastly, free thiol content was analyzed. Free thiol, while appearing greater for rituximab than bevacizumab, appeared to be related to less disulfide shuffling and less physical degradation, whereby free thiols were detected upon exposure over incubation. For bevacizumab, free thiol content also appeared related. Though less free thiols were detected, this is likely due to their participation in disulfide shuffling and degradation that was greater than that observed for rituximab.

## **4.2 Introduction**

Immunoglobulin Gs (IgGs) are comprised of 4 subtypes, IgG1-4, and are differentiated by the varied number and locations of their disulfide bonds.<sup>419,420</sup> Disulfide bonds are found throughout each IgG structure and are highly conserved across IgG



subtypes. The studied infliximab, rituximab and bevacizumab originator/biosimilar pairs are IgG1s, the largest IgG subtype for currently marketed products.<sup>421</sup> The three studied mAbs neutralize different antigens, including TNF- $\alpha$  (infliximab), VEGF (bevacizumab) and CD-20 (Rituximab). Infliximab and rituximab also rely on IgG's crystallizable fragment (Fc) domain interaction with target effector (immune) cells for their therapeutic activity through antibody-dependent cellular cytotoxicity (ADCC).<sup>422</sup> Another minor MOA that follows antigen-binding is the downstream complement cascade called complement dependent cytotoxicity (CDC); however, ADCC is more commonly understood to play the main role in therapeutic effect.<sup>422</sup>

Formation of shuffled disulfide bonds can lead to structural changes, which, in turn, can result in function changes such as reduced antigen binding (a potential efficacy concern) and formation of misfolded/aggregated mAbs (a potential immunogenicity concern). It is important to recognize that modifications of a protein's underlying structural backbone do occur and can result in functional changes.<sup>137,420,423</sup> Therefore, characterization of whether disulfide bonding within an IgG is retained (in its "expected" form) or has been modified can be a useful way to deduce whether protein function is expected to be retained.

## **IgG1 Structure: Disulfide Bonds**

Disulfide bonds are covalently formed between the thiol groups of two cysteine amino acid residues in a mAb. Not only do they contribute to protein stability, but also dictate protein folding during translation.<sup>424</sup> Disulfide bonds can occur either within HCs and LCs (intra-chain), between the HC and LC (inter-chain) of a mAb. Hinge region disulfide bonds are located between the Fab and Fc domains and occur between the two HCs (inter-chain). The IgG1 subtype has 12 intra-chain disulfide bonds and 4 inter-chain disulfide bonds.<sup>419</sup> There are two inter-chain disulfide bonds between the LCs and HCs, and two between the HCs (hinge region). There are two intra-chain disulfide bonds within each LC and four intra-chain disulfide bonds within each HC. Intra-chain disulfide bonds have been suggested to be responsible for the stabilization of tertiary structure while inter-chain disulfide bonds, which are more solvent accessible and susceptible to reduction, have been attributed to the stabilization of quaternary structure.<sup>425</sup> All together, these 16 disulfide bonds are what we consider to be “expected” bonds and will be referred to as such for the remainder of this presentation.

## **Methods of Disulfide Bond Characterization**

The standard techniques for disulfide bond characterization include a number of variations of liquid chromatography coupled to mass spectrometry (LC-MS). In “bottom-up” MS approaches, a large protein is digested into smaller peptide segments by digestion enzymes, which are then separated by LC prior to MS/MS analysis, a technique that has been implemented in several previous studies to detect, identify, quantify and compare expected disulfide bonds and related impurities in innovator/biosimilar mAb pairs.<sup>144,145,301,388,426</sup> Whereas previous studies have

characterized other chemical impurities through the use of reducing trypsin digestion, non-reducing trypsin digestions were used to prevent disulfide bond cleavage.

### **Disulfide Bond Shuffling**

Disulfide shuffling (thiol-disulfide interchange) has been commonly suggested and been understood to occur as a function of free thiol levels. When deprotonated, thiols form a highly reactive thiolate anion that can attack the sulfur of a disulfide moiety through SN2 type nucleophilic reactions.<sup>113–116</sup> Though not expected to occur as a result of high process control, previous studies have developed methods to detect small amounts of free thiols that can exist across recombinant subtypes and potentially serve as sources of disulfide shuffling.<sup>427,428</sup> Other studies have shown that disulfide bond shuffling can trigger IgG's aggregation pathway and result in the loss of stability, potency and activity (CDC and ADCC).<sup>115,429–433,</sup>

### **Trisulfide Bonding**

The formation of trisulfide bonds, although found in all IgG subtypes, is less studied as it is a relatively rare modification.<sup>119</sup> Resulting from a hypothesized redox reaction with excess dissolved hydrogen sulfide (H<sub>2</sub>S) in cell culture, trisulfides are thought to be formed by the insertion of a sulfur between two cysteines during fermentation.<sup>119,434,435</sup> However, trisulfides have neither been shown to reduce antigen binding nor impact the stability of proteins, both *in vitro* and *in vivo*.<sup>119,436</sup> Another study investigated the potential structural impact of trisulfide bonding in mAbs when developing antibody-drug conjugates (ADCs) and suggested precautionary monitoring of such modifications during development.<sup>437,438</sup> Again, while there are some studies investigating the formation of trisulfide bonds, current literature indicates that trisulfides

have a limited impact on stability or functionality, though their presence may indicate an underlying process variability between innovator/biosimilar mAb pairs.<sup>119</sup>

### 4.3 Methods

#### **MAb Sample Preparation/Stress Study Setup**

Originator and biosimilar samples of infliximab, rituximab and bevacizumab samples were acquired. Originator/biosimilar infliximab were supplied as lyophilized powders and were reconstituted using pure water for injection (WFI)(ThermoHyClone) to a concentration of 10 mg/mL as per the digest kit specifications. Originator/biosimilar rituximab were supplied as an aqueous formulation at a concentration of 10 mg/mL. Originator/biosimilar bevacizumab were supplied as an aqueous formulation at a concentration of 25 mg/mL that was then diluted to 10 mg/mL using pure WFI. All chemical reagents were of analytical grade or purer and were purchased from commercial suppliers. Only originator and biosimilar rituximab and bevacizumab pairs were subject to forced degradation at 37°C for up to 4 weeks.

#### **Trypsin Digestion (Infliximab)**

Originator and biosimilar infliximab samples were prepared at a concentration of 1 were digested at pH 5.6 using Promega's AccuMAP Low pH Protein Digestion Kits utilizing their non-reducing protocol to avoid disulfide bond cleavage (Promega, CAS # CS1895A01), which was generously provided.<sup>439,440</sup> This digest is referred to as "pH 5". Prior to digestion, antibody samples (5 µL) were denatured by a 9M Urea/AccuMAP denaturing solution (42 µL). Free cysteines were then blocked by mixing the denatured samples with 200 mM NEM (2 µL) and incubating for 30 minutes at 37°C. Pre-digestion protocols were completed by mixing the samples with AccuMAP Low pH Resistant rLys-

C (25  $\mu$ L) and incubating for 1 hour at 37°C. Digestion was completed after an addition of AccuMAP 10X Reaction Buffer (10  $\mu$ L) and AccuMAP Low pH Resistant rLys-C that had been diluted with NANOpure water (25/51  $\mu$ L). The reaction was terminated upon the addition of TFA (17  $\mu$ L). The pH was assessed to ensure termination of the reaction. Samples were stored at -20°C prior to analysis. These samples were then subjected to clean up/purification using SepPak C18 Plus light cartridges (Waters, SKU WAT051910) prior to injection onto LC-MS/MS.

### **Trypsin Digestion (Rituximab/Bevacizumab)**

Originator and biosimilar rituximab and bevacizumab were also digested at pH 5.6 using Promega's AccuMAP™ Low pH Protein Digestion Kit utilizing their non-reducing protocol to avoid disulfide bond cleavage (Promega, CAS # CS1895A01), which was generously provided. For this section, mAb digestion was modified from Promega's provided protocol to account for use of a PCR plate on an Agilent AssayMAP Bravo robot platform. Use of the Agilent AssayMAP Bravo platform and LC-MS/MS instrumentation was thanks to MS Bioworks (Ann Arbor). Solutions of 200 mM NEM, 50 mM acetic acid, trypsin diluent (CaCl<sub>2</sub> in acetic acid), "Platinum Trypsin" and termination solution (20%TFA) were prepared prior to digestion. 3  $\mu$ L of 10 mg/mL mAb was added to the PCR plate and then combined with 8M AccuMAP™ Denaturing Solution, low pH AccuMAP™ reaction buffer and NEM, which was then incubated at 37°C for 30 minutes in a water bath. Samples were then mixed with Lys-C and incubated at 37°C for 2.5 hours and then digested with a combination of low pH reaction buffer, lys-C and Trypsin Platinum. This mixture was then incubated overnight at 37°C in a water bath. 20% TFA was added to terminate the reaction at low pH, as confirmed by pH strips.

### **LC-MS/MS (Infliximab)**

Digested antibody samples (500 ng) were analyzed by nano UPLC-MS/MS with a Proxeon EASY-nLC 1000 HPLC system interfaced to a ThermoFisher Q Exactive HF mass spectrometer. Peptides were loaded on a trapping column and eluted over a 75  $\mu\text{m}$  x 50 cm analytical column (Thermo Fisher P/N ES803) at 300 nL/min with a 2-hour reverse phase gradient; both columns were packed with PepMap RSLC C18, 2 mm resin (Thermo Scientific). The mass spectrometer was operated in data-dependent mode, with MS and MS/MS performed in the Orbitrap at 70,000 and 17,500 FWHM resolution, respectively. The most abundant ions were selected for MS/MS.

### **LC-MS/MS (Rituximab/Bevacizumab)**

Data Dependent Acquisition (DDA) experiments were carried out using half of each enriched sample by nano LC-MS/MS using a Waters M-Class system interfaced to a ThermoFisher Fusion Lumos mass spectrometer. Peptides were loaded on a trapping column and eluted over a 75  $\mu\text{m}$  analytical column at 350 nL/min with a 30-minute reverse phase gradient; both columns were packed with Luna C18 resin (Phenomenex). The mass spectrometer was operated in a combined data dependent HCD mode, with MS and MS/MS performed in the Orbitrap at 60,000 FWHM resolution and 15,000 FWHM resolution, respectively. The instrument was run with a 3s cycle for MS and MS/MS. DDA data was processed in Byonic<sup>TM</sup> with a 10 ppm parent mass tolerance, 0.02 Da fragment mass error tolerance. Disulfide bonds and related impurities were reported as relative contribution, relative to the total sum of expected disulfide shuffled

disulfide and trisulfide bonds and normalized contribution, relative to the respective XIC AUC total. Trisulfides were reported as XIC AUCs when comparing pH.

### **Byonic™/Byologic® Workflow**

Analysis of LC-MS/MS outputs were identified, quantified and compared for expected disulfide, shuffled disulfide and trisulfide bonds by a Protein Metric workflow that is explained in previous publications.<sup>394</sup>

### **Gel Electrophoresis**

Originator/biosimilar rituximab and bevacizumab pairs were first qualitatively investigated for physical degradation by SDS-PAGE gels. Gels were optimized to find a balance between the visualization of minor components and the ability to avoid well overloading (data not shown). To do so, mAb samples were diluted to approximately 10 mg/mL and then further diluted to lower final concentrations ranging from 0.1-5 mg/mL. To prepare these final concentrations, we combined 5 µL of Loading Buffer (Thermo) to 15 µL of mAb sample (a 1:3 ratio). These samples, along with the 10µL of HiMark Pre-stained Protein Standard ladder (Thermo), were loaded onto 15 well 3-8% NuPAGE gels. Final mAb concentrations of 0.25 and 0.4 mg/mL were chosen for analysis of mAbs at different incubation time points and run at 150V for 1 hour. Gels were stained for 1 hour using SimplyBlue SafeStain (Thermo), cleaned with water, imaged and analyzed for relative component content using a Fluorchem M imager (ProteinSimple).

### **Size Exclusion Chromatography**

Originator/biosimilar rituximab and bevacizumab pairs were investigated for physical degradation by SEC on a Waters UPLC BEH450 SEC column (2.5µm, 4.6 x 150 mm) with a Waters 2707 autosampler connected to a 1525 binary UPLC pump,

interfaced with a 2489 UV/Vis detector. MAb samples were diluted with LC-MS grade water, from concentrations of approximately 10 mg/mL down to concentrations of approximately 1 mg/mL as confirmed by NanoDrop. The 1 mg/mL samples were injected onto the column at an injection volume of 10  $\mu$ L. Samples were isocratically delivered with a pH 7.4 1x PBS mobile phase at a flow rate of 0.4 mL/min over 10 minutes. MAb samples were detected and compared via UV absorbance chromatograms that were extracted at 280 nm.

### **Free Thiol Analysis**

Free thiols were analyzed through the use of a thiol-reactive probe, BODIPY<sup>TM</sup> FL N-(2-aminoethyl) maleimide (ThermoFisher Scientific). This probe is referred to as bodipy maleimide throughout the rest of the chapter. Bodipy maleimide stock solutions were prepared through reconstitution in DMSO at a concentration of 1 mg/mL and then then diluted to 0.2 mg/mL with 8M GuCl. Bodipy maleimide stock solutions (and any resulting solutions) were wrapped in aluminum foil to prevent light exposure. Stock solutions were kept at -20°C prior to usage. Rituximab and bevacizumab samples were adjusted to concentrations of approximately 2 mg/mL (concentrations recorded using a NanoDrop One Microvolume Spectrophotometer [ThermoFisher Scientific]) and mixed at a 1:1 (v/v) ratio with bodipy maleimide stock solution and incubated overnight at 4°C. Samples were then injected onto a Waters Acquity UPLC BEH450 SEC column (1.7 $\mu$ m, 2.1 x 150mm) at an injection volume of 10 $\mu$ L and isocratically delivered with a mobile phase composed of 20% ACN (0.1% TFA)/80% water (0.1% TFA) at a flow rate of 0.3 mL/min. MAb samples were detected and compared via fluorescence (excitation: 504



nm, emission: 514 nm). Fluorescence AUCs were normalized to concentration and compared.

#### 4.4 Results

##### Infliximab vs Rituximab Bevacizumab

First, we quantified and compared expected disulfide, shuffled disulfide and trisulfide bonds for originator and biosimilar infliximab. The relative contribution of expected bonds (relative to sum of expected disulfide, shuffled disulfide and trisulfide bonds) and normalized contributions (relative to total expected XIC AUC) of all isolated expected bond locations for originator/biosimilar infliximab are shown in Fig. 4-1. The relative contribution of expected bonds for originator infliximab ( $99.579 \pm 0.045\%$ ) was slightly higher than the biosimilar ( $99.447 \pm 0.004\%$ ,  $p < 0.05$ ). When normalized contributions were calculated for isolated expected bond locations, no differences were observed between the originator and the biosimilar. While variation appears high between expected bond locations, ranging between 0.2 and 27.0% normalized contribution, a fairly even distribution between expected bond locations was indicative of a successful and thorough digestion.

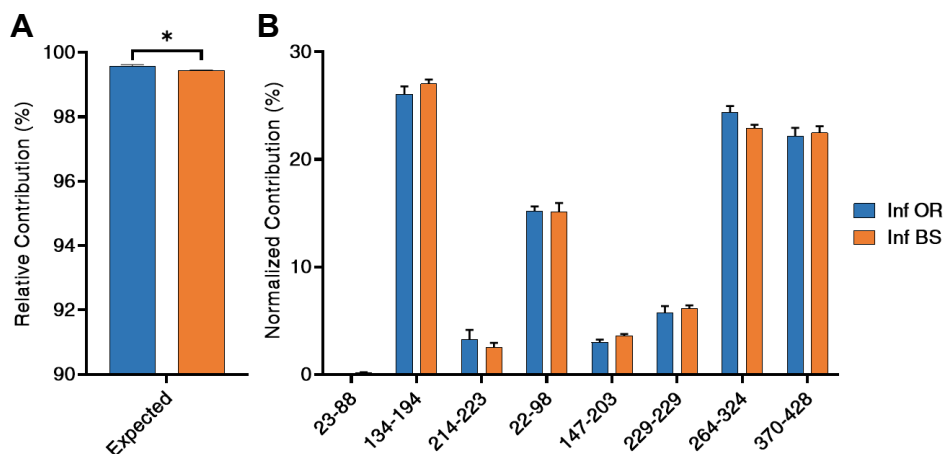


Figure 4-1. Comparison of infliximab originator/biosimilar by (A) relative expected contributions and (B) normalized contributions; Relative = divided by XIC AUC Totals of expected disulfide, shuffled disulfide and trisulfide bonds; Normalized = divided by specified XIC AUC total.

The relative contribution of shuffled disulfide bonds and the normalized contribution of the top ten most prevalent shuffled bond locations for originator and biosimilar infliximab are shown in Fig. 4-2.

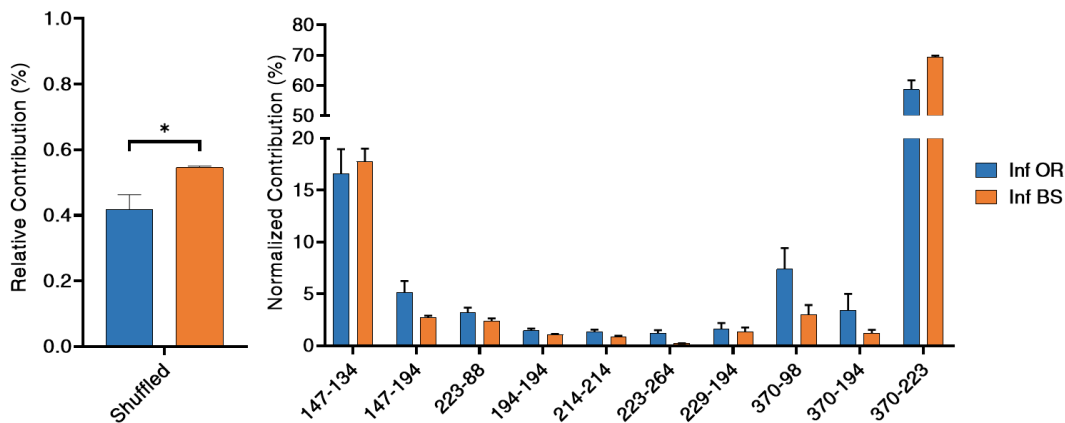


Figure 4-2. Comparison of shuffled disulfide bonds when trypsin digested at pH 5 for originator/biosimilar infliximab by (A) relative shuffled contributions and (B) normalized shuffled contributions for the top 10 shuffled bond locations.

The relative contribution of shuffled disulfide bonds for biosimilar infliximab ( $0.546 \pm 0.004\%$ ) was observed to be higher than the originator ( $0.418 \pm 0.044\%$ ,  $p < 0.05$ ). When comparing normalized contributions of the top ten shuffled bond locations, no significant differences were observed between originator and biosimilar infliximab. In addition, indicating that both originator and biosimilar infliximab undergo similar mechanisms of degradation. Of the ten listed shuffled disulfide bonds, five occur between cysteines in the variable region and five occur between a cysteine in the variable region and a cysteine in the constant region. Five of the listed shuffled disulfide bonds occur between the HC and LC (inter-chain), while two occur within the LC and three occur within the HC (intra-chain). The shuffled locations 194-194 and 214-214 stood out as examples of a limitation of the described method (see Discussion).

The relative contribution of trisulfide bonds and normalized contributions of the only two detected trisulfide bonds are shown in Fig. 4-3. The relative trisulfide contribution for originator infliximab (0.002%) was slightly lower than the biosimilar (0.006%). Originator/biosimilar infliximab had similar normalized contributions, though both were extremely low only appearing mainly at the 134-223 location.

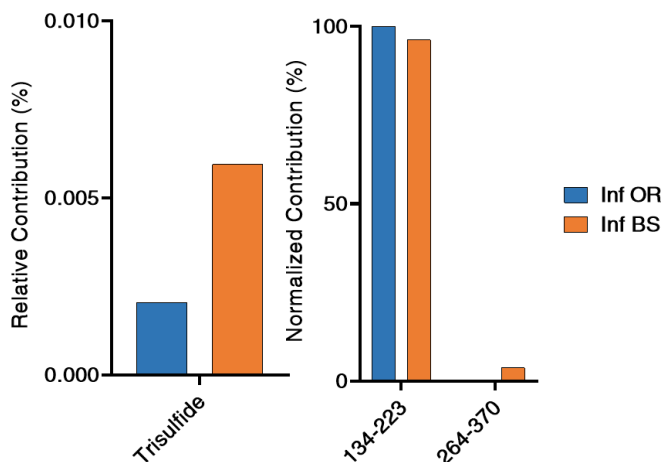


Figure 4-3. Comparison of trisulfide bonds for originator/biosimilar infliximab (A) relative trisulfide contributions and (B) prevalent normalized contribution locations.

Next, we quantified and compared expected disulfide, shuffled disulfide and trisulfide bonds for originator and biosimilar rituximab. The relative contribution of expected bonds (relative to sum of expected disulfide, shuffled disulfide and trisulfide bonds) and normalized contributions (relative to total expected XIC AUC) of all isolated expected bond locations for originator/biosimilar infliximab are shown in Fig. 4-4. The relative contribution of expected bonds for originator infliximab ( $99.76 \pm 0.12\%$ ) was identical to the biosimilar ( $99.73 \pm 0.04\%$ ). When normalized contributions were calculated for isolated expected bond locations, no differences were observed between the originator and the biosimilar. While variation appears high between expected bond locations, ranging between 0.1 and 63% contribution. This large range, in addition to a poor distribution between expected bond locations, was indicative of a digestion that

was not as thorough, relative to the digestion seen for infliximab expected bond locations.

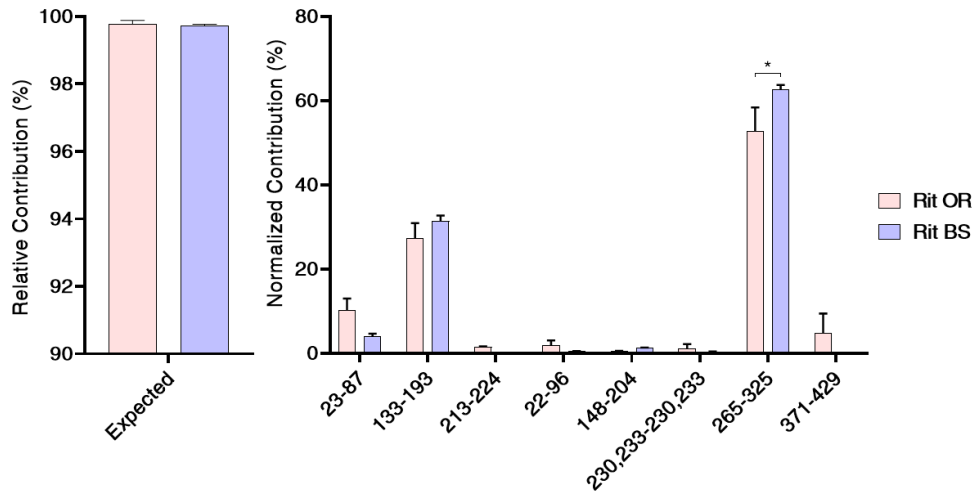


Figure 4-4. Comparison of originator/biosimilar rituximab by (A) relative expected contributions and (B) normalized contributions.

The relative contribution of shuffled disulfide bonds and the normalized contribution of the top ten most prevalent shuffled bond locations for originator and biosimilar infliximab are shown in Fig. 4-5.

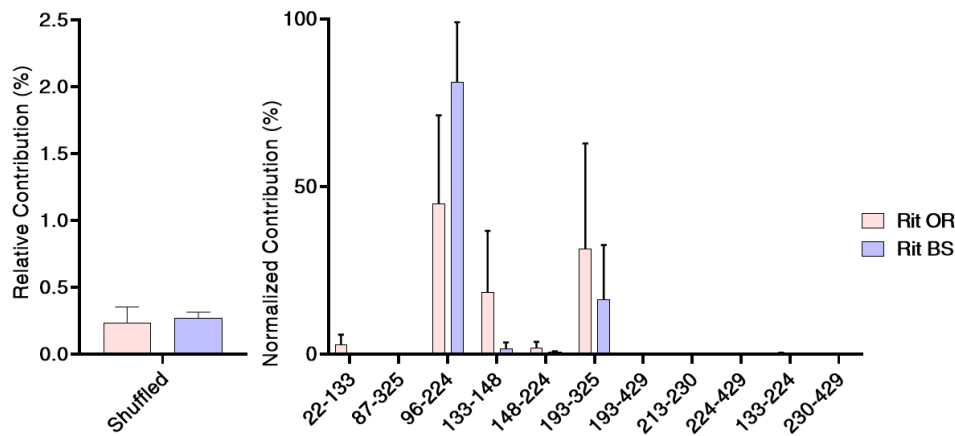


Figure 4-5. Comparison of originator/biosimilar rituximab by (A) relative shuffled contributions and (B) normalized contributions.

The relative contribution of shuffled disulfide bonds for originator rituximab ( $0.24 \pm 0.12\%$ ) was also observed to be identical to the biosimilar ( $0.27 \pm 0.04\%$ ). When comparing normalized contributions of the top ten shuffled bond locations, no significant

differences were observed between originator and biosimilar infliximab as variation was high. No trisulfides were detected for rituximab.

Next, we quantified and compared expected disulfide, shuffled disulfide and trisulfide bonds for originator and biosimilar bevacizumab. The relative contribution of expected bonds (relative to sum of expected disulfide, shuffled disulfide and trisulfide bonds) and normalized contributions (relative to total expected XIC AUC) of all isolated expected bond locations for originator/biosimilar bevacizumab are shown in Fig. 4-6. The relative contribution of expected bonds for originator bevacizumab ( $99.3 \pm 0.12\%$ ) was higher than the biosimilar ( $98.0 \pm 0.35\%$ ). When normalized contributions were calculated for isolated expected bond locations, two significant were observed that were not seen for both infliximab and rituximab, at the 134-194 and 267-327 locations. While variation again appears high between expected bond locations, this distribution appears to be similar to that seen for rituximab, indicative of a digestion that was not as thorough, relative to the digestion seen for infliximab expected bond locations.

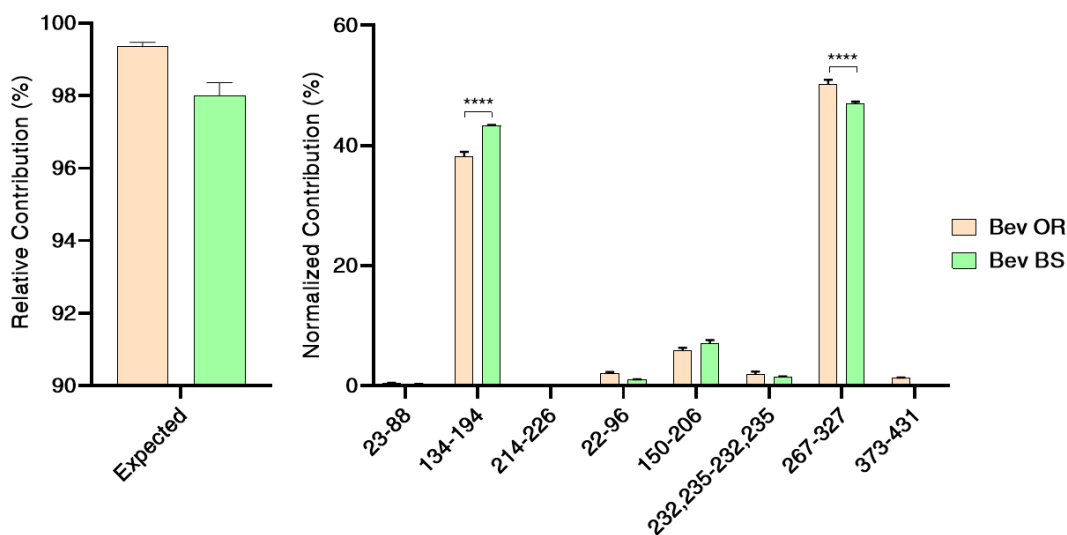


Figure 4-6. Comparison of originator/biosimilar bevacizumab by (A) relative expected contributions and (b) normalized contributions.

The relative contribution of shuffled disulfide bonds and the normalized contribution of the top ten most prevalent shuffled bond locations for originator and biosimilar bevacizumab are shown in Fig. 4-7.

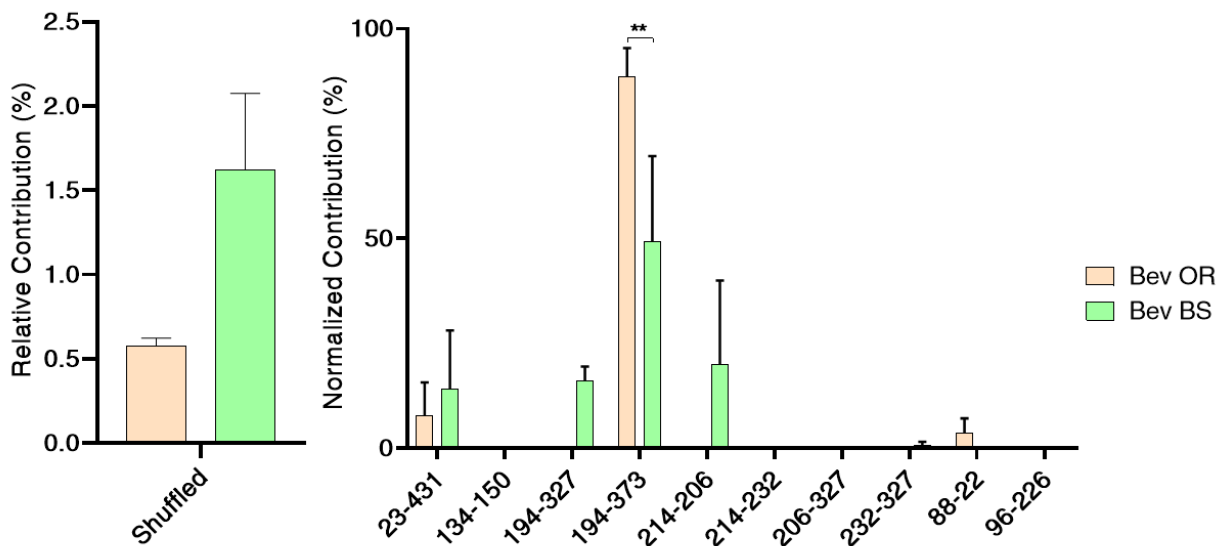


Figure 4-7. Comparison of originator/biosimilar bevacizumab by (A) relative shuffled contributions and (B) normalized contributions.

The relative contribution of shuffled disulfide bonds for the biosimilar ( $0.546 \pm 0.004\%$ ) was observed to be higher than the originator ( $0.418 \pm 0.044\%$ ,  $p < 0.05$ ) was observed to be less than the,  $p < 0.05$ ). When comparing normalized contributions of the top ten shuffled bond locations, significant differences were observed between originator and biosimilar infliximab at the 194-373 location (inter-chain). In addition, indicating that both originator and biosimilar infliximab undergo similar mechanisms of degradation. Of the ten listed shuffled disulfide bonds, five occur between cysteines in the variable region and five occur between a cysteine in the variable region and a cysteine in the constant region. Nine of the listed shuffled disulfide bonds occur between the HC and LC (inter-chain), while one occurs within the HC (intra-chain).

The relative contribution of trisulfide bonds and normalized contributions of the only two detected trisulfide bonds are shown in Fig. 4-8. The relative trisulfide contribution for originator infliximab (0.002%) was slightly lower than the biosimilar (0.006%). Originator/biosimilar infliximab had similar normalized contributions, though both were extremely low only appearing mainly at 22-96, an expected intra-chain bond, and 194-226, an inter-chain bond, locations.

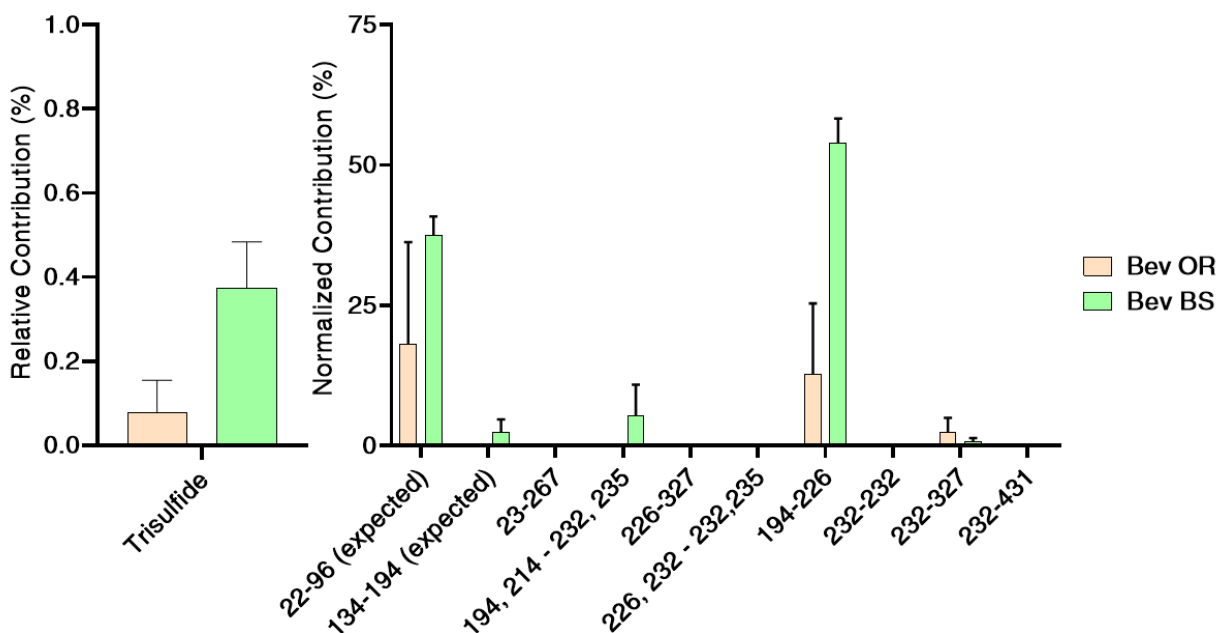


Figure 4-8. Comparison of trisulfide bonds for originator/biosimilar bevacizumab (A) relative trisulfide contributions and (B) prevalent normalized contribution locations.

Bevacizumab and infliximab biosimilars exhibited greater disulfide shuffling and trisulfide bonding than their originator counterparts, while rituximab originator and biosimilar were identical, where no trisulfide bonds were detected. In addition, we were able to rank order the originator and biosimilar pairs, where bevacizumab had the most disulfide shuffling and trisulfide bonding while rituximab had the least disulfide shuffling and no trisulfide bonds were detected.

Free thiol content for these originator and biosimilar infliximab, rituximab and bevacizumab pairs were determined. Chromatograms for samples labeled with bodipy maleimide are shown below in Fig. 4-9 and are quantified in Fig. 4-10.

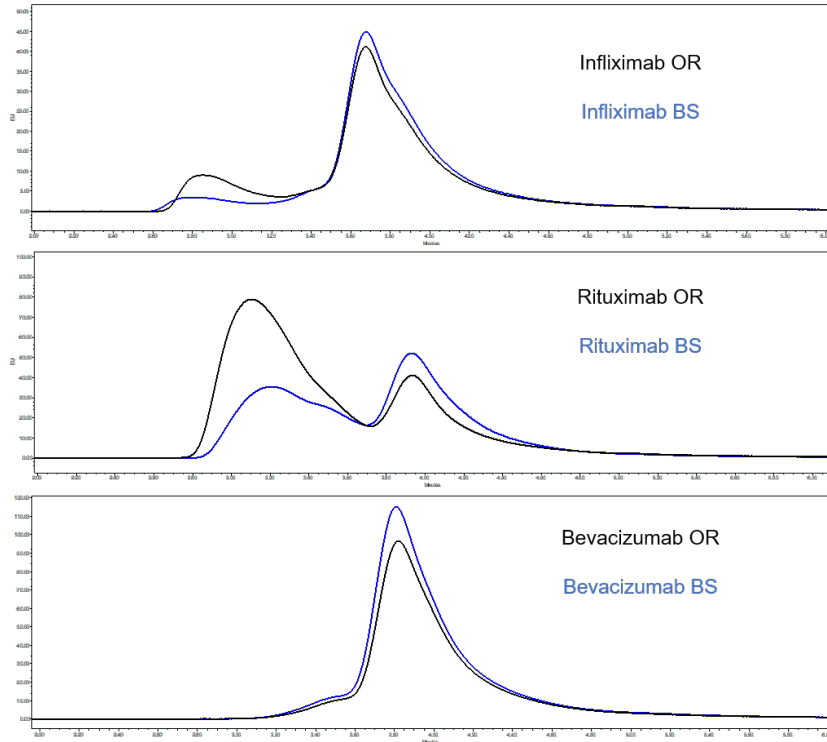


Figure 4-9. SEC-LC chromatogram overlays of originator/biosimilar (A) infliximab, (B) rituximab and (C) bevacizumab when labeled overnight with bodipy maleimide.

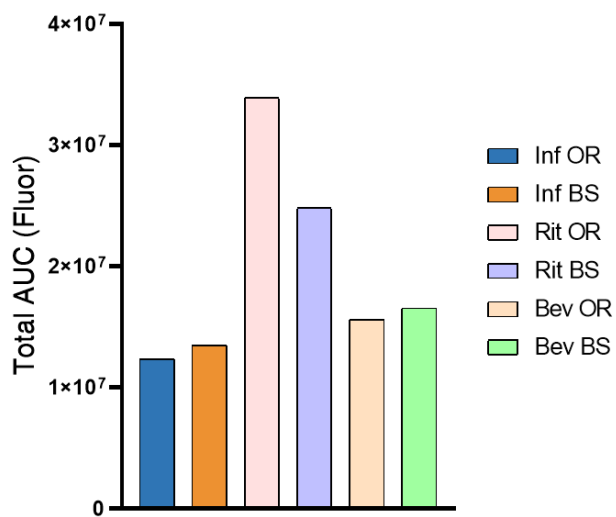


Figure 4-10. Quantified AUCs for SEC-LC chromatogram of originator/biosimilar infliximab, rituximab and bevacizumab when labeled overnight with bodipy maleimide.



The first noticeable difference observed was that observed between SEC-LC chromatograms of different mAb types, where originator and biosimilar infliximab, rituximab and bevacizumab all exhibited different distribution profiles. All three profiles have what appears to be a main peak at retention times between 3.6 and 3.9 minutes with significant tailing. While bevacizumab only has a minor secondary peak at approximately 3.4 minutes, infliximab has a noticeably larger secondary peak at 2.9 minutes while rituximab has a secondary peak at approximately 3.1 minutes. While profile distributions may seem of interest, understanding of contributing peaks is rendered less useful due to the use of 20% ACN organic phase in the mobile phase. Therefore, AUC was quantified and compared totals between approximately 2 and 6 minute retention times, where AUCs were representative of free thiol content.

We first compared originators against biosimilars, where we observed more thiol content for biosimilar infliximab and bevacizumab than their originators. For rituximab, though, the originator had a more free thiols than the biosimilar. In addition, rituximab had the most free thiols. In relations to disulfide shuffling, the biosimilar for both infliximab and bevacizumab exhibited greater disulfide shuffling and trisulfide bonding, seemingly indicating a relationship between free thiol content and disulfide shuffling. For rituximab, though, the originator had more free thiols while disulfide shuffling was similar for both. Unlike the other two mAb, this would seem to indicate that there is no relationship between free thiols and disulfide shuffling. This would likely be explained by the fact that the free thiol assay is limited by when free thiols are detected. For rituximab, newly exposed free thiols seem to be detected while free thiols for bevacizumab are lower, already participating in disulfide shuffling.

## Originator/Biosimilar Rituximab and Bevacizumab Subject to Forced Degradation Electrophoresis Gels

Gels were run at concentrations of 0.25 and 0.4 mg/mL to visualize the presence of minor aggregate and fragment component bands (Fig. 4-11).

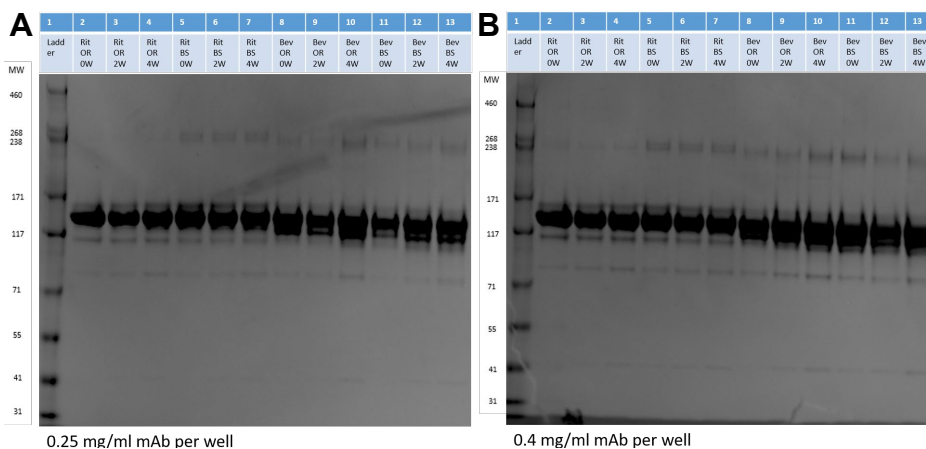


Figure 4-11. SDS PAGE gels for bevacizumab and rituximab originator and biosimilar mAb pairs at (A) 0.25 and (B) 0.4 mg/mL comparing HiMark Prestained Protein Ladder against mAb pairs after 0, 2 and 4 weeks of incubation at 37°C; n = 1.

The main monomer bands appear at a MW of approximately 145 and 150 kD, which matches the expected MWs reported in package inserts as 145 and 149 kD, respectively.<sup>441,442</sup> While difficult to precisely quantify due to band overlap, there are some observed trends observed where the originator/biosimilar mAb pairs differed over the course of incubation. When comparing rituximab originator/biosimilar, we noticed that initial amounts of aggregates (~155 kD) and fragments (~115 kD) were present that did not seem to change over the course of incubation. In terms of differences observed, the rituximab biosimilar had distinct initial aggregates (~255 kD, not present in the originator) that did not appear to change over the course of incubation. The innovator's 85 kD fragment does appear to increase over the course of incubation, but only after 4 weeks. Bevacizumab originator and biosimilar appeared similar in terms of levels of aggregates and fragments both initially and over the course of incubation. In terms of all

mAbs, a small fragment component at ~41 kD was present at 0.4 mg/mL and seemed to be the most intense after 4 weeks of incubation. On the whole, it appears that our rituximab and bevacizumab originator/biosimilar pairs to start with initial degradant components that also changed over the course of incubation. It is of note that these studies were performed on expired mAb products. The relative contribution from aggregate, monomer and fragment species were quantified and shown in Fig. 4-12.

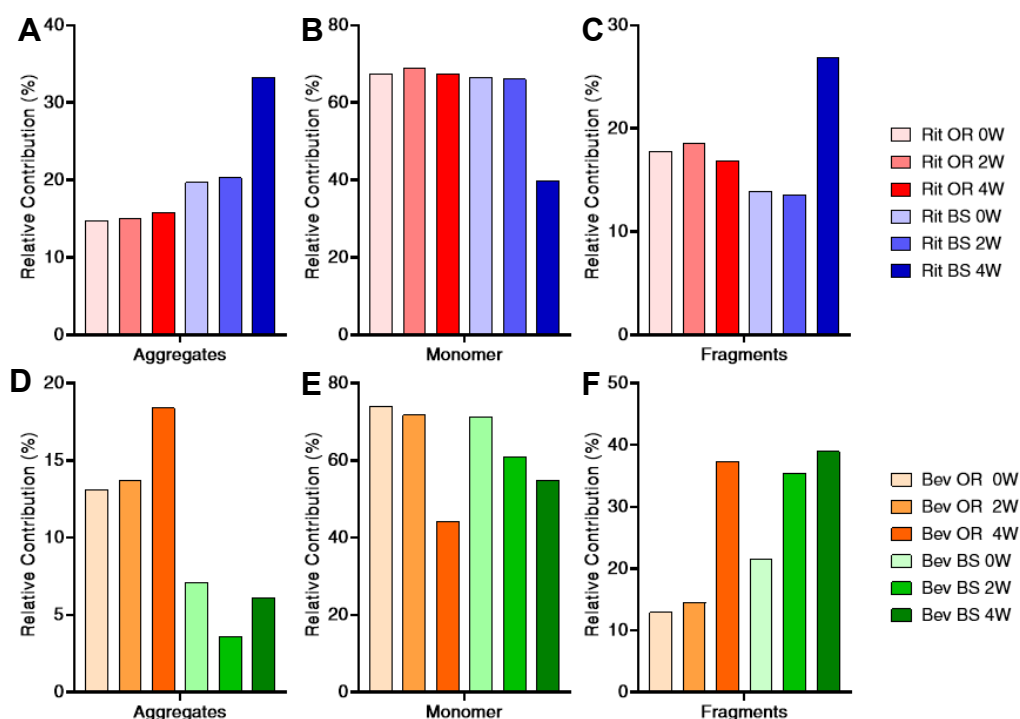


Figure 4-12. SDS-PAGE relative contributions for rituximab originator/biosimilar (A) aggregates, (B) monomer and (C) fragments and relative contributions for bevacizumab originator/biosimilar (D) aggregates, (E) monomer and (F) fragments over the course of 4 weeks of incubation at 37°C; n = 1.

### SEC Physical Degradation Analysis

Physical degradation of bevacizumab and rituximab originator/biosimilar pairs were also compared by SEC over the course of incubation and were quantified as a function of change of levels of monomer and degradants, including aggregates and fragments. SEC-LC chromatograms are shown below in Fig. 4-13 and are quantified in Fig. 4-14, where marked differences were observed both initially and over the course of incubation. The samples analyzed were the same as those that run on SDS-PAGE gels.

The purpose was to investigate if similar trends of degradation were observable by orthogonal methods prior to analysis by LC-MS/MS, the main focus of this chapter.

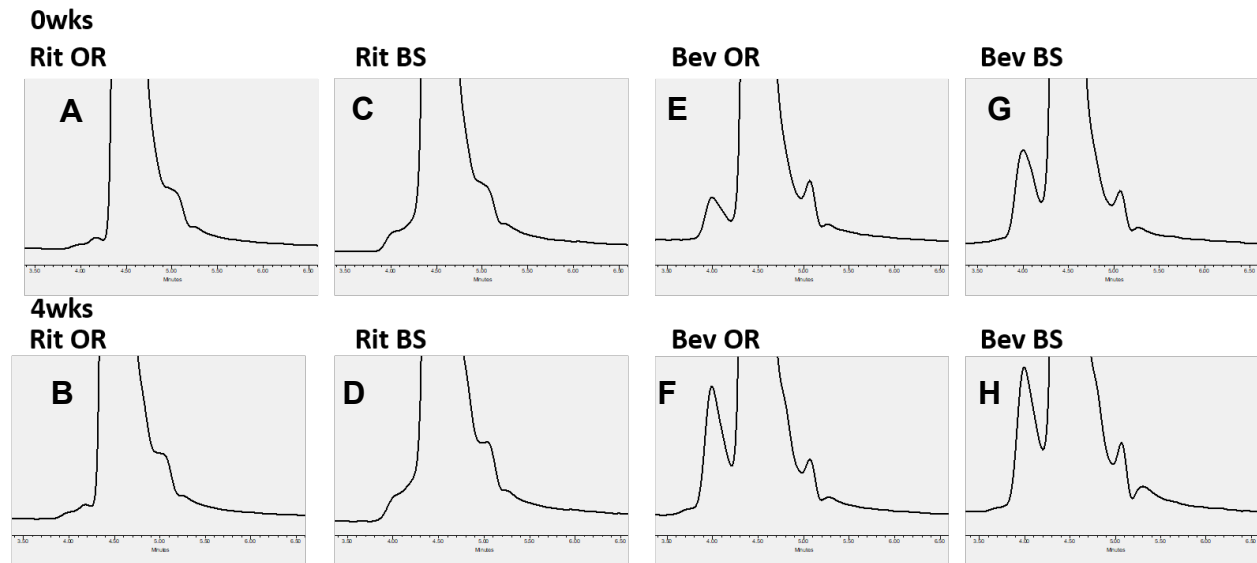


Figure 4-13. SEC-LC chromatograms of rituximab originator at (A) 0 and (B) 4 and biosimilar at (C) 0 and (D) 4 weeks of incubation at 37°C. Bevacizumab originator at (E) 0 and (F) 4 and biosimilar at (G) 0 and (H) 4 weeks of incubation at 37°C.

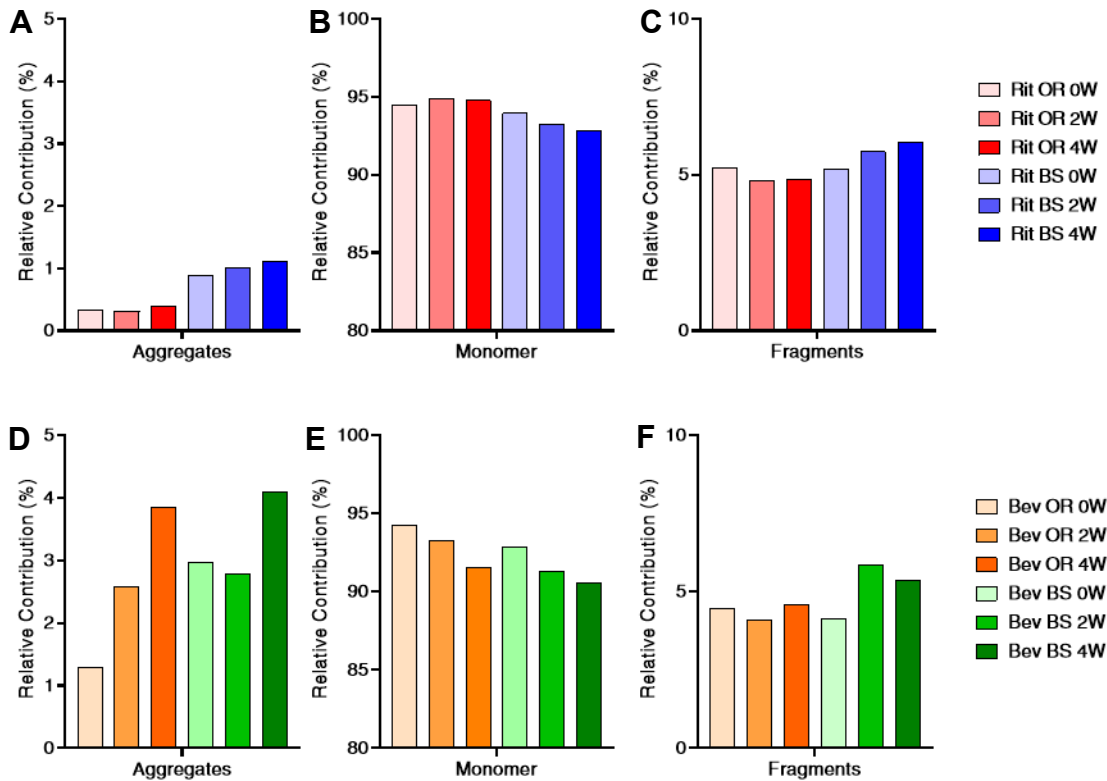


Figure 4-14. SEC relative contributions for rituximab originator/biosimilar (A) aggregates, (B) monomer and (C) fragments and relative contributions for bevacizumab originator/biosimilar (D) aggregates, (E) monomer and (F) fragments over the course of 4 weeks of incubation at 37°C. (n = 1)

The rituximab originator was observed to have the most amount of initial monomer content (94.4%), least amount of initial degradants, which included mainly fragments (5.2%) and small amounts of aggregates (0.3%). Rituximab did not exhibit monomer loss over incubation. Lower levels of initial monomer content (94.0%) were observed for the rituximab biosimilar (94.0%), which reflected an elevated level of aggregates (0.9%), while levels of fragments were similar (5.2%). Unlike rituximab originator, the biosimilar exhibited a decrease in monomer content over incubation, with increases of fragments (to 6.1%) and aggregates (to 1.1%) after 4 weeks. 4-week originator/biosimilar rituximab/bevacizumab chromatograms qualitatively show observable differences for the relative contribution of aggregates and fragments.

While the bevacizumab originator had similar initial levels of monomer content (94.3%) as the rituximab originator, there were relatively more aggregates (1.3%) for bevacizumab. Again, the main degradant species were fragments. The bevacizumab biosimilar had the least initial monomer content (92.9%). While having the most relative amounts of aggregates, fragments were the main degradant observed. Both bevacizumab originator/biosimilar degraded to a greater extent than rituximab originator/biosimilar, with monomer content decreasing to 91.6% to 90.6% over incubation, respectively. While fragments make up the largest relative degradant species, further bevacizumab originator degradation, increasing to 3.85% over incubation. Degradation of bevacizumab biosimilar appeared to be driven by both aggregation, increasing to 4.09%, and fragmentation, increasing to 5.37%, after 4 weeks of incubation.

## Disulfide Bond Analysis: Expected vs Shuffled vs Trisulfide

Expected disulfide bond locations for rituximab and bevacizumab are shown below in Fig. 4-15. Upon inspection of their amino acid sequences, expected disulfide bond locations and number of cysteines (32, the minimum number required for expected bonds) were confirmed to be similar, as is expected for IgG1 mAbs. Figures were generated from Protein Metrics Byonic/Byologic workflow, where mAbs were compared as a function of quantifiable XIC AUCs. Relative contributions of expected disulfide, shuffled disulfide and trisulfide bonds, when detected, for originator and biosimilar rituximab and bevacizumab pairs over the course of incubation are shown below in Fig. 4-16.

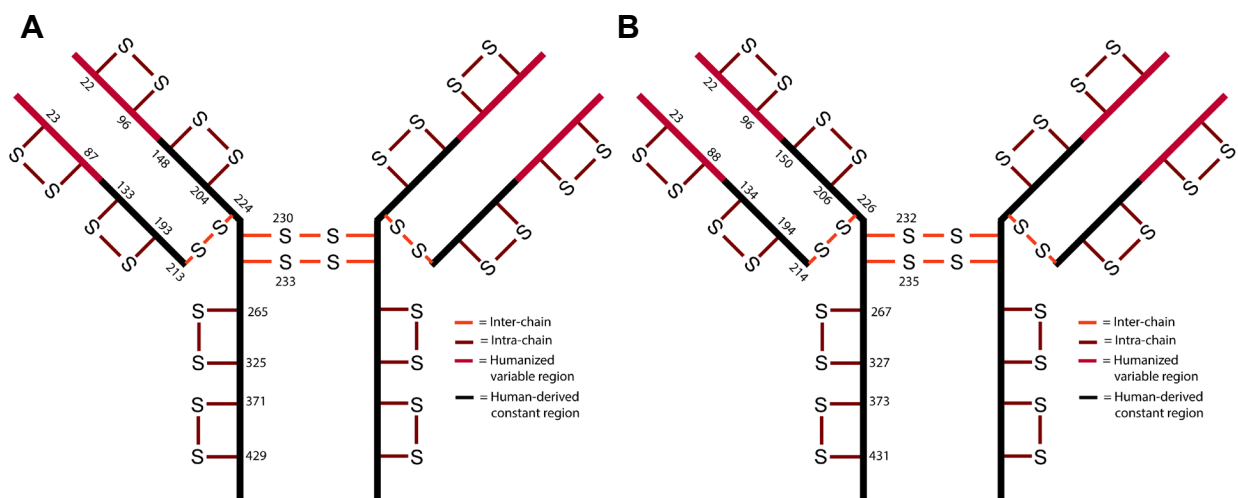


Figure 4-15. Labeled cysteines and expected disulfide bond locations for (A) rituximab and (B) bevacizumab.

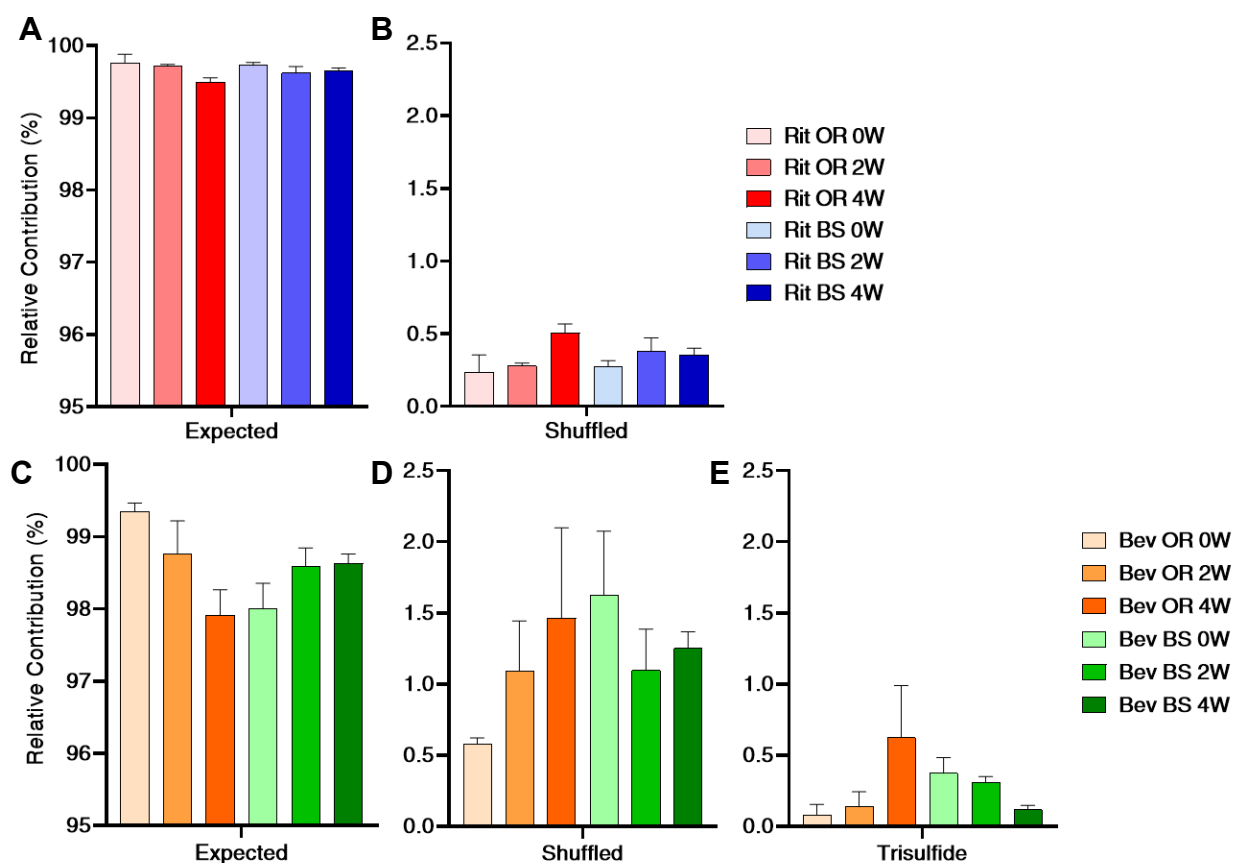


Figure 4-16. Relative contributions of expected disulfide bonds, shuffled disulfide bonds and trisulfide bonds for (A) rituximab originator/biosimilar and (B) bevacizumab originator/biosimilar over the course of 4 weeks of incubation at 37°C. n = 3, mean ± SEM.

As shown previously, the initial relative contribution from expected and shuffled disulfide bonds for rituximab originator and biosimilar were similar, where no trisulfide bonds were detected. Minor decreases of expected disulfide bonds were matched by similar increases of shuffled disulfide bonds for the originator (to  $0.28 \pm 0.02$  and  $0.51 \pm 0.06\%$ ) and biosimilar (to  $0.38 \pm 0.09$  and  $0.35 \pm 0.05\%$ ) after 2 and 4 weeks of incubation, respectively. The relative contributions and trends of changes of expected bonds seem to support the trends observed for physical degradation analyzed by SEC and SDS-PAGE, where rituximab originator and biosimilar appeared to undergo less

degradation over incubation than bevacizumab. Both the originator and biosimilar have increases of disulfide shuffling over the incubation.

For bevacizumab, the initial relative contribution from expected disulfide bonds was observed to be greater for the originator than the biosimilar. This difference which was matched by greater amounts of shuffled and trisulfide disulfide bonds for the biosimilar than the originator ( $1.62 \pm 0.45$  and  $0.37 \pm 0.11\%$ ). In addition, the trends of degradation by disulfide bond analysis appeared different over the incubation. Whereas the trend of degradation for the originator appears normal, where a decrease of relative expected contribution (to  $98.8 \pm 0.45$  and  $97.91 \pm 0.35\%$ ) is matched by an increase of relative shuffled contribution (to  $1.09 \pm 0.35$  and  $1.46 \pm 0.64\%$ ) and increase of relative trisulfide contribution (to  $0.14 \pm 0.10$  and  $0.62 \pm 0.37\%$ ) after 2 and 4 weeks, respectively. The trend of degradation for the biosimilar appears to be inverse, where the initial time point is the most degraded with a decrease of relative shuffled contribution (to  $1.09 \pm 0.35$  and  $1.46 \pm 0.64\%$ ) and a decrease of relative trisulfide contribution (to  $0.31 \pm 0.04$  and  $0.12 \pm 0.03\%$ ) after 2 and 4 weeks, respectively. While unusual, these results appear to match physical degradation results when analyzed by SEC and SDS-PAGE, where bevacizumab initially has more degradants, though the relationship between the two becomes muddled over incubation, where loss of shuffled and trisulfide bond contributions may be likely due to precipitation of the biosimilar.



## Shuffled/Trisulfide Bonds

Distributions and locations of shuffled bonds were identified and compared for rituximab and bevacizumab originator/biosimilar over the course of incubation and are reported as normalized contributions to shuffled XIC AUC totals (Fig. 4-17). Shuffled bond locations were organized as a function of inter-chain and intra-chain bonds. Intra-chain bonds were observed to make up the clear minority of shuffled bonds for both rituximab (133-224 and 230-429) and bevacizumab (22-88 and 96-226). It should also be noted that the digestion again appears incomplete as sample-to-sample variations were high, with only few locations having shuffling across all 3 samples.

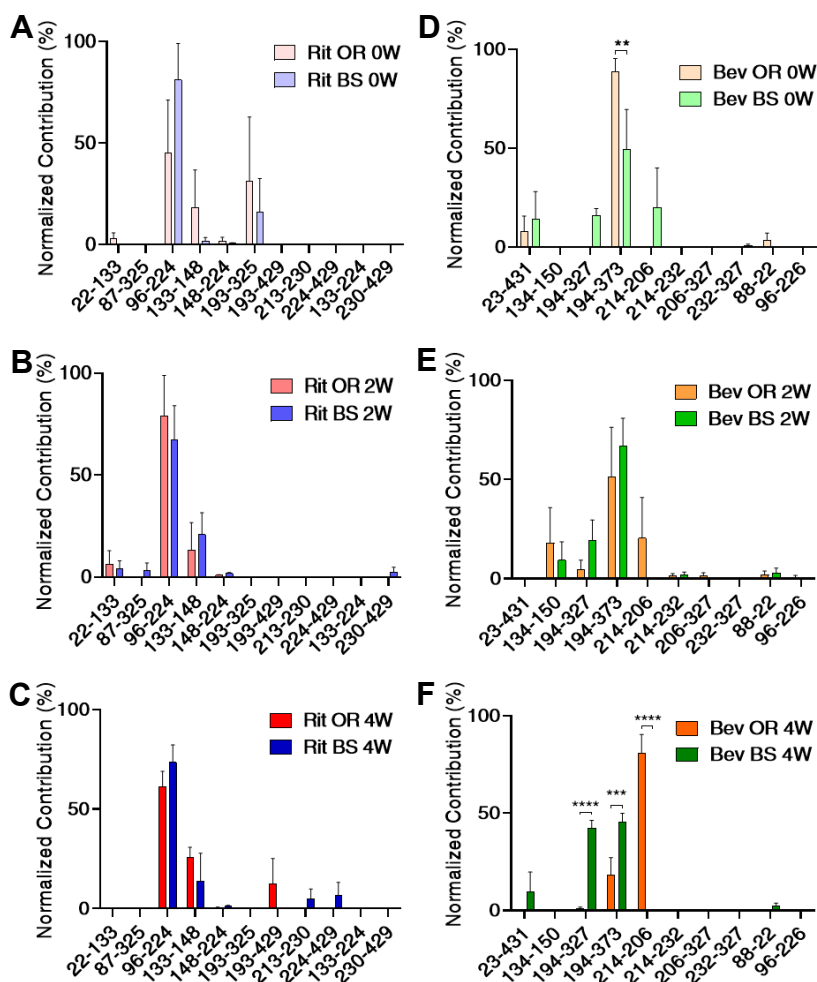


Figure 4-17. Normalized contributions of shuffled bonds comparing originator/biosimilar rituximab at (A) 0, (B) 2 and (C) 4 weeks and bevacizumab at (D) 0, (E) 2 and (F) 4 weeks of incubation at 37°C; n = 3, mean ± SEM.

For rituximab, there were no significant differences detected between the originator/biosimilar at all time points. In addition, shuffled bond distributions for rituximab remained somewhat similar over the course of incubation. Though not statistically significant, a general trend of similarity was indicated by the normalized contribution of the largest 2 shuffled bond species at 96-224 and 133-148 locations for the originator and biosimilar at,  $63.4 \pm 55.1\%$  and  $82.9 \pm 28.0$ ,  $92.6 \pm 10.9\%$  and  $88.2 \pm 17.1\%$  and  $86.8 \pm 22.0\%$  and  $87.4 \pm 9.4\%$  at 0, 2 and 4 weeks, respectively. These two shuffled bond locations were the only ones detected across all 3 samples.

For bevacizumab, there was only 1 observed statistically significant difference at the 194-373 location, which made up  $88.6 \pm 6.8\%$  (originator) and  $49.3 \pm 20.4\%$  (biosimilar) at 0 weeks ( $p < 0.01$ ). Though no statistically significant differences were observed at 2 weeks, the most significant differences were observed at 4 weeks at the following shuffled bond location; 194-327,  $0.9 \pm 1.6\%$  vs  $42.2 \pm 7.3\%$  ( $p < 0.001$ ), 194-373,  $18.1 \pm 15.8\%$  vs  $45.4 \pm 8.1\%$  ( $p < 0.005$ ), and 214-206,  $81.0 \pm 16.5\%$  vs  $0\%$  ( $p < 0.001$ ). Trends in shifts of distributions of shuffled disulfide bonds are specifically indicated through the 194-373 location, which makes up  $88.6 \pm 11.8\%$  and  $49.3 \pm 35.3\%$ ,  $51.5 \pm 43.0\%$  and  $67.1 \pm 23.9\%$  and  $18.1 \pm 15.8\%$  and  $45.4 \pm 8.1\%$  for the originator and biosimilar at 0, 2 and 4 weeks, respectively. This single location is the only location detected across all three samples. The shift in distribution of shuffled bonds for bevacizumab indicates not only that there is a difference between bevacizumab originator/biosimilar, but also that bevacizumab degraded more extensively than rituximab.

Trisulfide bonds were only identified in bevacizumab. Trisulfide bond distributions were compared between bevacizumab originator/biosimilar over the course of incubation and are shown as normalized contributions to trisulfide XIC AUC totals (Fig. 4-18). Trisulfide bond locations were observed at expected, inter-chain and intra-chain locations. The majority of trisulfide bonds were observed as a subset of the 22-96 (expected) and 194-226 (shuffled) bond locations. Distributions were observed to shift over the course of incubation, which, unlike rituximab matches the increased degradation and shifts of shuffled disulfide bond distributions for bevacizumab.

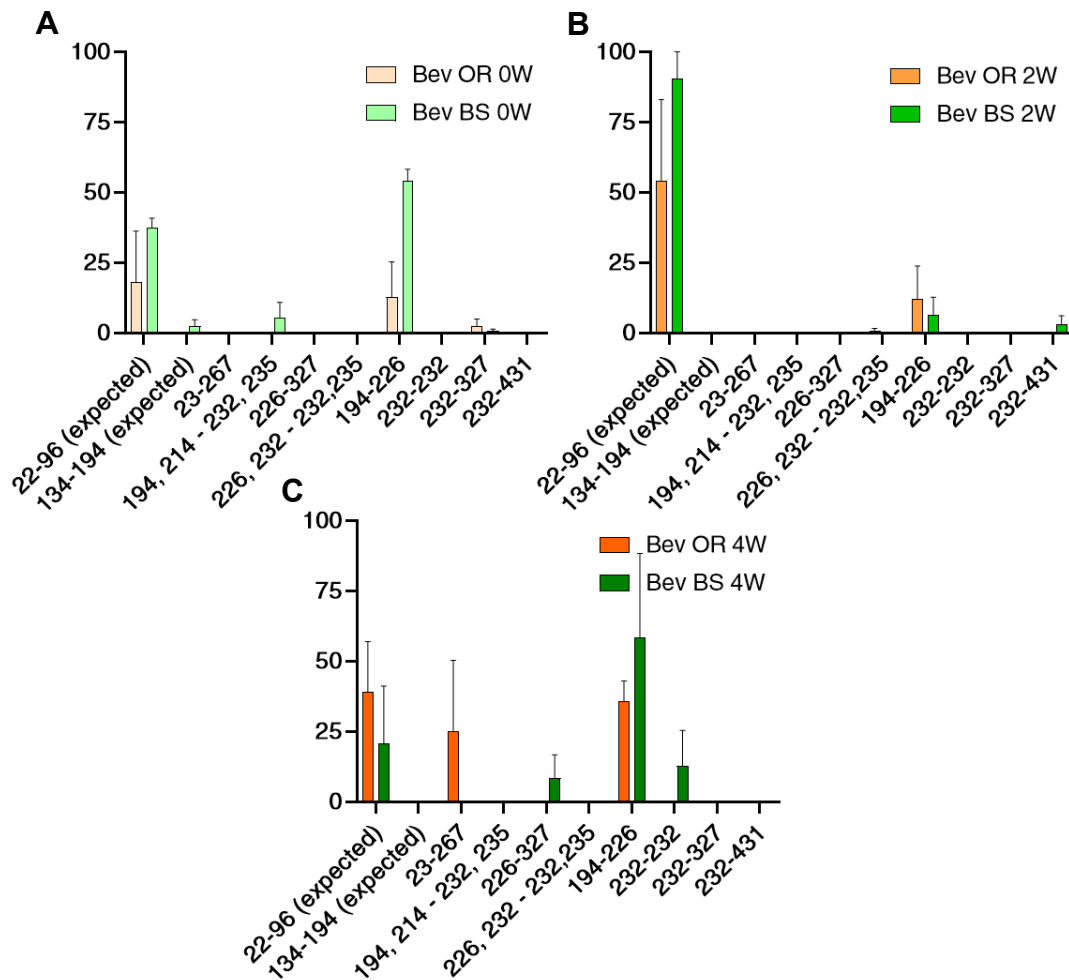


Figure 4-18. Normalized trisulfide contributions for bevacizumab at (A) 0, (B) 2 and (C) 4 weeks of incubation at 37°C; n = 3, mean ± SEM.

## Free Thiol Analysis: Maleimide

Bodipy maleimide was used to investigate the potential relationship of free thiols to physical degradation and disulfide shuffling. Bodipy maleimide is a free thiol probe, where conjugation allows for detection by fluorescence. Free thiols were compared as a function of total AUC as organic is used in the mobile phase. The main assumption for this method was that a higher AUC is an indicator of larger amounts of free thiols.

Samples were the same as those previously characterized by SDS PAGE and SEC.

Fluorescence SEC-LC chromatograms for bodipy maleimide labeled originator rituximab and bevacizumab samples over the course of incubation are shown in Fig. 4-19 and are quantified in Fig. 4-20.

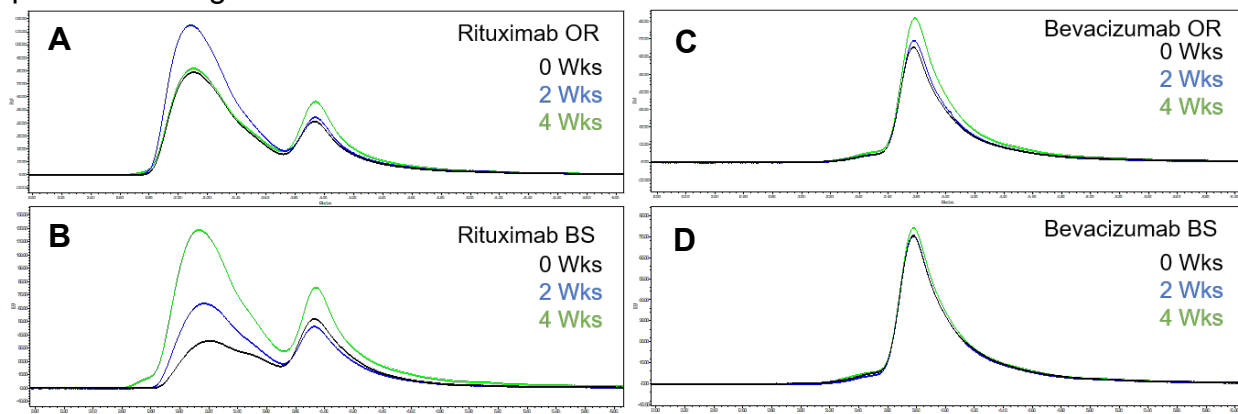


Figure 4-19. Fluorescence SEC-LC chromatograms overlays of OR/BS at 0,2 and 4 weeks of incubation for rituximab (A) OR and (B) BS and bevacizumab (C) OR and (D) BS incubated with bodipy maleimide.

For both rituximab and bevacizumab, the unlabeled blanks appeared at a retention time of approximately 4 minutes (data not shown). While a similar retention time appears for mAb samples labeled with bodipy maleimide, rituximab exhibits the formation of a secondary species at a retention time of approximately 3.1 minutes, while bevacizumab shows a small secondary peak at approximately 3.4 minutes. In addition, the main component for both appears to have significant tailing starting at approximately 4.05 minutes. A current limitation of this technique arises due to the use of organic phase ACN, which muddles our ability to differentiate the identity of each individual component in such chromatograms, hence why total AUCs are compared, as shown in Fig. 4-20.

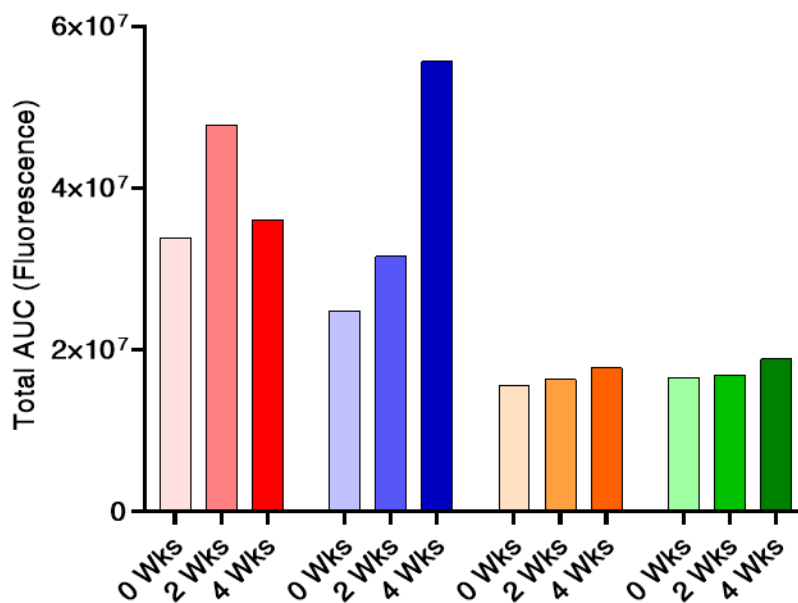


Figure 4-20. Free thiol total fluorescence AUCs for rituximab and bevacizumab OR/BS at 0, 2 and 4 weeks of incubation at 37°C; n = 1.

Changes of AUCs for originator/biosimilar rituximab/bevacizumab were compared over the course of incubation. Relative to 0 weeks, the rituximab originator AUC was 29.9 and 10.1% higher at 2 and 4 weeks, respectively. The AUC for the biosimilar, while initially less than the originator, increased approximately 24.4 and

120.8% after 2 and 4 weeks of incubation, respectively. Relative to the rituximab originator made up for 67.7% and 64.9% of total AUC at 0 and 2 weeks, respectively. At 4 weeks, though the biosimilar AUC was 35.9% higher than the originator. While disulfide shuffling was similar, increasing over the incubation, physical degradation was also the greatest for the biosimilar after 4 weeks of incubation.

Relative to 0 weeks, AUC for the bevacizumab originator increased by 4.9 and 14.1%, while the biosimilar increased similarly by 2.6 and 14.4% after 2 and 4 weeks of incubation, respectively. When comparing the AUC of the biosimilar against the originator, a consistent trend emerged, whereby the biosimilar was relatively higher than the originator at by 6.1%, 3.7% and 6.3% at 0, 2 and 4 weeks, respectively. This trend would make sense in conjunction with results seen for physical degradation and disulfide shuffling, where the biosimilar was more prone to aggregation and disulfide shuffling than the originator, though both were more prone to degradation than rituximab. In addition, free thiols for rituximab ranged between 2- and 3-fold higher than the bevacizumab samples at all time points. Again, the trend of less amounts of free thiols for bevacizumab would seem to be related to the fact that they are already participating in disulfide shuffling and aggregation, whereas newly exposed free thiols for rituximab are being detected.

## 4.5 Discussion

### Disulfide Analysis of Infliximab, Rituximab and Bevacizumab Pairs

The relative contribution of expected disulfide bonds was found to be significantly lower for biosimilar infliximab and bevacizumab than their originator, with both having greater disulfide shuffling and trisulfide bonding. While there were no significant differences observed when comparing the normalized contributions of isolated expected bond locations between originator and biosimilar infliximab, there were significant differences detected between originator and biosimilar bevacizumab. It is important to note the variation of normalized contributions across expected bond locations, with values ranging over two orders of magnitude. This variation is inherent to the LC-MS/MS method and is attributed to differences between ionization efficiencies of peptide sequences as one sequence may not “fly” similarly to another.<sup>443</sup> Therefore, further probing into the values of the distribution of expected bond locations should be taken into consideration, especially when evaluating if the digestion was complete and thorough. Relative to infliximab, the normalized expected contributions from rituximab and bevacizumab would imply their digestions were not complete and thorough. Even so, this variability is resolved by focusing on the comparability between the originator and biosimilar. While the top ten most prevalent shuffled locations were identical for originator and biosimilar infliximab and rituximab, indicating similarity of degradation pathways, they were not similar for originator and biosimilar bevacizumab. In terms of trisulfide bonding, there were only two trisulfide bonds detected at very low amounts for infliximab (less than 0.01%), while trisulfide bonding was markedly higher for the bevacizumab originator (~0.1%) and biosimilar (~0.5%). As a whole, rituximab originator

and biosimilar had the least amount of disulfide shuffling and no trisulfide bonding. Originator and biosimilar infliximab had slightly more disulfide shuffling and trisulfide bonding, while originator and biosimilar bevacizumab had the most disulfide shuffling and trisulfide bonding.

### **Intramolecular vs Intermolecular Disulfide Shuffling**

Another concept that must be accounted for is the difference of disulfide shuffling that occurs within a molecule (intra-molecular) and disulfide shuffling that occurs between two different molecules (inter-molecular). This is exemplified by the 194-194 and 214-214 shuffled bond locations (Fig. 4-2), which require intermolecular bonding. The addition of an orthogonal technique with high resolution of minimally present and intact degraded/shuffled species would be useful.

### **Effect of Forced Degradation on Rituximab and Bevacizumab Pairs**

#### **Disulfide Bond Analysis**

Though trends of decrease of relative expected contribution were observed for both originator and biosimilar rituximab, decreases were only slight and matched by increases of disulfide shuffling. No trisulfide bonds were detected for rituximab. Relative to rituximab, though originator and biosimilar bevacizumab had markedly reduced relative expected contributions and increased amounts of disulfide shuffling and trisulfide bonding. Within rituximab, the originator and biosimilar were similar, increasing over the incubation. Within bevacizumab, though the biosimilar had the largest amount of shuffling and trisulfide bonding at 0 weeks, which decreased after 2 and 4 weeks of incubation, potentially indicating its precipitation that resulted in decreased levels of



disulfide shuffling and trisulfide bonding. Even with the observed trends, changes of disulfide shuffling and trisulfide bonding were not statistically significant.

Normalized contributions of shuffled disulfide and trisulfide bond locations were then compared. Disulfide bonds for originator and biosimilar rituximab, indicated by similar distribution profiles of disulfide bond locations, were similar both initially and over the course of incubation, indicating that forced degradation did not cause the formation of differences. This was not the case for bevacizumab. In addition to significant initial differences in terms of disulfide bond locations, these initial differences appear to be exacerbated by incubation, with distributions becoming even more different after 4 weeks of incubation. This shift in distribution is a key indicator that bevacizumab seems to be not only more prone to degradation both the originator and biosimilar rituximab, but also a difference in degradation between the originator and biosimilar bevacizumab. A similar trend for normalized trisulfide contributions was observed as that seen for disulfide bonds, having both initial differences that were exacerbated over incubation.

### **Relationship Between Physical Degradation, Disulfide Shuffling and Free Thiols**

Common orthogonal physical characterization techniques were implemented to understand the potential relationship of physical degradants with disulfide shuffling. Similar trends in terms of the relative contributions from aggregate, monomer and fragment species were observed by both SDS-PAGE and SEC-LC. Originator and biosimilar rituximab remained similar over the course of incubation, though the biosimilar was slightly more degraded. On the other hand, originator and biosimilar bevacizumab were more initially degraded. Where differences were exacerbated with the application of forced degradation. This was even more so the case for the biosimilar

bevacizumab. The routes of physical degradation of rituximab and bevacizumab appeared to differ, where rituximab degradation was characterized mainly by the presence (and increase) of fragments while bevacizumab degradation was characterized by the increase of aggregates and fragments. The trends of increases of shuffled and trisulfide bonding for both seemed to match the degree and rate of physical degradation observed by these techniques.

The method developed for free thiol analysis was a result of several unsuccessful attempts using several previous approaches that are often used to determine free thiols. The first method tested was with Ellman's reagent, which was only applied to bevacizumab. We were unable to observe any free thiols, which may imply that bevacizumab does not have enough free thiols to appropriately reach the limit of detection. We then tried a technique found in a previously published paper, whereby the authors tested conjugation of various maleimide reagents with analysis by RPLC and UV detection.<sup>158</sup> Results using that method differed vastly from those reported (data not shown). We then found bodipy maleimide that imparts fluorescence and adjusted a common SEC method (that used 1x PBS as a mobile phase) by introducing 20% ACN to the mobile phase, the upper limit for our specified column. As far as we are aware, this bodipy maleimide method is not currently found in the literature for this application.

There are 2 potential underlying hypotheses that influence how free thiol data may be understood. The first hypothesis is that a greater amount of free thiols may induce degradation; the second hypothesis is that free thiol content increases as mAbs degrade. As there are no current publications on the changes of free thiol levels for

mAbs subjected to force degradation, one must consider types of physical degradants that may form.

To address the first hypothesis, where increased initial free thiol content could result in increased degradation, we notice that rituximab originator/biosimilar have approximately twice the AUC relative to bevacizumab. These results do not support such a hypothesis as rituximab undergoes less physical degradation and disulfide shuffling. On the other hand, the bevacizumab biosimilar was observed to have higher free thiol AUC at all time points relative to the originator and exhibited increased physical degradation and disulfide shuffling. In combination, these would seem to indicate that we can only compare initial free thiol content between an originator and a biosimilar. To address the second hypothesis, higher free thiol content was observed over the course of incubation for all mAb samples. Free thiol increases that were observed for rituximab originator/biosimilar were markedly higher than for bevacizumab. Additionally, increases for the rituximab biosimilar were higher than the originator, while increases for bevacizumab originator/biosimilar were approximately the same. This would seem to support such a hypothesis, though direct comparison between originator/biosimilar becomes more complex. Further studies would be necessary to elucidate whether the proposed hypothesis is valid.

Our results seem to indicate a limitation of our assay, where we are unable to determine when free thiols are detected. It appears that for rituximab, newly exposed free thiols are detected, hence a large increase. For bevacizumab, free thiols are detected after participating in disulfide shuffling and physical degradation, hence the low levels of free thiols for originator and biosimilar bevacizumab at all time points.

## **Chapter 5: Conclusions and Future Directions**

The work presented in this thesis focuses on aspects related to the development of peptide and mAb biopharmaceutical products. Via forced degradation, a combination of state-of-the-art and orthogonal characterization techniques provide valuable and comprehensive information on various instability mechanisms of biopharmaceutical products.

The first chapter provides a general introduction on the state of approval of biopharmaceutical products and their generic/biosimilar versions, analytical methodologies used to prove biosimilarity and typical instability mechanisms observed during forced-degradation studies of peptide and protein products. In the second chapter, we investigated the long-term stability of exenatide, a 39 amino acid GLP-1 receptor agonist peptide that is used to treat type 2 diabetes. While patent expirations for exenatide products are looming, novel extended-release formulation of GLP-1 agonists and recent co-formulations with insulin analogs warranted investigation of exenatide's stability profile as a representation of potential GLP-1 agonist degradation mechanisms. In addition, a recent focus on the effect of peptide degradants on immunogenic responses is a critical regulatory consideration for the approval of generic versions of exenatide as well as novel sustained-released formulations of peptide. When exenatide was studied at elevated pH, rapid chemical and physical degradation occurred. Chemical degradation was characterized by a pH-dependent increase of

deamidation impurities while physical degradation was mainly attributed to dimerization, aggregation and loss of  $\alpha$ -helicity, which was matched by an increase of unordered structural content. Aggregation was proposed to be a function of Trp-cage disruption. The addition of common excipients to the peptide solution, despite some of their presumed protective functions, were unable to prevent degradation at elevated pH 7.5. In fact, trehalose seemed to further destabilize exenatide. While a previous publication has investigated the impact of deamidation chemical impurities on GLP-1R binding, we observed the formation of multiple additional oxidation chemical impurities, that had yet to be characterized for their biological activities. In addition, while we do see the formation of multiple oxidation and deamidation impurities, we are unsure of the locations of the modified amino acid residues. There are three sets of future studies that may be applicable as a follow-up. The first, detailed identification of the locations of chemical modifications on exenatide's sequence and understanding of how individual modifications impact a GLP-1R receptor binding. The second study could be focused on development of an understanding of how chemical and physical impurities of exenatide impact peptide immunogenicity. This study will be critical for the approval of generic version of Byetta and Bydureon. The third set of future studies, though not of exenatide itself, would be the generation of stability profiles of currently marketed GLP-1R/insulin analog co-formulations (Xultophy and Soliqua).

In the third and fourth chapters, comparability studies of originator/biosimilar infliximab, rituximab and bevacizumab pairs were performed. In both chapters, we investigated the applicability of tandem mass spectrometry (LC-MS/MS) to elucidate initial differences and enhance the purity information provided by traditional analytical

methods like gel electrophoresis (SDS-page) and size exclusion chromatography (SEC). We also investigated whether initial purity differences between originator and biosimilar pairs would be amplified over the course of forced degradation studies to provide additional information on the biosimilarity of different products.

In the third chapter, minor differences between infliximab originator and biosimilar were found over the course of incubation, including differences of heat capacity, intrinsic fluorescence, subvisible particulates, deamidation tendencies and fragmentation levels, though these differences were not determined to be statistically significant between originator and biosimilar products. Degradation mechanisms and kinetics were found to be highly similar.

In the first part of the fourth chapter, tandem mass spectrometry (LC-MS/MS) was used to compare disulfide bonding for an originator/biosimilar infliximab, rituximab and bevacizumab pairs, where LC-MS/MS outputs were analyzed using a Protein Metrics' Byonic™ and Byologic® workflow, which allowed for the detection, identification, quantification and comparison of expected disulfide bonds and related impurities (shuffled disulfide and trisulfide bonds). The relative contribution of shuffled and trisulfide bonds were found to be higher for biosimilar infliximab and biosimilar bevacizumab than their respective originators. On the other hand, for rituximab, the relative contribution of shuffling for the biosimilar was identical to that seen for originator and no trisulfides were detected. These differences of disulfide shuffling would seem to indicate underlying differences between originator and biosimilar infliximab and bevacizumab.

In the second part of the fourth chapter, originator and biosimilar rituximab and bevacizumab were subject to forced degradation, where these pairs were incubated at 37°C for 4 weeks. LC-MS/MS was used to compare changes of shuffled disulfide and trisulfide bonds over the course of incubation. The relative contribution of shuffled disulfide bonds for originator/biosimilar rituximab were similar over the course of incubation. The relative contribution of disulfide shuffling for originator and biosimilar bevacizumab not only started with higher initial levels of disulfide shuffling and trisulfide bonding but also had greater extents of shuffling over incubation. In addition, the relative contribution of disulfide shuffling for biosimilar bevacizumab was greater than the originator. Physical degradation characterization (SDS PAGE and SEC) was then used to assess and confirm the relationship of protein degradation to disulfide shuffling. It was observed that bevacizumab was more prone to both physical degradation and disulfide shuffling than rituximab, where again the biosimilar bevacizumab had more initial degradation than the originator. Lastly, free thiol content was analyzed. Free thiol, while appearing greater for rituximab than bevacizumab, appeared to be related to less disulfide shuffling and less physical degradation, whereby free thiols were detected upon exposure over incubation. For bevacizumab, free thiol content also appeared related. Though less free thiols were detected, this is likely due to their participation in disulfide shuffling and degradation that was greater than that observed for rituximab.

Current limitations of the fourth chapter include a lack of understanding of intra- versus inter-molecular disulfide shuffling, as exhibited by 194-194 and 214-214 shuffled bond location for originator/biosimilar infliximab. This could be accounted for by a method where the shuffled antibodies are left intact. Also, we currently do not

understand the percentage of these aggregates that are covalent by nature. Further studies could also include investigation between discrepancies resulting from the high variability of trypsin digestion that were seen between the two sections of this chapter. Normalized expected, shuffled and trisulfide bonds contributions appeared more evenly distributed than those detected for rituximab and bevacizumab samples, where large variabilities occur likely as a result of an incomplete digestion, exemplified the two shuffled locations that were expressed for all three samples of rituximab originator and biosimilar.

Other future studies potentially lie in the understanding of the free thiol analysis method that we have developed using bodipy maleimide as a free thiol probe. Current literature on this method is lacking. In addition, further identification of contributing peaks (determined by SEC fluorescence) would prove useful. Lastly, the generation and generation of large numbers of aggregate and fragment species, followed by fractionation, would additionally allow for us to determine the relative contributions from mAb fragments and aggregates. Further investigation of the underlying mechanisms of disulfide shuffling as a function of free thiol content is also warranted.

Additionally, analysis of disulfide shuffling, in combination with orthogonal physical degradation characterization techniques can be applied to any protein containing two or more disulfide bonds. As an example, this could be applied to insulin analogs. Although fibrillation of insulin analogs has been studied, the role of disulfide shuffling remains unknown.



Overall, each of these projects is useful to companies seeking regulatory approval for a wide variety of biotherapeutic products. The second chapter applies specifically to development of generic and novel delivery technologies of GLP-1RAs, which have recently included the advent of co-formulation with long-acting insulin analogs (Fig. 5-1). The third chapter applies to any and all future biotherapeutic products while the fourth chapter applies to all future biotherapeutic products that contain two or more disulfide bonds.

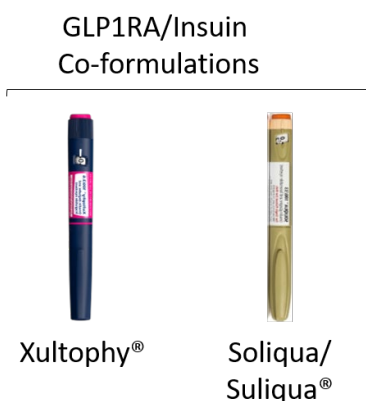


Figure 5-1. Currently marketed GLP-1 receptor agonist/long-acting insulin analog co-formulations.

While information derived from analytical characterization is useful within the regulatory space, it provides a backdrop for the continued desirability to correlate specific impurities with immunogenic responses, a focus of big pharma. The more information that is known about chemical and physical impurities, the more likely we are to find these correlations. To do so, investigation of mAbs that have died in clinical testing may prove useful to optimizing biopharmaceutical product development and approval. While immunogenicity has relied upon the formation of ADAs through

adaptive immune response, there has been a shift in focus towards innate immune responses, which occur upstream of ADA formation (Fig. 5-2).

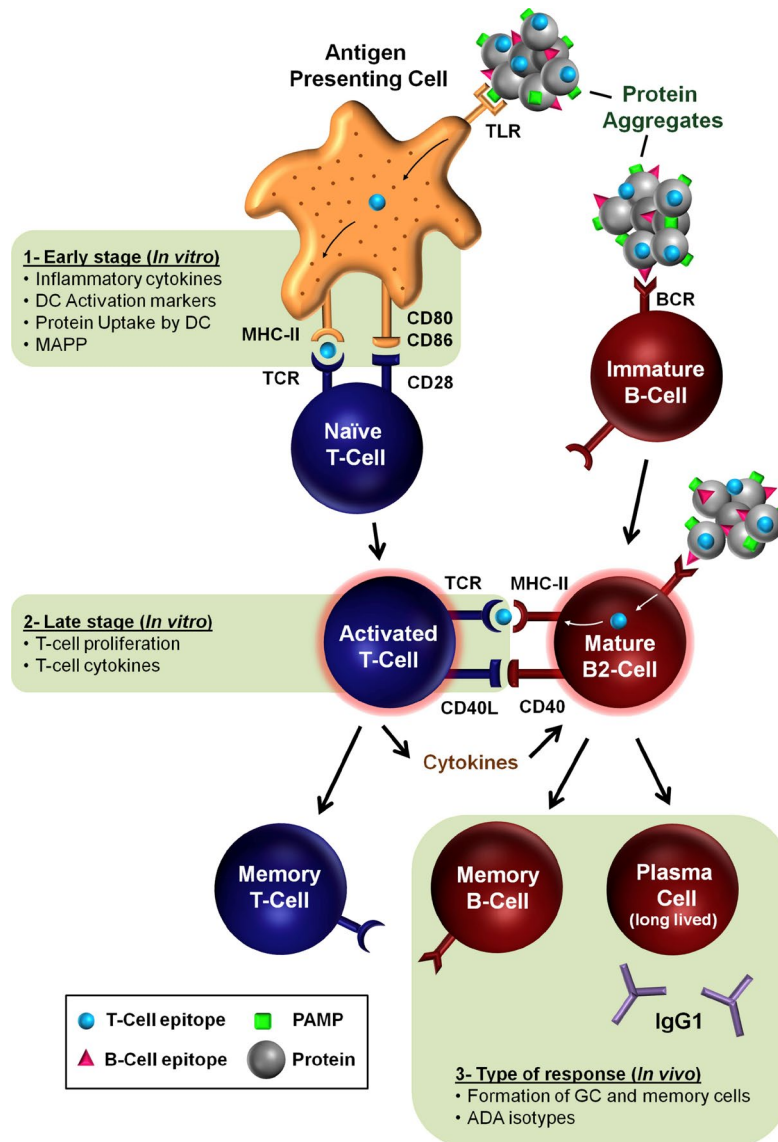


Figure 5-2 Hypothesis of TD mechanism of ADA formation by aggregates. (1) Early stage: activated APCs stimulate naïve T-cells through interactions of MHC-II and costimulatory molecules (presented on the surface of activated APCs) with TCRs and CD28 (presented on T-cells), respectively, turning them into activated T-cells. (2) Late-stage: activated T cells differentiate into cytokine secreting T helper cells type 2 (Th2). Both antigen binding to BCRs (IgM or IgD) and costimulation of B-cells with antigen-specific Th2 cells are required to activate naïve B-cells in the T-cell-rich zones of the secondary lymphoid tissues into B2-cells. Mature B2-cells develop oligoclonal monoreactive GCs in the B-cell follicles, in which B-cells undergo site-directed hypermutation in the Ig variable domain and clonal expansion. Finally, B-cells proliferate and differentiate into memory and antibody-secreting plasma cells. The response also involves antibody isotype class switching, in which the Ig class is switched (i.e., from IgM or IgD to IgG, IgE, or IgA) by alternatively splicing the Ig heavy chain in the constant region. Green rectangles denote stages at which studies have evaluated the potential immunogenicity of protein aggregates. BCR = B-cell receptors; GC = germinal centers; TCR = T-cell receptor; TD = thymus dependent. Adapted with permission.

## Bibliography

1. Chiavenna SM, Jaworski JP, Vendrell A. State of the art in anti-cancer mAbs. *J Biomed Sci.* 2017;24:1-12.
2. Rodney J. Y. H, Milo G. Hematopoietic Growth and Coagulation Factors. In: *Biotechnology and Biopharmaceuticals: Transforming Proteins and Genes into Drugs.* 2nd ed. John Wiley & Sons, Inc; 2013:211-250.
3. Rosman Z, Shoenfeld Y, Zandman-Goddard G. Biologic therapy for autoimmune diseases: An update. *BMC Med.* 2013;11:1-12.
4. Marston HD, Paules CI, Fauci AS. Monoclonal Antibodies for Emerging Infectious Diseases — Borrowing from History. *Perspective.* 2018;378(16):1469-1472.  
doi:10.1056/NEJMp1002530
5. Statistica. No Title.
6. Chames P, Van Regenmortel M, Weiss E, Baty D. Therapeutic antibodies: Successes, limitations and hopes for the future. *Br J Pharmacol.* 2009;157(2):220-233. doi:10.1111/j.1476-5381.2009.00190.x
7. Neves H, Kwok HF. Recent advances in the field of anti-cancer immunotherapy. *BBA Clin.* 2015;3:280-288. doi:10.1016/j.bbacli.2015.04.001
8. Iwamoto N, Shimada T. Recent advances in mass spectrometry-based approaches for proteomics and biologics: Great contribution for developing therapeutic antibodies. *Pharmacol Ther.* 2018;185:147-154.

doi:10.1016/j.pharmthera.2017.12.007

9. U.S. Food and Drug Administration. What Are “Biologics” Questions and Answers.
10. Kang J. Analytical Comparability Strategies for Originators and Biosimilars.  
Published online 2019. <https://deepblue.lib.umich.edu/handle/2027.42/153400>
11. Declerck PJ. Biologicals and biosimilars: a review of the science and its implications. *Generics Biosimilars Initiat J.* 2012;1(1):13-16.  
doi:10.5639/gabij.2012.0101.005
12. Reynolds T, de Zafra C, Kim A, Gelzleichter TR. Overview of Biopharmaceuticals and Comparison with Small-molecule Drug Development. In: *Nonclinical Development of Novel Biologics, Biosimilars, Vaccines and Specialty Biologics.* ; 2013:3-33. doi:10.1016/B978-0-12-394810-6.00001-0
13. Morrow T, Felcone LH. Defining the difference: What Makes Biologics Unique. *Biotechnol Healthc.* 2004;1(4):24-29. doi:10.1177/2050640615590302
14. U.S. Food and Drug Administration. Biosimilar and Interchangeable Products.
15. U.S. Food and Drug Administration. Biosimilar Development, Review and Approval.
16. GaBI. Biosimilars Approved in Europe.
17. CDER. *List of Licensed Biological Products.*; 2018.
18. European Medicines Agency. European public assessment reports on authorised biosimilar medicines.
19. U.S. Food and Drug Administration. *Good ANDA Submission Practices Guidance for Industry.*; 2018.
20. European Medicines Agency. *European Medicines Agency Procedural Advice for*

- Users of the Centralised Procedure for Generic/Hybrid Applications.*; 2017.
21. Tsuruta LR, Lopes dos Santos M, Moro AM. Biosimilars advancements: Moving on to the future. *Biotechnol Prog.* 2015;31(5):1139-1149. doi:10.1002/btpr.2066
  22. Socinski MA, Curigliano G, Jacobs I, Gumbiner B, MacDonald J, Thomas D. Clinical considerations for the development of biosimilars in oncology. *MAbs.* 2015;7(2):286-293. doi:10.1080/19420862.2015.1008346
  23. European Medicines Agency. *Guideline on Process Validation for the Manufacture of Biotechnology-Derived Active Substances and Data to Be Provided in the Regulatory Submission* Title.; 2016.
  24. U.S. Food and Drug Administration. *Analytical Procedures and Methods Validation for Drugs and Biologics Guidance for Industry.*; 2015.
  25. U.S. Food and Drug Administration. *Chemistry, Manufacturing, and Controls Changes to an Approved Application: Certain Biological Products Draft Guidance for Industry.*; 2017.
  26. U.S. Food and Drug Administration. *Guidance for Industry Q5E Comparability of Biotechnological/Biological Products Subject to Changes in Their Manufacturing Process.*; 2005.
  27. European Medicines Agency. *Guideline on Comparability of Biotechnology-Derived Medicinal Products after a Change in the Manufacturing Process.*; 2007.
  28. International Conference on Harmonisation (ICH). *ICH Harmonised Tripartite Guideline Pharmaceutical Development Q8(R2).*; 2009.
  29. Vandekerckhove K, Seidl A, Gutka H, et al. Rational Selection , Criticality Assessment , and Tiering of Quality Attributes and Test Methods for Analytical

- Similarity Evaluation of Biosimilars. Published online 2018:1-9.  
doi:10.1208/s12248-018-0230-9
30. Chow S-C, Liu L. Analytical Similarity Assessment. In: Endrenyi L, Declerck PJ, Chow S-C, eds. *Biosimilar Drug Product Development*. Taylor & Francis Group; 2017:83-108.
  31. U.S. Food and Drug Administration. FDA Withdraws Draft Guidance for Industry: Statistical Approaches to Evaluate Analytical Similarity.
  32. European Medicines Agency. *Meeting Report : Workshop on the Draft Reflection Paper on Statistical Methodology for the Comparative Assessment of Quality Attributes in Drug Development.*; 2018.
  33. Beck A, Sanglier-Cianférani S, Van Dorsselaer A. Biosimilar, biobetter, and next generation antibody characterization by mass spectrometry. *Anal Chem*. 2012;84(11):4637-4646. doi:10.1021/ac3002885
  34. Xie H, Chakraborty A, Ahn J, et al. Rapid comparison of a candidate biosimilar to an innovator monoclonal antibody with advanced liquid chromatography and mass spectrometry technologies. *MABs*. 2010;2(4):379-394.  
doi:10.4161/mabs.11986
  35. Kirchhoff CF, Wang XZM, Conlon HD, Anderson S, Ryan AM, Bose A. Biosimilars: Key regulatory considerations and similarity assessment tools. *Biotechnol Bioeng*. 2017;114(12):2696-2705. doi:10.1002/bit.26438
  36. Olson EJ, Coleman DA. *FDA Draft Guidance for Industry: Statistical Approaches to Evaluate Analytical Similarity Docket No. FDA-2017-D-5525: Comments from Genentech a Member of the Roche Group.*; 2017.

37. Brenna Z. Sandoz Raises Questions With FDA Draft Guidance on Statistical Approaches for Biosimilars. *Regulatory Focus*.
38. American Association of Pharmaceutical Scientists. *Comments on Draft Guidance: Statistical Approaches to Evaluate Analytical Similarity Docket No. FDA-2017-D-5525*.; 2017.
39. Cai X-Y, Wake A, Gouty D. Analytical and bioanalytical assay challenges to support comparability studies for biosimilar drug development. *Bioanalysis*. 2013;5(5):517-520. doi:10.4155/bio.13.1
40. Nowak C, K. Cheung J, M. Dellatore S, et al. Forced degradation of recombinant monoclonal antibodies: A practical guide. *MAbs*. Published online 2017. doi:10.1080/19420862.2017.1368602
41. European Biopharmaceutical enterprises. *Forced Degradation Studies for Therapeutic Proteins*.; 5019.
42. Blessy M, Patel RD, Prajapati PN, Agrawal YK. Development of forced degradation and stability indicating studies of drugs - A review. *J Pharm Anal*. Published online 2014. doi:10.1016/j.jpha.2013.09.003
43. U.S. Food and Drug Administration. *FDA Briefing Document Arthritis Advisory Committee Meeting BLA 125544 CT-P13 , a Proposed Biosimilar to Remicade*.; 2016.
44. U.S. Food and Drug Administration. *FDA Briefing Document Oncologic Drugs Advisory Committee Meeting BLA 761074 MYL-1401O, a Proposed Biosimilar to Herceptin (Trastuzumab)*.; 2017.
45. U.S. Food and Drug Administration. *FDA Advisory Committee Briefing Document*

- CT-P10, a Proposed Biosimilar to Rituxan.*; 2018.
46. U.S. Food and Drug Administration. *FDA Briefing Document Arthritis Advisory Committee Meeting BLA 761024 ABP-501, a Proposed Biosimilar to Humira (Adalimumab).*; 2016.
  47. U.S. Food and Drug Administration. *FDA Briefing Document Oncologic Drugs Advisory Committee BLA 761028 ABP215, a Proposed Biosimilar to Avastin (Bevacizumab).*; 2017.
  48. *Guidance for Industry Q1A(R2) Stability Testing of New Drug Substances and Products.*; 2003.
  49. Dall'Ozzo S, Tartas S, Paintaud G, et al. Rituximab-dependent cytotoxicity by natural killer cells: Influence of FCGR3A polymorphism on the concentration-effect relationship. *Cancer Res.* Published online 2004. doi:10.1158/0008-5472.CAN-03-2862
  50. Bowles JA, Wang SY, Link BK, et al. Anti-CD20 monoclonal antibody with enhanced affinity for CD16 activates NK cells at lower concentrations and more effectively than rituximab. *Blood.* Published online 2006. doi:10.1182/blood-2006-04-020057
  51. Liu L. Antibody glycosylation and its impact on the pharmacokinetics and pharmacodynamics of monoclonal antibodies and Fc-fusion proteins. *J Pharm Sci.* Published online 2015. doi:10.1002/jps.24444
  52. Niwa R, Hatanaka S, Shoji-Hosaka E, et al. Enhancement of the antibody-dependent cellular cytotoxicity of low-fucose IgG1 is independent of FcγRIIIa functional polymorphism. *Clin Cancer Res.* Published online 2004.



doi:10.1158/1078-0432.CCR-04-0850

53. Iida S, Kuni-Kamochi R, Mori K, et al. Two mechanisms of the enhanced antibody-dependent cellular cytotoxicity (ADCC) efficacy of non-fucosylated therapeutic antibodies in human blood. *BMC Cancer*. Published online 2009. doi:10.1186/1471-2407-9-58
54. Greenwald M, Tesser J, Sewell KL. Biosimilars Have Arrived: Rituximab. *Arthritis*. Published online 2018. doi:10.1155/2018/3762864
55. European Medicines Agency. *EPAR Summary for the Public: Truxima.*; 2017.
56. European Medicines Agency. *EPAR Summary for the Public: Rixathon.*; 2017.
57. Althoff E. Sandoz decides not to pursue US biosimilar rituximab; will focus on robust biosimilar portfolio for unmet access and sustainability needs.
58. Gabi. Biosimilars of rituximab.  
<http://www.gabionline.net/Biosimilars/General/Biosimilars-ofrituximab.%0D>
59. Filipe V, Jiskoot W, Basmeh AH, Halim A, Schellekens H, Brinks V. Immunogenicity of different stressed IgG monoclonal antibody formulations in immune tolerant transgenic mice. *MAbs*. 2012;4(6):740-752. doi:10.4161/mabs.22066
60. Dotan E, Aggarwal C, Smith MR. Impact of rituximab (Rituxan) on the treatment of B-cell non-Hodgkin's lymphoma. *P T*. Published online 2010.
61. Welch AR. Russia's Biosimilar Market At A Glance.
62. ICH. Stability Testing: Photostability testing of new drug substances and products Q1B. *Int Conf Harmon*. Published online 2003. doi:10.1136/bmj.333.7574.873-a
63. Du P, Liu W, Cao H, Zhao H, Huang CH. Oxidation of amino acids by peracetic

- acid: Reaction kinetics, pathways and theoretical calculations. *Water Res X*.  
Published online 2018. doi:10.1016/j.wroa.2018.09.002
64. Siew Adeline. Impurity Testing of Biologic Drug Products. *BioPharm Int*. Published online 2018.
65. U.S. Food and Drug Administration. Guidance for industry Q6B specifications: Test procedures and acceptance criteria for biotechnological/biological products. Published online 1999:1-24. doi:10.1093/elt/40.2.121
66. Walsh G, Jefferis R. Post-translational modifications in the context of therapeutic proteins. *Nat Biotechnol*. 2006;24(10):1241-1252. doi:10.1038/nbt1252
67. Kuriakose A, Chirmule N, Nair P. Immunogenicity of Biotherapeutics: Causes and Association with Posttranslational Modifications. *J Immunol Res*. Published online 2016. doi:10.1155/2016/1298473
68. Walsh CT, Garneau-Tsodikova S, Gatto GJ. Protein posttranslational modifications: The chemistry of proteome diversifications. *Angew Chemie - Int Ed*. 2005;44(45):7342-7372. doi:10.1002/anie.200501023
69. Jefferis R. Characterization of Biosimilar Biologics The Link between Structure and Functions. In: Endrenyi L, Declerck PJ, Chow S-C, eds. *Biosimilar Drug Product Development*. CRC Press, Taylor & Frances group; 2017:109-150.
70. Li W, Kerwin JL, Schiel J, et al. Structural elucidation of post-translational modifications in monoclonal antibodies. *ACS Symp Ser*. 2015;1201:119-183. doi:10.1021/bk-2015-1201.ch003
71. Nathan JJ, Ramchandani M, Kaur P. Manufacturing of Biologics. In: Yamauchi PS, ed. *Biologic and Systemic Agents in Dermatology*. Springer International

- Publishing; 2018:101-110.
72. Shacter E. Quantification and significance of protein oxidation in biological samples. In: *Drug Metabolism Reviews.* ; 2000. doi:10.1081/DMR-100102336
  73. Scislowski PW, Foster AR, Fuller MF. Regulation of oxidative degradation of L-lysine in rat liver mitochondria. *Biochem J.* 1994;300 ( Pt 3(Pt 3):887-891. doi:10.1042/bj3000887
  74. Hovorka SW, Schöneich C. Oxidative degradation of pharmaceuticals: Theory, mechanisms and inhibition. *J Pharm Sci.* Published online 2001. doi:10.1002/1520-6017(200103)90:3<253::AID-JPS1>3.0.CO;2-W
  75. Slavica A, Dib I, Nidetzky B. Single-site oxidation, cysteine 108 to cysteine sulfinic acid, in D-amino acid oxidase from *Trigonopsis variabilis* and its structural and functional consequences. *Appl Environ Microbiol.* Published online 2005. doi:10.1128/AEM.71.12.8061-8068.2005
  76. Lu HS, Fausset PR, Narhi LO, et al. Chemical modification and site-directed mutagenesis of methionine residues in recombinant human granulocyte colony-stimulating factor: effect on stability and biological activity. *Arch Biochem Biophys.* 1999;362(1):1-11. doi:10.1006/abbi.1998.1022
  77. Stadtman ER, Moskovitz J, Berlett BS, Levine RL. Cyclic oxidation and reduction of protein methionine residues is an important antioxidant mechanism. *Mol Cell Biochem.* Published online 2002. doi:10.1023/A:1015916831583
  78. Davies MJ. The oxidative environment and protein damage. *Biochim Biophys Acta - Proteins Proteomics.* Published online 2005. doi:10.1016/j.bbapap.2004.08.007

79. Valley CC, Cembran A, Perlmutter JD, et al. The methionine-aromatic motif plays a unique role in stabilizing protein structure. *J Biol Chem*. Published online 2012. doi:10.1074/jbc.M112.374504
80. Chao CC, Ma YS, Stadtman ER. Modification of protein surface hydrophobicity and methionine oxidation by oxidative systems. *Proc Natl Acad Sci U S A*. Published online 1997. doi:10.1073/pnas.94.7.2969
81. LIEBSTER J, KOPOLDOVÁ J. The Radiation Chemistry of Amino Acids. In: AUGENSTEIN LG, MASON R, QUASTLER HBT-A in RB, eds. Vol 1. Elsevier; 1964:157-226. doi:https://doi.org/10.1016/B978-1-4832-3120-4.50010-3
82. Levine RL, Mosoni L, Berlett BS, Stadtman ER. Methionine residues as endogenous antioxidants in proteins. *Proc Natl Acad Sci U S A*. Published online 1996. doi:10.1073/pnas.93.26.15036
83. Geiger T, Clarke S. Deamidation, isomerization, and racemization at asparaginyl and aspartyl residues in peptides. Succinimide-linked reactions that contribute to protein degradation. *J Biol Chem*. Published online 1987.
84. Patel K, Borchardt RT. Chemical Pathways of Peptide Degradation. III. Effect of Primary Sequence on the Pathways of Deamidation of Asparaginyl Residues in Hexapeptides. *Pharm Res An Off J Am Assoc Pharm Sci*. Published online 1990. doi:10.1023/A:1015999012852
85. Liu S, Moulton KR, Auclair JR, Zhou ZS. Mildly acidic conditions eliminate deamidation artifact during proteolysis: Digestion with endoprotease Glu-C at pH 4.5. *Amino Acids*. Published online 2016. doi:10.1007/s00726-015-2166-z
86. Yan Q, Huang M, Lewis MJ, Hu P. Structure Based Prediction of Asparagine

- Deamidation Propensity in Monoclonal Antibodies. *MAbs*. Published online 2018.  
doi:10.1080/19420862.2018.1478646
87. Robinson NE, Robinson AB. Molecular clocks. *Proc Natl Acad Sci U S A*.  
Published online 2001. doi:10.1073/pnas.98.3.944
88. Geiger T, Clarke S. Aspartyl Residues in Peptides. *J Biol Chem*. Published online  
1987.
89. Li B, Borchardt RT, Topp EM, VanderVelde D, Schowen RL. Racemization of an  
asparagine residue during peptide deamidation. *J Am Chem Soc*. Published  
online 2003. doi:10.1021/ja0360992
90. Joshi AB, Kirsch LE. The relative rates of glutamine and asparagine deamidation  
in glucagon fragment 22-29 under acidic conditions. *J Pharm Sci*. Published  
online 2002. doi:10.1002/jps.10213
91. Oliyai C, Borchardt RT. Chemical Pathways of Peptide Degradation. IV.  
Pathways, Kinetics, and Mechanism of Degradation of an Aspartyl Residue in a  
Model Hexapeptide. *Pharm Res An Off J Am Assoc Pharm Sci*. Published online  
1993. doi:10.1023/A:1018981231468
92. Capasso S. Estimation of the deamidation rate of asparagine side chains. *J Pept  
Res*. Published online 2000. doi:10.1034/j.1399-3011.2000.00172.x
93. Jenkins N. Modifications of therapeutic proteins: Challenges and prospects. In:  
*Cytotechnology*. Vol 53. ; 2007:121-125. doi:10.1007/s10616-007-9075-2
94. Huang L, Lu J, Wroblewski VJ, Beals JM, Riggin RM. In vivo deamidation  
characterization of monoclonal antibody by LC/MS/MS. *Anal Chem*. Published  
online 2005. doi:10.1021/ac0494174

95. Zhang W, Czupryn MJ, Boyle PT, Amari J. Characterization of asparagine deamidation and aspartate isomerization in recombinant human interleukin-11. *Pharm Res*. Published online 2002. doi:10.1023/A:1019814713428
96. CLARKE S. Propensity for spontaneous succinimide formation from aspartyl and asparaginyl residues in cellular proteins. *Int J Pept Protein Res*. Published online 1987. doi:10.1111/j.1399-3011.1987.tb03390.x
97. Harris RJ, Kabakoff B, Macchi FD, et al. Identification of multiple sources of charge heterogeneity in a recombinant antibody. *J Chromatogr B Biomed Sci Appl*. 2001;752(2):233-245. doi:10.1016/S0378-4347(00)00548-X
98. Chelius D, Jing K, Lueras A, et al. Formation of pyroglutamic acid from N-terminal glutamic acid in immunoglobulin gamma antibodies. *Anal Chem*. Published online 2006. doi:10.1021/ac051827k
99. DIMARCHI RD, TAM JP, KENT SBH, MERRIFIELD RB. Weak acid-catalyzed pyrrolidone carboxylic acid formation from glutamine during solid phase peptide synthesis: Minimization by rapid coupling. *Int J Pept Protein Res*. Published online 1982. doi:10.1111/j.1399-3011.1982.tb03027.x
100. Shih FF. Analysis of glutamine, glutamic acid and pyroglutamic acid in protein hydrolysates by high-performance liquid chromatography. *J Chromatogr A*. Published online 1985. doi:10.1016/S0021-9673(01)97681-2
101. Suzuki Y, Motoi H, Sato K. Quantitative analysis of pyroglutamic acid in peptides. *J Agric Food Chem*. Published online 1999. doi:10.1021/jf990003z
102. Liu H, Caza-Bulsecu G, Faldu D, Chumsae C, Sun J. Heterogeneity of monoclonal antibodies. *J Pharm Sci*. 2008;97(7):2426-2447.

doi:10.1002/jps.21180

103. Khawli LA, Goswami S, Hutchinson R, et al. Charge variants in IgG1: Isolation, characterization, in vitro binding properties and pharmacokinetics in rats. *MAbs*. 2010;2(6):613-624. doi:10.4161/mabs.2.6.13333
104. Niazi SK. Stability and formulation considerations. In: *Biosimilars and Interchangeable Biologics: Tactical Elements*. Taylor & Francis Group; 2016:83-122.
105. Robinson NE. Protein deamidation. *Proc Natl Acad Sci*. 2002;99(8):5283-5288. doi:10.1073/pnas.082102799
106. Cook KM, Hogg PJ. Post-Translational Control of Protein Function by Disulfide Bond Cleavage. *Antioxid Redox Signal*. 2013;18(15):1987-2015. doi:10.1089/ars.2012.4807
107. Azimi I, Wong JWH, Hogg PJ. Control of Mature Protein Function by Allosteric Disulfide Bonds. *Antioxid Redox Signal*. 2011;14(1):113-126. doi:10.1089/ars.2010.3620
108. Holder PG, Rabuka D. Technologies for Antibody-Drug Conjugation. In: Liu C, Morrow Jr. KJ, eds. *Biosimilars of Monoclonal Antibodies A Practical Guide to Manufacturing, Preclinical, and Clinical Development*. John Wiley & Sons, Inc; 2017:591-640.
109. Zhang W, Czupryn MJ. Free sulfhydryl in recombinant monoclonal antibodies. *Biotechnol Prog*. 2002;18(3):509-513. doi:10.1021/bp025511z
110. Dillon TM, Bondarenko P V., Rehder DS, Pipes GD, Kleemann GR, Ricci MS. Optimization of a reversed-phase high-performance liquid chromatography/mass

- spectrometry method for characterizing recombinant antibody heterogeneity and stability. *J Chromatogr A*. 2006;1120(1-2):112-120.  
doi:10.1016/j.chroma.2006.01.016
111. Trexler-Schmidt M, Sargis S, Chiu J, et al. Identification and prevention of antibody disulfide bond reduction during cell culture manufacturing. *Biotechnol Bioeng*. 2010;106(3):452-461. doi:10.1002/bit.22699
112. Hutterer KM, Hong RW, Lull J, et al. Monoclonal antibody disulfide reduction during manufacturing Untangling process effects from product effects. *MABs*. 2013;5(4):608-613. doi:10.4161/mabs.24725
113. Fernandes PA, Ramos MJ. Theoretical insights into the mechanism for thiol/disulfide exchange. *Chem - A Eur J*. Published online 2004.  
doi:10.1002/chem.200305343
114. Fava A, Iliceto A, Camera E. Kinetics of the thiol-disulfide exchange. *J Am Chem Soc*. 1957;79(4):833-838. doi:10.1021/ja01561a014
115. Lacy ER, Baker M, Brigham-Burke M. Free sulfhydryl measurement as an indicator of antibody stability. *Anal Biochem*. Published online 2008.  
doi:10.1016/j.ab.2008.07.016
116. Bach RD, Dmitrenko O, Thorpe C. Mechanism of thiolate-disulfide interchange reactions in biochemistry. *J Org Chem*. Published online 2008.  
doi:10.1021/jo702051f
117. Seibel R, Maier S, Schnellbaecher A, et al. Impact of S-sulfocysteine on fragments and trisulfide bond linkages in monoclonal antibodies. *MABs*. Published online 2017. doi:10.1080/19420862.2017.1333212



118. Okado-Matsumoto A, Guan Z, Fridovich I. Modification of Cysteine 111 in human Cu,Zn-superoxide dismutase. *Free Radic Biol Med*. Published online 2006. doi:10.1016/j.freeradbiomed.2006.09.011
119. Gu S, Wen D, Weinreb PH, et al. Characterization of trisulfide modification in antibodies. *Anal Biochem*. Published online 2010. doi:10.1016/j.ab.2010.01.019
120. Mulinacci F, Poirier E, Capelle MAH, Gurny R, Arvinte T. Influence of methionine oxidation on the aggregation of recombinant human growth hormone. *Eur J Pharm Biopharm*. 2013;85(1):42-52. doi:10.1016/j.ejpb.2013.03.015
121. Hu D, Qin Z, Xue B, Fink AL, Uversky VN. Effect of methionine oxidation on the structural properties, conformational stability, and aggregation of immunoglobulin light chain LEN. *Biochemistry*. 2008;47(33):8665-8677. doi:10.1021/bi800806d
122. Van Beers MMC, Sauerborn M, Gilli F, Brinks V, Schellekens H, Jiskoot W. Oxidized and aggregated recombinant human interferon beta is immunogenic in human interferon beta transgenic mice. *Pharm Res*. 2011;28(10):2393-2402. doi:10.1007/s11095-011-0451-4
123. Mirzaei H, Regnier F. Protein:protein aggregation induced by protein oxidation. *J Chromatogr B Anal Technol Biomed Life Sci*. 2008;873(1):8-14. doi:10.1016/j.jchromb.2008.04.025
124. Sohal RS. Role of oxidative stress and protein oxidation in the aging process. *Free Radic Biol Med*. 2002;33(1):37-44. doi:10.1016/S0891-5849(02)00856-0
125. Davies MJ. Protein oxidation and peroxidation. *Biochem J*. 2016;473(7):805-825. doi:10.1042/BJ20151227
126. Kuo TT, Aveson VG. Neonatal Fc receptor and IgG-based therapeutics. *MAbs*.

- 2011;3(5):422-430. doi:10.4161/mabs.3.5.16983
127. Mo J, Yan Q, So CK, Soden T, Lewis MJ, Hu P. Understanding the Impact of Methionine Oxidation on the Biological Functions of IgG1 Antibodies Using Hydrogen/Deuterium Exchange Mass Spectrometry. *Anal Chem*. 2016;88(19):9495-9502. doi:10.1021/acs.analchem.6b01958
128. Bertolotti-Ciarlet A, Wang W, Lownes R, et al. Impact of methionine oxidation on the binding of human IgG1 to Fc Rn and Fc gamma receptors. *Mol Immunol*. 2009;46(8-9):1878-1882. doi:10.1016/j.molimm.2009.02.002
129. Liu D, Ren D, Huang H, et al. Structure and stability changes of human IgG1 Fc as a consequence of methionine oxidation. *Biochemistry*. 2008;47(18):5088-5100. doi:10.1021/bi702238b
130. Pan H, Chen K, Chu L, Kinderman F, Apostol I, Huang G. Methionine oxidation in human IgG2 Fc decreases binding affinities to protein A and FcRn. *Protein Sci*. 2009;18(2):424-433. doi:10.1002/pro.45
131. Phillips JJ, Buchanan A, Andrews J, et al. Rate of Asparagine Deamidation in a Monoclonal Antibody Correlating with Hydrogen Exchange Rate at Adjacent Downstream Residues. *Anal Chem*. 2017;89(4):2361-2368. doi:10.1021/acs.analchem.6b04158
132. Doyle HA, Zhou J, Wolff MJ, et al. Isoaspartyl post-translational modification triggers anti-tumor T and B lymphocyte immunity. *J Biol Chem*. 2006;281(43):32676-32683. doi:10.1074/jbc.M604847200
133. Yu L, Vigel A, Huff MB, Young M, Remmele RL, He B. Investigation of N-terminal glutamate cyclization of recombinant monoclonal antibody in formulation

- development. *J Pharm Biomed Anal.* 2006;42(4):455-463.  
doi:10.1016/j.jpba.2006.05.008
134. Lyubarskaya Y, Houde D, Woodard J, Murphy D, Mhatre R. Analysis of recombinant monoclonal antibody isoforms by electrospray ionization mass spectrometry as a strategy for streamlining characterization of recombinant monoclonal antibody charge heterogeneity. *Anal Biochem.* 2006;348(1):24-39.  
doi:10.1016/j.ab.2005.10.003
135. Liu YD, Goetze AM, Bass RB, Flynn GC. N-terminal glutamate to pyroglutamate conversion in vivo for human IgG2 antibodies. *J Biol Chem.* 2011;286(13):11211-11217. doi:10.1074/jbc.M110.185041
136. Jung SK, Lee KH, Jeon JW, et al. Physicochemical characterization of Remsima®. *MAbs.* 2014;6(5):1163-1177. doi:10.4161/mabs.32221
137. Lamanna WC, Mayer RE, Rupprechter A, et al. The structure-function relationship of disulfide bonds in etanercept. *Sci Rep.* 2017;7(1):3951. doi:10.1038/s41598-017-04320-5
138. Cho IH, Lee N, Song D, et al. Evaluation of the structural, physicochemical, and biological characteristics of SB4, a biosimilar of etanercept. *MAbs.* 2016;8(6):1136-1155. doi:10.1080/19420862.2016.1193659
139. U.S. Food and Drug Administration. *FDA Briefing Document Arthritis Advisory Committee Meeting BLA 761042 GP2015, a Proposed Biosimilar to Enbrel (Etanercept).*; 2016.
140. Wang W, Meeler AR, Bergerud LT, Hesselberg M, Byrne M, Wu Z. Quantification and characterization of antibody deamidation by peptide mapping with mass

- spectrometry. *Int J Mass Spectrom.* 2012;312:107-113.  
doi:10.1016/j.ijms.2011.06.006
141. Chelius D, Render DS, Bondarenko P V. Identification and characterization of deamidation sites in the conserved regions of human immunoglobulin gamma antibodies. *Anal Chem.* 2005;77(18):6004-6011. doi:10.1021/ac050672d
142. Timm V, Gruber P, Wasiliu M, Lindhofer H, Chelius D. Identification and characterization of oxidation and deamidation sites in monoclonal rat/mouse hybrid antibodies. *J Chromatogr B Anal Technol Biomed Life Sci.* 2010;878(9-10):777-784. doi:10.1016/j.jchromb.2010.01.036
143. Holzmann J, Hausberger A, Rupprechter A, Toll H. Top-down MS for rapid methionine oxidation site assignment in filgrastim. *Anal Bioanal Chem.* 2013;405(21):6667-6674. doi:10.1007/s00216-013-7138-0
144. Pisupati K, Benet A, Tian Y, et al. Biosimilarity under stress: A forced degradation study of Remicade® and Remsima™. *MABs.* Published online 2017. doi:10.1080/19420862.2017.1347741
145. Kang J, Kim SY, Vallejo D, et al. Multifaceted assessment of rituximab biosimilarity: The impact of glycan microheterogeneity on Fc function. *Eur J Pharm Biopharm.* Published online 2020. doi:10.1016/j.ejpb.2019.12.003
146. Kahle J, Watzig H. Determination of protein charge variants with (imaged) capillary isoelectric focusing and capillary zone electrophoresis. *Electrophoresis.* 2018;0:1-20.
147. Fekete S, Beck A, Fekete J, Guillarme D. Method development for the separation of monoclonal antibody charge variants in cation exchange chromatography, Part

- II: PH gradient approach. *J Pharm Biomed Anal.* 2015;102:282-289.  
doi:10.1016/j.jpba.2014.09.032
148. Yamamoto S, Ishihara T. Resolution and retention of proteins near Isoelectric points in ion-exchange chromatography. Molecular recognition in electrostatic interaction chromatography. *Sep Sci Technol.* 2000;35(11):1707-1717.  
doi:10.1081/SS-100102489
149. Ahamed T, Nfor BK, Verhaert PDEM, et al. pH-gradient ion-exchange chromatography: An analytical tool for design and optimization of protein separations. *J Chromatogr A.* 2007;1164(1-2):181-188.  
doi:10.1016/j.chroma.2007.07.010
150. Fekete S, Gassner A-LL, Rudaz S, Schappler J, Guillarme D. Analytical strategies for the characterization of therapeutic monoclonal antibodies. *TrAC - Trends Anal Chem.* 2013;42:74-83. doi:10.1016/j.trac.2012.09.012
151. Moorhouse KG, Nashabeh W, Deveney J, Bjork NS, Mulkerrin MG, Ryskamp T. Validation of an HPLC method for the analysis of the charge heterogeneity of the recombinant monoclonal antibody IDEC-C2B8 after papain digestion. *J Pharm Biomed Anal.* 1997;16(4):593-603. doi:10.1016/S0731-7085(97)00178-7
152. Flores-Ortiz LF, Campos-García VR, Perdomo-Abúndez FC, Pérez NO, Medina-Rivero E. Physicochemical properties of Rituximab. *J Liq Chromatogr Relat Technol.* 2014;37(10):1438-1452. doi:10.1080/10826076.2013.794738
153. Voeten RLC, Ventouri IK, Haselberg R, Somsen GW. Capillary Electrophoresis: Trends and Recent Advances. *Anal Chem.* Published online 2018:1464-1481.  
doi:10.1021/acs.analchem.8b00015

154. Wu S-L, Jiang H, Lu Q, Dai S, Hancock WS, Karger BL. Mass Spectrometric Determination of Disulfide Linkages in Recombinant Therapeutic Proteins Using On-line LC-MS with Electron Transfer Dissociation (ETD). *Anal Chem*. 2009;81(1):112-122. doi:10.1021/ac801560k
155. Bean MF, Carr SA. Characterization of disulfide bond position in proteins and sequence analysis of cystine-bridged peptides by tandem mass spectrometry. *Anal Biochem*. 1992;201(2):216-226. doi:10.1016/0003-2697(92)90331-Z
156. Jiang W, Liu S, Zhong Z. Product Analysis of Biosimilar Antibodies. In: Liu C, Morrow, Jr. KJ, eds. *Biosimilars of Monoclonal Antibodies A Practical Guide to Manufacturing, Preclinical, and Clinical Development*. 1st ed. John Wiley & Sons, Inc; 2017:427-458.
157. Chen X, Zhou Y, Peng X, Yoon J. Fluorescent and colorimetric probes for detection of thiols. *Chem Soc Rev*. 2010;39(6):2120-2135. doi:10.1039/b925092a
158. Welch L, Dong X, Hewitt D, et al. Facile quantitation of free thiols in a recombinant monoclonal antibody by reversed-phase high performance liquid chromatography with hydrophobicity-tailored thiol derivatization. *J Chromatogr B Anal Technol Biomed Life Sci*. Published online 2018. doi:10.1016/j.jchromb.2018.05.039
159. He F, Phan DH, Hogan S, et al. Detection of IgG aggregation by a high throughput method based on extrinsic fluorescence. *J Pharm Sci*. Published online 2010. doi:10.1002/jps.22036
160. Filipe V, Jiskoot W, Basmeh AH, Halim A, Schellekens H, Brinks V. Immunogenicity of different stressed IgG monoclonal antibody formulations in

- immune tolerant transgenic mice. *MAbs*. Published online 2012.  
doi:10.4161/mabs.22066
161. CDER/CBER, FDA. *Quality Considerations in Demonstrating Biosimilarity of a Therapeutic Protein Product to a Reference Product.*; 2015.
162. Berkowitz SA, Engen JR, Mazzeo JR, Jones GB. Analytical tools for characterizing biopharmaceuticals and the implications for biosimilars. *Nat Rev Drug Discov*. 2012;11(7):527-540. doi:10.1038/nrd3746
163. Den Engelsman J, Garidel P, Smulders R, et al. Strategies for the assessment of protein aggregates in pharmaceutical biotech product development. *Pharm Res*. 2011;28(4):920-933. doi:10.1007/s11095-010-0297-1
164. Vugmeyster Y. Pharmacokinetics and toxicology of therapeutic proteins: Advances and challenges. *World J Biol Chem*. 2012;3(4):73.  
doi:10.4331/wjbc.v3.i4.73
165. Roberts CJ. Protein aggregation and its impact on product quality. *Curr Opin Biotechnol*. 2014;30:211-217. doi:10.1016/j.copbio.2014.08.001
166. Meager A, Dolman C, Dilger P, et al. An Assessment of Biological Potency and Molecular Characteristics of Different Innovator and Noninnovator Interferon-Beta Products. *J Interf Cytokine Res*. 2011;31(4):383-392. doi:10.1089/jir.2010.0113
167. Hochuli E. Interferon immunogenicity: technical evaluation of interferon-alpha 2a. *J Interferon Cytokine Res*. 1997;17 Suppl 1:S15-21.
168. Fradkin AH, Carpenter JF, Randolph TW. Immunogenicity of aggregates of recombinant human growth hormone in mouse models. *J Pharm Sci*. 2009;98(9):3247-3264. doi:10.1002/jps.21834

169. Pathak JA, Sologuren RR, Narwal R. Do clustering monoclonal antibody solutions really have a concentration dependence of viscosity? *Biophys J*. 2013;104(4):913-923. doi:10.1016/j.bpj.2013.01.007
170. Moussa EM, Panchal JP, Moorthy BS, et al. Immunogenicity of Therapeutic Protein Aggregates. *J Pharm Sci*. 2016;105(2):417-430. doi:10.1016/j.xphs.2015.11.002
171. Barth HG, Boyes BE, Jackson C. Size Exclusion Chromatography and Related Separation Techniques. *Anal Chem*. 1998;70(12):251-278. doi:10.1021/a1980015t
172. Wen J, Arakawa T, Philo JS. Size-exclusion chromatography with on-line light-scattering, absorbance, and refractive index detectors for studying proteins and their interactions. *Anal Biochem*. 1996;240(2):155-166. doi:10.1006/abio.1996.0345
173. Mahler HC, Friess W, Grauschopf U, Kiese S. Protein aggregation: Pathways, induction factors and analysis. *J Pharm Sci*. 2009;98(9):2909-2934. doi:10.1002/jps.21566
174. Liu J, Andya JD, Shire SJ. A critical review of analytical ultracentrifugation and field flow fractionation methods for measuring protein aggregation. *AAPS J*. 2006;8(3):E580-E589. doi:10.1208/aapsj080367
175. Wagner M, Holzschuh S, Traeger A, Fahr A, Schubert US. Asymmetric flow field-flow fractionation in the field of nanomedicine. *Anal Chem*. 2014;86(11):5201-5210. doi:10.1021/ac501664t
176. Rebolj K, Pahovnik D, Žagar E. Characterization of a protein conjugate using an



- asymmetrical-flow field-flow fractionation and a size-exclusion chromatography with multi-detection system. *Anal Chem.* 2012;84(17):7374-7383.  
doi:10.1021/ac3010378
177. Cole JL, Lary JW, Moody T, Laue TM. Analytical Ultracentrifugation: Sedimentation Velocity and Sedimentation Equilibrium. *Methods Cell Biol.* 2008;84(07):143-179. doi:10.1016/S0091-679X(07)84006-4. Analytical
178. Lebowitz J, Lewis MS, Schuck P. Modern analytical ultracentrifugation in protein science: A tutorial review. *Protein Sci.* 2009;11(9):2067-2079.  
doi:10.1110/ps.0207702
179. Filipe V, Hawe A, Jiskoot W. Critical evaluation of nanoparticle tracking analysis (NTA) by NanoSight for the measurement of nanoparticles and protein aggregates. *Pharm Res.* 2010;27(5):796-810. doi:10.1007/s11095-010-0073-2
180. Patapoff TW, Tani TH, Cromwell MEM. A low-volume, short-path length dynamic light scattering sample cell for highly turbid suspensions. *Anal Biochem.* 1999;270(2):338-340. doi:10.1006/abio.1999.4108
181. Hassan P a, Rana S, Verma G. Making sense of brownian motion: colloid characterization by dynamic light scattering. *Langmuir.* 2015;31(1):3-12.  
doi:10.1021/la501789z
182. Gallego-Urrea JA, Tuoriniemi J, Hassellöv M. Applications of particle-tracking analysis to the determination of size distributions and concentrations of nanoparticles in environmental, biological and food samples. *TrAC - Trends Anal Chem.* 2011;30(3):473-483. doi:10.1016/j.trac.2011.01.005
183. Bandyopadhyay S, Mahajan M, Mehta T, et al. Physicochemical and functional

- characterization of a biosimilar adalimumab ZRC-3197. *Biosimilars*. 2014;5:1-18.  
doi:10.2147/BS.S75573
184. Liu J, Eris T, Li C, Cao S, Kuhns S. Assessing Analytical Similarity of Proposed Amgen Biosimilar ABP 501 to Adalimumab. *BioDrugs*. 2016;30(4):321-338.  
doi:10.1007/s40259-016-0184-3
185. Pelton JT, McLean LR. Spectroscopic methods for analysis of protein secondary structure. *Anal Biochem*. 2000;277(2):167-176. doi:10.1006/abio.1999.4320 M4 - Citavi
186. Visser J, Feuerstein I, Stangler T, Schmiederer T, Fritsch C, Schiestl M. Physicochemical and functional comparability between the proposed biosimilar rituximab GP2013 and originator rituximab. *BioDrugs*. 2013;27(5):495-507.  
doi:10.1007/s40259-013-0036-3
187. Magnenat L, Palmese A, Fremaux C, et al. Demonstration of physicochemical and functional similarity between the proposed biosimilar adalimumab MSB11022 and Humira®. *MAbs*. 2017;9(1):127-139. doi:10.1080/19420862.2016.1259046
188. Deechongkit S, Aoki KH, Park SS, Kerwin BA. Biophysical comparability of the same protein from different manufacturers: A case study using Epoetin alfa from Epogen® and Eprex®. *J Pharm Sci*. 2006;95(9):1931-1943.  
doi:10.1002/jps.20649
189. Hong J, Lee Y, Lee C, et al. Physicochemical and biological characterization of SB2, a biosimilar of Remicade® (infliximab). *MAbs*. 2017;9(2):364-382.  
doi:10.1080/19420862.2016.1264550
190. Barth A. Infrared spectroscopy of proteins. *Biochim Biophys Acta - Bioenerg*.

- 2007;1767(9):1073-1101. doi:10.1016/j.bbabbio.2007.06.004
191. Jackson M, Mantsch HH. The Use and Misuse of FTIR Spectroscopy in the Determination of Protein Structure. *Crit Rev Biochem Mol Biol.* 1995;30(2):95-120. doi:10.3109/10409239509085140
  192. Greenfield NJ. Using circular dichroism spectra to estimate protein secondary structure. *Nat Protoc.* 2006;1(6):2876-2890. doi:10.1038/nprot.2006.202.Using
  193. Sorgel F, Schwebig A, Holzmann J, Prasch S, Singh P, Kinzig M. Comparability of biosimilar filgrastim with originator filgrastim: Protein characterization, pharmacodynamics, and pharmacokinetics. *BioDrugs.* 2015;29(2):123-131. doi:10.1007/s40259-015-0124-7
  194. U.S. Food and Drug Administration. *FDA Briefing Document Oncologic Drugs Advisory Committee Meeting BLA 125553 EP2006, a Proposed Biosimilar to Neupogen (Filgrastim).*; 2015.
  195. Kelly SMMM, Price NCCC. The use of circular dichroism in the investigation of protein structure and function. *Curr Protein Pept Sci.* 2000;1(4):349-384. doi:10.2174/1389203003381315
  196. Kelly SM, Jess TJ, Price NC. How to study proteins by circular dichroism. *Biochim Biophys Acta - Proteins Proteomics.* 2005;1751(2):119-139. doi:10.1016/j.bbapap.2005.06.005
  197. Prasad PN. Fundamentals of Light–Matter Interactions. In: *Introduction to Biophotonics.* ; 2004:92-128. doi:10.1002/0471465380.ch4
  198. Bruylants G, Wouters J, Michaux C. Differential Scanning Calorimetry in Life Science: Thermodynamics, Stability, Molecular Recognition and Application in

- Drug Design. *Curr Med Chem*. 2005;12(17):2011-2020.  
doi:10.2174/0929867054546564
199. Clas S, Dalton C, Hancock B. Differential scanning calorimetry: applications in drug development. *Pharm Sci Technolo Today*. 1999;2(8):311-320.  
doi:http://dx.doi.org/10.1016/S1461-5347(99)00181-9
200. Johnson CM. Differential scanning calorimetry as a tool for protein folding and stability. *Arch Biochem Biophys*. 2013;531:100-109.  
doi:10.1016/j.abb.2012.09.008
201. Berkowitz SA. Analytical Characterization Structural Assessment of Biosimilarity. In: Endrenyi L, Declerck P, Chow S-C, eds. *Biosimilar Drug Product Development*. ; 2017:15-82.
202. Fang J, Doneanu C, Alley WR, Yu YQ, Beck A, Chen W. Advanced assessment of the physicochemical characteristics of Remicade® and Inflectra® by sensitive LC/MS techniques. *MAbs*. 2016;8(6):1021-1034.  
doi:10.1080/19420862.2016.1193661
203. Masson GR, Jenkins ML, Burke JE. An overview of hydrogen deuterium exchange mass spectrometry (HDX-MS) in drug discovery. *Expert Opin Drug Discov*. 2017;12(10):981-994. doi:10.1080/17460441.2017.1363734
204. Tian Y, Han L, Buckner AC, Ruotolo BT. Collision Induced Unfolding of Intact Antibodies: Rapid Characterization of Disulfide Bonding Patterns, Glycosylation, and Structures. *Anal Chem*. 2015;87(22):11509-11515.  
doi:10.1021/acs.analchem.5b03291
205. Guo J, Kumar S, Prashad A, Starkey J, Singh SK. Assessment of physical

- stability of an antibody drug conjugate by higher order structure analysis: Impact of thiol-maleimide chemistry. *Pharm Res.* 2014;31(7):1710-1723.  
doi:10.1007/s11095-013-1274-2
206. Beck A, Wagner-Rousset E, Ayoub D, Van Dorsselaer A, Sanglier-Cianféran S. Characterization of therapeutic antibodies and related products. *Anal Chem.* 2013;85(2):715-736. doi:10.1021/ac3032355
207. Beck A, Debaene F, Diemer H, et al. Cutting-edge mass spectrometry characterization of originator, biosimilar and biobetter antibodies. *J Mass Spectrom.* 2015;50(2):285-297. doi:10.1002/jms.3554
208. Tian Y, Ruotolo BT. Collision induced unfolding detects subtle differences in intact antibody glycoforms and associated fragments. *Int J Mass Spectrom.* 2018;425:1-9. doi:10.1016/j.ijms.2017.12.005
209. Eschweiler JD, Rabuck-Gibbons JN, Tian Y, Ruotolo BT. CIUSuite: A Quantitative Analysis Package for Collision Induced Unfolding Measurements of Gas-Phase Protein Ions. *Anal Chem.* 2015;87(22):11516-11522.  
doi:10.1021/acs.analchem.5b03292
210. Han L, Ruotolo BT. Traveling-wave ion mobility-mass spectrometry reveals additional mechanistic details in the stabilization of protein complex ions through tuned salt additives. *Int J Ion Mobil Spectrom.* 2013;16(1):41-50.  
doi:10.1007/s12127-013-0121-9
211. Pisupati K, Tian Y, Okbazghi S, et al. A multidimensional analytical comparison of Remicade and the biosimilar Remsima. *Anal Chem.* Published online 2017.  
doi:10.1021/acs.analchem.6b04436

212. Japelj B, Ilc G, Marušič J, Senčar J, Kuzman D, Plavec J. Biosimilar structural comparability assessment by NMR: From small proteins to monoclonal antibodies. *Sci Rep.* 2016;6:1-12. doi:10.1038/srep32201
213. Research FC for DE and. *Immunogenicity Assessment for Therapeutic Protein Products.*; 2014. <https://www.fda.gov/downloads/drugs/guidances/ucm338856.pdf>
214. Casadevall N, Nataf J, Viron B, et al. Pure red-cell aplasia and antierythropoietin antibodies in patients treated with recombinant erythropoietin. *N Engl J Med.* Published online 2002. doi:10.1056/NEJMoa011931
215. Sciences SL. Immunogenicity. <https://www.synexagroup.com/immunogenicity/>
216. Morgan H, Tseng SY, Gallais Y, et al. Evaluation of in vitro assays to assess the modulation of dendritic cells functions by therapeutic antibodies and aggregates. *Front Immunol.* Published online 2019. doi:10.3389/fimmu.2019.00601
217. Moussa EM, Kotarek J, Blum JS, Marszal E, Topp EM. Physical Characterization and Innate Immunogenicity of Aggregated Intravenous Immunoglobulin (IGIV) in an In Vitro Cell-Based Model. *Pharm Res.* Published online 2016. doi:10.1007/s11095-016-1914-4
218. Karle AC. Applying MAPPs Assays to Assess Drug Immunogenicity. *Front Immunol.* Published online 2020. doi:10.3389/fimmu.2020.00698
219. Alakhras NS, Qiu J, Rocha G V., et al. FcγRIIIa-dependent IFN-γ release in whole blood assay is predictive of therapeutic IgG1 antibodies safety. *MAbs.* Published online 2018. doi:10.1080/19420862.2018.1474996
220. Joubert MK, Deshpande M, Yang J, et al. Use of in vitro assays to assess immunogenicity risk of antibody-based biotherapeutics. *PLoS One.* Published

- online 2016. doi:10.1371/journal.pone.0159328
221. Joubert MK, Hokom M, Eakin C, et al. Highly aggregated antibody therapeutics can enhance the in vitro innate and late-stage T-cell immune responses. *J Biol Chem*. Published online 2012. doi:10.1074/jbc.M111.330902
222. Lee ACL, Harris JL, Khanna KK, Hong JH. A comprehensive review on current advances in peptide drug development and design. *Int J Mol Sci*. Published online 2019. doi:10.3390/ijms20102383
223. Lau JL, Dunn MK. Therapeutic peptides: Historical perspectives, current development trends, and future directions. *Bioorganic Med Chem*. Published online 2018. doi:10.1016/j.bmc.2017.06.052
224. Manning MC, Chou DK, Murphy BM, Payne RW, Katayama DS. Stability of protein pharmaceuticals: An update. *Pharm Res*. Published online 2010. doi:10.1007/s11095-009-0045-6
225. Topp EM, Zhang L, Zhao H, Payne RW, Evans GJ, Manning MC. Chemical Instability in Peptide and Protein Pharmaceuticals. In: *Formulation and Process Development Strategies for Manufacturing Biopharmaceuticals*. John Wiley & Sons, Inc.; 2010:41-67. doi:10.1002/9780470595886.ch2
226. Kossiakoff AA. Tertiary structure is a principal determinant to protein deamidation. *Science (80- )*. Published online 1988. doi:10.1126/science.3353715
227. Grassi L, Cabrele C. Susceptibility of protein therapeutics to spontaneous chemical modifications by oxidation, cyclization, and elimination reactions. *Amino Acids*. Published online 2019. doi:10.1007/s00726-019-02787-2
228. Capasso S, Salvadori S. Effect of the three-dimensional structure on the

- deamidation reaction of ribonuclease A. *J Pept Res*. Published online 1999.  
doi:10.1034/j.1399-3011.1999.00111.x
229. Capasso S, Di Cerbo P. Kinetic and thermodynamic control of the relative yield of the deamidation of asparagine and isomerization of aspartic acid residues. *J Pept Res*. Published online 2000. doi:10.1034/j.1399-3011.2000.00778.x
230. Bak A, Leung D, Barrett SE, et al. Physicochemical and Formulation Developability Assessment for Therapeutic Peptide Delivery—A Primer. *AAPS J*. Published online 2015. doi:10.1208/s12248-014-9688-2
231. Trainor K, Broom A, Meiering EM. Exploring the relationships between protein sequence, structure and solubility. *Curr Opin Struct Biol*. Published online 2017. doi:10.1016/j.sbi.2017.01.004
232. Riek R, Eisenberg DS. The activities of amyloids from a structural perspective. *Nature*. Published online 2016. doi:10.1038/nature20416
233. Woods RJ, Alarcoń J, McVey E, Pettis RJ. Intrinsic fibrillation of fast-acting insulin analogs. *J Diabetes Sci Technol*. Published online 2012. doi:10.1177/193229681200600209
234. Mikiewicz D, Bierzynska-Krzysik A, Sobolewska A, et al. Soluble insulin analogs combining rapid- and long-acting hypoglycemic properties  $\pm$  from an efficient *E. coli* expression system to a pharmaceutical formulation. *PLoS One*. Published online 2017. doi:10.1371/journal.pone.0172600
235. Tonie Wright H, Urry DW. Nonenzymatic deamidation of asparaginyl and glutaminyl residues in protein. *Crit Rev Biochem Mol Biol*. Published online 1991. doi:10.3109/10409239109081719



236. Rivers J, McDonald L, Edwards IJ, Beynon RJ. Asparagine deamidation and the role of higher order protein structure. *J Proteome Res.* 2008;7(3):921-927.  
doi:10.1021/pr070425l
237. Tyler-Cross R, Schirch V. Effects of amino acid sequence, buffers, and ionic strength on the rate and mechanism of deamidation of asparagine residues in small peptides. *J Biol Chem.* Published online 1991.  
doi:papers3://publication/uuid/91D1D08A-6EF8-49FE-85CC-5085C345C1D6
238. Brange J, Langkj\sgmaelig;r L, Havelund S, V\olund A. Chemical Stability of Insulin. 1. Hydrolytic Degradation During Storage of Pharmaceutical Preparations. *Pharm Res An Off J Am Assoc Pharm Sci.* Published online 1992.  
doi:10.1023/A:1015835017916
239. Nilsson MR, Driscoll M, Raleigh DP. Low levels of asparagine deamidation can have a dramatic effect on aggregation of amyloidogenic peptides: Implications for the study of amyloid formation. *Protein Sci.* Published online 2009.  
doi:10.1110/ps.48702
240. Harms MJ. Laser light-scattering evidence for an altered association of B1-crystallin deamidated in the connecting peptide. *Protein Sci.* Published online 2004. doi:10.1110/ps.03427504
241. Harn NR, Jeng YN, Kostelc JG, Middaugh CR. Spectroscopic analysis of highly concentrated suspensions of bovine somatotropin in sesame oil. *J Pharm Sci.* Published online 2005. doi:10.1002/jps.20464
242. Khossravi M, Shire SJ, Borchardt RT. Evidence for the involvement of histidine A(12) in the aggregation and precipitation of human relaxin induced by metal-

- catalyzed oxidation. *Biochemistry*. Published online 2000. doi:10.1021/bi9924720
243. Li S, Schöneich C, Borchardt RT, Nguyen TH. Aggregation and Precipitation of Human Relaxin Induced by Metal-Catalyzed Oxidation. *Biochemistry*. Published online 1995. doi:10.1021/bi00017a008
244. Gaudiano MC, Colone M, Bombelli C, Chistolini P, Valvo L, Diociaiuti M. Early stages of salmon calcitonin aggregation: Effect induced by ageing and oxidation processes in water and in the presence of model membranes. *Biochim Biophys Acta - Proteins Proteomics*. Published online 2005. doi:10.1016/j.bbapap.2005.04.008
245. Zapadka KL, Becher FJ, Gomes dos Santos AL, Jackson SE. Factors affecting the physical stability (aggregation) of peptide therapeutics. *Interface Focus*. Published online 2017. doi:10.1098/rsfs.2017.0030
246. Ahmad A, Uversky VN, Hong D, Fink AL. Early in the fibrillation of monomeric insulin. *J Biol Chem*. Published online 2005. doi:10.1074/jbc.M504298200
247. Hawe A, Sutter M, Jiskoot W. Extrinsic fluorescent dyes as tools for protein characterization. *Pharm Res*. Published online 2008. doi:10.1007/s11095-007-9516-9
248. Nielsen L, Khurana R, Coats A, et al. Effect of environmental factors on the kinetics of insulin fibril formation: Elucidation of the molecular mechanism. *Biochemistry*. Published online 2001. doi:10.1021/bi002555c
249. Bouchard M, Zurdo J, Nettleton EJ, Dobson CM, Robinson C V. Formation of insulin amyloid fibrils followed by FTIR simultaneously with CD and electron microscopy. *Protein Sci*. Published online 2000. doi:10.1110/ps.9.10.1960

250. Moorthy BS, Ghomi HT, Lill MA, Topp EM. Structural transitions and interactions in the early stages of human glucagon amyloid fibrillation. *Biophys J*. Published online 2015. doi:10.1016/j.bpj.2015.01.004
251. Ali MK, Bullard KMK, Saaddine JB, Cowie CC, Imperatore G, Gregg EW. Achievement of goals in U.S. diabetes care, 1999-2010. *N Engl J Med*. Published online 2013. doi:10.1056/NEJMsa1213829
252. Marathe PH, Gao HX, Close KL. American Diabetes Association Standards of Medical Care in Diabetes 2017. *J Diabetes*. Published online 2017. doi:10.1111/1753-0407.12524
253. Meloni AR, Deyoung MB, Lowe C, Parkes DG. GLP-1 receptor activated insulin secretion from pancreatic  $\beta$ -cells: Mechanism and glucose dependence. *Diabetes, Obes Metab*. Published online 2013. doi:10.1111/j.1463-1326.2012.01663.x
254. Baggio LL, Drucker DJ. Biology of Incretins: GLP-1 and GIP. *Gastroenterology*. Published online 2007. doi:10.1053/j.gastro.2007.03.054
255. Holst JJ. The physiology of glucagon-like peptide 1. *Physiol Rev*. Published online 2007. doi:10.1152/physrev.00034.2006
256. Franek E, Gajos G, Gumprecht J, Kretowski A, Zahorska-Markiewicz B, Malecki MT. The role of glucagon-like peptide 1 in glucose homeostasis and in other aspects of human physiology. *Pol Arch Med Wewn*. 2009;119(11):743—751. <http://europepmc.org/abstract/MED/19920800>
257. Li Y, Hansotia T, Yusta B, Ris F, Halban PA, Drueker DJ. Glucagon-like peptide-1 receptor signaling modulates  $\beta$  cell apoptosis. *J Biol Chem*. Published online 2003. doi:10.1074/jbc.M209423200

258. Yusta B, Baggio LL, Estall JL, et al. GLP-1 receptor activation improves  $\beta$  cell function and survival following induction of endoplasmic reticulum stress. *Cell Metab*. Published online 2006. doi:10.1016/j.cmet.2006.10.001
259. Cornu M, Thorens B. GLP-1 protects  $\beta$ -cells against apoptosis by enhancing the activity of an IGF-2/IGF1-receptor autocrine loop. *Islets*. 2009;1(3):280-282. doi:10.4161/isl.1.3.9932
260. Grieco M, Giorgi A, Gentile MC, et al. Glucagon-Like Peptide-1: A Focus on Neurodegenerative Diseases. *Front Neurosci*. Published online 2019. doi:10.3389/fnins.2019.01112
261. Aviles-Olmos I, Dickson J, Kefalopoulou Z, et al. Exenatide and the treatment of patients with Parkinson's disease. *J Clin Invest*. Published online 2013. doi:10.1172/JCI68295
262. Athauda D, Foltynie T. The glucagon-like peptide 1 (GLP) receptor as a therapeutic target in Parkinson's disease: Mechanisms of action. *Drug Discov Today*. Published online 2016. doi:10.1016/j.drudis.2016.01.013
263. Yu M, Benjamin MM, Srinivasan S, et al. Battle of GLP-1 delivery technologies. *Adv Drug Deliv Rev*. Published online 2018. doi:https://doi.org/10.1016/j.addr.2018.07.009
264. Hoare SRJ. Mechanisms of peptide and nonpeptide ligand binding to Class B G-protein-coupled receptors. *Drug Discov Today*. Published online 2005. doi:10.1016/S1359-6446(05)03370-2
265. Thorens B. Expression cloning of the pancreatic  $\beta$  cell receptor for the glucorecretin hormone glucagon-like peptide 1. *Proc Natl Acad Sci U S A*. Published

- online 1992. doi:10.1073/pnas.89.18.8641
266. Dillon JS, Tanizawa Y, Wheeler MB, et al. Cloning and functional expression of the human glucagon-like peptide-1 (GLP-1) receptor. *Endocrinology*. Published online 1993. doi:10.1210/endo.133.4.8404634
267. Graziano MP, Hey PJ, Borkowski D, Chicchi GG, Strader CD. Cloning and functional expression of a human glucagon-like peptide-1 receptor. *Biochem Biophys Res Commun*. Published online 1993. doi:10.1006/bbrc.1993.2226
268. Bergwitz C, Gardella TJ, Flannery MR, et al. Full activation of chimeric receptors by hybrids between parathyroid hormone and calcitonin. Evidence for a common pattern of ligand-receptor interaction. *J Biol Chem*. Published online 1996. doi:10.1074/jbc.271.43.26469
269. Suzuki S, Kawai K, Ohashi S, Mukai H, Yamashita K. Comparison of the effects of various C-terminal and N-terminal fragment peptides of glucagon-like peptide-1 on insulin and glucagon release from the isolated perfused rat pancreas. *Endocrinology*. Published online 1989. doi:10.1210/endo-125-6-3109
270. MOJSOV S. Structural requirements for biological activity of glucagon-like peptide-I. *Int J Pept Protein Res*. Published online 1992. doi:10.1111/j.1399-3011.1992.tb00309.x
271. Gallwitz B, Schmidt WE, Conlon JM, Creutzfeldt W. Glucagon-like peptide-1(7-36)amide: Characterization of the domain responsible for binding to its receptor on rat insulinoma RINm5F cells. *J Mol Endocrinol*. Published online 1990. doi:10.1677/jme.0.0050033
272. Wimley WC, White SH. Membrane Partitioning: Distinguishing Bilayer Effects

- from the Hydrophobic Effect. *Biochemistry*. Published online 1993.  
doi:10.1021/bi00076a001
273. Wimley WC, White SH. Experimentally determined hydrophobicity scale for proteins at membrane interfaces. *Nat Struct Biol*. Published online 1996.  
doi:10.1038/nsb1096-842
274. Henry GD, Sykes BD. Methods to study membrane protein structure in solution. *Methods Enzymol*. Published online 1994. doi:10.1016/S0076-6879(94)39020-7
275. Neidigh JW, Fesinmeyer RM, Prickett KS, Andersen NH. Exendin-4 and glucagon-like-peptide-1: NMR structural comparisons in the solution and micelle-associated states. *Biochemistry*. Published online 2001. doi:10.1021/bi010902s
276. Eng J, Kleinman WA, Singh L, Singh G, Raufman JP. Isolation and characterization of exendin-4, an exendin-3 analogue, from *Heloderma suspectum* venom. Further evidence for an exendin receptor on dispersed acini from guinea pig pancreas. *J Biol Chem*. Published online 1992.
277. Raufman JP, Singh L, Eng J. Exendin-3, a novel peptide from *Heloderma horridum* venom, interacts with vasoactive intestinal peptide receptors and a newly described receptor on dispersed acini from guinea pig pancreas: Description of exendin-3(9-39) amide, a specific exendin receptor. *J Biol Chem*. Published online 1991.
278. Goke R, Fehmann HC, Linn T, et al. Exendin-4 is a high potency agonist and truncated exendin-(9-39)-amide an antagonist at the glucagon-like peptide 1-(7-36)-amide receptor of insulin-secreting  $\beta$ -cells. *J Biol Chem*. Published online 1993.

279. Schepp W, Schmidtler J, Riedel T, et al. Exendin-4 and exendin-(9-39)NH<sub>2</sub>: agonist and antagonist, respectively, at the rat parietal cell receptor for glucagon-like peptide-1-(7-36)NH<sub>2</sub>. *Eur J Pharmacol Mol Pharmacol*. Published online 1994. doi:10.1016/0922-4106(94)90085-X
280. Kolligs F, Fehmann HC, Göke R, Göke B. Reduction of the incretin effect in rats by the glucagon-like peptide 1 receptor antagonist exendin (9-39) amide. *Diabetes*. Published online 1995. doi:10.2337/diab.44.1.16
281. Astrazeneca. *Byetta [Package Insert]*.; 2018.  
<https://www.azpicentral.com/byetta/byetta.pdf#page=1>
282. Astrazeneca. *Bydureon [Package Insert]*.; 2018.  
<https://www.azpicentral.com/bydureon/bydureon.pdf#page=1>
283. Shi Y, Sun X, Zhang L, et al. Fc-modified exenatide-loaded nanoparticles for oral delivery to improve hypoglycemic effects in mice. *Sci Rep*. Published online 2018. doi:10.1038/s41598-018-19170-y
284. Schneider EL, Hearn BR, Pfaff SJ, et al. A Hydrogel-Microsphere Drug Delivery System That Supports Once-Monthly Administration of a GLP-1 Receptor Agonist. *ACS Chem Biol*. Published online 2017. doi:10.1021/acscchembio.7b00218
285. Hudson FM, Andersen NH. Exenatide: NMR/CD evaluation of the medium dependence of conformation and aggregation state. In: *Biopolymers - Peptide Science Section*. ; 2004. doi:10.1002/bip.20126
286. Jäger M, Nguyen H, Crane JC, Kelly JW, Gruebele M. The folding mechanism of a  $\beta$ -sheet: The WW domain. *J Mol Biol*. Published online 2001.

doi:10.1006/jmbi.2001.4873

287. Neidigh JW, Andersen NH. Peptide conformational changes induced by tryptophan-phosphocholine interactions in a micelle. *Biopolymers*. Published online 2002. doi:10.1002/bip.10272
288. Cochran AG, Skelton NJ, Starovasnik MA. Tryptophan zippers: Stable, monomeric  $\beta$ -hairpins. *Proc Natl Acad Sci U S A*. Published online 2001. doi:10.1073/pnas.091100898
289. Kay BK, Williamson MP, Sudol M. The importance of being proline: the interaction of proline-rich motifs in signaling proteins with their cognate domains. *FASEB J*. Published online 2000. doi:10.1096/fasebj.14.2.231
290. Barua B, Lin JC, Williams VD, Kummler P, Neidigh JW, Andersen NH. The Trp-cage: Optimizing the stability of a globular miniprotein. *Protein Eng Des Sel*. Published online 2008. doi:10.1093/protein/gzm082
291. Neidigh JW, Fesinmeyer RM, Andersen NH. Designing a 20-residue protein. *Nat Struct Biol*. Published online 2002. doi:10.1038/nsb798
292. Rovó P, Farkas V, Stráner P, et al. Rational design of  $\alpha$ -helix-stabilized exendin-4 analogues. *Biochemistry*. Published online 2014. doi:10.1021/bi500033c
293. Andersen NH, Brodsky Y, Neidigh JW, Prickett KS. Medium-dependence of the secondary structure of exendin-4 and glucagon-like-peptide-1. *Bioorganic Med Chem*. Published online 2002. doi:10.1016/S0968-0896(01)00263-2
294. Dos Santos ML, Quintilio W, Manieri TM, Tsuruta LR, Moro AM. Advances and challenges in therapeutic monoclonal antibodies drug development. *Brazilian J Pharm Sci*. Published online 2018. doi:10.1590/s2175-97902018000001007



295. Vermeire S, Gils A, Accossato P, Lula S, Marren A. Immunogenicity of biologics in inflammatory bowel disease. *Therap Adv Gastroenterol*. Published online 2018. doi:10.1177/1756283X17750355
296. Johnson J&. *2019 Annual Report.*; 2020. <https://www.investor.jnj.com/annual-meeting-materials/2019-annual-report>
297. Pfizer. *2019 Financial Report.*; 2020. [https://s21.q4cdn.com/317678438/files/doc\\_financials/2018/ar/Pfizer-2019-Financial-Report.pdf](https://s21.q4cdn.com/317678438/files/doc_financials/2018/ar/Pfizer-2019-Financial-Report.pdf)
298. Samsung Bioepis. *2019 Annual Report.*; 2020. <https://samsungbiologics.com/ir/financial-info/annual-business-report>
299. Merck. *2019 Annual Report on Form 10-K.* [https://s21.q4cdn.com/488056881/files/doc\\_financials/2019/q4/2019-Form-10-K-Final.pdf](https://s21.q4cdn.com/488056881/files/doc_financials/2019/q4/2019-Form-10-K-Final.pdf)
300. European Medicines Agency. *Assessment Report: Inflectra.*; 2013.
301. Kang J, Pisupati K, Benet A, Ruotolo BT, Schwendeman SP, Schwendeman A. Infliximab biosimilars in the age of personalized medicine. *Trends Biotechnol*. Published online 2018. doi:10.1016/j.tibtech.2018.05.002
302. Dörner T, Kay J. Biosimilars in rheumatology: Current perspectives and lessons learnt. *Nat Rev Rheumatol*. 2015;11(12):713-724. doi:10.1038/nrrheum.2015.110
303. Braun J, Kudrin A. Switching to biosimilar infliximab (CT-P13): Evidence of clinical safety, effectiveness and impact on public health. *Biologicals*. Published online 2016. doi:10.1016/j.biologicals.2016.03.006
304. Danese S, Gomollon F. ECCO position statement: The use of biosimilar

- medicines in the treatment of inflammatory bowel disease (IBD). *J Crohn's Colitis*. 2013;7(7):586-589. doi:10.1016/j.crohns.2013.03.011
305. Ben-Horin S, Vande Casteele N, Schreiber S, Lakatos PL. Biosimilars in Inflammatory Bowel Disease: Facts and Fears of Extrapolation. *Clin Gastroenterol Hepatol*. Published online 2016. doi:10.1016/j.cgh.2016.05.023
306. Blauvelt A, Puig L, Chimenti S, et al. Biosimilars for psoriasis: clinical studies to determine similarity. *Br J Dermatol*. Published online 2017. doi:10.1111/bjd.15067
307. Park W, Hrycaj P, Jeka S, et al. A randomised, double-blind, multicentre, parallel-group, prospective study comparing the pharmacokinetics, safety, and efficacy of CT-P13 and innovator infliximab in patients with ankylosing spondylitis: the PLANETAS study. *Ann Rheum Dis*. 2013;72(10):1605 LP - 1612. <http://ard.bmj.com/content/72/10/1605.abstract>
308. Yoo DH, Hrycaj P, Miranda P, et al. A randomised, double-blind, parallel-group study to demonstrate equivalence in efficacy and safety of CT-P13 compared with innovator infliximab when coadministered with methotrexate in patients with active rheumatoid arthritis: the PLANETRA study. *Ann Rheum Dis*. 2013;72(10):1613 LP - 1620. <http://ard.bmj.com/content/72/10/1613.abstract>
309. Jørgensen KK, Olsen IC, Goll GL, et al. Switching from originator infliximab to biosimilar CT-P13 compared with maintained treatment with originator infliximab (NOR-SWITCH): a 52-week, randomised, double-blind, non-inferiority trial. *Lancet*. 2017;389(10086):2304-2316. doi:10.1016/S0140-6736(17)30068-5
310. Yoo DH, Prodanovic N, Jaworski J, et al. Efficacy and safety of CT-P13 (biosimilar infliximab) in patients with rheumatoid arthritis: Comparison between

- switching from reference infliximab to CT-P13 and continuing CT-P13 in the PLANETRA extension study. *Ann Rheum Dis*. Published online 2017.  
doi:10.1136/annrheumdis-2015-208786
311. Park W, Yoo DH, Miranda P, et al. Efficacy and safety of switching from reference infliximab to CT-P13 compared with maintenance of CT-P13 in ankylosing spondylitis: 102-week data from the PLANETAS extension study. *Ann Rheum Dis*. Published online 2017. doi:10.1136/annrheumdis-2015-208783
312. Cohen HP, Blauvelt A, Rifkin RM, Danese S, Gokhale SB, Woollett G. Switching Reference Medicines to Biosimilars: A Systematic Literature Review of Clinical Outcomes. *Drugs*. Published online 2018. doi:10.1007/s40265-018-0881-y
313. Singh LR, Poddar NK, Dar TA, Kumar R, Ahmad F. Protein and DNA destabilization by osmolytes: The other side of the coin. *Life Sci*. Published online 2011. doi:10.1016/j.lfs.2010.10.020
314. Wang W, Singh S, Zeng DL, King K, Nema S. Antibody structure, instability, and formulation. *J Pharm Sci*. Published online 2007. doi:10.1002/jps.20727
315. Information about IgG antibodies.  
[https://www.agrisera.com/en/info/igg.html#:~:text=IgG is the main low,up 75%25 of serum immunoglobulins.&text=Isoelectric point 6.1-8.5 \(7.3,a pool of various classes\)](https://www.agrisera.com/en/info/igg.html#:~:text=IgG is the main low,up 75%25 of serum immunoglobulins.&text=Isoelectric point 6.1-8.5 (7.3,a pool of various classes)).
316. Le Roith D. Insulin glargine and receptor-mediated signalling: Clinical implications in treating type 2 diabetes. *Diabetes Metab Res Rev*. Published online 2007.  
doi:10.1002/dmrr.776
317. Campbell RK, White JR, Levien T, Baker D. Insulin glargine. *Clin Ther*. Published

- online 2001. doi:10.1016/S0149-2918(01)80148-X
318. Jorgensen L, Hostrup S, Moeller EH, Grohganz H. Recent trends in stabilising peptides and proteins in pharmaceutical formulation - Considerations in the choice of excipients. *Expert Opin Drug Deliv*. Published online 2009. doi:10.1517/17425240903199143
319. Akbarian M, Ghasemi Y, Uversky VN, Yousefi R. Chemical modifications of insulin: Finding a compromise between stability and pharmaceutical performance. *Int J Pharm*. Published online 2018. doi:10.1016/j.ijpharm.2018.06.023
320. Jain NK, Roy I. Trehalose and protein stability. *Curr Protoc Protein Sci*. Published online 2010. doi:10.1002/0471140864.ps0409s59
321. Habib S, Khan MA, Younus H. Thermal destabilization of stem bromelain by trehalose. *Protein J*. Published online 2007. doi:10.1007/s10930-006-9052-1
322. Pikal MJ, Dellerman KM, Roy ML, Riggin RM. The Effects of Formulation Variables on the Stability of Freeze-Dried Human Growth Hormone. *Pharm Res An Off J Am Assoc Pharm Sci*. Published online 1991. doi:10.1023/A:1015834724528
323. Pikal MJ, Dellerman K, Roy ML. Formulation and stability of freeze-dried proteins: effects of moisture and oxygen on the stability of freeze-dried formulations of human growth hormone. *Dev Biol Stand*. Published online 1992.
324. Lai MC, Topp EM. Solid-state chemical stability of proteins and peptides. *J Pharm Sci*. Published online 1999. doi:10.1021/js980374e
325. Chang L, Shepherd D, Sun J, et al. Mechanism of protein stabilization by sugars during freeze-drying and storage: Native structure preservation, specific

- interaction, and/or immobilization in a glassy matrix? *J Pharm Sci*. Published online 2005. doi:10.1002/jps.20364
326. Costantino HR, Pikal MJ. Freeze-drying Process Development for Protein Pharmaceuticals in Lyophilization of biopharmaceuticals. *Am Assoc Pharm Sci*. Published online 2004.
327. Franks F, Hatley RHM, Mathias S. Materials Science and the Production of Shelf-Stable Biologicals. *Biopharm-The Technol Buissness Biopharm*. Published online 1991.
328. Reid DS, Levine H. Beyond Water Activity: Recent Advances Based on an Alternative Approach to the Assessment of Food Quality and Safety. *Crit Rev Food Sci Nutr*. Published online 1991. doi:10.1080/10408399109527543
329. Carpenter JF, Prestrelski SJ, Arakawa T. Separation of Freezing- and Drying-Induced Denaturation of Lyophilized Proteins Using Stress-Specific Stabilization: I. Enzyme Activity and Calorimetric Studies. *Arch Biochem Biophys*. Published online 1993. doi:10.1006/abbi.1993.1309
330. Carpenter JF, Crowe JH. An infrared spectroscopic study of the interactions of carbohydrates with dried proteins. *Biochemistry*. Published online 1989. doi:10.1021/bi00435a044
331. Crowe JH, Crowe LM, Carpenter JF. Preserving dry biomaterials: the water replacement hypothesis. *Biopharm*. Published online 1993.
332. Duddu SP, Zhang G, Dal Monte PR. The relationship between protein aggregation and molecular mobility below the glass transition temperature of lyophilized formulations containing a monoclonal antibody. *Pharm Res*. Published

- online 1997. doi:10.1023/A:1012196826905
333. Banting FG, Best CH. The internal secretion of the pancreas. *J Lab Clin Med*.  
Published online 1922. doi:10.1093/ajcp/21.4.364
334. Alcántara-Aragón V. Improving patient self-care using diabetes technologies. *Ther Adv Endocrinol Metab*. Published online 2019. doi:10.1177/2042018818824215
335. Rex J, Jensen KH, Lawton SA. A review of 20 years' experience with the NovoPen® family of insulin injection devices. *Clin Drug Investig*. Published online 2006. doi:10.2165/00044011-200626070-00001
336. Weaver KW, Hirsch IB. The Hybrid Closed-Loop System: Evolution and Practical Applications. *Diabetes Technol Ther*. Published online 2018.  
doi:10.1089/dia.2018.0091
337. Turner R. Intensive blood-glucose control with sulphonylureas or insulin compared with conventional treatment and risk of complications in patients with type 2 diabetes (UKPDS 33). *Lancet*. Published online 1998. doi:10.1016/S0140-6736(98)07019-6
338. Kesavadev J, Saboo B, Krishna MB, Krishnan G. Evolution of Insulin Delivery Devices: From Syringes, Pens, and Pumps to DIY Artificial Pancreas. *Diabetes Ther*. Published online 2020. doi:10.1007/s13300-020-00831-z
339. Singh R, Samuel C, Jacob JJ. A comparison of insulin pen devices and disposable plastic syringes - Simplicity, safety, convenience and cost differences. *Eur Endocrinol*. Published online 2018. doi:10.17925/EE.2018.14.1.47
340. Guerci B, Chanan N, Kaur S, Jasso-Mosqueda JG, Lew E. Lack of treatment persistence and treatment nonadherence as barriers to glycaemic control in

- patients with type 2 diabetes. *Diabetes Ther.* Published online 2019.  
doi:10.1007/s13300-019-0590-x
341. Bailey TS, Stone JY. A novel pen-based Bluetooth-enabled insulin delivery system with insulin dose tracking and advice. *Expert Opin Drug Deliv.* Published online 2017. doi:10.1080/17425247.2017.1313831
342. Gildon BW. InPen smart insulin pen system: Product review and user experience. *Diabetes Spectr.* Published online 2018. doi:10.2337/ds18-0011
343. Peters AL, Ahmann AJ, Battelino T, et al. Diabetes technology-continuous subcutaneous insulin infusion therapy and continuous glucose monitoring in adults: An endocrine society clinical practice guideline. *J Clin Endocrinol Metab.* Published online 2016. doi:10.1210/jc.2016-2534
344. Pozzilli P, Battelino T, Danne T, Hovorka R, Jarosz-Chobot P, Renard E. Continuous subcutaneous insulin infusion in diabetes: Patient populations, safety, efficacy, and pharmacoeconomics. *Diabetes Metab Res Rev.* Published online 2016. doi:10.1002/dmrr.2653
345. Hovorka R. Closed-loop insulin delivery: From bench to clinical practice. *Nat Rev Endocrinol.* Published online 2011. doi:10.1038/nrendo.2011.32
346. Zisser H. Quantifying the impact of a short-interval interruption of insulin-pump infusion sets on glycemic excursions. *Diabetes Care.* Published online 2008. doi:10.2337/dc07-1757
347. Kerr D, Wizemann E, Senstius J, Zacho M, Ampudia-Blasco FJ. Stability and performance of rapid-acting insulin analogs used for continuous subcutaneous insulin infusion: A systematic review. *J Diabetes Sci Technol.* Published online

2013. doi:10.1177/193229681300700620
348. Kerr D, Morton J, Whately-Smith C, Everett J, Begley JP. Laboratory-based non-clinical comparison of occlusion rates using three rapid-acting insulin analogs in continuous subcutaneous insulin infusion catheters using low flow rates. *J Diabetes Sci Technol*. Published online 2008. doi:10.1177/193229680800200314
349. Bode BW. Comparison of pharmacokinetic properties, physicochemical stability, and pump compatibility of 3 rapid-acting insulin analogues-aspart, lispro, and glulisine. *Endocr Pract*. Published online 2011. doi:10.4158/EP10260.RA
350. Nauck MA, Meier JJ. MANAGEMENT OF ENDOCRINE DISEASE: Are all GLP-1 agonists equal in the treatment of type 2 diabetes? *Eur J Endocrinol*. Published online 2019. doi:10.1530/eje-19-0566
351. Nauck MA, Quast DR, Wefers J, Meier JJ. GLP-1 receptor agonists in the treatment of type 2 diabetes – state-of-the-art. *Mol Metab*. Published online 2020. doi:10.1016/j.molmet.2020.101102
352. Abd El Aziz MS, Kahle M, Meier JJ, Nauck MA. A meta-analysis comparing clinical effects of short- or long-acting GLP-1 receptor agonists versus insulin treatment from head-to-head studies in type 2 diabetic patients. *Diabetes, Obes Metab*. Published online 2017. doi:10.1111/dom.12804
353. Singh S, Wright EE, Kwan AYM, et al. Glucagon-like peptide-1 receptor agonists compared with basal insulins for the treatment of type 2 diabetes mellitus: a systematic review and meta-analysis. *Diabetes, Obes Metab*. Published online 2017. doi:10.1111/dom.12805
354. Mueller C, Altenburger U, Mohl S. Challenges for the pharmaceutical technical



- development of protein coformulations. *J Pharm Pharmacol*. Published online 2018. doi:10.1111/jphp.12731
355. European Medicines Agency. *Suliqua, INN*.  
[https://www.ema.europa.eu/en/documents/product-information/suliqua-epar-product-information\\_en.pdf](https://www.ema.europa.eu/en/documents/product-information/suliqua-epar-product-information_en.pdf)
356. European Medicines Agency. *Xultophy, INN*.  
[https://www.ema.europa.eu/en/documents/product-information/xultophy-epar-product-information\\_en.pdf](https://www.ema.europa.eu/en/documents/product-information/xultophy-epar-product-information_en.pdf)
357. Gough SCL, Bode B, Woo V, et al. Efficacy and safety of a fixed-ratio combination of insulin degludec and liraglutide (IDegLira) compared with its components given alone: Results of a phase 3, open-label, randomised, 26-week, treat-to-target trial in insulin-naive patients with type 2 di. *Lancet Diabetes Endocrinol*. Published online 2014. doi:10.1016/S2213-8587(14)70174-3
358. Nauck MA, Meier JJ. GLP-1 analogues and insulin: sound the wedding bells? *Nat Rev Endocrinol*. 2011;7(4):193-195. doi:10.1038/nrendo.2011.30
359. Buse JB, Bergenstal RM, Glass LC, et al. Use of twice-daily exenatide in basal insulin-treated patients with type 2 diabetes. *Ann Intern Med*. Published online 2011. doi:10.7326/0003-4819-154-2-201101180-00300
360. Ahmann A, Rodbard HW, Rosenstock J, et al. Efficacy and safety of liraglutide versus placebo added to basal insulin analogues (with or without metformin) in patients with type 2 diabetes: A randomized, placebo-controlled trial. *Diabetes, Obes Metab*. Published online 2015. doi:10.1111/dom.12539
361. Pozzilli P, Norwood P, Jódar E, et al. Placebo-controlled, randomized trial of the

- addition of once-weekly glucagon-like peptide-1 receptor agonist dulaglutide to titrated daily insulin glargine in patients with type 2 diabetes (AWARD-9). *Diabetes, Obes Metab*. Published online 2017. doi:10.1111/dom.12937
362. Leiter LA, Gross JL, Chow F, Miller D, Johnson S, Ahrén B. Once weekly glucagon-like peptide-1 receptor agonist albiglutide vs. prandial insulin added to basal insulin in patients with type 2 diabetes mellitus: Results over 52 weeks. *J Diabetes Complications*. Published online 2017. doi:10.1016/j.jdiacomp.2017.05.010
363. Rodbard HW, Lingvay I, Reed J, et al. Semaglutide Added to Basal Insulin in Type 2 Diabetes (SUSTAIN 5): A Randomized, Controlled Trial. *J Clin Endocrinol Metab*. Published online 2018. doi:10.1210/jc.2018-00070
364. Zinman B, Aroda VR, Buse JB, et al. Efficacy, safety, and tolerability of oral semaglutide versus placebo added to insulin with or without metformin in patients with type 2 diabetes: The PioNEER 8 trial. *Diabetes Care*. Published online 2019. doi:10.2337/dc19-0898
365. Syed YY, McCormack PL. Exenatide Extended-Release: An Updated Review of Its Use in Type 2 Diabetes Mellitus. *Drugs*. Published online 2015. doi:10.1007/s40265-015-0420-z
366. Young AA, Gedulin BR, Bhavsar S, et al. Glucose-lowering and insulin-sensitizing actions of exendin-4: Studies in obese diabetic (ob/ob, db/db) mice, diabetic fatty Zucker rats, and diabetic rhesus monkeys (*Macaca mulatta*). *Diabetes*. Published online 1999. doi:10.2337/diabetes.48.5.1026
367. Kolterman OG, Kim DD, Shen L, et al. Pharmacokinetics, pharmacodynamics,

- and safety of exenatide in patients with type 2 diabetes mellitus. *Am J Heal Pharm*. Published online 2005. doi:10.1177/0091270008323750
368. Joy S V, Rodgers PT, Scates AC. Incretin mimetics as emerging treatments for type 2 diabetes. *Ann Pharmacother*. Published online 2005. doi:10.1345/aph.1E245
369. *AstraZeneca Annual Report and Form 20-F Information 2017.*; 2017.
370. Business Wire. Teva Settles Patent Litigation with AstraZeneca Allowing Teva to Commercialize its Generic Version of Byetta (Exenatide Injection) in the United States. Published 2016. <https://www.businesswire.com/news/home/20160623005356/en/Teva-Settles-Patent-Litigation-with-AstraZeneca-Allowing-Teva-to-Commercialize-Its-Generic-Version-of-Byetta-Exenatide-Injection-in-the-United-States>
371. Drug.com. Generic Byetta Availability. <https://www.drugs.com/availability/generic-byetta.html>
372. *Drugs Coming Off Patent by 2022*. [https://www.pti-nps.com/nps/wp-content/uploads/2017/04/NPS\\_Drugs-Coming-Off-Patent-by-2022-Web.pdf](https://www.pti-nps.com/nps/wp-content/uploads/2017/04/NPS_Drugs-Coming-Off-Patent-by-2022-Web.pdf)
373. Li T, Chandrashekar A, Beig A, et al. Characterization of attributes and in vitro performance of exenatide-loaded PLGA long-acting release microspheres. *Eur J Pharm Biopharm*. Published online 2021. doi:10.1016/j.ejpb.2020.10.008
374. Lim SM, Eom HN, Jiang HH, Sohn M, Lee KC. Evaluation of PEGylated exendin-4 released from poly (lactic-co-glycolic acid) microspheres for antidiabetic therapy. *J Pharm Sci*. Published online 2015. doi:10.1002/jps.24238
375. Wang P, Zhuo X, Chu W, Tang X. Exenatide-loaded microsphere/thermosensitive

- hydrogel long-acting delivery system with high drug bioactivity. *Int J Pharm.*  
Published online 2017. doi:10.1016/j.ijpharm.2017.05.069
376. CDER. *ANDAs for Certain Highly Purified Synthetic Peptide Drug Products That Refer to Listed Drugs of RDNA Origin.*; 2021.  
<https://www.fda.gov/media/107622/download>
377. Srivastava V, ed. *Peptide Therapeutics*. The Royal Society of Chemistry; 2019.  
doi:10.1039/9781788016445
378. Liang R, Zhang R, Li X, et al. Stability of exenatide in poly(D,L-lactide-co-glycolide) solutions: A simplified investigation on the peptide degradation by the polymer. *Eur J Pharm Sci*. Published online 2013. doi:10.1016/j.ejps.2013.08.014
379. EMA. Byetta : EPAR - Product Information. *Internet Eur Integr*. Published online 2009.
380. Sigma-Aldrich. Mass Changes. Accessed January 6, 2017.  
<https://www.sigmaaldrich.com/life-science/proteomics/post-translational-analysis/phosphorylation/mass-changes.html>
381. Griffiths SW, Cooney CL. Relationship between protein structure and methionine oxidation in recombinant human  $\alpha$ 1-antitrypsin. *Biochemistry*. Published online 2002. doi:10.1021/bi025599p
382. Ji JA, Zhang B, Cheng W, Wang YJ. Methionine, tryptophan, and histidine oxidation in a model protein, PTH: Mechanisms and stabilization. *J Pharm Sci*.  
Published online 2009. doi:10.1002/jps.21746
383. *AF4 Comparability Study of Generic Exenatide Injection and Originator Samples.*; 2017.

384. Zapadka KL, Becher FJ, Uddin S, et al. A pH-Induced Switch in Human Glucagon-like Peptide-1 Aggregation Kinetics. *J Am Chem Soc*. Published online 2016. doi:10.1021/jacs.6b05025
385. Fineman MS, Mace KF, Diamant M, et al. Clinical relevance of anti-exenatide antibodies: Safety, efficacy and cross-reactivity with long-term treatment. *Diabetes, Obes Metab*. Published online 2012. doi:10.1111/j.1463-1326.2012.01561.x
386. Konara CS, Barnard RT, Hine D, Siegel E, Ferro V. The Tortoise and the Hare: Evolving Regulatory Landscapes for Biosimilars. *Trends Biotechnol*. Published online 2016. doi:10.1016/j.tibtech.2015.10.009
387. AstraZeneca. *Remicade [Packageinsert]*.; 2015.
388. Pisupati K, Tian Y, Okbazghi S, et al. A Multidimensional Analytical Comparison of Remicade and the Biosimilar Remsima. *Anal Chem*. Published online 2017. doi:10.1021/acs.analchem.6b04436
389. Hawe A, Wiggernhorn M, van de Weert M, Garbe JHO, Mahler HC, Jiskoot W. Forced degradation of therapeutic proteins. *J Pharm Sci*. Published online 2012. doi:10.1002/jps.22812
390. Luo Q, Joubert MK, Stevenson R, Ketchum RR, Narhi LO, Wypych J. Chemical modifications in therapeutic protein aggregates generated under different stress conditions. *J Biol Chem*. Published online 2011. doi:10.1074/jbc.M110.160440
391. Chan CP. Forced degradation studies: current trends and future perspectives for protein-based therapeutics. *Expert Rev Proteomics*. Published online 2016. doi:10.1080/14789450.2016.1200469

392. AstraZeneca. *Remsima [Package Insert]*.; 2014.
393. Greenspan L. Humidity Fixed Points of Binary Saturated Aqueous Solutions. *J Res Natl Bur Stand Sect A Phys Chem*. Published online 1977.  
doi:10.6028/jres.081A.011
394. Bern M, Kil YJ, Becker C. Byonic: Advanced peptide and protein identification software. *Curr Protoc Bioinforma*. 2012;40(1):13.20.1-13.20.14.  
doi:10.1002/0471250953.bi1320s40
395. Bern M, Cai Y, Goldberg D. Lookup peaks: A hybrid of de novo sequencing and database search for protein identification by tandem mass spectrometry. *Anal Chem*. 2007;79(4):1393-1400. doi:10.1021/ac0617013
396. Zhong Y, Hyung S-J, Ruotolo BT. Characterizing the resolution and accuracy of a second-generation traveling-wave ion mobility separator for biomolecular ions. *Analyst*. 2011;136(17):3534-3541. doi:10.1039/c0an00987c
397. Giles K, Williams JP, Campuzano I. Enhancements in travelling wave ion mobility resolution. *Rapid Commun Mass Spectrom*. 2011;25(11):1559-1566.  
doi:10.1002/rcm.5013
398. Tito MA, Tars K, Vallengard K, Hajdu J, Robinson C V. Electrospray time-of-flight mass spectrometry of the intact MS2 virus capsid [15]. *J Am Chem Soc*.  
Published online 2000. doi:10.1021/ja993740k
399. McKay AR, Ruotolo BT, Ilag LL, Robinson C V. Mass measurements of increased accuracy resolve heterogeneous populations of intact ribosomes. *J Am Chem Soc*. 2006;128(35):11433-11442. doi:10.1021/ja061468q
400. Okbazghi SZ, More AS, White DR, et al. Production, Characterization, and

- Biological Evaluation of Well-Defined IgG1 Fc Glycoforms as a Model System for Biosimilarity Analysis. *J Pharm Sci.* 2016;105(2):559-574.  
doi:10.1016/j.xphs.2015.11.003
401. Alsenaidy MA, Okbazghi SZ, Kim JH, et al. Physical stability comparisons of IgG1-Fc variants: Effects of N-glycosylation site occupancy and Asp/gln residues at site asn 297. *J Pharm Sci.* 2014;103(6):1613-1627. doi:10.1002/jps.23975
402. Lakowicz JR. *Principles of Fluorescence Spectroscopy*. Third edit. (Lakowicz JR, ed.). Springer; 2006. doi:10.1007/978-0-387-46312-4
403. Ohadi K, Legge RL, Budman HM. Intrinsic fluorescence-based at situ soft sensor for monitoring monoclonal antibody aggregation. *Biotechnol Prog.* Published online 2015. doi:10.1002/btpr.2140
404. Garidel P, Hegyi M, Bassarab S, Weichel M. A rapid, sensitive and economical assessment of monoclonal antibody conformational stability by intrinsic tryptophan fluorescence spectroscopy. *Biotechnol J.* Published online 2008. doi:10.1002/biot.200800091
405. Cathou RE, Kulczycki A, Haber E. Structural Features of  $\gamma$ -Immunoglobulin, Antibody, and Their Fragments. Circular Dichroism Studies. *Biochemistry.* Published online 1968. doi:10.1021/bi00851a024
406. Joshi V, Shivach T, Yadav N, Rathore AS. Circular dichroism spectroscopy as a tool for monitoring aggregation in monoclonal antibody therapeutics. *Anal Chem.* Published online 2014. doi:10.1021/ac503140j
407. Houde DJ, Berkowitz SA. *Biophysical Characterization of Proteins in Developing Biopharmaceuticals.*; 2019. doi:10.1016/C2017-0-03008-2

408. Houde D, Peng Y, Berkowitz SA, Engen JR. Post-translational modifications differentially affect IgG1 conformation and receptor binding. *Mol Cell Proteomics*. Published online 2010. doi:10.1074/mcp.M900540-MCP200
409. Wang W, Vlasak J, Li Y, et al. Impact of methionine oxidation in human IgG1 Fc on serum half-life of monoclonal antibodies. *Mol Immunol*. Published online 2011. doi:10.1016/j.molimm.2010.12.009
410. Zhu J. Mammalian cell protein expression for biopharmaceutical production. *Biotechnol Adv*. Published online 2012. doi:10.1016/j.biotechadv.2011.08.022
411. Hmiel LK, Brorson KA, Boyne M.T. II. Post-translational structural modifications of immunoglobulin G and their effect on biological activity. *Anal Bioanal Chem*. 2015;407(1):79-94. doi:10.1007/s00216-014-8108-x
412. Carpenter JF, Randolph TW, Jiskoot W, Crommelin DJA, Middaugh CR, Winter G. Potential inaccurate quantitation and sizing of protein aggregates by size exclusion chromatography: Essential need to use orthogonal methods to assure the quality of therapeutic protein products. *J Pharm Sci*. Published online 2010. doi:10.1002/jps.21989
413. *Remsima: Summary Basis of Decision.*; 2014.
414. Feagan BG, Choquette D, Ghosh S, et al. The challenge of indication extrapolation for infliximab biosimilars. *Biologicals*. 2014;42(4):177-183. doi:10.1016/j.biologicals.2014.05.005
415. Ahmadi M, Bryson CJ, Cloake EA, et al. Small amounts of sub-visible aggregates enhance the immunogenic potential of monoclonal antibody therapeutics. *Pharm Res*. Published online 2015. doi:10.1007/s11095-014-1541-x



416. Paul R, Graff-Meyer A, Stahlberg H, et al. Structure and function of purified monoclonal antibody dimers induced by different stress conditions. *Pharm Res*. Published online 2012. doi:10.1007/s11095-012-0732-6
417. Bi V, Jawa V, Joubert MK, et al. Development of a human antibody tolerant mouse model to assess the immunogenicity risk due to aggregated biotherapeutics. *J Pharm Sci*. Published online 2013. doi:10.1002/jps.23663
418. Rombach-Riegraf V, Karle AC, Wolf B, et al. Aggregation of human recombinant monoclonal antibodies influences the capacity of dendritic cells to stimulate adaptive T-cell responses in vitro. *PLoS One*. Published online 2014. doi:10.1371/journal.pone.0086322
419. Liu H, May K. Disulfide bond structures of IgG molecules: Structural variations, chemical modifications and possible impacts to stability and biological function. *MAbs*. Published online 2012. doi:10.4161/mabs.4.1.18347
420. Vidarsson G, Dekkers G, Rispens T. IgG subclasses and allotypes: From structure to effector functions. *Front Immunol*. Published online 2014. doi:10.3389/fimmu.2014.00520
421. Ryman JT, Meibohm B. Pharmacokinetics of monoclonal antibodies. *CPT Pharmacometrics Syst Pharmacol*. Published online 2017. doi:10.1002/psp4.12224
422. Arora T, Padaki R, Liu L, et al. Differences in binding and effector functions between classes of TNF antagonists. *Cytokine*. 2009;45(2):124-131. doi:10.1016/j.cyto.2008.11.008
423. Gupta A, Van Vlijmen HWT, Singh J. A classification of disulfide patterns and its

- relationship to protein structure and function. *Protein Sci.* Published online 2004.  
doi:10.1110/ps.04613004
424. Trivedi M, Laurence J, Siahaan T. The Role of Thiols and Disulfides on Protein Stability. *Curr Protein Pept Sci.* Published online 2009.  
doi:10.2174/138920309789630534
425. Liu H, Chumsae C, Gaza-Bulseco G, Hurkmans K, Radziejewski CH. Ranking the susceptibility of disulfide bonds in human IgG1 antibodies by reduction, differential alkylation, and LC-MS analysis. *Anal Chem.* Published online 2010.  
doi:10.1021/ac100575n
426. Kang J, Halseth T, Vallejo D, et al. Assessment of biosimilarity under native and heat-stressed conditions: rituximab, bevacizumab, and trastuzumab originators and biosimilars. *Anal Bioanal Chem.* Published online 2020. doi:10.1007/s00216-019-02298-9
427. Xiang T, Chumsae C, Liu H. Localization and quantitation of free sulfhydryl in recombinant monoclonal antibodies by differential labeling with <sup>12</sup>C and <sup>13</sup>C iodoacetic acid and LC-MS analysis. *Anal Chem.* Published online 2009.  
doi:10.1021/ac901311y
428. Chumsae C, Gaza-Bulseco G, Liu H. Identification and localization of unpaired cysteine residues in monoclonal antibodies by fluorescence labeling and mass spectrometry. *Anal Chem.* Published online 2009. doi:10.1021/ac900815z
429. Harris RJ. Heterogeneity of recombinant antibodies: Linking structure to function. In: *Developments in Biologicals.* ; 2005.
430. Thies MJW, Talamo F, Mayer M, et al. Folding and oxidation of the antibody

- domain C(H)3. *J Mol Biol.* 2002;319(5):1267-1277. doi:10.1016/S0022-2836(02)00375-3
431. Van Buren N, Rehder D, Gadgil H, Matsumura M, Jacob J. Elucidation of two major aggregation pathways in an IgG2 antibody. *J Pharm Sci.* 2009;98(9):3013-3030. doi:10.1002/jps.21514
432. Brych SR, Gokarn YR, Hultgen H, Stevenson RJ, Rajan R, Matsumura M. Characterization of antibody aggregation: Role of buried, unpaired cysteines in particle formation. *J Pharm Sci.* Published online 2010. doi:10.1002/jps.21868
433. Dorai H, Wesolowski JS, Gillies SD. Role of inter-heavy and light chain disulfide bonds in the effector functions of human immunoglobulin IgG1. *Mol Immunol.* Published online 1992. doi:10.1016/0161-5890(92)90222-J
434. Pristatsky P, Cohen SL, Krantz D, Acevedo J, Ionescu R, Vlasak J. Evidence for trisulfide bonds in a recombinant variant of a human IgG2 monoclonal antibody. *Anal Chem.* Published online 2009. doi:10.1021/ac9006254
435. Kshirsagar R, Mcelearney K, Gilbert A, Sinacore M, Ryll T. Controlling trisulfide modification in recombinant monoclonal antibody produced in fed-batch cell culture. *Biotechnol Bioeng.* Published online 2012. doi:10.1002/bit.24511
436. Thomsen MK, Hansen BS, Nilsson P, et al. Pharmacological Characterization of a Biosynthetic Trisulfide-Containing Hydrophobic Derivative of Human Growth Hormone: Comparison with Standard 22 K Growth Hormone. *Pharmacol Toxicol.* Published online 1994. doi:10.1111/j.1600-0773.1994.tb01372.x
437. Cumnock K, Tully T, Cornell C, et al. Trisulfide modification impacts the reduction step in antibody-drug conjugation process. *Bioconjug Chem.* Published online

2013. doi:10.1021/bc4000299
438. Liu R, Chen X, Dushime J, et al. The impact of trisulfide modification of antibodies on the properties of antibody-drug conjugates manufactured using thiol chemistry. *MAbs*. 2017;9(3):490-497. doi:10.1080/19420862.2017.1285478
439. Cao M, Xu W, Niu B, et al. An Automated and Qualified Platform Method for Site-Specific Succinimide and Deamidation Quantitation Using Low-pH Peptide Mapping. *J Pharm Sci*. Published online 2019. doi:10.1016/j.xphs.2019.07.019
440. Nowak C, Ponniah G, Neill A, Liu H. Characterization of succinimide stability during trypsin digestion for LC-MS analysis. *Anal Biochem*. Published online 2017. doi:10.1016/j.ab.2017.03.005
441. Genentech/Biogen. *Rituxan [Package Insert]*.; 2010.  
[https://www.accessdata.fda.gov/drugsatfda\\_docs/label/2010/103705s5311lbl.pdf](https://www.accessdata.fda.gov/drugsatfda_docs/label/2010/103705s5311lbl.pdf)
442. Genentech. *Bevacizumab [Package Insert]*.; 2017.  
[https://www.accessdata.fda.gov/drugsatfda\\_docs/label/2017/125085s319lbl.pdf](https://www.accessdata.fda.gov/drugsatfda_docs/label/2017/125085s319lbl.pdf)
443. Tang L, Kebarle P. Dependence of ion intensity in electrospray mass spectrometry on the concentration of the analytes in the electrosprayed solution. *Anal Chem*. Published online 1993. doi:10.1021/ac00072a020